Contour Integration and Principles of Perceptual Grouping

Inaugural-Dissertation
zur Erlangung des akademischen Grades
eines Dr. phil.
vorgelegt dem Fachbereich 02

Sozialwissenschaften, Medien und Sport
der Johannes Gutenberg-Universität Mainz
von

Dipl.-Psych. Malte Persike
aus Hannover

Mainz 2008

Tag des Prüfungskolloquiums: 15. April 2008

Those to whom I owe so much, who lent their support in every conceivable way, who encouraged, endorsed, and guided me - you know who you are. Thank you.

Contents

List of Figures

List of Tables

1 Introduction

1.1 Perceptual Grouping and Gestalt Rules

A fundamental task of vision is to identify parts of a visual scene that belong together and combine these parts into meaningful wholes. Processes which accomplish the integration of identified parts into a unique percept are commonly subsumed under the term *perceptual grouping*. The human visual system implements grouping mechanisms at several levels in the visual hierarchy, based on spatial, temporal, and chromatic features of the stimulus (Beck, 1966; Pashler, 1988; Grossberg & Pessoa, 1998; S. H. Lee & Blake, 2001). Many of these grouping mechanisms relate to a set of rules formulated by Gestalt psychologists early in the last century to govern the principles of perceptual organization (Koffka, 1935; Wertheimer, 1958). Gestalt theory is centered around the precept of conciseness, according to which perception tends to be organized in a regular, simple, and meaningful manner.

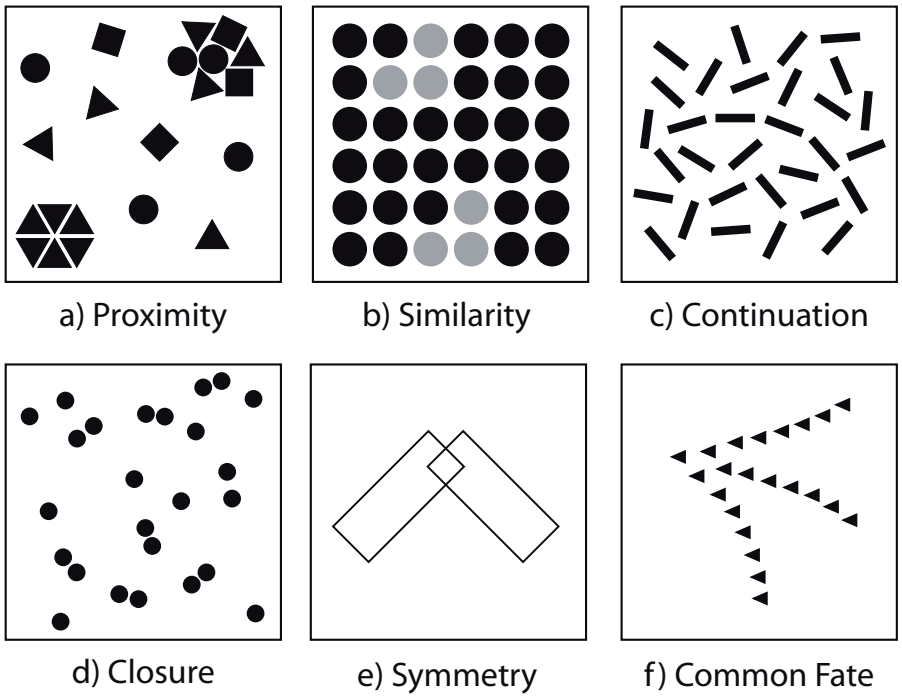

Figure 1.1: Stimulus examples of perceptual grouping phenomena relating to Gestalt rules.

Based upon this fundamental proposition, more specific rules have been devised to account for prominent patterns of perceptual grouping. Among these Gestalt rules, the two principles ascribed with the highest salience for perceptual organization are proximity and similarity. According to the *rule of proximity*, distinct elements are likely to be perceived as a collective or whole if they are in the spatial or temporal vicinity of each other (Figure 1.1a). The *rule of similarity* states that elements are perceived as a whole if they share common features like color, depth, or size (Figure 1.1b). Four other principles are comprised in the original assembly of Gestalt rules. The *rule of good continuation*, as shown in Figure 1.1c, derives from the notion that a sequence of separate objects aligned with a common spatial or temporal trajectory will be grouped due to the perceived nonaccidental relationship among the elements. Exemplified in Figure 1.1d is the *rule of closure*, claiming that elements will be grouped if they follow a closed overall shape. Although the spatial configuration of the dots in Figure 1.1d would allow for the perception of two opposite open arcs, the visual system favors to integrate the dots into a closed circle. The *rule of symmetry* captures the notion that objects in a visual scene tend to be organized by means of symmetrical shapes. Figure 1.1e is therefore most likely to be interpreted as two overlapping rectangular frames rather than two polygons bordering on a central small diamond shape. The last in the set of Gestalt principles is the *rule of common fate*, predominantly conceived for moving objects, whereby elements with the same motion direction or destination are perceived as a single entity or collective of conjoint elements. The significant difference between the rules of common fate and good continuation becomes apparent in Figure 1.1f. While good continuation does only account for the grouping of local elements into three rays, common fate integrates all three rays into a whole percept.

1.1.1 Gestalt Rules as a Perceptual Framework

Intuitive and plausible as the set of Gestalt rules may accrue from illustrations such as provided in Figure 1.1, these principles of perceptual grouping have frequently been found to elude theoretical formalization, pointedly expressed by Leeuwenberg and Boselie (1988) who stated “The Gestalt laws have been formulated to specify the perceptual organization of patterns, but their own organization is lacking” (p. 490). One of the first critical examinations of the validity of Gestalt rules was attempted by Rock and Brosgole (1964) in a study on the determinants of proximity grouping. The authors constructed a rectangular array of dots with a row separation of 3 inches and a column separation of 4 inches, inducing the percept of groups of dots organized into columns. The dot array could be rotated away from the observer in arbitrary angles around its vertical axis, thereby reducing the horizontal retinal distance between the columns and imposing a weak impression of slant. A rotation angle of $41.4°$ would yield equal retinal separation of rows and columns, marking the point of indifferent arrangement of dots into rows or columns. Congruent with the

rule of proximity, when viewed from the frontal parallel plane, subjects perceived the dots to form vertical columns. However, even with randomized presentation order of rotation angles, the perceptual 'switch' to grouping the dots into rows rather than columns did not occur until a rotation angle of $43.0°$ under monocular viewing conditions and $53.3°$ when viewed binocularly. Subjects apparently were able to take both slant and binocular disparity into account when estimating the horizontal and vertical distances between the dots, giving rise to the hypothesis that not the physical or retinal distance between elements but the perceived distance determines perceptual grouping by proximity, and consequently deeming the rule of proximity tautological (Rock & Brosgole, 1964).

Discordant results have also been obtained for the Gestalt rule of similarity in human vision. Goldstone, Medin, and Gentner (1991) let human observers evaluate the similarity of different sets of visual shapes. Similarity between the sets was modulated either by identical attributes such as "circle at first position in both sets", or identical relations between elements, e.g., "same element at first and second position in both sets". The authors found intransitivities in the judgements of set similarity. Increasing similarity in one category (i.e., attributes or relations) and decreasing similarity in the other did not invariably produce the same overall change in perceived similarity but could either enhance or degrade the similarity percept, depending on the specific set configuration. Goldstone et al. (1991) concluded that the Gestalt rule of similarity is not to be taken as an independent mechanism subserving perceptual organization at the expense of other grouping principles but is modulated by contextual information.

The Gestalt rule of good continuation has also received considerable critical examination. Prytulak (1974) constructed stimuli in which dots were aligned with one of three trajectories. The trajectories extended from a common point of origin toward different directions, hence creating variants of a 'Y' shape. The two short upper segments could take arbitrary angular juxtapositions relative to the longer bottom segment, denoted as the 'shaft', and the whole shape was rotated by a random angle around the origin. Subjects were asked to judge which of the shorter segments best continued the shaft and how appropriate this continuation was. The author found perceived continuation not to be predicted properly by the sole juxtaposition angle between segments, as originally proposed by Wertheimer (1958), but by a nonlinear combination of segment angle, the orientation of the whole shape, and the area enclosed by the imaginary triangle spanned by each segment and the shaft. Later studies to formalize the rule of good continuation by some form of geometrical quantification identified several determinants of perceptual goodness of continuation, part of which are not covered by the notion of continuation originally held by Gestaltists (Wertheimer, 1923). Among these factors are the magnitude of curvature (Smits & Vos, 1987), the number of distractor elements not belonging to the trajectory (Tripathy, Mussap, & Barlow, 1999), the length of the trajectory (Pettet, 1999), and the number of changes in curvature polarity, i.e., alterations between convex and concave segments (Feldman &

Singh, 2005; Mathes & Fahle, 2007a). A recent study by Singh and Fulvio (2007) suggested that the rule of good continuation may not even relate to continuation but to the perceived curvature of parts of the trajectory, combined with an estimation bias. The authors used curved lines, the tail of which being obscured by an occluding shape. Subjects were asked to extrapolate where the line would come out from behind the occluder (Figure 1.2). Results showed that the change of curvature prior to the occluder (the 'curvature gradient') did not exhibit any systematic effect on line extrapolation. Instead, extrapolation performance was well predicted by a simple estimation of the curvature shortly before the occluder, corrected by a general tendency of human observers to minimize curvature, regardless of whether line curvature was increasing or decreasing as it approached the occluder. Results contradicted the notion of good continuation as a highly dynamic and adaptive extrapolation process which exploits manifold geometric properties of a contour such as curvature angle and curvature gradients, turning points, or length. Similar findings were also obtained by Liu, Jacobs, and Basri (1999) who found that perceptual completion of a partly occluded contour was modulated by just the degree of convexity of the contour, not the extrapolation of a smooth trajectory based on the spatial course of the visible contour parts. Subjects' contour completion performance degraded with the introduction of turning points to the contour although cues to good continuation based on the global course of the contour were held equivalent in all experimental conditions.

Research on the interplay and mutual dependencies among multiple Gestalt rules has yielded equally ambiguous results. According to Quinlan and Wilton (1998), two cardinal forms of interaction between Gestalt rules may be distinguished. *Cooperation* on the one hand refers to multiple Gestalt rules acting in concert to serve perceptual grouping. *Competition* on the other hand describes stimulus configurations in which coexistent Gestalt rules indicate different, often incompatible perceptual organizations. Several examples of cooperativity are comprised in the grouping examples in Figure 1.1. The collection of shapes in the upper right corner of Figure 1.1a is defined by element proximity alone, whereas grouping of the elements in the lower left is mediated by proximity, similarity, and symmetry. To most observers, the elements in the upper right will therefore appear as just a cluster of nearby elements, opposed to the group of elements in the lower left which form a structured geometric whole. The stimulus example in Figure 1.1b defines groups of elements by similarity and further employs distance information to segregate two otherwise similar objects from each other. The closure illustration in Figure 1.1d combines closure with the rule of good continuation to outline the circular shape. Good continuation is also used to define the rays in Figure 1.1f which are then bound together due to the rule of common fate. The effects of cooperativity among multiple Gestalt rules have been investigated in a number of studies for different combinations of Gestalt rules, converging on the notion that cooperation disambiguates perceptual organization and tends to produce more robust object vision. Evidence for beneficial cooperative interactions of Gestalt rules have been reported for

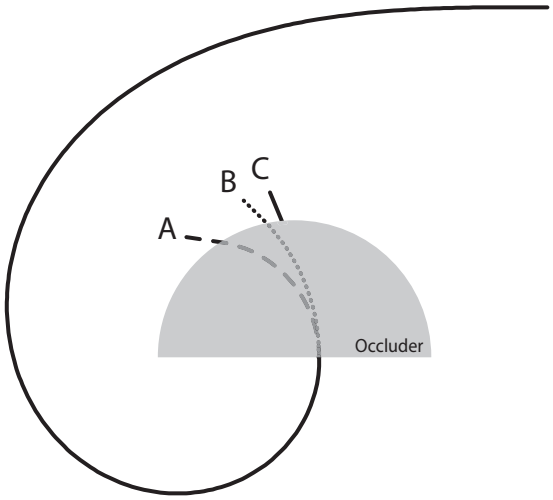

Figure 1.2: Extrapolation of curved shapes based on good continuation, curvature, and prior expectancy (Singh & Fulvio, 2007). The end part of an Euler's Curve is obscured by an occluder. Subjects were asked to continue the line behind the occluder. If good continuation would take into account the increasing curvature gradient, the line should be extrapolated towards point (A). If only the curvature of the last part of the line before the occluder determined the estimated course of the line, subjects should mark (B) as the continuation point. However, most subjects chose a point close to (C), indicating a tendency to minimize extrapolated curvature.

combinations such as good continuation and proximity (Beaudot & Mullen, 2003), good continuation and common fate (S. H. Lee & Blake, 2001), closure and proximity (Kovacs & Julesz, 1993), and similarity and proximity (Zucker, Stevens, & Sander, 1983; Quinlan & Wilton, 1998). The study by Quinlan and Wilton (1998), however, demonstrated that no one Gestalt rule or combination of rules is apt to govern perceptual organization in an invariable manner. The authors found evidence not only for cooperative interaction among the Gestalt rules of proximity and similarity but also for substantial competition. Stimulus displays comprised rows of seven basic shapes, taking different chromatic attributes and proximity relations (see Figure 1.3), and subjects were asked whether they perceived the middle element as belonging to either the three elements on the left or on the right side, or as an element of its own. Consistent with previous research, the authors found stable perceptual grouping either when proximity and similarity acted alone or cooperatively (Figure 1.3a-c), or in certain conditions of competition between proximity and similarity. In Figure 1.3d, the combination of proximity and color similarity outweighs the shape similarity cue, while in Figure 1.3e proximity alone suffices to group the leftmost black square with the white squares despite the contradictory similarity cue. Conflicts between competing Gestalt

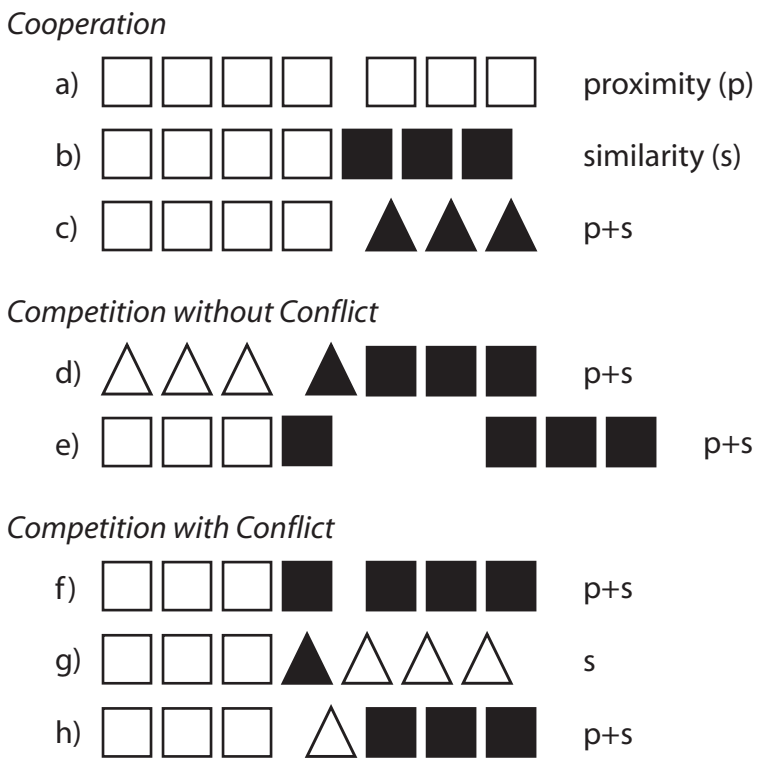

Figure 1.3: Cooperation and competition among grouping principles in the stimuli used by Quinlan and Wilton (1998).

rules resulting in ambiguous object vision are depicted in Figure 1.3f-h. Although subjects are not consistent in their evaluation of the membership of the leftmost black square to one of the two groups in Figure 1.3f, most subjects still tend to favor one interpretation over the other and assign the leftmost black element to either the left or the right group of squares. This does not hold for the last two illustrations, where shape similarity is not sufficient for stable perceptual grouping in Figure 1.3g, and proximity does not prevail against color similarity in Figure 1.3h. Consequently, the middle shape is perceived as a single object by most subjects. A related study furthermore showed that the quantitative relations between grouping by similarity and proximity differ contingent on the feature by which similarity is conveyed (Masin, 2001). Results indicated that similarity of achromatic colors determines grouping jointly or in equitable competition with proximity, whereas similarity of chromatic colors is overruled by proximity in the majority of cases. Apart from the interaction of proximity and similarity, empirical evidence on competitive interplay between Gestalt rules include the precedence of closure over proximity (Koffka, 1935) and perceptual rivalry between motion similarity and good continuation (Poom & Borjesson, 2004).

Notwithstanding the difficulty to construe a systematic quantitative formalization of Gestalt theory, the Gestalt rules have proven as a useful descriptive framework in which

phenomena of perceptual grouping can be organized, evaluated, and compared (see Spillmann, 1999). More importantly, the Gestalt approach has guided a wealth of psychophysical, neurophysiological, and computational research to translate the mere perceptual qualities of Gestalt phenomena into neural correlates of perceptual organization (Ehrenstein, Spillmann, & Sarris, 2003). Research on contextual modulation of single neurons, for example, has provided evidence for the representation of objecthood very early in the visual pathway. Lamme (1995) found cell responses in the primary visual cortex toward identical stimulation of the receptive field to depend on whether the stimulus element within the receptive field belonged to a well-defined figure or the background. Lamme suggested that context-sensitivity of neuronal responses within primary visual cortex serves to evaluate a visual stimulus with respect to its perceptual context, thus challenging the traditional view of receptive fields as independent feature processing units. Further research supported the idea that receptive fields in many visual areas perform complex analyses that allow for dynamic, multi-purpose organization of the visual scene, rather than being limited to the analysis of specific basic visual attributes (Schiller, 1996). The Gestalt notions of spatial proximity and similarity are also well reflected by patterns of cortical organization. Synaptic interconnections of cells in the visual cortex span preferentially between neurons with nearby receptive fields (Tootell, Switkes, Silverman, & Hamilton, 1988; Das & Gilbert, 1999; Levitt & Lund, 2002) and similar feature tunings (Livingstone & Hubel, 1984; Ts'o & Gilbert, 1988; Schmidt, Goebel, Lowel, & Singer, 1997), which allows for lateral interaction of cells encoding similar and/or spatially proximate visual features. Results from a neurophysiological study by Zhou, Friedman, and von der Heydt (2000) indicated a neural correlate of the Gestalt rule of closure. The rule of closure states that a straight or curved contour is perceived as just an ordinary line, not an area or an object, while a closed path appears as a surface figure bounded by the contour, thus acquiring a unique perceptual quality (Koffka, 1935). Using single-cell recordings in areas V1, V2, and V4 of awake monkeys, Zhou et al. (2000) observed that a considerable number of edge detector neurons not only encoded contrast polarity of edges within their receptive field but selectively responded if the edge belonged to an object and this object extended in a specific direction. Response modulation due to 'border-ownership' occurred at latencies too short to enable top-down influence from higher visual areas. The authors reasoned that neurons in early visual areas are capable of encoding Gestalt information required for figure-ground segregation. Von der Heydt, Peterhans, and Baumgartner (1984) discovered a neural correlate for the continuation of disconnected contours. Neurons in certain areas of the primary visual cortex whose receptive fields covered only the gap between stimulus elements inducing an illusionary contour responded as if a real line or edge was present in their receptive field. Modifications that decreased the perceptual salience of the illusionary contour also weakened the neuronal responses.

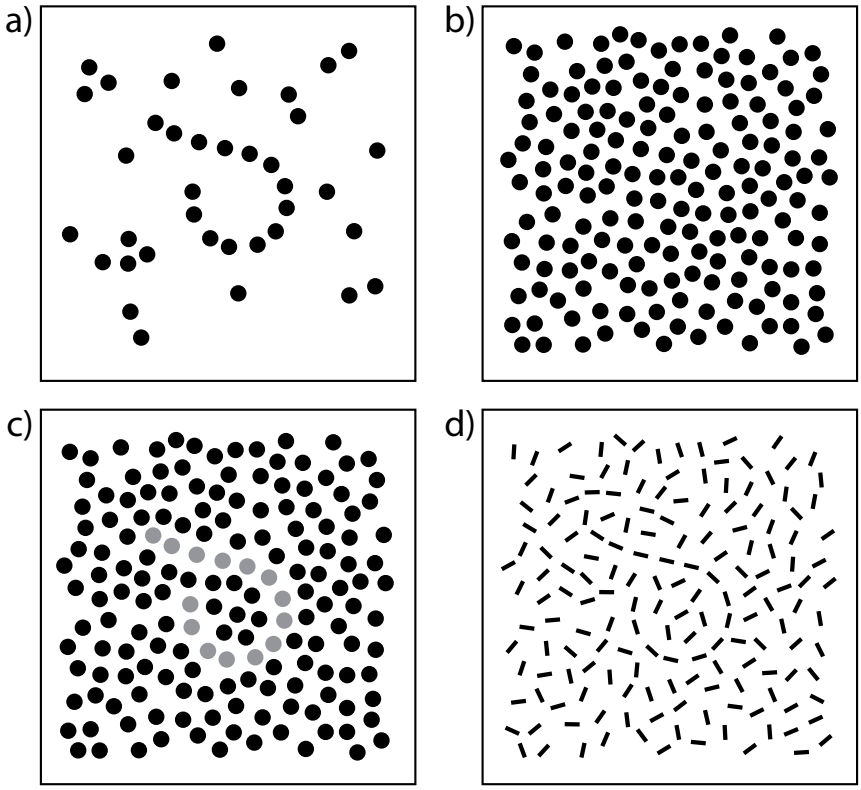

Figure 1.4: Illustration of principles of good continuation and proximity. In panel (a) the contour is defined by the rule of good continuation, combined with the density principle of proximity. Equalization of the density distributions among contour and background elements renders the path invisible (b). Perceptual grouping is again enabled either by adding a further Gestalt cue, like the rule of similarity (c), or by complementing the local elements with orientation collinearity (d). Note that element positions are identical among all four stimuli.

This thesis will put under experimental scrutiny the visual task of 'contour integration', such as illustrated in Figure 1.1c, capitalizing on the rich descriptive framework set up by Gestalt theory. Perceptual grouping of local elements into a global contour involves a variety of Gestalt rules, the most relevant of which are the rules of good continuation, proximity, and similarity. The next section will discuss these grouping principles in the light of contour integration, and propose significant conceptual refinements to account for the intricacies of specific variants of contour integration.

1.1.2 Good Continuation, Proximity, and Similarity Revisited

One of the most prominent psychophysical approaches to the integration of visual contours is the 'pathfinder paradigm', first presented in the seminal paper of Field, Hayes, and Hess (1993). A typical pathfinder stimulus comprises a smooth spatial path defined by oriented local elements with collinear alignment, embedded in a background field of randomly oriented elements (see Figure 1.4d). Subjects are required to detect the path by means of perceptual grouping. Contour integration in most variants of the pathfinder paradigm is conceived as borrowing from the Gestalt rules of proximity and good continuation: local elements are likely to be perceptually grouped if they are nearby and align with a piecewise smooth path (Hess & Field, 1999; Geisler, Perry, Super, & Gallogly, 2001). This definition, however, falls short of providing a concise description of the Gestalt principles inherent to the specific stimulus configuration in pathfinder displays.

Many textbook illustrations of the rule of good continuation resemble the stimulus examples given in Figure 1.4a or Figure 1.4d (e.g., Anderson, 2004; Metzger, 1975; for an English translation see Metzger, 2006). Both examples comprise visual contours that implement the rule of good continuation by aligning a group of discrete but contiguous local elements with a smooth global trajectory. These examples, however, confound the rule of good continuation with other salient grouping principles. The contour in Figure 1.4a is defined by the combination of good continuation and a spatial density difference between the tightly packed contour elements and the sparsely populated background. Contour integration in Figure 1.4d is facilitated by local tangent information provided by the orientation of the line segments. Upon elimination of the additional cue, good continuation alone does not suffice to establish the percept of a visual contour (see Figure 1.4b), although close examination of the stimulus display will eventually allow for the detection of the hidden path, owing to its reasonably regular geometric structure. The Gestalt rule of good continuation may thus represent a fairly weak principle of perceptual grouping, insufficient for the integration of local elements solely due to their orderly geometric relationship. Good continuation instead bears the necessity of being supported by additional visual cues in order to gain perceptual salience.

Consideration of the role of proximity in the pathfinder paradigm points to a second important differentiation. The Gestalt rule of proximity covers two separate aspects of spatial distances between grouped elements, namely the *density* principle of proximity and the *contiguity* principle of proximity. In the introductory example of Figure 1.1a the clusters of elements in the lower left and upper right corner are defined by different spatial densities of elements belonging to the respective cluster compared to the surround. Proximity due to density therefore facilitates perceptual grouping of regions of dense element spacing, embedded in a background of sparse filling. A similar pattern of proximity grouping by element density constitutes the contour integration example in Figure 1.4a, where the density

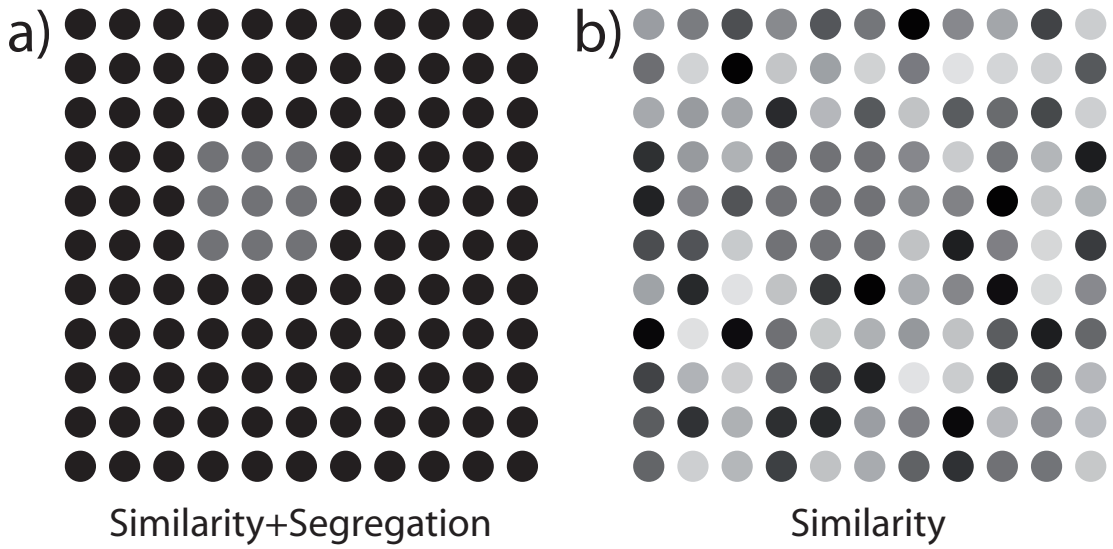

Figure 1.5: Contribution of a feature contrast cue to similarity grouping. The left panel (a) depicts a typical stimulus example employed to illustrate the Gestalt rule of similarity. Similarity grouping is enhanced by a strong feature contrast cue resulting from different luminance parameters of grouped elements and their surround. The right panel (b) implements an unconfounded similarity principle: all elements belonging to the square exhibit the same luminance value which is not matched by any background element. The visibility impairment due to the elimination of the feature contrast cue is perceptually evident.

of background elements is low in the vicinity of the contour, thus having the contour appear as a formation of tightly packed elements. However, generation algorithms for well-formed pathfinder displays have been devised under the pivotal premise to eliminate any cues accruing from different element density distributions of contour and background elements in order to reduce confoundation of artificial spatial or configurational cues with the primary feature cue intended to be studied. A well-formed pathfinder stimulus practically devoid of density cues to the contour is depicted in Figure 1.4b-d, leaving the contour undetectable if only defined by the principles good continuation and contiguity (Figure 1.4b). Rather than pertaining to the density distribution of local elements, the Gestalt rule of proximity in pathfinder displays manifests itself as the degree of contiguity among grouped elements. This form of neighbor relation emerging from spatial adjacency of elements is denoted as the contiguity principle of proximity. Contiguity may be reduced by interspersing the contour with nonaligned background elements, or by increasing the inter-element distances among all elements in a stimulus display.

A last conceptual refinement is needed for the Gestalt rule of similarity. Many demonstrations of similarity grouping employ stimuli built up from a number of separate objects, a

subset of which is distinguished from the surround by strong feature contrast. Such cases of similarity grouping are illustrated in the introductory example of Figure 1.1a, and the stimulus in Figure 1.5a. However, two different cues to perceptual grouping are confounded in such stimuli. Complementary to the similarity of grouped elements, a segregation cue resulting from luminance contrast between grouped elements and their background significantly promotes the figure-ground percept in both stimulus examples. The contribution of the feature contrast cue becomes apparent upon inspection of the stimulus displays in Figure 1.5. The target square in Figure 1.5a is defined by setting the luminance of background elements to zero (black) and assigning the grouped elements a luminance value corresponding to a mean grey, hence generating element similarity as well as a feature contrast cue which segregates the square from its surround. Feature contrast is eliminated in Figure 1.5b, where background elements take luminance parameters from a broad interval of possible values ranging from black to a light grey, while asserting that no background element is identical to an element within the target square. Perceptual grouping is still enabled with just the similarity cue present, but at the cost of significantly reduced visual salience of the target square.

1.1.3 A Special Case of Good Continuation

Let a working definition of contour integration that roots in the framework of Gestalt rules and takes into account the terminology discussed in the foregoing section be derived as follows. The task of grouping local elements into a contiguous whole is denoted as contour integration if the grouped elements satisfy the rule of good continuation. The rule of good continuation may therefore be held as a necessary definitory condition for contour integration: a contour is mandatory to be outlined by discrete local elements that align with a smooth global trajectory. The principle of good continuation, however, will in most cases not suffice to readily enable perceptual grouping of contour elements. Sufficient conditions for contour integration may then be established by complementary measures. Good continuation can be reinforced by providing local elements with information about the course of the global trajectory such as orientation collinearity, or be augmented with additional Gestalt rules like proximity, similarity, or closure, as well as with salient feature contrast cues.

This definition abstracts from the prototypical pathfinder paradigm by assuming a more general view of the task of contour integration operating on a variety of visual cues. A typical pathfinder stimulus with collinearly oriented and adjacent local elements combines the principle of good continuation, the contiguity principle of proximity, and a local collinearity cue (Figure 1.4d). This is, however, just one possible conjunction of good continuation with other grouping principles enabling contour integration. Within the realm of the proposed definition, other combinations are easily conceivable, such as contours de-

fined by good continuation and the density principle of proximity as in Figure 1.4a, good continuation backed by contiguity, similarity, and feature contrast (Figure 1.4c), or good continuation in concert with density and closure, shown in the introductory Figure 1.1d. The definition also sets apart contour integration from other figure detection tasks, such as illustrated by the introductory example in Figure 1.1f. Contour integration here only accounts for perceptual grouping of local elements into three separate paths, whereas the acute-angled connection between the three rays does not comply with the principle of good continuation. Instead, the rule of common fate is required for grouping the three rays into a whole percept.

1.2 Contour Integration

1.2.1 Early Research

Initial attempts to develop an explanatory foundation for contour integration considered the task too complex for being achieved by local feature processing units early in the visual pathway, but argued in favor of a globally precedent mechanism that integrates information from multiple feature dimensions in order to reconstruct a visual object (Uttal, Davis, Welke, & Kakarala, 1988; Beck, Rosenfeld, & Ivry, 1989). This notion was challenged by a number of psychophysical (Field et al., 1993; Kovacs, 1996; McIlhagga & Mullen, 1996; Roelfsema, Scholte, & Spekreijse, 1999; Feldman, 2001; Morita, Morita, & Kumada, 2003), neurophysiological (C. Y. Li & Li, 1994; Bauer & Heinze, 2002; Mandon & Kreiter, 2005; Samonds, Zhou, Bernard, & Bonds, 2006), neuroimaging (Altmann, Bülthoff, & Kourtzi, 2003; Kourtzi, Tolias, Altmann, Augath, & Logothetis, 2003; Altmann, Deubelius, & Kourtzi, 2004), and computational studies (Gigus & Malik, 1991; Pettet, McKee, & Grzywacz, 1998; Z. Li, 1998; Choe & Miikkulainen, 2004; Kubota, 2004; Schinkel, Pawelzik, & Ernst, 2005), from which a general concept has emerged about how contour grouping is implemented by the visual system. The task of contour integration can accordingly be summarized by a sequence of three processing stages at different levels of the visual hierarchy. In the early *filtering stage*, local features of stimulus elements are extracted by dedicated spatial filters with properties similar to those observed in primary visual cortex. In the subsequent *linking stage*, element bindings are established as a function of local characteristics like proximity, element orientation, or spatial frequency. Finally, in the *integration stage*, a higher-order process exploits the local linking strengths to group individual elements into a whole contour and thereby constructs a global percept (Geisler et al., 2001).

While neural processes covering the integration stage are still subject to lively debate, research has converged on a common notion about the neural basis of the filtering and linking stages. Early algorithmic models proposed specialized types of feature detectors

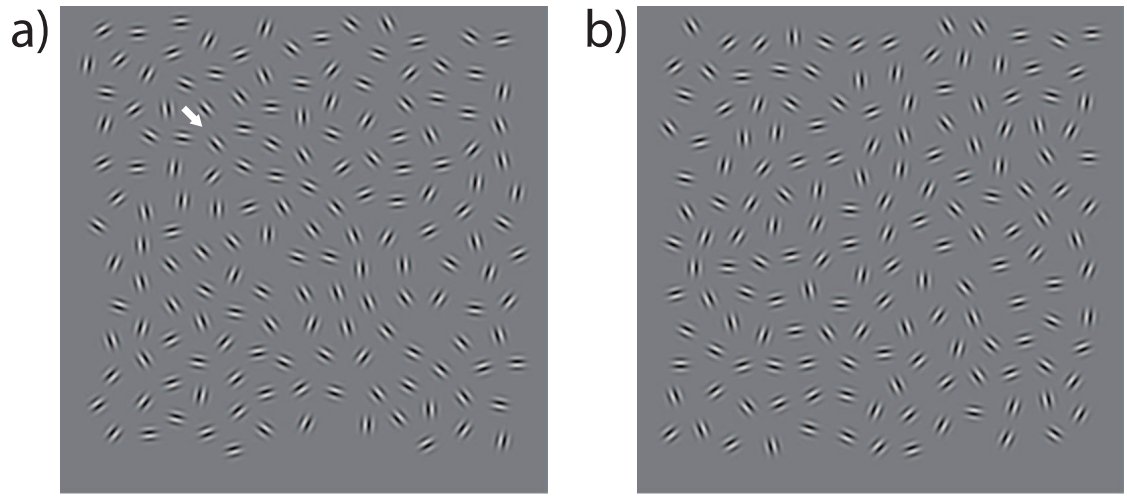

Figure 1.6: Examples of contour integration stimuli. The stimulus displays are composed of randomly placed Gabor patches, a subset of which is aligned with a smooth path. The left panel (a) shows a target stimulus with an embedded contour, marked by an arrow. The right panel (b) depicts a distractor display with no visible path.

responsible for the extraction of curvilinearly aligned elements, such as non-circular symmetric gaussian receptive field profiles (Smits, Vos, & Oeffelen, 1985), circular arc detectors (Gigus & Malik, 1991), or edge and tangent detectors (Parent & Zucker, 1989). The subsequent integration of outputs from feature detectors in order to link neighboring elements was attributed to rather complex mechanisms such as sequential tracking operators (Farag & Delp, 1992), template matching (Parent & Zucker, 1989), or iterative optimization (Ullman & Sha'ashua, 1988). However, no conclusive support for many of these theoretical assumptions could be obtained from neurophysiological studies, which largely failed to provide evidence of the proposed types of receptive fields and neural linking operators (Gigus & Malik, 1991; Hess & Field, 1999).

1.2.2 The 'Association Field'

A simple approach to govern both the filtering stage and the linking stage by a single cortical mechanism was suggested by Field et al. (1993) on the basis of psychophysical experiments employing the pathfinder paradigm. Subjects were presented with random fields of oriented local elements, a subset of which were aligned along a smooth path (see Figure 1.6 for an example). The path was constructed from local band-pass elements whose spatial frequency and orientation properties resembled those of cortical cells in area V1; the background consisted of similar elements with random orientation and position. Based

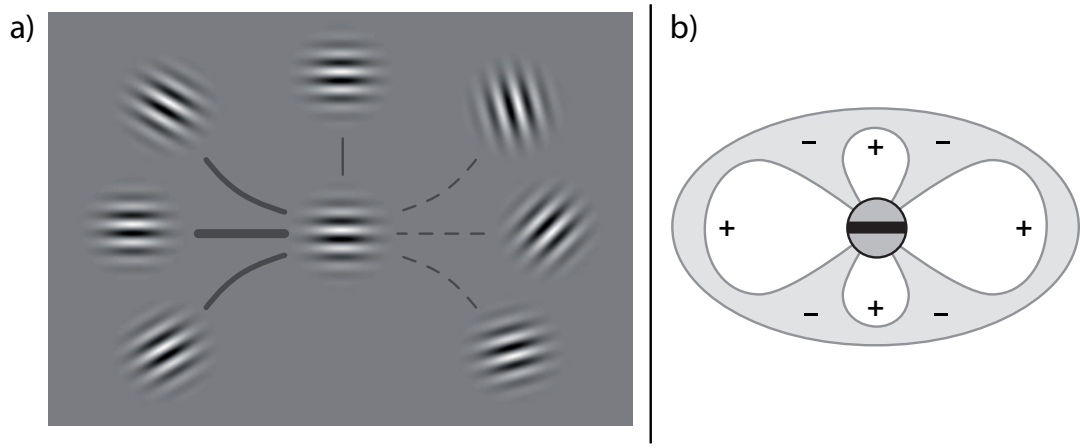

Figure 1.7: Illustration of the 'association field' model. The left panel (a) depicts a cutout of a typical stimulus display used in contour integration experiments (see Figure 1.6). Linking between the oriented elements is marked by solid lines, the link strength is indicated by line thickness, which is maximum for elements along the same axis and degrades with increasing deviation, until weak excitatory interactions are again found for elements along a perpendicular axis. Dashed lines denote the absence of element linking. The right panel (b) holds a schematic representation of the association field model according to Field et al. (1993). Excitatory connections extend along the preferred orientation of the respective neural unit, weaker excitatory cones project in perpendicular orientation, intercepted by regions with inhibitory or no interaction.

upon their findings, Field et al. (1993) proposed an *association field* to explain how spatially distributed local elements of collinear orientation become integrated into a coherent percept very early in the visual pathway. The authors claimed that interconnections between local orientation detectors in area V1 form the neural basis for contour integration. Such long-range lateral connections in the visual cortex are assumed to span preferentially between neurons with similar orientation tuning and collinear alignment, as described for inter-columnar synaptic fibres in the visual cortex of the macaque (Malach, Amir, Harel, & Grinvald, 1993), the tree shrew (Bosking, Zhang, Schofield, & Fitzpatrick, 1997), and the cat (Schmidt et al., 1997).

In addition to the work by Field and colleagues utilizing the pathfinder paradigm (see Ledgeway, Hess, & Geisler, 2005, for an overview), the association field hypothesis has been supported by psychophysical experiments on the effect of collateral and collinear flanking stimuli upon the detection of central contrast targets (Polat & Sagi, 1993; Polat, 1999; Polat & Bonneh, 2000), and was further substantiated by V1 cell recordings (Ts'o, Gilbert, & Wiesel, 1986; Gilbert, Ito, Kapadia, & Westheimer, 2000; Bauer & Heinze,

2002). As illustrated in Figure 1.7a, lateral connections enable the mutual facilitation of collinearly aligned neural units with similar orientation tuning. Excitatory interactions between neighboring elements gradually reduce with decreasing collinearity or increasing displacement of local elements from an imaginary underlying contour, until they are superseded by suppressive effects of nearby elements with oblique orientation (see Figure 1.7b). Facilitative effects of flanking elements on the contrast detection threshold have again been found in perpendicular direction of the preferred orientation, although markedly weaker than for collinear units (Polat & Sagi, 1994a). Consistent with the notion of an association field projecting both in collinear and perpendicular direction, paths composed of orthogonally aligned elements are well detected in contour integration tasks, but evince less visibility than collateral paths (Hess, Ledgeway, & Dakin, 2000; Bex, Simmers, & Dakin, 2001; May & Hess, 2007a, 2007b). The assumption of excitatory cones projecting along the orthogonal axis of a receptive field, however, did not receive univocal support. Polat and Bonneh (2000) failed to obtain any interactory effects of orthogonal flanking stimuli on the luminance contrast detection threshold of a central target element in psychophysical experiments, and Kapadia, Westheimer, and Gilbert (2000) even observed inhibitory contextual interactions along the perpendicular axis of V1 neurons of alert monkeys, thus raising doubts about the presumed excitatory nature of local interactions. Closer examination proved the polarity of lateral interactions to depend on the luminance contrast ratio of flanking and central elements (Polat, Mizobe, Pettet, Kasamatsu, & Norcia, 1998; Kapadia, Westheimer, & Gilbert, 1999). Collateral elements of higher luminance compared to the center element emitted excitatory cones, whereas flankers of lower luminance elicited inhibitory interactions. Psychophysical and neurophysiological studies again converge on the presumed geometry of the association field with respect to the extension of lateral interconnections at increasing angular differences between adjacent neural units. In studies employing the target-flanker paradigm (Polat & Sagi, 1994a; Polat & Bonneh, 2000), considerable interactions between local elements were found for orientation differences up to approximately $45° \pm 10°$, which complies with results from pathfinder experiments, where contours were shown to become undetectable at similar deviations of inter-element angles (Field et al., 1993; Hess et al., 2000). Neurophysiological evidence conform with these figures, showing that approximately 60% to 80% of lateral synaptic connections in V1 span between neurons exhibiting similar orientation tunings within a range of $\pm 45°$ (Malach et al., 1993).

1.2.3 Determinants of Contour Integration Performance

Several factors have an effect on contour visibility and thus modulate contour integration performance. Inherent to the association field model is the impact of local element orientation. An increase in orientation difference between neighboring contour elements at-

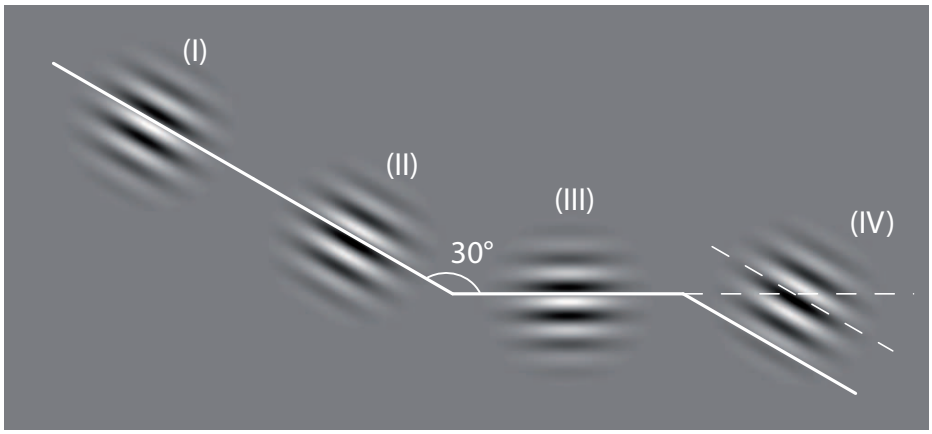

Figure 1.8: Collinearity, curvature, and tilt angle among contour elements. Elements (I) and (II) are justified along a straight line and hence collinear by definition. Elements (II) and (III) deviate in local element orientation by $30°$ but align with an angular path outlining the element positions, and, within the pathfinder paradigm, also become labeled collinear. Elements (III) and (IV) deviate in local orientation by the same angle as elements (II) and (III), yet they do not follow the curvature of the global path. Therefore, element (IV) is assumed to be tilted away from an imaginary straight connection with the previous element by a 'tilt angle' of $v = 30°$.

tenuates contour visibility due to the diminishing lateral connection strength between the respective neural units. However, two concepts of orientation differences between path elements need to be kept distinct. The contour *curvature* on the one hand pertains to the global spatial geometry of the path and determines the orientation differences between adjacent path elements. Contours with a straight or smooth curved overall shape comprise elements with small inter-element angles, whereas irregular and highly bent contours are characterized by large angular differences between local elements. Within the pathfinder paradigm, all local elements which align with a global path are defined as collinear. Local elements may thus differ significantly in orientation but can still be labeled perfectly collinear relative to the global curvature of the path. In Figure 1.8, the three leftmost stimulus patches are aligned collinearly, although only the first two elements fall onto a straight path and have identical local orientations. The *tilt angle* on the other hand describes the deviation of local element orientation from its perfect alignment with global path curvature, as illustrated by the two rightmost stimulus patches in Figure 1.8, where the second patch deviates from collinear alignment by a tilt angle of $30°$. In the scope of the pathfinder paradigm, the tilt angle is thus conceived as the obverse of collinearity. Among those two types of orientation differences, only changes to the tilt angle of path elements qualify as

a predominantly local operation, since altering the curvature of the path necessarily recasts its global spatial structure.

Curvature is the most thoroughly examined global spatial characteristic in the scope of pathfinder experiments. In their original study, Field et al. (1993) varied global curvature by modulating the angular difference between adjacent collinear path elements from 15° up to 75°. The authors found contour visibility to reduce gradually with increasing curvature until detection performance fell to chance level for an inter-element angle of about 60°. The deterioration of contour detection performance due to higher curvature has subsequently been corroborated by a number of studies (Dakin & Hess, 1998; Pettet, 1999; Hess et al., 2000; Hess, Beaudot, & Mullen, 2001; Persike & Meinhardt, 2005; Mathes & Fahle, 2007a), in which contour curvature was either subject to investigation or served as a modulatory variable to control path visibility. A global contour property closely related to curvature is polarity, describing the alteration between concave and convex segments along a visual contour caused by reversals of the sign of inter-element angles, often referred to as 'turning points'. A change in orientation polarity without variation of the absolute value of inter-element angles significantly degrades contour detection performance compared to fully convex paths (Pettet, 1999; Mathes & Fahle, 2007a). The results comply with evidence from a variety of psychophysical tasks other than contour integration, where considerable performance advantages for fully convex shapes have been reported for the judgement of target position (Gibson, 1994; Bertamini & Farrant, 2006), figure-ground discrimination (Hoffman & Singh, 1997; Bertamini & Croucher, 2003), and visual search (Elder & Zucker, 1993).

Another global spatial property of contour stimuli known to modulate contour integration performance is the number of elements defining the path, commonly denoted as 'path length'. Results indicate a direct relationship between the number of collinear path elements and contour detection performance (Dakin & Hess, 1998; Tversky, Geisler, & Perry, 2004). A minimum of 5 to 6 elements is required to readily enable contour integration (Feldman, 2001; Kiorpes & Bassin, 2003), and detection performance saturates when a contour comprises at least 10 to 12 elements (Braun, 1999). Often confounded with path length in psychophysical experiments is the eccentricity of a contour. A number of studies have shown that contour integration degrades with higher eccentricity of the contour (Hess & Dakin, 1999; Nugent, Keswani, Woods, & Peli, 2003; May & Hess, 2007a) until a contour becomes invisible when it is located far in the peripheral field at approximately 20° visual angle (Hess & Dakin, 1997).

Finally, the contiguity principle of proximity and the Gestalt rule of closure have been subject to extensive psychophysical examination. Kovacs and Julesz (1993) varied the inter-element distance of path elements and found contour integration performance to decrease with higher distances between local elements (see also Beaudot & Mullen, 2003). Results from the same study by Kovacs and Julesz furthermore showed that fragmented

contours were better detected in cluttered backgrounds when their global shape outline was closed. Subsequent studies endorsed the notion of a detection advantage accruing from closure, when contours are embedded in noisy surrounds (Elder & Zucker, 1993; Saarinen & Levi, 1999; Mathes & Fahle, 2007a). However, the proposal of a unique perceptual quality emerging from closure (Kovacs & Julesz, 1993) has been challenged on several grounds by results from psychophysical experiments (Braun, 1999; Tversky et al., 2004) and computational studies (Elder & Goldberg, 2002; Choe & Miikkulainen, 2004). The role of perceptual closure in contour integration will be elaborated in the next section, and put under experimental scrutiny in Chapter 3.

Ample research has been concerned with the contribution of *local* stimulus features to contour integration. A feature inherent to the association field model is the orientation tilt angle which determines the angular deviation of a contour element from its perfect collinearity with the path. Several studies have demonstrated that contour detection performance degrades with higher tilt angles (Hess & Demanins, 1998; Bex et al., 2001; Persike & Meinhardt, 2007). Particularly, Mathes and Fahle (2007a) measured detection thresholds based on tilt angle for contours that exhibited different degrees of curvature and closure. Tolerance against disrupted collinearity increased with lower curvature and was generally superior for closed contours compared to open contours at similar inter-element angles. One of the first local features other than element orientation to have been put under experimental investigation was the carrier spatial frequency of contour and background elements. Dakin and Hess (1998) reported that contour locking between local elements of identical carrier spatial frequency is maintained at steady perceptual levels over a wide range of spatial frequencies from 1.0 cycles per degree (cpd) up to approximately 8.0 cpd. More importantly though, the authors found the degree of tolerable spatial-frequency difference between successive contour elements to be inversely related to path curvature, indicating a pronounced spatial frequency selectivity of visual contour detection. Although at first glance, psychophysical evidence obtained by Dakin and Hess (1998; see also Dakin & Hess, 1999) seemingly sustain the association field hypothesis implying that inter-element locking is accomplished by lateral connections between neural units with bandpass properties such as found in early visual areas, the results can be called into question on account of the psychophysical paradigm used in the study. A detailed discussion is given in section 1.2.5, substantiated by experimental results presented in Chapter 4.

In general, empirical evidence about the role of features other than orientation alignment in contour integration tasks converges on a straightforward notion. Additional feature or configurational cues coincident with the primary orientation cue tend to facilitate contour detection, while incoherent cues as well as elevated feature noise in the background impair human performance. Experimental results consistent with this pattern have been obtained for spatial phase (Field, Hayes, & Hess, 2000), depth (Hess & Field, 1995), texture (Dakin, Williams, & Hess, 1999), motion (Ledgeway & Hess, 2002; Lorenceau, Giersch, & Series,

2005; Ledgeway & Hess, 2006), color (Mullen, Beaudot, & McIlhagga, 2000; Beaudot & Mullen, 2003; Mathes & Fahle, 2007a), flicker (Bex et al., 2001), and context (Rivest & Cavanagh, 1996). However, defining contours by path alignment and supplemental cues such as motion (Ledgeway et al., 2005) and color (Mathes & Fahle, 2007a) led to the disappointing result that these other features combine with orientation alignment as independently processed cues, yielding just a moderate increase of perceptual contour salience when added to the collinearity cue. The impact of cue combination on contour integration performance will be revisited in Section 1.2.6, followed by a thorough experimental evaluation in Chapter 5, using spatial frequency feature contrast as the additional cue.

1.2.4 The Effect of Closure on Contour Integration Efficiency

The Gestalt principle of closure states that line elements, or parts of a contour, are preferably grouped if the ends can be connected to form a closed 'whole'. Kovacs and Julesz (1993) were able to show that fragmented contours were better detected in cluttered backgrounds when their smooth global form was closed. In their study, Kovacs and Julesz created stimulus displays similar to those used in the pathfinder paradigm by Field et al. (1993). Target contours were built up by 15 local bandpass elements aligned with an invisible angular backbone having a random inter-element angle within a $\pm 30^{\circ}$ range. Contour visibility was modulated through the spatial separation between path elements, measured in wavelength λ of the carrier spatial frequency. Contours were either closed, although not perfectly circular, or open with a jagged overall shape. Stimulus examples of open and closed contours are depicted in Figure 1.9. By measuring psychometric functions on element separation as the modulatory variable, the authors found detection performance to be halved at an element separation of 6.0λ for closed contours, as opposed to only 3.3λ for jagged open contours, thus indicating a significant visibility advantage resulting from closure. A second experiment in the same study proved that the removal of just two local elements from closed contours with a length of 12 elements disrupted the closure percept and had contour detection performance drop to chance level.

The authors concluded that the performance benefit observed for closed contours is due to the global form characteristic of closure. Kovacs (1996) interpreted the results towards a synergistic neural process in early vision that implements the Gestalt rule of closure. The distinctive role of closure was supported by results from a set of visual search experiments, showing that processing speed is rapid for closed forms but slow for open forms (Elder & Zucker, 1993). The authors presented stimulus displays with target outline figures consisting of multiple line segments, embedded in a background of distractor elements with a slightly different spatial configuration. The 'closure state' within a given stimulus display was identical, i.e. all shapes in a stimulus shared the same degree of closure. Elder and Zucker found reaction times for the detection of open targets among open distractors to be

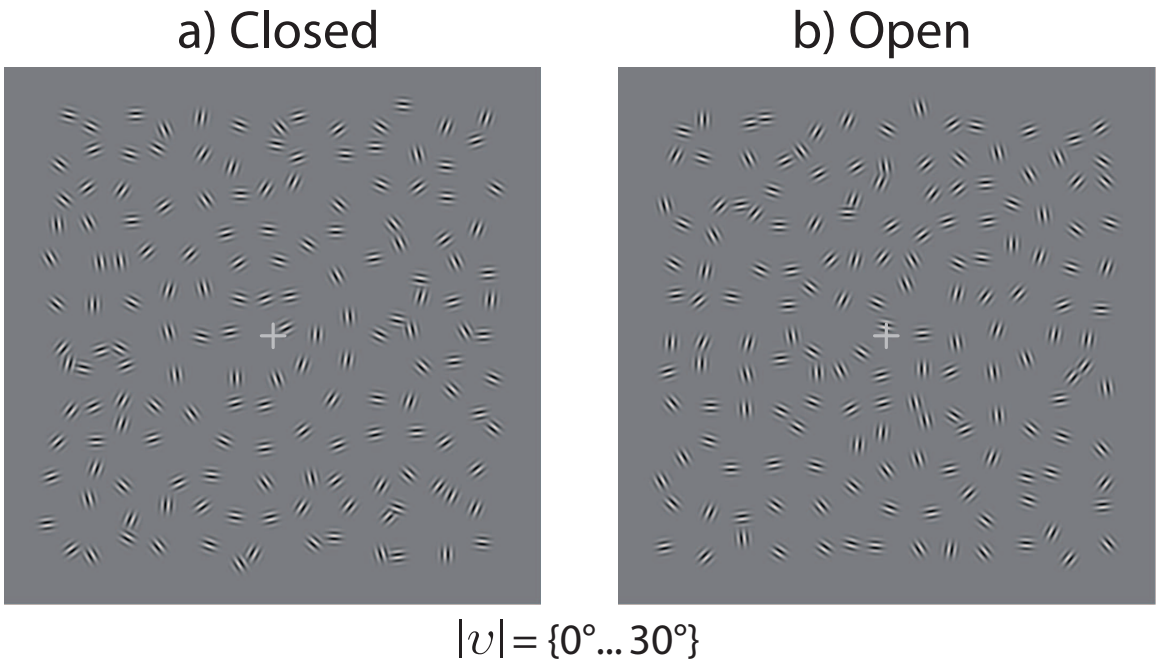

Figure 1.9: Examples of contour stimuli used by Kovacs and Julesz (1993). Panel (a) shows a closed contour, panel (b) an open contour traversing from the upper right to the lower left corner of the stimulus display. Both contours have a maximum inter-element angle of $v = \pm 30°$. Note the higher eccentricity of parts of the open contour compared to the more central location of the closed path.

at least twice as high as for closed targets in a background of closed distractor figures (see also Elder & Zucker, 1994). A similar result was obtained by Saarinen and Levi (1999) for the accuracy of shape perception. The authors presented open and closed figures constructed from local elongated bandpass elements (Gabors) and let human observers judge the aspect ratio of the shapes. When expressed as a threshold ratio measure, discrimination performance was similar among different types of closed forms but far superior compared to open figures.

The closure benefit in contour integration reported by Kovacs and Julesz (1993) was taken to indicate a reverberating excitatory circuit operating on closed contours (Polat & Sagi, 1994a), which may enhance figure ground segregation of the enclosed area. Pettet et al. (1998) found further evidence for such a hypothetical mechanism, substantiating the serious impairment of contour integration performance caused by corners and gaps, and showing superior robustness of closed contours against an increasing number of background noise elements. In a computational approach, Z. Li (1998) developed a neural model for contour integration in the primary visual cortex that only incorporated such neural units and organizational patterns known to exist in area V1. Although not intentionally

targeted at an explanation of the closure advantage, the model predicted a more robust integration of closed contours based on highly synchronous activities of a closed chain of neural units carrying a reverberating excitatory impulse.

Further study of the closure effect, however, raised doubts about its distinctive notion and perceptual generality. The findings of Kovacs and Julesz (1993) have been challenged by both empirical evidence and theoretical reasoning. The first criticism addressed the goodness of the contour generation algorithm (Braun, 1999). If contour and background elements exhibit different spatial statistical properties, artificial distance cues are introduced which may modulate contour salience. In stimulus displays with different distribution functions of contour and background element distances, contour elements have neighboring elements at distances that background elements do not. Braun (1999) investigated the spatial statistical properties of the contour stimuli used in the study of Kovacs and Julesz by calculating the pairwise distances between a local element and all neighboring elements within a defined perimeter. The author reasoned that a well-formed stimulus devoid of spatial cues originating from different spatial distributions of the stimulus elements should be characterized by identical density functions for contour and background elements. Braun demonstrated that contour and background elements in the contour stimuli of Kovacs and Julesz have markedly different spatial density functions, as shown in Figure 1.10. While the element density function is flat for background elements, indicating equal probabilities for a wide range of inter-element distances, the density distribution of contour elements peaks at a spatial wavelength separation of 6λ and 12λ. Further analysis revealed that the peaks were caused by just the adjacent and next by one contour elements, since Kovacs and Julesz omitted to match the positional uncertainty of contour elements with that of background patches but established steady pairwise distances among neighboring contour elements. A contour element was hence most likely to have a contour neighbor at regular distances, thereby acquiring a spatial property which background elements lacked (see Figure 1.10a). This disparity is more pronounced for closed paths with only few elements since the contour 'endpoints' are neighbors to each other, whereas for open contours, the endpoints are surrounded only by background elements. Hence, the disparate element density functions of contour and background elements may contribute differentially to the salience of closed and open paths, particulary with short contours.

A second objection raised by Braun (1999) pertained to the eccentricity of the contours presented in the study of Kovacs and Julesz, who generated most of the open contours by decreasing the inter-element angle along short sections of the path, effectively bending apart the contour. This algorithm yields open contours with a more elongated overall structure, extending over a wider area of the stimulus display and consequently taking higher eccentricities than closed contours (see Figure 1.9, for an example). According to Hess and Dakin (1997, 1999) and Nugent et al. (2003), contour integration performance deteriorates in the peripheral field, which may have further impaired the visibility of open jagged

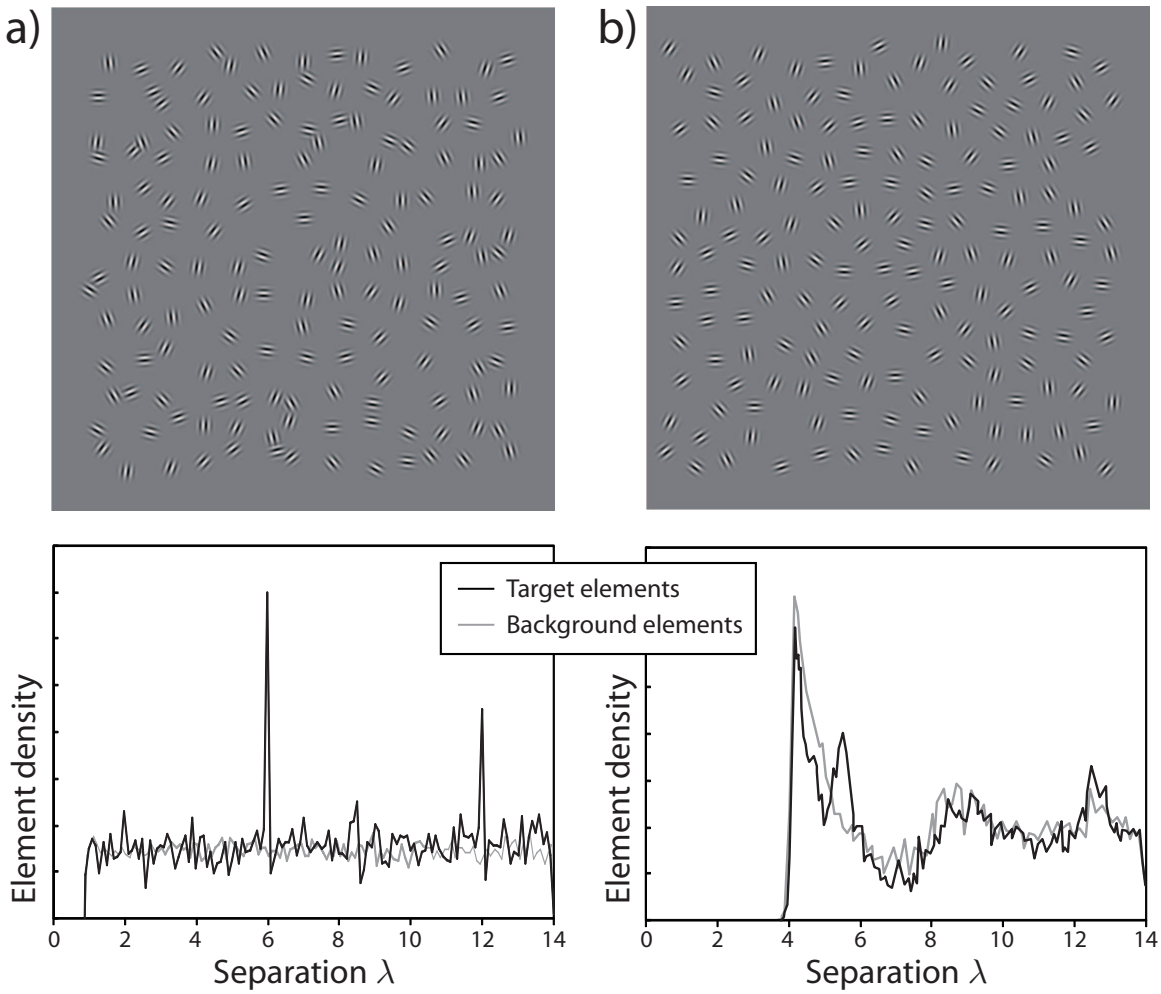

Figure 1.10: Illustrations of spatial density cues in contour integration. The upper row depicts stimulus displays of Kovacs et al. (1994) in (a) and Braun (1999) in (b). The second row shows characteristic element density distributions of the respective stimulus generation algorithms (see text) measured in spatial units of wavelength λ. Element density is expressed in arbitrary units.

contours in the stimulus displays of Kovacs and Julesz.

To put the closure advantage proposed by Kovacs and Julesz (1993) under critical scrutiny, Braun (1999) devised stimulus generation routines which precluded both density and eccentricity cues, as well as visibility differences due to dissimilar numbers of contour elements (see Figure 1.10b). Contour salience was therefore presumed to be established by local orientation collinearity alone. Subjects had to detect closed and open contours with a length of 21 elements in backgrounds of randomly oriented bandpass elements. Results confirmed a significant closure benefit, but of much smaller effect size compared to the

figures reported by Kovacs and Julesz. Braun concludes that, while his results lend support to the general notion of higher perceptual salience contingent on closure, the magnitude of the closure advantage has probably been overestimated by Kovacs and Julesz due to the presence of several confounding factors in the stimulus displays. More importantly, a second experiment conducted by Braun (1999) called into question the hypothesis of a rather dichotomous nature of closure as a global geometric characteristic which is either present in a stimulus or not. When deleting elements from a closed contour of 21 elements, Braun did not observe instantaneous disruption of contour integration performance, as previously suggested by Kovacs and Julesz (1993) who reported contour integration performance to drop to chance level if only two elements were deleted from a 12 element contour. Instead, the closure advantage gradually declined until partly closed contours finally leveled off with open contours of identical length. This notion of closure as a perceptual continuum rather than a dichotomy has received further support from the study by Elder and Zucker (1993) who provided a systematic evaluation of closure effects by modulating the degree of closure among target figures constructed from disjoint line segments. The authors showed that response times in a visual search task can be characterized as a monotonic decreasing function of the degree of closure. A similar pattern was obtained by Mathes and Fahle (2007a) who 'sliced open' closed contours by reducing the inter-element angle between contour elements, thus gradually changing a circle or ellipsis into an open arc of lower curvature without altering the number of path elements (see Figure 1.11). Results consistently showed that the closure advantage ceases smoothly with larger gap size, opposing the notion of a dichotomous perceptual quality of closure.

A straightforward explanation for the closure advantage has been suggested by Tversky et al. (2004), which dispenses with the assumption of higher-order neural processes to account for the more sensitive inference of closed figures from local signals. Upon controlling for artificial visual cues like eccentricity and spatial certainty, and precluding any density cues to the global contour, Tversky et al. (2004) obtained no decisive closure advantage when the robustness of contour detection against orientation jitter was examined with contours made up made up from more than the critical length of 12 contour elements (Kovacs & Julesz, 1993). In another experiment with no orientation jitter along the contour the authors observed a substantial closure effect for contour detection performance when contour length was varied up to 12 elements. However, this advantage was found to be compatible with probability summation among 5 element substrings, the minimum number of elements that is seemingly grouped according to Kovacs and Julesz. With the same number of elements, a closed contour falls into more possible groups of 5 element substrings than an open contour, and, as the authors argue, if contour detection is implemented as a process where all possible 5 element strings independently compete for threshold, the observed advantage of closed contours should emerge, and the closure benefit was just an artifact of a higher combinatorial chance.

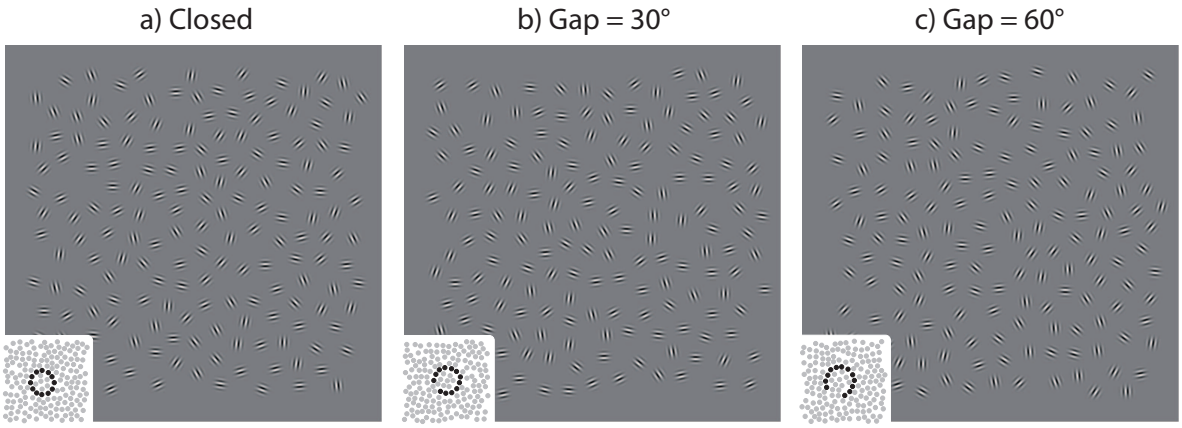

Figure 1.11: Contour visibility with different degrees of closure. The leftmost stimulus (a) shows a circular contour embedded in a surround of randomly oriented distractor elements, stimulus display (b) an open contour with a gap size of $30°$, and (c) an open contour with a gap size of $60°$. All contour elements are assigned a tilt angle of $v = \pm 15°$. Iconic figures represent the exact locations of contour and background elements. Open contours were created by reducing contour curvature while keeping the number of path elements constant. Despite the lower curvature of open contours, the visibility reduction due to decreasing closure is perceptually evident.

If the detection advantage for closed contours with a larger number of elements is indeed small, as reported by Braun (1999) and Tversky et al. (2004), the proposed explanation of probability summation among substrings is difficult to rule out, and therefore the proof of special routines involved with closure will be hard to obtain. A promising approach emerges from consideration of the psychometric measures used in the empirical studies to date, where the integration of open and closed contours was consistently compared by different variants of performance advantage measures. However, for robustness of contour detection in noisy surrounds as the variable of interest, a detection advantage is just one indicator. When analyzing detection stability, also the slope of psychometric curves should be taken into account. If there is a hypothetical closure mechanism serving to stabilize detection of contours in cluttered backgrounds, then psychometric curves recorded for orientation tilt angle along the contour (Hess et al., 2001) should be more steep for closed contours, compared to open ones. The crucial problem to be addressed is that a detection advantage pertaining to closure will most probably involve a mean shift, and, consequently, the slopes of psychometric curves cannot directly be compared for open and closed contours at the same location on the orientation tilt angle scale.

In Chapter 3, a ‘variation coefficient’ is derived as a means to factor both the location

and slope of a psychometric curve into a single measure. The variation coefficient is then employed to assess the perceptual efficacy of the integration of open and closed contours, embedded in backgrounds with different levels of feature noise. Psychometric curves for open and closed contours are found to be similar in overall steepness once the mean shift of the curves is taken into account. While closed contours are proven to be easier to detect, no evidence is found that detection is more efficient in noise, suggesting that there are no particularly efficient detection routines involved with closure. The results comply with the current state of research on the effects of closure in contour integration. Upon careful elimination of confounding factors, no study has so far provided decisive evidence in favor of a dedicated closure mechanism subserving the detection of visual contours.

1.2.5 Spatial Frequency Selectivity of Contour Integration

Remarkably few studies have been devoted to the role of spatial frequency in contour integration (Dakin & Hess, 1998, 1999; Ledgeway & Hess, 2006) despite the significance of spatial frequency within the columnar topology of area V1 (see Sagi, 1991). Although primary sensory mechanisms in V1 are jointly tuned to both parameters, orientation collinearity was the local feature cue particularly focused upon in experiments employing the pathfinder paradigm. Whether aimed at global path characteristics like curvature, closure, and inter-element spacing, or local features like color, motion, and depth, most studies on determinants of visual contour integration were carried out at fixed carrier spatial frequencies of the bandpass elements constituting the stimulus displays. With regard to the validation of association field models, too little consideration was given to the implications of spatial frequency selectivity in contour integration tasks. Generally, knowing the bandpass properties of lateral interconnections in V1 should allow for precise predictions about contour integration performance within and across spatial frequency bands. A number of studies explored how local spatial frequencies interact across space (Chubb, Sperling, & Solomon, 1989; Sagi & Hochstein, 1985). The most systematic contribution comes from experiments by Polat and Sagi (1993, 1994a). The authors studied how the contrast threshold of a central bandpass patch is affected by the presence of suprathreshold flanking patches and proved that the contrast detection threshold of the central probe can be characterized as a function of the spatial probe to flanker distance. Threshold curves were biphasic, with a small inhibitory lobe superseded by larger excitatory ones, existent up to a probe to flanker distance of approximately 8 wavelength units. Additional manipulation of the similarity of probe and flanker in orientation and spatial frequency allowed for an estimate of how the threshold curve modulation alleviates with increasing dissimilarity of probe and flanker elements in the respective feature. For spatial frequency Polat and Sagi (1993) found the amplitude of excitatory interaction to be more than halved at probe-flanker wavelength ratios of 1 octave and cease completely at ratios of 2 octaves, indicating selec-

tive contextual interactions between orientation and spatial frequency tuned mechanisms. Hence, if the spatial frequency tuning of human contour integration performance could be predicted from the bandpass tuning of local contextual interaction, this would lend further support to the local association field model proposed by Field et al. (1993). If, on the other hand, contour integration was found to operate across larger or smaller spatial frequency bands than predicted by the bandpass tuning of lateral interconnections, this would be evidence for the involvement of additional mechanisms and higher order integration processes in contour grouping.

The spatial frequency tuning of contour integration in cluttered images was first studied by Dakin and Hess (1998). The authors used the pathfinder paradigm to measure the detection of contours composed of local bandpass elements embedded in fields of randomly oriented background elements. Contour and background elements could take two distinct spatial frequency values (see Figure 1.12a). Contour elements were nearly perfectly collinear to the path, and the effect of spatial frequency separation between the two concurrent micropattern families on contour detection performance was measured. The authors found proportions correct to be halved in the range of $^5/_4$ octaves for straight contours down to $^3/_4$ octaves for jagged curves with an inter-element angle of 30°. In a later study, Dakin and Hess (1999) used narrowband elements (Gabors) and broadband patches (luminance contrast edges with Gaussian profiles) to construct stimulus displays. Results closely resembled the earlier findings. While contour integration is readily enabled among Gabors with nearby spatial frequencies, as well as among broadband edges, detection performance dropped sharply when the two micropattern types were blended into the same stimulus display, thereby pointing to a bandpass tuning of human contour integration (Dakin & Hess, 1999). Although these results seemingly substantiate local inter-element locking of early orientation and spatial frequency tuned mechanisms at first glance, it is worth looking at the actual stimulus arrangement in the experiment.

Contour detection in random fields with alternating spatial frequencies is a tedious task, because the observer has to monitor the outputs of two channel families across space to differentiate between false positives and proper targets. Experiments on the detection of second order feature modulation have shown that the use of two concurrent spatial frequency bands deteriorates detection of orientation modulated waveforms (Kingdom & Keeble, 2000). Besides the adverse effect of elevated feature noise, deterioration is due to higher level influence, since concurrent groupings by element similarity and proximity occur in two separated spatial frequency bands. Figure 1.12 illustrates the perceptual impact of such concurrent grouping processes. Spatial frequency jitter in both stimulus displays is sampled from $f \in [1.0, 8.0]$ cycles per degree (cpd). Figure 1.12a exemplifies the type of stimuli used by Dakin and Hess (1998), where the stimulus comprised just two distinct spatial frequency families (i.e., the interval limits 1.0 and 8.0 cpd). In contrast, spatial frequency parameters in Figure 1.12b follow a continuous distribution, ranging from 1.0 to

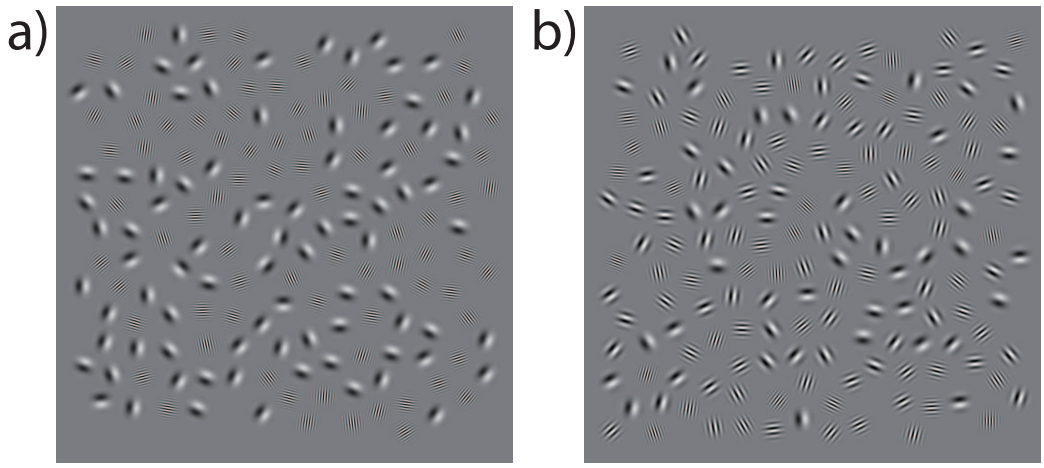

Figure 1.12: Impact of discrete and continuous spatial frequency variability on contour visibility. Each panel contains an S-type contour with zero tilt angle embedded in a background with random orientation. In (a), each stimulus patch is assigned one of two possible spatial frequency levels, either 1.0 or 8.0 cycles per degree (cpd). In (b), spatial frequency values are sampled from a continuous distribution in exactly this interval (1.0 to 8.0 cpd).

8.0 cpd. The stimulus setup from Dakin and Hess inevitably leads to competition between multiple grouping principles. Sampling the spatial frequency parameter of local elements from only two possible values most likely produces clusters of elements with identical spatial frequency, alternating with regions densely populated with elements from the other family. The contour percept is therefore disrupted by intersecting groups of contiguous elements with identical spatial frequency. From a Gestalt perspective, the principle of good continuation along collinear contour elements conflicts with the Gestalt rule of similarity. It is perceptually evident from Figure 1.12a that concurrent element grouping due to spatial frequency similarity degrades integration of the target contour, hence the higher contour visibility in Figure 1.12b. The entanglement of multiple competing grouping principles let the dual frequency band configuration appear inappropriate for studying the role of a low level property such as spatial frequency bandwidth in contour integration.

In Chapter 4, the spatial frequency tuning of human contour detection is revisited using random fields continuously jittering in spatial frequency and orientation. It is shown that after elimination of the conflicting similarity cue contour integration can be done at reasonable performance levels even if the critical frequency separation of the elements along the contour is larger than 2 octaves (see Figure 1.13a,b). The results pose a severe penalty for the association field model since the well-known spatial frequency selectivity of the lateral

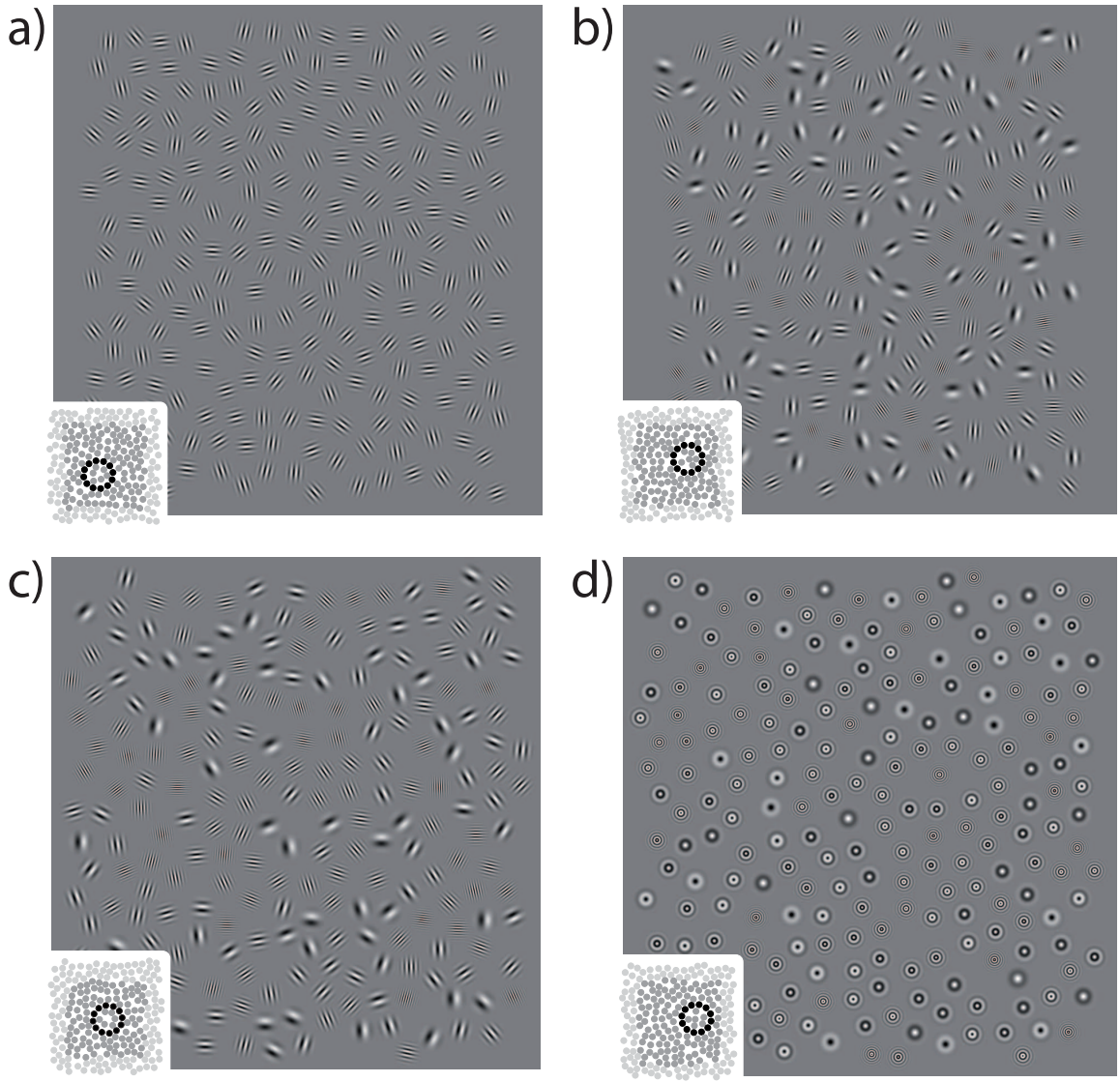

Figure 1.13: The effect of spatial frequency variability on contour visibility. The iconic figures in the lower left corner of each panel are exact symbolic representations of the larger stimulus displays. Both stimulus examples contain a circular contour with zero local tilt angle. In (a), the spatial frequency of all elements is fixed, in (b) it varies continuously over approximately 3 octaves with the same mean value as in (a).

interconnections between V1 neurons is not reflected by the broad spatial frequency tuning of human contour integration performance.

The stimulus examples in Figure 1.13 bring into focus another fundamental characteristic of the association field model. Contour grouping in early vision is assumed to occur

based on lateral interactions of neurons with similar orientation tuning (Field et al., 1993). Applicability of the association field model is therefore constrained on contours that are defined by local elements carrying some sort of orientation signal. In Gestalt terms, only element collinearity is apt to augment good continuation with local information about the global course of the contour, whenever stationary stimulus displays with random element positions like in the original pathfinder paradigm are used. However, good continuation is but one of several principles of perceptual grouping that might serve contour integration when combined with element contiguity. Extending the association field model beyond the scope of an orientation selective mechanism hence requires the identification of other grouping principles that allow for contour integration. Considering the rationale underlying the construction of pathfinder displays, grouping by similarity presents itself as a promising candidate. Instead of assigning random orientations to background elements and establish a contour by coaligning nearby local elements like in Figure 1.13a,b, target contours may alternatively be defined by feature similarity of adjacent path elements, embedded in backgrounds with high variability in the respective feature domain. An illustration is given in Figure 1.13c,d. If in such stimulus arrangements features like depth, color, or spatial frequency readily enabled contour integration, the association field model would qualify as a general functional principle of neural organization, governing the grouping of local elements into a perceptual whole due to combinations of the rule of good continuation with several other grouping principles.

Hess, Hayes, and Kingdom (1997) devised a variant of the pathfinder paradigm in order to probe contour integration through the combination of good continuation and similarity grouping, using depth as the local feature cue. Stimulus displays were built up from non-oriented Gaussian blobs at two different depth planes of ± 3.9 or ± 7.8 arcmin binocular disparity. All elements of a target contour were either bound to one depth plane or traversed smoothly from one depth plane to the other. In distractor displays contours were randomly assigned one of the two depth values, thereby limiting salience of distractor contours to emerge solely from element density cues and the regular global form of the path. Target contours were defined by highlighting contour elements by some form of similarity or feature contrast cue. Stimulus examples are depicted in Figure 1.14, where depth is illustrated by different micropattern sizes, shading, and drop shadow. Hess et al. found distractor contours to be practically invisible (Figure 1.14a) while contours bound to one fixed depth plane (Figure 1.14b) were detected significantly above chance level. Highest detection performances were obtained for paths traversing through depth (Figure 1.14c). Based on their findings Hess et al. concluded that the visual system links the outputs of neurons tuned to depth by means of an association field similar to that for orientation detectors. From a Gestalt perspective, such an association field would serve to promote contour integration by combining the Gestalt principles of good continuation and similarity rather than adding a collinearity cue to good continuation.

A closer look at the stimulus configuration of Hess et al. (1997) renders this conclusion equivocal. All depth defined contours exhibited some form of salient feature contrast cue, emerging from local or global feature contrast between contour and background elements. For contours bound to one depth plane, a global first-order cue was present in all target stimulus displays, i.e. a different frequency histogram in the depth parameter. Background elements were set at random to a disparity of either ± 3.9 or ± 7.8 arcmin, depending on experimental condition, which amounts to an average disparity of 0.0 arcmin if depth values are integrated over the whole stimulus display. A contour bound to one depth plane thus deviated from the average depth of the surround by 3.9 or 7.8 arcmin. Disparity contrasts of such magnitude have been proven sufficient to elicit a salient feature contrast percept and render a target figure visible (Mallot, Arndt, & Bülthoff, 1996). Taking a Gestalt view, stimulus displays contained target contours defined by the two Gestalt rules of good continuation and similarity, complemented by a salient feature contrast cue (Figure 1.14b). Although the feature contrast cue is not as strong as in the introductory example of Figure 1.1b, as well as Figure 1.4c, where grouped target elements exhibit unique feature values inexistent throughout the background, different mean values between target and background parameters entail a first-order cue for the visual system to exploit. The presence of a first-order cue imposes the possibility that detection of target contours did not even require any integrative grouping processes but was accomplished simply by summation within a single large receptive field or a population of cells with similar properties, a model commonly referred to as linear filtering. Results from the second experiment in the study of Hess et al. further promoted this alternative explanation. A contour traversing from one background depth plane to the other comprises local elements that are distinguished from all background as well as contour elements by their depth, again introducing a highly salient feature contrast cue along the contour and, more importantly, reducing the Gestalt cue of similarity among contour elements (see stimulus example in Figure 1.14c). Every contour element is unique in the sense that its depth parameter is absent in the remainder of the stimulus, hence facilitating visual pop-out of contour elements (Treisman & Gelade, 1980; Wolfe, 1994) and preventing the formation of false positive contours within one depth family. Hess et al. (1997) found detection performance for target contours traversing through depth to be highest in the entire series of experiments, which gives weight to the hypothesis that a feature contrast cue rather than the Gestalt rule of similarity enabled the detection of the depth defined target contours. With feature contrast being the primary cue to the contour in the stimulus displays of Hess et al., the assumption of an association field operating on depth similarity is expendable because simple feedforward processing by a bank of dedicated depth selective neurons or a single large receptive field would suffice to detect first-order depth contrast cues (Hess, Baker, & Wilcox, 1999), requiring no lateral interconnections between neural units of similar depth tuning.

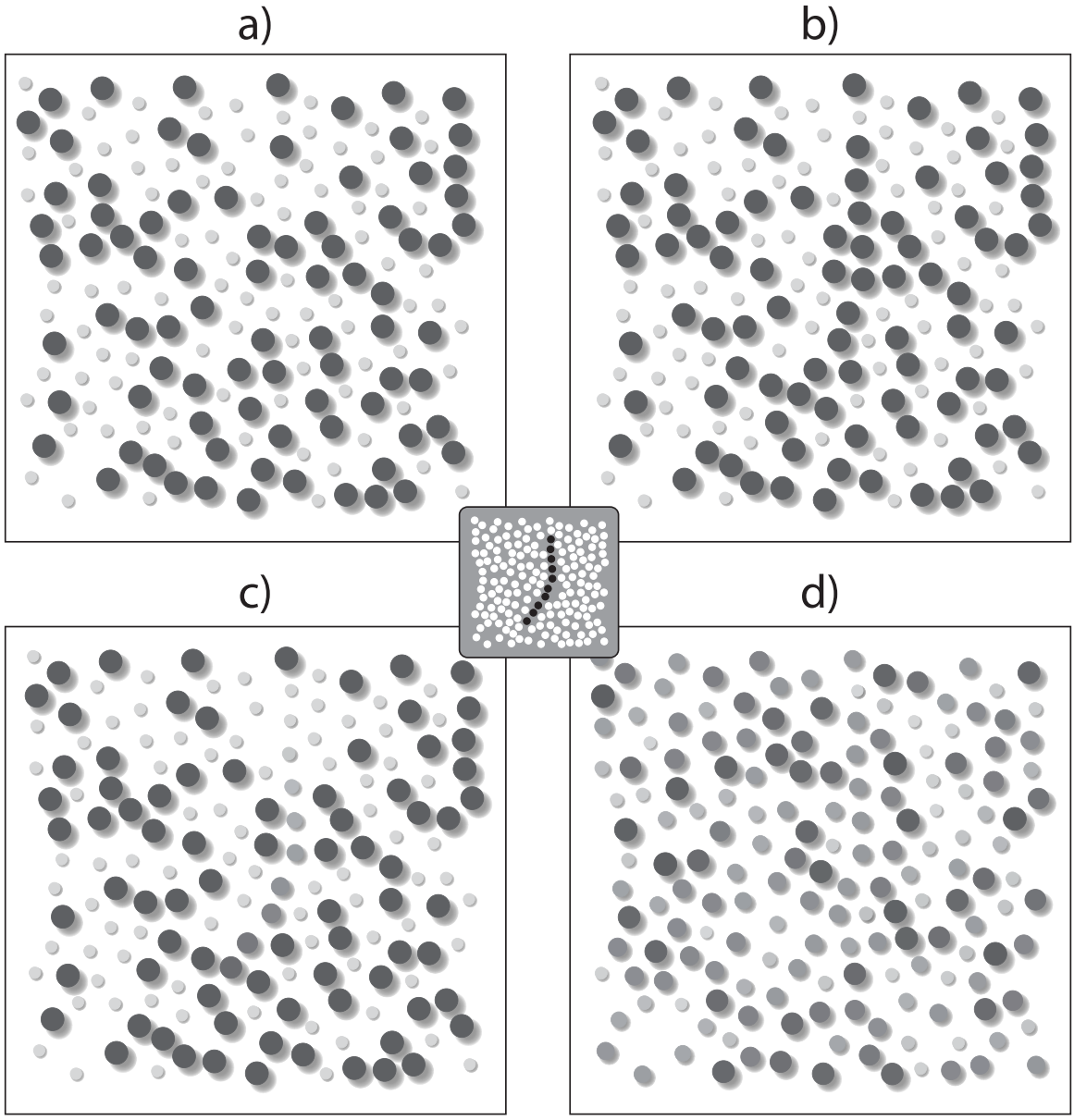

Figure 1.14: Contour grouping by good continuation and depth segregation. In all stimuli exemplified here, depth is illustrated by element size, shading and displacement of the drop shadow. Panels (a) through (c) are stimulus examples used by Hess et al. (1997). A distractor stimulus with no depth cue to the contour is given in (a), a target contour contour traversing through depth in (b), and a target stimulus with contour elements bound to one depth plane in (c). A contour stimulus devoid of feature contrast cues to contour elements, defining the contour only by the grouping principles of proximity and similarity is exemplified in panel (d).

Stimulus displays appropriate for studying contour integration based on element contiguity and similarity evidently demand generation algorithms that obviate any first-order feature contrast cues along the contour. An effective way to construct such stimulus displays is to assign high levels of feature noise to background elements and homogenize contour elements onto the mean feature parameter of the background. This approach translates the high magnitudes of background orientation jitter innate to pathfinder displays into other feature dimensions and consequently augments the good continuation cue with feature similarity at the absence of a confounding feature contrast cue (see Figure 1.14d).

The second experiment of Chapter 4 is designed to examine the ability of the visual system to integrate contours defined by good continuation in combination with grouping cues other than local orientation collinearity. A modified pathfinder paradigm is described that adds a feature similarity cue to the principle of good continuation, while carefully precluding additional cues such as spatial density or element pop-out due to feature contrast. Stimulus displays were created from Gabor patches with fully random orientations, as well as from circular sinusoidal micropatterns. Spatial frequency of background elements was sampled from a broad interval, and similarity of contour elements was established by homogenizing the spatial frequency parameter onto the mean value of the background distribution (Figure 1.15a,b). Contour integration performance is found to not exceed chance level when spatial frequency homogeneity is the only feature cue to the contour in an otherwise random element field. Hence, good continuation in combination with similarity grouping does not suffice to yield salient contours when spatial frequency is used as the local feature. The results presented here clearly object the assumption of an association field operating on spatial frequency similarity, as well as the hypothesis of a universal association field principle in human vision, which would allow for contour integration by mere similarity of features rather than collinearity of local elements. The addition of a salient feature contrast cue to a similarity cue appears mandatory to integrate visual contours devoid of local collinearity information.

1.2.6 Contour Integration with Multiple Cues

The dynamic interplay of multiple Gestalt rules during the process of perceptual organization is one of the key characteristics of the Gestalt framework. As has been shown in previous sections, Gestalt rules can interact in a variety of ways, including cooperation, competition, conflict, or mere independence. Despite the rich body of research in the field of contour integration, evidence on the contribution of other Gestalt rules like similarity or common fate to contour grouping is rare and largely incidental.

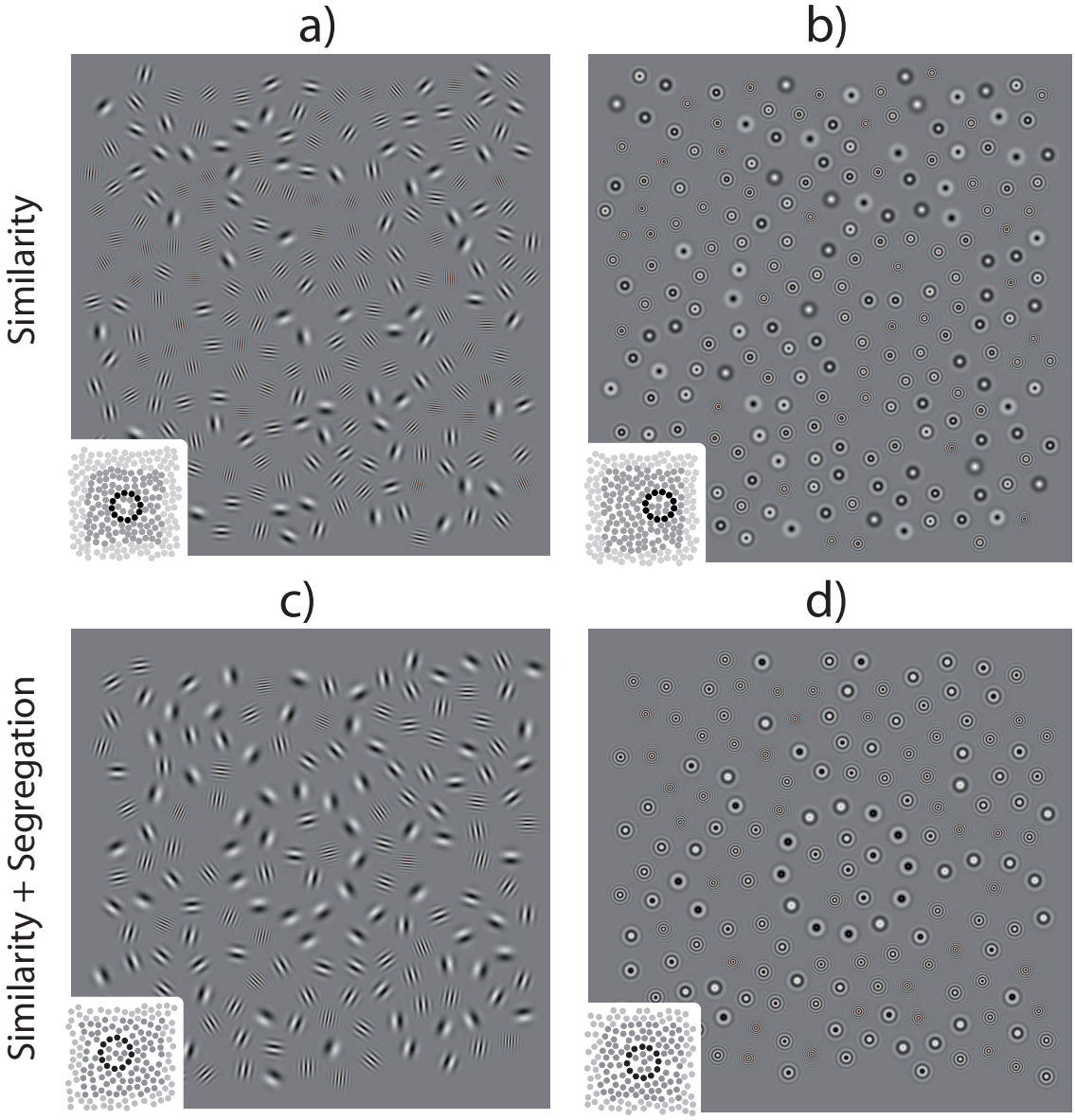

Figure 1.15: Contour visibility due to spatial frequency similarity and feature contrast. Spatial frequency jitter of background elements is identical to Figure 1.13b-d. Stimuli in the left column are built up from Gabor elements with random orientations, displays in the right column comprise circular sinusoidal patches devoid of any orientation information. Panels (a) and (b) are illustrations of a contour integration task mediated by the Gestalt rule of similarity alone. Similarity between path elements is established by setting the spatial frequency of contour elements to the mean value of the background distribution of spatial frequencies, thereby avoiding a first-order feature contrast cue between contour and background. In (c) and (d) the similarity cue is combined with a feature contrast cue by assigning all path elements a spatial frequency near the lower bound of the background distribution.

Effects of cooperative interplay between multiple Gestalt rules in contour integration became apparent in the study of Hess et al. (1997), discussed in the previous section. Contours defined by a good continuation cue alone were practically undetectable (Figure 1.14a), until a similarity and a feature cue were established among the contour elements (Figure 1.14b,c). Unfortunately, the stimulus setup employed by Hess et al. left open the question whether perceptual grouping occurred due to element similarity, feature contrast, or a combination of both. The second experiment presented in Chapter 4 indicates that the Gestalt rule of similarity alone does not suffice to establish perceptual salience when added to the rule of good continuation. For the stimulus displays used in Chapter 4, the perceptual effect of supplementing similarity grouping with a feature contrast cue is illustrated in Figure 1.15c and d. Spatial frequency similarity of the contour elements is augmented with a feature contrast cue induced by setting the spatial frequency values of contour elements to the lower bound of the background spatial frequency distribution, rather than their mean value as in Figure 1.15a and b. Similar cooperative interactions of a feature contrast cue with good continuation have also been found for depth (Hess & Field, 1995) and color (Mullen et al., 2000), as well for deviation of flicker frequency between contour and background (Hess et al., 2001). Segregation cues emanating from different feature properties of figure and ground apparently qualify as a viable means to improve perceptual grouping in contour integration tasks when combined with a good continuation cue.

Systematic quantifications of the effects of additional grouping cues on contour integration performance have, however, been attempted in very few studies. The first quantitative assessment of the combination of multiple Gestalt rules in the scope of pathfinder experiments was conducted by S. H. Lee and Blake (2001). The authors generated stimuli resembling typical pathfinder displays (see Figure 1.6). Target stimuli contained a smooth path consisting of nine Gabor elements, embedded in a background of randomly positioned elements. Contours were defined by orientation collinearity of Gabor elements, temporal synchrony of feature changes, or the combination of collinearity and temporal synchrony. Two variants of temporal synchrony were employed, either due to phase-shift motion in perpendicular direction of the Gabor orientation, or luminance contrast changes of Gabor elements. Temporal synchrony of phase-shift motion was established by coherent alterations of motion direction, synchrony of luminance contrast changes by coherent luminance pulsation The stimulus setup hence allowed for two possible combinations of orientation collinearity with a temporal synchrony cue. From a Gestalt perspective, orientation collinearity was combined with common fate (motion cue) or similarity (luminance contrast cue) to augment the principle of good continuation. Contour visibility was modulated by increasing the tilt angle of local elements until contour detection performance dropped to chance level. Psychometric curves were then measured for the orientation collinearity cue alone and for its conjunction with each of the temporal synchrony cues. For both combinations of cues, S. H. Lee and Blake (2001) observed significant increases of contour

integration performance. The tilt angle required to reduce contour integration performance to threshold level approximately doubled when contour elements exhibited fully coherent temporal synchrony in addition to the orientation collinearity cue. Detection performance was elevated from the 75% threshold for orientation collinearity alone to proportion correct levels of about 90% for the combination with each of the temporal synchrony cues, thus far exceeding what would be expected from independent feature processing. The authors concluded that the synergistic interaction between spatial and temporal cues suggests an integrated spatio-temporal circuit underlying contour integration which enables the visual system to exploit combinations of grouping cues in a highly efficient manner.

The experiment by S. H. Lee and Blake (2001), however, has since remained the only study to support the notion of synergistic processing of multiple grouping principles in contour integration. A study by Ledgeway et al. (2005), using a paradigm very similar to that of S. H. Lee and Blake, yielded conflicting results. Ledgeway et al. sought to determine the effect of combining element collinearity with a salient motion cue upon contour integration performance of human observers. Collinear alignment of oriented broadband contour elements was combined with coherent motion in perpendicular direction of the orientation axis. The motion cue used by Ledgeway et al. (2005) differed from that of S. H. Lee and Blake (2001) only insofar as the latter amplified the motion cue by having motion direction alternate coherently along the contour and randomly for background elements, while Ledgeway et al. established a steady motion direction among contour elements. Ledgeway et al. (2005) first measured detection performance levels for contours defined by either collinear orientation or motion direction, after which the two cues were combined and the performance gain due to the interaction of grouping principles was estimated. The authors found motion direction to yield just a moderate increase of overall contour salience when added to the alignment cue. Unlike the results obtained by S. H. Lee and Blake (2001), this increase was compatible with the notion of separate feature channels responsible for the processing of orientation and motion signals, thus indicating perceptual independence of the rule of good continuation from the processing of motion cues in contour integration.

Evidence from a study by on the combination of the element collinearity with a chromatic color cue point in a similar direction (Mathes, Trenner, & Fahle, 2006b). Using pathfinder stimuli, the authors first determined the 25% color contrast detection threshold for a contour of randomly oriented Gabor stimuli, embedded in a random field of achromatic Gabors. Perceptual salience of contour elements was modulated by adding color intensity to the green component channel (Figure 1.16a). Contour integration was then measured depending on the tilt angle of contour elements. Contours were defined either by orientation collinearity alone (Figure 1.16b) or the combination of collinearity with a color contrast cue corresponding to the previously obtained 25% threshold level (Figure 1.16c). Although contour integration performance was amplified by the combination of both cues, the visibility gain remained rather weak and attested to an independent processing scheme

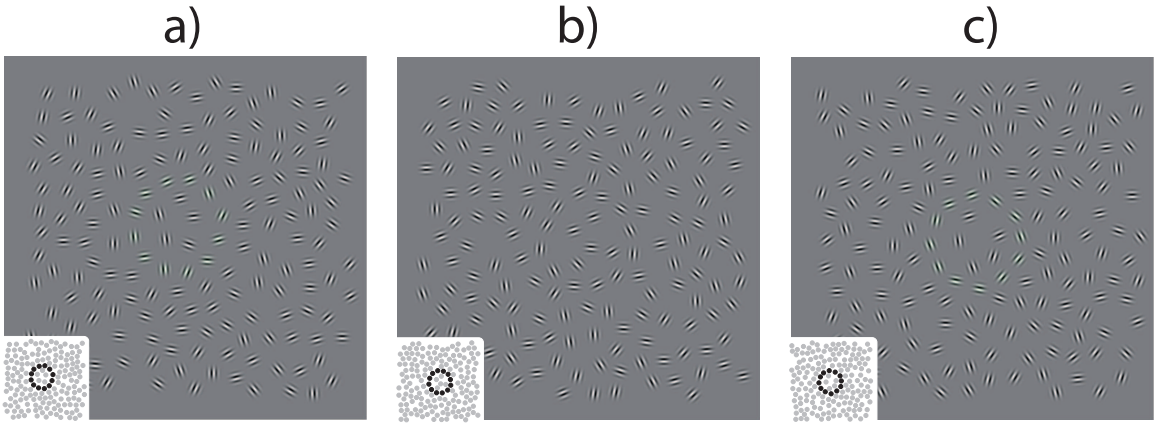

Figure 1.16: Combination of color and collinearity cues in contour integration (Mathes et al., 2006b). Contour elements in the leftmost stimulus are assigned a faint green hue (a), the contour in (b) is highlighted by orientation collinearity of local elements with a tilt angle of $v = \pm 10°$. Green hue and orientation collinearity are combined to define the contour in the rightmost stimulus (c), yielding only a moderate salience gain.

of the orientation collinearity cue and the color feature contrast cue.

Nothdurft (2000) conducted a series of experiments to quantify the salience benefit attributable to combinations of different features. Stimuli were texture patterns made of oblique line elements with identical orientation. One of the line elements displayed feature contrast in orientation, motion, luminance, or color contrast, or pairwise combinations of these. Targets with feature contrast in two dimensions were consistently found to be more salient than targets with a single feature contrast property, but the magnitude of the salience gain was highly dependent on the specific pairing of features, and the task under study. While color and orientation did not show much salience summation, while adding a luminance cue to any of the other features produced a much stronger salience gain. The results give rise to the hypothesis that different patterns of interactions between feature processing mechanisms are implemented along the visual pathway, ranging from independent processing to near linear summation.

As propagated by Sagi (1988), combinations of orientation and spatial frequency are jointly coded on an early site by neurons optimally tuned to a specific combination of orientation and spatial frequency. The joint coding hypothesis is supported by psychophysical evidence from masking experiments (Wilson, McFarlane, & Phillips, 1983), texture discrimination (Rubenstein & Sagi, 1990; Prins & Kingdom, 2003), feature contrast detection (Meinhardt, Schmidt, Persike, & Röers, 2004), and figure identification tasks (Persike & Meinhardt, 2008), as well as neurophysiological studies on the orientation and spatial fre-

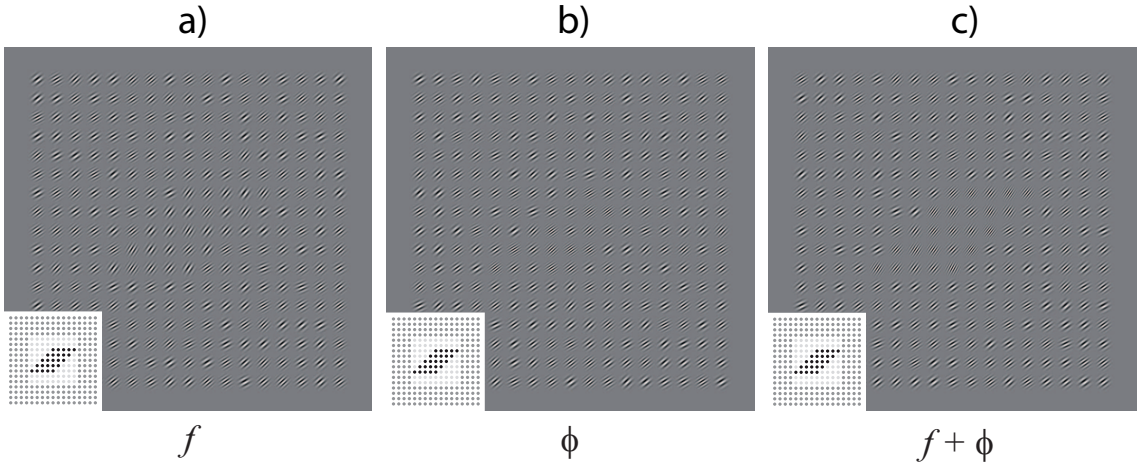

Figure 1.17: Cue combination in a feature detection and figure identification task (Meinhardt & Persike, 2007). All figures are rightward tilted lozenges, defined by feature contrast in spatial frequency (a), orientation (b), and both features (c). With only a single feature cue the mean parameter difference of the inner and the outer region barely enables feature contrast detection and is too small for the identification of target shape. With the same parameter difference given simultaneously in both feature dimensions (double cue target definition) detection performance is significantly improved and the shape of a the lozenge figure becomes apparent.

quency selectivity of cells in primary visual cortex (Webster & De Valois, 1985; Bradley, Skottun, Ohzawa, Sclar, & Freeman, 1987; Sirovich & Uglesich, 2004). In a recent psychophysical study, Meinhardt, Persike, Mesenholl, and Hagemann (2006) investigated how orientation and spatial frequency interact in a combined feature contrast detection and figure discrimination task. Target figures were embedded in Gabor random fields, and were defined by feature contrast in spatial frequency, orientation, or both cues (see Figure 1.17). The authors obtained a substantial salience gain due to the combination of cues for all target figures in both the feature contrast detection and figure identification task, which was incompatible in magnitude with the assumption of independent feature processing mechanisms. Moreover, cue summation was generally larger in the identification than the detection task, indicating higher salience gains when processes of object formation are involved. Meinhardt et al. (2006) interpreted their findings toward a joint coding model of feature processing and element grouping in early vision, apt to improve spatial form completion and figure-ground segregation in noisy environments, and thereby leading to more stable object vision.

Spatial frequency thus lends itself as a promising feature to evaluate quantitative effects

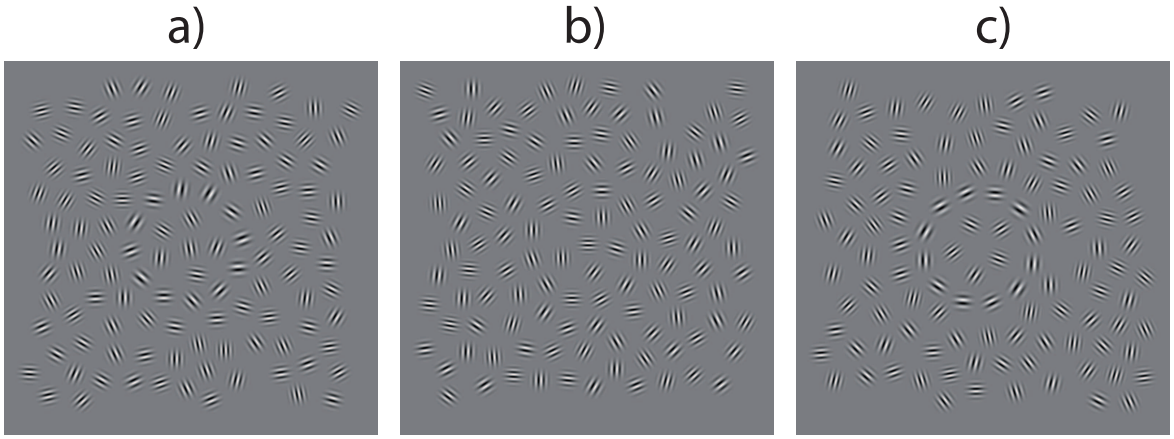

Figure 1.18: Perceptual effects of feature contrast, alignment, and similarity cues on the salience of a circular contour in Gabor random fields. In (a) the twelve contour defining elements have the same random orientation than the surrounding elements, but an octave lower carrier frequency. The contour defining elements segregate from the surround, and are similar to each other. (b) shows contour defining elements with local orientations aligned with the global path. Elements belonging to the contour have the same carrier frequency than the surrounding elements. In (c) the contour defining principles of a) and b) are combined, which makes the global path highly salient.

of cue combination in contour integration tasks. Since in the framework of association field models, contour integration is viewed as the result of inter-element locking of orientation and spatial frequency selective units located early in the visual pathway, it is straightforward to ask whether combining orientation collinearity with a spatial frequency feature contrast cue yields a strong contour detection gain. Figure 1.18 illustrates the effect of combining the orientation collinearity cue with a perceptually equivalent feature contrast cue due to spatial frequency feature contrast. Figure 1.18a comprises Gabor elements with a carrier spatial frequency about half an octave lower compared to the surround which are arranged along a circular path, producing the vague impression of a circular shape. In Figure 1.18b Gabor elements of the same carrier frequency as the surround are aligned with the path, which also results in a weak figure percept. In Figure 1.18c the variations from Figure 1.18a and Figure 1.18b are combined. Gabor elements are aligned with the path and have lower carrier frequency than the surround. The perceptual result is a highly salient circular figure. In a Gestaltist approach, one may conjecture that augmenting collinearly aligned elements with the Gestalt rule of similarity and a feature contrast cue results in strong visibility enhancement of the global contour.

In Chapter 5, the effect of combining feature contrast, similarity grouping, and element

collinearity is investigated by using stimuli akin to those in Figure 1.18. Results confirm that cue combination of an orientation collinearity cue with a spatial frequency feature contrast cue significantly enhances contour integration performance, thereby leading to more stable object vision. Performance gains due to the combination of multiple grouping cues, denoted as 'cue summation', were higher than predicted by the assumption of independent feature processing, and in certain conditions even exceeded linear summation that would result from joint coding of both cues by one cortical mechanism. An illustration of oversummative visibility advantages is given in Figure 1.18, where the figure-ground percept due to the combination of cues (Figure 1.18c) is much more pronounced than with only the single cues (Figure 1.18a,b). Findings also substantiate the notion of a differential role of spatial frequency deviations in contour integration. Cue summation due to cue combination was particularly large when the spatial frequency contrast of contour elements was realized by lowering the carrier frequency of the contour elements relative to the background (see Figure 1.18), far outweighing the visibility advantage when spatial frequency contrast in upward direction was established. Oversummativity and the cue summation asymmetry are taken to counter the notion of passive integration of multiple grouping rules along the visual pathway. Instead, two distinct Gestalt-based mechanisms of contour grouping are proposed. The first implements good continuation of collinearly aligned local elements, the second exploits the collaboration of similarity grouping and a feature contrast cue. Upon combination of these two mechanisms, highly efficient processing streams are tapped, involving such mechanisms as attentional preselection (Kimchi, Yeshurun, & Cohen-Savransky, 2007) or adaptive reweighing of feature specific layers due to feedback connections (Bredfeldt & Ringach, 2002; Goolsby, Grabowecky, & Suzuki, 2005).

1.3 Thesis Outline

This thesis is organized into four parts: Introduction and General Methods (**Chapter 1** and **2**), Experiments 1 to 3 (**Chapter 3** through **5**), and General Discussion (**Chapter 6**), concluded with a proposal of most promising directions of future work (**Chapter 7**).

Chapter 2 elaborates on the experimental methods and procedures common to all experiments presented in subsequent chapters.

In **Chapter 3**, the perceptual efficacy of the integration of open and closed contours embedded in backgrounds with different levels of spatial frequency noise is studied.

In **Chapter 4**, the spatial frequency selectivity of human contour detection is revisited using random fields continuously jittering in spatial frequency and orientation. A second experiment clarifies whether contour integration in spatial frequency heterogenous surrounds is possible solely by similarity grouping among local elements with homogenous spatial

frequency.

In **Chapter 5**, the effect of combining orientation collinearity and two kinds of spatial frequency feature contrast cues on contour integration performance is studied.

Chapter 6 presents a joint discussion of the results from all three studies. Careful consideration is given to the contribution of good continuation, element collinearity, similarity grouping, and feature contrast to contour salience in cluttered displays. Finally, the association field model is evaluated in the context of the new insights emerging from the work presented here.

The thesis ends on a concluding remark in **Chapter 7**. A generalization is attempted upon how the studied rules of perceptual organization contribute to contour integration, when combined with the principle of good continuation. It is proposed that the patterns of interaction between good continuation, similarity, and feature contrast, which are covered in Chapter 3 through Chapter 5, are not constrained to the spatial frequency domain but may be extended to other basic features like chromatic color.

2 General methods

2.1 Stimulus Micropatterns

In all experiments presented here, stimulus displays comprised contour paths made up from local micropatterns, embedded in random fields of the same micropattern type. Two types of micropatterns were used throughout the experiments, being Gabor patches and Gaussian patches of circular sinusoidal waves. Circular sinusoidal patches were employed only in the second experiment of Chapter 4. Micropatterns were spatially limited to a diameter of 1.0° visual angle by setting the standard deviation σ of the bivariate Gaussian envelope to 0.2° and clipping beyond a radius of 2.5 σ-units. Gabor elements were defined by

$$g\left(x,y\right)=\exp\left(-\frac{x^2+y^2}{2\sigma^2}\right)\sin\left(2\pi f\left(x\cos\left(\omega\right)-y\sin\left(\omega\right)\right)\right). \tag{2.1}$$

In (2.1) $\omega=\frac{\varphi}{180}\pi$, with φ the rotation angle measured in degrees.

Circular sinusoidal patches were defined as the product of a bivariate Gaussian envelope with a circular sinusoid:

$$g\left(x,y\right)=\exp\left(-\frac{x^2+y^2}{s^2}\right)\sin\left(2\pi f\sqrt{x^2+y^2}\right). \tag{2.2}$$

The phase of all micropatterns alternated randomly, taking values of 0 (sine phase) and π (anti-sine phase) with equal likelihood. Stimulus properties specific to each experiment will be explicated in the methods section of the respective chapter.

2.2 Stimuli

2.2.1 Contour Generation

Contours were generated in a procedure adopted from (Field et al., 1993; see Figure 2.1). First, a virtual path of N_{cont} connected line segments was created. Each line element had a constant length D that was chosen so that D equaled the mean pairwise natural neighbor distance of background elements (see section 2.2.3). The orientation of each line segment deviated from that of its predecessor by an inter-element angle θ in order to form curved paths. Micropatterns were placed at the midpoint of each line segment and, in case of

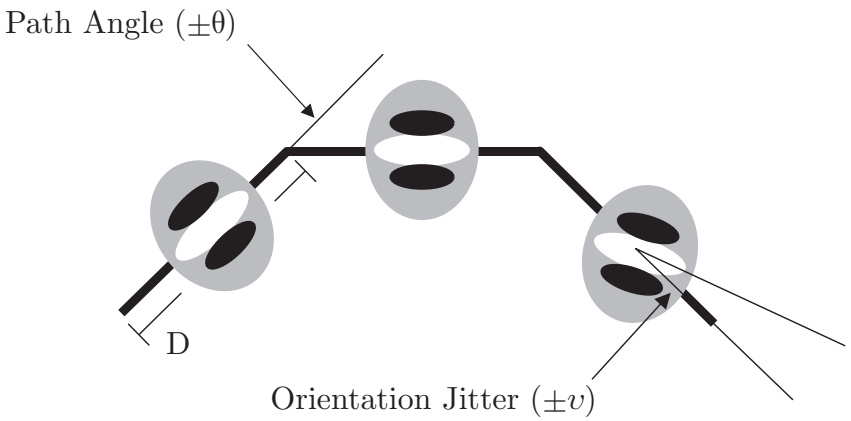

Figure 2.1: Generation of contours. A virtual path of N_{cont} connected line segments of constant length D is created and the angle between an adjacent pair of line segments set to θ. Micropatterns are placed at the midpoint of each line segment and, in case of oriented micropatterns, element orientation set congruent with the orientation of the corresponding line segment. Detectability of target contours made up from oriented micropatterns can be modulated by rotating an element away from its perfect alignment with the contour by an angle v. Increasing this 'tilt angle' results in decreasing contour detection performance.

Gabor micropatterns, element orientation was set congruent with the orientation of the corresponding line segment, thereby yielding contours of highest possible visibility given the inter-element angle θ. As outlined in the introduction, the deviation of the orientation of a local contour element from its perfect alignment with the contour, denoted as 'tilt angle', is the only cue involving local element orientation that does not affect the overall spatial geometry of the contour, unlike curvature or the number or turning points. Detectability of target contours made up from Gabor micropatterns was therefore modulated by rotating a Gabor element away from its perfect alignment with the contour by an angle v. Increasing the tilt angle results in decreasing contour detection performance. The perceptual effect of different tilt angles is illustrated in Figure 2.3. A completed path was finally embedded at a given location into a background of randomly positioned stimulus elements, as outlined in the following section.

2.2.2 Construction of Stimulus Fields

Stimulus construction generally split into four stages (see Figure 2.2). First, a hexagonal grid was filled with $N_{bg} = 225$ background element positions (Figure 2.2a). Second, a contour was constructed as described in the previous section and superimposed onto the background grid. Background elements overlapped by contour elements were removed

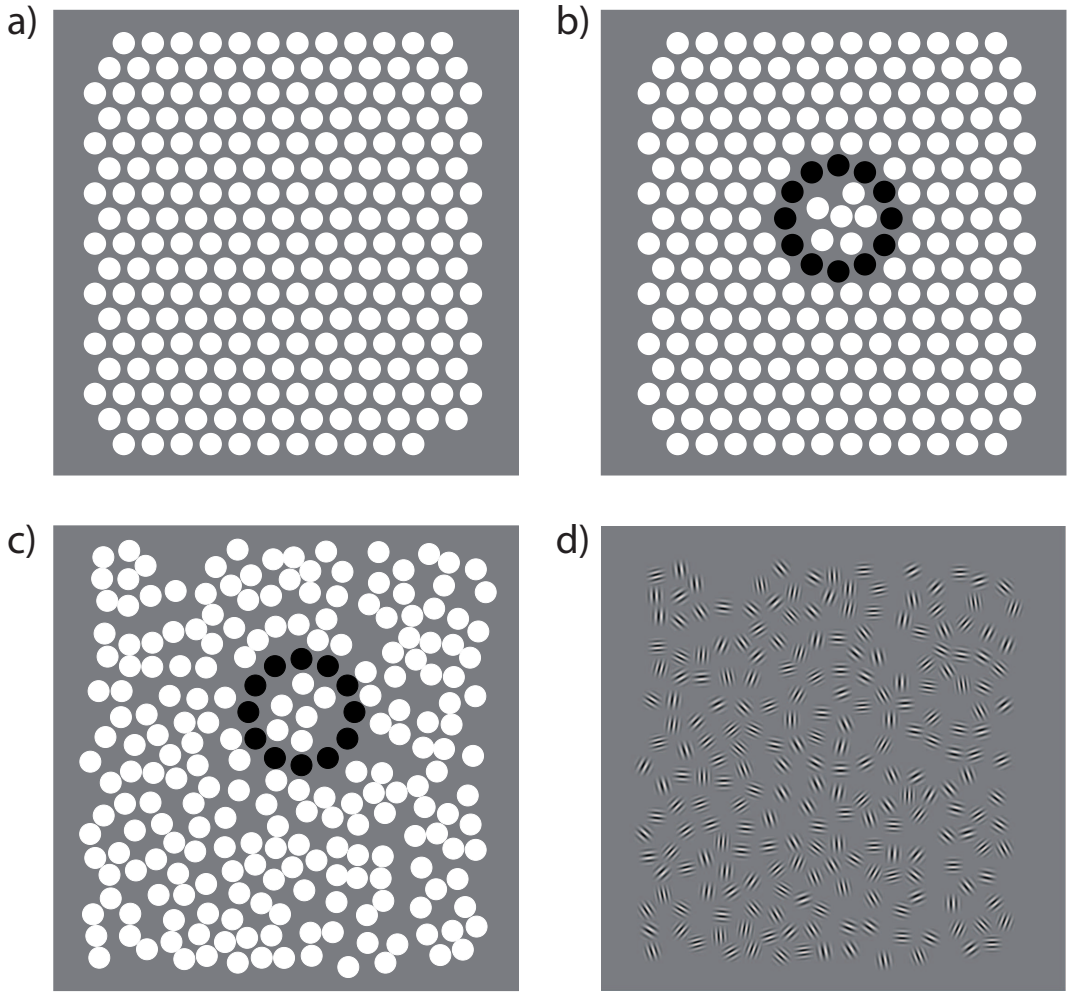

Figure 2.2: Construction of stimulus displays. After setting up a hexagonal grid with 225 element positions (a), a contour is added to the grid (b). Background positions that are overlapped by contour element positions are removed from the grid and the inner region of closed contours is filled with supplemental element positions in order to match the element density outside of the contour. All background element positions are then displaced during iterative perturbations (c). Finally, stimulus patches are placed onto the element positions, and orientation and spatial frequency values become assigned (d).

from the grid. This procedure implies a high likelihood to yield unequal spatial densities of elements within and outside of closed contours. Therefore, supplementary elements were added to the inside area of a closed contour until the element density inside the contour was similar to the background (Figure 2.2b). Third, background elements were displaced by employing an iterative perturbation technique on the initial hexagonal configuration.

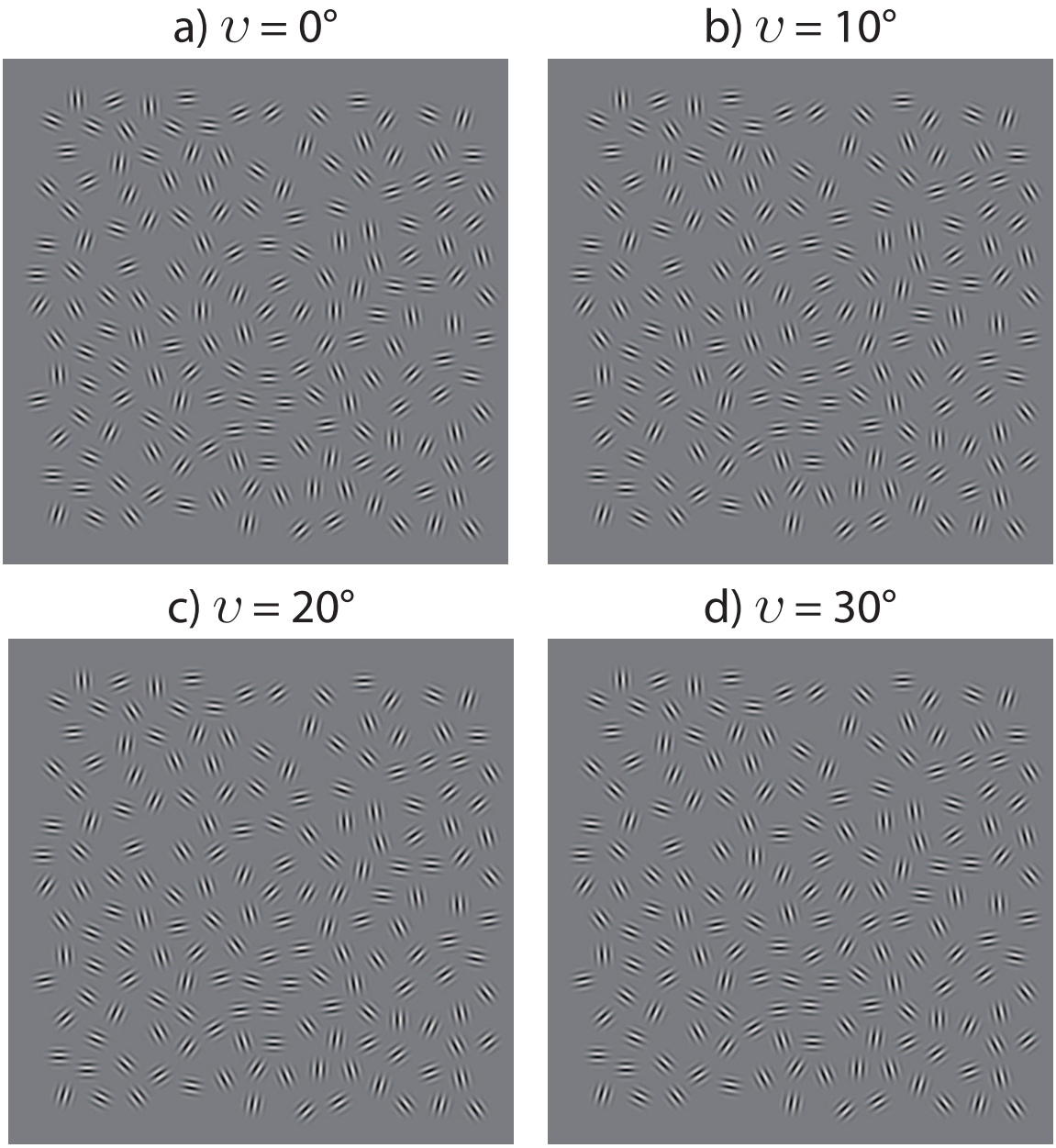

Figure 2.3: Contour detectability at different tilt angles v. The figure illustrates the deterioration of contour visibility with increasing tilt angle v of local elements. The background field and contour location are identical in all four panels, only the orientations of contour elements take different levels of deviation from the global contour curvature. In (a), the contour elements are perfectly aligned with the contour curvature, panels (b) to (d) depict tilt angles increasing in steps of $10°$, up to $30°$ in panel (d), where the contour becomes practically indetectable. Note that due to the global path curvature of $\theta = 30°$ used for the circular contour displayed here, a tilt angle of $v = 30°$ has inter-element orientation differences add up to $60°$.

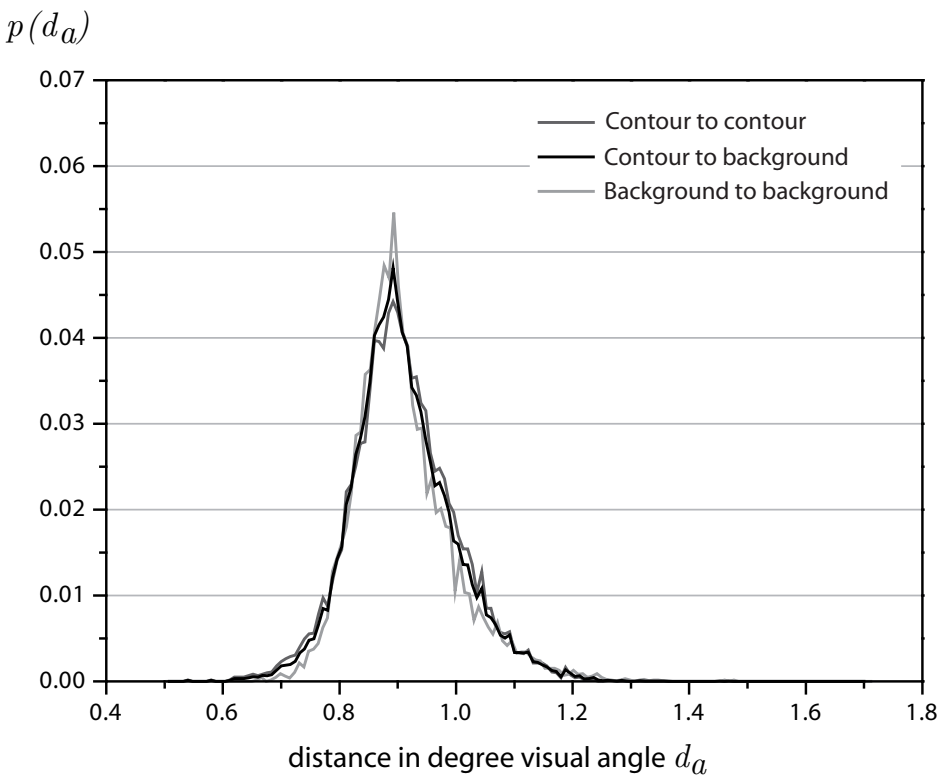

Figure 2.4: Statistical properties of stimulus displays. Probability of mean distance $p(d_a)$ is plotted as a function of distance in units of degree visual angle d_a, with an ordinate resolution of $0.01°$. Distances were computed as mean natural neighbour separations (see text) from 50.000 generated stimulus displays for every local element in a stimulus. Natural neighbour distances split into three classes, which are presented as separate graphs in the figure.

A detailed description of the diffusion algorithm is given by Braun (1999). Pairwise euclidian distances between the contour elements were also jittered in an iterative random process in order to approximate the distribution of natural neighbor distances of the background (Figure 2.2c; see following section). Finally, micropatterns were placed onto the element positions and assigned the feature values to be used in the respective experiment (Figure 2.2d).

2.2.3 Spatial Statistical Properties of Contour Displays

If contour and background elements exhibit different spatial statistical properties, undesirable 'distance cues' are introduced which may contribute significantly to contour salience. In stimulus displays with different distance distribution functions of contour and back-

ground elements, contour elements have neighboring elements at distances that background elements do not, which potentially affects contour integration performance. The spatial statistical properties of stimulus displays can be put under scrutiny by calculating *natural neighbor* distances for each micropattern comprised in the stimulus. To obtain natural neighbor statistics, a planar Delaunay triangulation (D. T. Lee & Schachter, 1980) is constructed upon the stimulus, after which a mean euclidian distance can be calculated for each stimulus element with all other elements it connects to within the Delaunay mesh. Mean natural neighbor distances may be computed for three possible pairwise distance types, i.e. only among background elements, only among contour elements, and between contour and background elements. A stimulus devoid of spatial cues originating from natural neighbor statistics of the stimulus elements is characterized by identical probability distribution functions for each of the three distance types. The stimulus displays used here comply with this notion reasonably well (Figure 2.4). Distance distributions shown in the figure were obtained by generating 50.000 stimulus displays containing a target contour and computing natural neighbor distances for background-background, contour-contour, and contour-background element connections. The present stimulus displays have salient distance cues practically eliminated, so that contour detection performance is most likely to be based on the orientation of local contour elements alone.

2.2.4 Outline and Spatial Arrangement of Target Stimuli

Target contours consisted of $N_{cont} = 12$ elements with an inter-element angle of $\theta = 30^\circ$ and were embedded in fields of about $N_{cont} \approx 213$ background elements. Contours were either a closed circle, or an open path with the shape of an 'S'. By reason of the unknown effects of curvature, curvature gradient, and polarity on the visibility of contours (see Introduction, section 1.1.1), global curvature was held fixed for all contours in the experiment. Curvature of open contours was the same as for closed contours except for the turning point at half length. The global orientation of open contours was limited so that the first cardinal axis of the imaginary bounding rectangle pointed in horizontal direction, with a small variability within $[-7.5^\circ, 7.5^\circ]$. The restriction on sideways S-type contours was introduced to account for the greater spatial uncertainty of open shapes as compared to circular closed contours. The bounding box of a contour always fell within a $10^\circ \times 10^\circ$ square in the center of the whole $17^\circ \times 17^\circ$ background lattice (see Figure 2.5).

2.3 Psychophysical Task

A 2AFC detection and identification task was used in all experiments (see Figure 2.6). Subjects saw two subsequent stimulus frames, one of which contained a target contour, the other only a background of local stimulus elements with random orientation and spatial

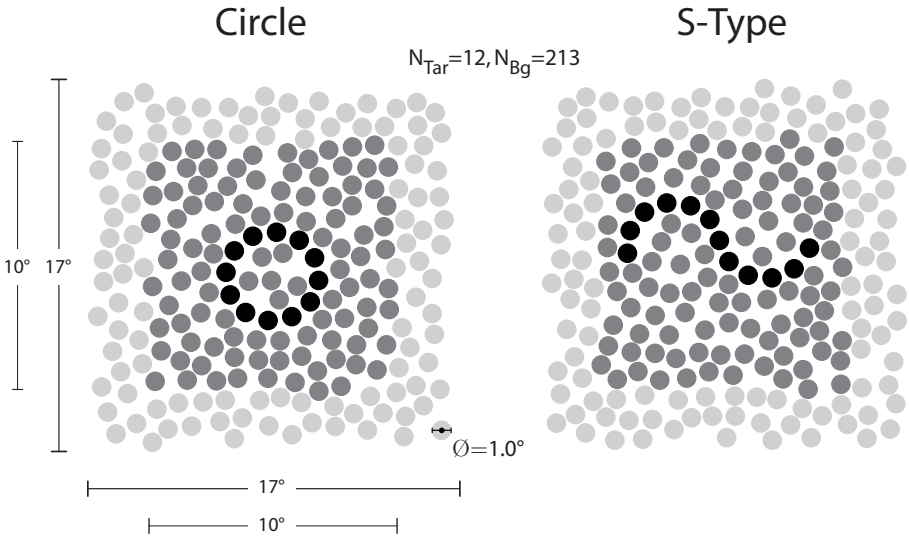

Figure 2.5: Illustration of the stimulus field geometry and the spatial outline of closed circular (left) and open S-type (right) target contours. Target and background Gabor element placement was done using the algorithm of Braun (1999). Elements in medium gray mark the area of possible contour placement.

frequencies sampled from the reference distribution. With the first button press subjects indicated whether the first or the second frame contained a target, with the second button press they indicated whether the target contour was a circle or an S-type figure. Contour type was randomly chosen with equal likelihood on each trial. The identification task was implemented to warrant that subjects did not only encode arbitrary contour fragments, including false positives, but saw a sufficiently large part of the intended contour. Detection and identification performance ought therefore not differ considerably. Acoustical feedback was provided about correctness for both judgements by a brief tone signal. Stimulus frame presentation was terminated by masking with spatial noise at a grain resolution of 3 pixels. Stimulus presentation time was selected according to the results of Braun (1999) who found saturating contour integration performance of human observers at inspection times of 350 ms. The temporal order of events was fixation (500 msec) - SOA (400 msec) - 1st stimulus frame (350 msec) - mask (400 msec) - SOA (400 msec) - 2nd stimulus frame (350 msec) - mask (400 msec) - blank frame until response.

2.4 Apparatus

Patterns were generated on a ViSaGe stimulus generator system manufactured by Cambridge Research Systems and displayed on a Samsung 959NF color monitor. The mean luminance of the screen was 50 cd/m^2. Stimuli were displayed with a fixed Michelson con-

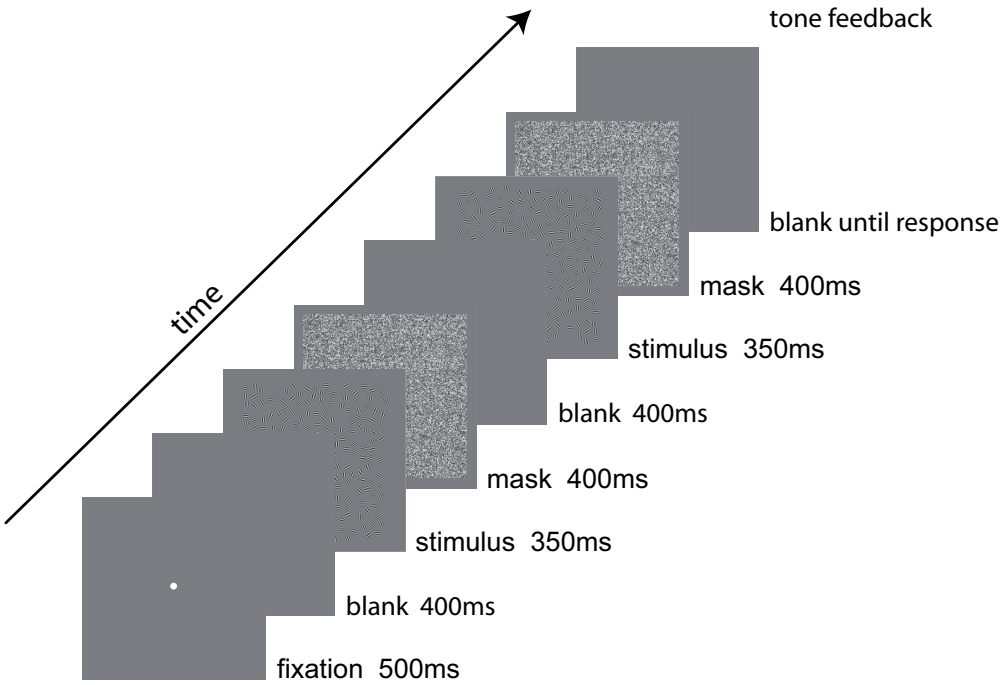

Figure 2.6: Temporal order of events in an experimental trial. A screen containing a small fixation mark initialized the sequence of events, which proceeded as shown. Depending on the experimental paradigm, subjects had to provide either one or two responses. The correctness of every response was immediately signaled by tone feedback.

trast of 0.85. Color values were taken from a linear grey staircase consisting of 255 steps chosen from a palette of 4096 possible grey values. The relation between grey level entries and the luminance on the screen was linearized by means of gamma correction tables. This linearity was checked before the experiment using a calibration program which determined the relation between grey value number (1 to 255) and luminance in cd/m^2 measured by a Cambridge Research Systems ColorCAL colorimeter. The determination coefficient of the regression line was in all cases larger than 0.98. The refresh rate of the monitor was 80 Hz at a horizontal frequency of 84.62 kHz, the pixel resolution was set to 1348×1006 pixels. The room was darkened so that the ambient illumination approximately matched the illumination of the screen. Patterns were viewed binocularly at a distance of 70 cm. Subjects used a chin rest for head stabilization and gave their responses with their dominant hand via an external response keyboard.

3 Perceptual Efficiency at Integrating Open and Closed Contours

Synopsis

Detection of smooth contours in cluttered backgrounds is often easier with contours enclosing an area of the stimulus field than with open contours. This led to speculations that there are special sensory routines for closure, stabilizing contour detection and rendering closed forms particularly robust against noise. To investigate whether detection of closed contours is more efficient we measured contour detection performance as a function of the element tilt angle along the contour, for various degrees of spatial frequency jitter in background and contour. Generally, contour detection performance declined with increasing spatial frequency jitter. Closed contours showed a clear detection advantage compared to open contours, with the same detection performance achieved at larger tilt angles at all spatial frequency jitter levels. Slope comparison in terms of the variation coefficient revealed that psychometric curves for closed contours are not steeper once the mean shift of the curves is taken into account. We thus prove that closed contours are easier to detect, but found no evidence that detection is more efficient in noise, suggesting that there are no particularly efficient detection routines involved with closure.

3.1 Introduction

Visual processing requires to decompose a visual scene into features, and to link features across space in order to form shapes and objects. Early in the twenties of the last century phenomenological laws of perceptual organization were formulated by the Gestalt psychologists (see Spillmann, 1999, for a review), which still have great impact on current attempts to understand sensory mechanisms involved in feature binding and object perception.

One prominent Gestalt principle is closure, meaning that line elements, or parts of a contour, are preferably grouped if their ends can be connected to form a closed 'whole'. Kovacs and Julesz (1993) were able to show that fragmented contours were better detected in cluttered backgrounds when their smooth global form was closed. Particularly, they

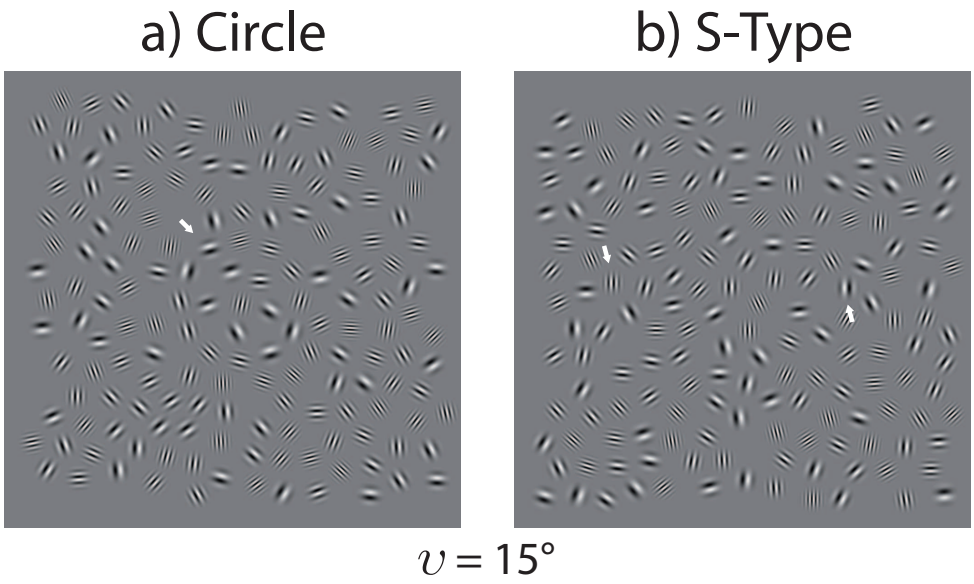

Figure 3.1: Illustration of the closure effect in contour integration. Each panel comprises a contour (highlighted by arrows) embedded in a stimulus random field varying both in orientation and spatial frequency. Panel (a) shows a closed circular contour, panel (b) contains an open contour with the shape of an 'S'. Inter-element angles are $30°$ for both contours, the only difference being the turning point at half length to generate the S-type contour. Local tilt angles are held constant at $\upsilon = 15°$ for both contours. The visibility advantage of the closed contour is immediately perceived.

showed that contour integration with closed contours is more robust against enlarged element spacing than with open contours. For closed contours larger gaps along the contour could be bridged, indicating a global influence on local integration of neighboring line elements of similar orientation. Further, closing a contour by adding missing final elements was found to produce a synergistic jump in the overall contour detection performance (see Figure 3.1), and contrast discrimination of line elements was facilitated inside a closed contour, compared to outside. The findings of Kovacs and Julesz were taken to indicate a reverberating excitatory circuit in closed contours, which may enhance figure ground segregation of the surrounded area. Pettet and coworkers found further evidence for such a hypothetical mechanism, substantiating the disruption in contour integration caused by corners and gaps, and showing larger robustness of closed contours against an increasing number of background noise elements (Pettet et al., 1998).

Further study of the closure effect revealed that it is not as general as initially thought. Braun (1999) showed that the advantage of closed contours is limited to contours formed by a small number of elements. He observed that the closure effect is relatively small when

contours exceed a critical length of about 12 elements. Moreover, it was pointed out that other important variables affecting contour detection performance, namely path angle and curvature, eccentricity, spatial certainty and local element density, are hard to balance such that a possible contour detection advantage is uniquely attributable to just closure with no confounds (Tversky et al., 2004). Controlling for eccentricity and spatial certainty, and precluding any density cues to the global contour in cluttered backgrounds, Tversky et al. obtained no clear closure advantage when the robustness of contour detection against orientation jitter was examined with contours made up made up by more than 12 contour elements. In another experiment with no orientation jitter along the contour they found a substantiate closure effect for contour detection performance when contour length was varied up to the critical 12 element length. However, this advantage was found to be compatible with probability summation among 5 element substrings, the minimum number of elements that is seemingly grouped as suggested by Kovacs and Julesz. With the same number of elements, a closed contour falls into more possible groups of 5 element substrings than an open contour, and, as the authors argue, if contour detection is conceived as a process where all possible 5 element strings independently compete for threshold, the observed advantage of closed contours should emerge, and the advantage for closed contours would just be an artifact of a higher combinatorial chance.

In the stimulus arrangement used by Tversky et al. the open contours used for performance reference had turning points, i.e. their form changed from convex to concave, while the closed forms were fully convex. The effect of turning points was recently studied by Mathes and Fahle (2007a), demonstrating that turning points usually impair contour detection, while closed contours still have some small detection advantage once the effect of turning points is canceled out. The remaining advantage, since it is small, does not uniquely point to closure, since it may be attributable to other clues of closed contour which are hard to control, or it may simply be due to probability summation among independent substrings.

Hence, if the detection advantage for closed contours with a larger number of elements is small, then it will be difficult to rule out the alternative explanation of probability summation among substrings, and therefore it will not be easy to prove that special routines are involved with closure. However, as argued by Kovacs and Julesz, contour integration may be more robust in noise for closed shapes. This points to another aspect of performance. For robustness of contour detection as the variable of interest a detection advantage effect is just one indicator. When analyzing detection stability, also the slope of psychometric curves should be taken into account. If there is a hypothetical closure mechanism serving to stabilize detection of contours in cluttered backgrounds, then psychometric curves recorded for orientation jitter along the contour (Field et al., 1993) should be more steep for closed contours, compared to open ones. However, one problem is that if there is a closure effect, then there will also be a mean shift, and, consequently, the slopes of psychometric curves cannot directly be compared for open and contours at the same location

on the orientation jitter scale.

As shown in early attempts of psychometric curve analysis (Crozier, 1936) the ratio of standard deviation to mean parameter, known as *variation coefficient*, gives valuable hints about the efficiency of a detector system. If the variation coefficient is constant across different mean parameters, then this means that the standard deviation of the underlying distribution rises proportional to the mean parameter, which is a common behavior of many statistical variables, such as mental test scores (Lord & Novick, 1968). In sensory analysis constancy of the variation coefficient was observed in simple discrimination tasks under various conditions (Crozier & Holway, 1937; Blackwell, 1963), which is known as *Crozier's law*, after its discoverer. Roufs (1974) was able to show that Crozier's law implies detector operation at a constant signal to noise ratio. Larger values of the variation coefficient imply stronger internal noise at the detection criterion, and therefore less efficient detection (Roufs, 1974; Mortensen & Suhl, 1991).

The analyses of Roufs were done within the framework of linear systems analysis, assuming separability of physical intensity and system response. This assumption, and the assumption of temporal peak detection made it possible to derive the direct correspondence of the variation coefficient with the ratio of the standard deviation of the internal noise to the sensory threshold. While temporal peak detection seems to be a reasonable assumption in many experimental situations (Mortensen & Suhl, 1991; Mortensen, 2002, 2007a, 2007b), separability of the amount of jitter and (nonlinear) response of the underlying contour detection circuit can surely not be assumed, precluding a direct correspondence of the variation coefficient with an internal noise to threshold ratio. However, this does not imply that an analysis in terms of psychometric curve slopes and variation coefficients does not lead to valuable insights about a possibly higher detection efficiency of closed contours in the vicinity of the detection threshold. If there are particular sensory routines involved with closure, such as reverberating stabilizing circuits, internal noise reduction should result in higher slopes of psychometric curves for the same mean parameters. This means that variation coefficients should generally tend to be smaller for closed contours, irrespective of a direct interpretation in terms of internal noise and threshold parameters.

3.2 Methods

3.2.1 Experimental Rationale

Aim of the experiment was to measure the effects of three experimental conditions differing by the degree of Gabor carrier spatial frequency jitter applied to contour and background elements on contour detection performance, and to compare the performance for open and closed contours within these conditions. Comparison was along three performance measures. These were tilt angle threshold (Field et al., 1993), defined as the 0.75 point v_0 of the

psychometric curve for a 2AFC measurement, the standard deviation measure, as derived from the slope estimate in x_0, and the generalized variation coefficient q_0, as calculated from the first two measures. Estimates of v_0 and σ were taken for three different levels of spatial frequency jitter in order to prove whether robustness of detection in noise is different for open and closed contours. Data preparation and outlier analysis was done such that univariate statistical analysis of each measurement variable, as well as bivariate analysis was enabled by verifying bivariate normality with an appropriate test.

3.2.2 Stimulus Micropatterns

Stimulus displays consisted of contours made up by Gabor micropatterns aligned along a smooth path, embedded in Gabor random fields. Detectability of target contours was modulated by rotating a Gabor element away from its perfect alignment with the contour by an angle of v. Increasing this tilt angle results in decreasing contour detection performance. Gabor micropatterns were defined according to (2.1).

3.2.3 Orientation and Spatial Frequency Jitter

Orientation jitter was applied to the background elements in all experimental conditions. Orientation jitter was maximum, sampling φ uniformly from the interval $[0°, 180°]$.
There were three conditions of spatial frequency jitter:

1) Spatial frequency was constant for both the contour and the background elements with $f_{cont} = f_{bg} = \overline{f}$ (see below);

2) Spatial frequency was constant for the contour elements ($f_{cont} = \overline{f}$) and heterogenous for the background. In the background, spatial frequency was randomly sampled (see below);

3) Spatial frequency was heterogenous for both contour and background. For elements of both, spatial frequency was randomly sampled (see below).

For obtaining spatial frequencies of a random distribution we defined spatial frequencies as $f = 2^u$ and sampled u from a uniform distribution in the interval $[1, 3]$. So spatial frequencies were in the interval $[2, 8]$, measured in units of cycles per degree, (cpd). The expected value of the exponential spatial frequency distribution resulting from this procedure is $\overline{f} = 4.33$ cpd[1]. This constant value was used in the first condition with no spatial frequency jitter for background and contour elements, and in the second condition for spatial frequency values along the contour. Stimulus examples for the three spatial frequency jitter conditions, for open and closed contours, are shown in Figure 3.2.

[1]The arithmetic mean μ_f in cycles per degree (cpd) of the density function $f(u) = 2^u$ in the interval $u = [u_l, u_h]$, can be easily derived as $\mu_f = \frac{F(u_h)-F(u_l)}{u_h-u_l}$, with $F(u) = \frac{2^u}{\log 2}$ the integral of $f(u)$.

3.3 Procedure

3.3.1 Subjects

22 undergraduate students served as observers. Fourteen subjects were female, eight male. All subjects had normal or corrected to normal vision. The students had no former psychophysical experience, were paid and not informed about the purpose of the experiment.

3.3.2 Preparation Measurements and Calibration of Individual Parameter Values

Tilt angles v were calibrated at five performance levels for both contour types and all three spatial frequency conditions, and individually for each subject. In preparation measurements psychometric function data were recorded, and fit with Weibull distribution functions. This was done twice, and separately for each target condition. On the basis of the curve fitting results of the second measurement a set of tilt angles was extrapolated for each experimental condition, which corresponded to five fixed levels of proportions of correct judgements. These levels were selected as rates of 0.59, 0.67, 0.75, 0.83 and 0.91. In the main experiment the individually calibrated sets of tilt angles were used in the six target conditions for each subject. Measuring detection rates twice at 5 tilt angles, each with 32 replications, for 6 target conditions means that each subject had to get through 1920 trials before the main experiment, which took about two hours.

3.3.3 Main Experiment

After calibration of the tilt angle sets for each subject the main experiment was executed where all target conditions were randomly intermixed in a single experimental block. With 5 tilt angles, 6 target conditions and 32 replications each subject had to complete 960 trials, which took about one hour. The trials were completely randomized and administered in a single session with a brief pause.

3.4 The Variation Coefficient Obtained from Psychometric Curves

To judge the processing efficiency with which open and closed contours are integrated, a variation coefficient q, whereupon data analysis will be predominantly based, is be derived in what follows.

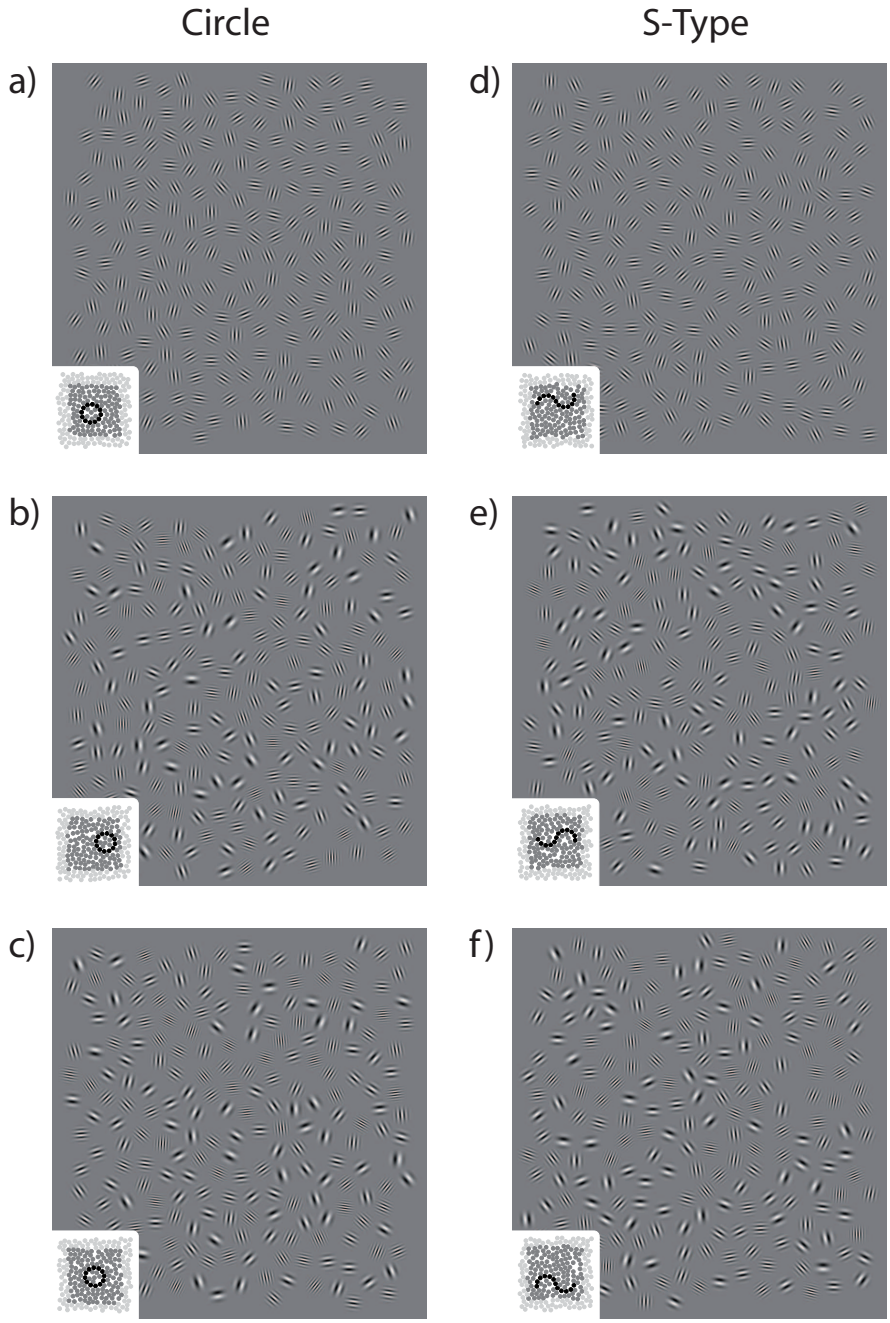

Figure 3.2: Examples of Gabor stimulus displays with closed target contours (left panel) and open target contours (right panel), without spatial frequency jitter (upper panel, (a) and (d)), with spatial frequency jitter only in background (middle panel, (d) and (e)), and spatial frequency jitter in background and along the contour (lower panel, (c) and (f)). In the examples, the tilt angle, i.e. the rotation angle of the Gabor elements relative to the contour path, is set to $0°$. The pictographs in each image indicate the position of the contour in the field.

Let x be a physical nonnegative variable describing a stimulus quantity. Then, in a two alternative forced choice experiment, the psychometric function obtained for this quantity has the general form

$$P(x) = 1 - (1 - g)\,(1 - F(x))\,. \tag{3.1}$$

Here, g is the probability of guessing, which is $g = 0.5$ for two choice alternatives, and $F(x)$ is the probability that the internal decision criterion is surpassed given the stimulus quantity x. Suppose that the distribution function $F(x)$ can be described by an integrated Gaussian

$$F(x) = \frac{1}{\sqrt{2\pi}\sigma} \int_{-\infty}^{x} \exp\left(-\frac{1}{2}\left(\frac{v-\mu}{\sigma}\right)^2\right) dv. \tag{3.2}$$

The slope of F at μ is given by

$$\delta = \left.\frac{dF}{dx}\right|_{\mu} = \left(\sqrt{2\pi}\sigma\right)^{-1} \tag{3.3}$$

The standard deviation σ of the underlying distribution $f(x)$ can thus be obtained directly from the determination of the slope of F:

$$\sigma = \left(\delta\sqrt{2\pi}\right)^{-1}. \tag{3.4}$$

The ratio of standard deviation to expected value

$$\rho = \frac{\sigma}{\mu} = \frac{\delta^{-1}}{\mu}\left(\sqrt{2\pi}\right)^{-1} \tag{3.5}$$

is called the *variation coefficient*. Since the standard deviation is inversely proportional to the slope at μ, the variation coefficient reflects the spread of $f(x)$ relative to the location on the scale. As can be shown, if the variation coefficient is constant, then the corresponding distribution functions are parallel when the physical quantity x is expressed on a logarithmic scale (see Appendix A).

It is possible to define a generalized variation coefficient by evaluating the ratio of the reciprocal of slope in a particular quantile x_0 relative to this quantile of a distribution function. The ratio

$$q_0 = \frac{\delta^{-1}}{x_0} = (\delta x_0)^{-1} \tag{3.6}$$

with $x_0 = F^{-1}(p_0)$ and $\delta = dF/dx|_{x_0}$ is proportional to the variation coefficient for a normal distribution with $p_0 = 0.5$ (see equation (3.5)) and can be used with other distribution functions, as the Weibull. For a Weibull distribution function

$$F\,(x) = 1 - \exp\left(-ax^b\right) \tag{3.7}$$

the generalized variation coefficient takes the form

$$q_0 = (\delta x_0)^{-1} = \frac{e}{b} \tag{3.8}$$

for $p_0 = 1 - 1/e$ (≈ 0.632). For $p_0 = 0.5$, which corresponds to a detection probability of 0.75 in a 2AFC task, one obtains

$$q_0 = \frac{e^{\ln(2)}}{b \ln(2)}. \tag{3.9}$$

(see Appendix B). Equations (3.8) and (3.9) show that the variation coefficient taken from Weibull functions is independent of the scale parameter, just the shape parameter b enters.

3.5 Results

3.5.1 Psychometric Curves

Psychometric curves were obtained for each subject in each of the six experimental conditions. As a function of the tilt level v, they had the general form

$$P(v) = 1 - 0.5F(v), \tag{3.10}$$

which means that detection rates *decrease* with increasing tilt angle v. For fitting psychometric curves the Weibull model

$$F(v) = 1 - c \exp\left(-av^b\right) \tag{3.11}$$

was used and its three parameters a, b and c were estimated with the Levenberg-Marquardt algorithm. Figure 3.3 gives an overview of the results, and Tables 3.1 and 3.2 list the parameter estimates, as well as the absolute 0.75 point (v_0), and the standard deviation estimate (σ_0), as derived from (3.11) by using (3.4). This means that the Weibull model was used for convenience to estimate the mean and standard deviation parameters of an assumed normal distribution, i.e. the Weibull model was used as an approximation, which is known to work fairly well (see Quick, 1974). A shrink parameter c was estimated to account for saturation performance below 1, but this parameter was necessary in only few cases, and it was canceled out in the slope estimate to avoid that the shrink parameter enters the estimate of the standard deviation parameter.[2]

[2]The slope was estimated for the quantile where the Weibull function was at half amplitude, $c/2$. So $p_0 = 0.5 + 0.25c$ was the criterion detection rate for the estimation of slope δ. Since, for most of the cases, c was 1, this quantile was the 0.75 point of the psychometric curve (3.10). Note that, with respect to the distribution function, different half amplitudes $c/2$ correspond to the same point $v_0 = \left(\frac{\ln 2}{a}\right)^{1/b}$, i.e. relative to the function, the same point is estimated for different values of c. Since the constant c enters the slope estimate, it was canceled out in order to obtain a slope estimate which is independent of a possible shrink parameter $c < 1$. Curve fitting accuracy was generally high, reaching a ratio of explained to total variation of $\eta^2 > .85$ on average. The quality of the fit was substantially poorer in only some cases.

	UNI							SEMI-MULTI							MULTI						
no.	a	b	c	η^2	v_0	σ_0		a	b	c	η^2	v_0	σ_0		a	b	c	η^2	v_0	σ_0	
1	.053	2.72	1.00	.77	16.54	7.01		.047	2.92	1.00	.82	18.96	7.48		.057	3.65	1.00	.98	15.81	4.99	
2	.043	3.46	1.00	.74	20.81	6.93		.047	4.54	1.00	.99	19.47	4.93		.052	3.88	1.00	.90	17.45	5.17	
3	.045	5.83	1.00	.96	20.69	4.09		.043	6.50	1.00	.95	21.89	3.88		.048	3.76	1.00	.78	18.75	5.74	
4	.043	8.06	1.00	.98	22.39	3.20		.035	3.41	1.00	.98	25.66	8.66		.047	3.61	1.00	.97	19.37	6.17	
5	.054	2.31	1.00	.50	15.82	7.87		.063	2.31	1.00	.74	13.48	6.72		.062	4.65	1.00	.97	14.83	3.67	
6	.066	2.28	1.00	.53	12.95	6.53		.088	1.93	1.00	.74	9.38	5.60		.083	2.83	1.00	.97	10.65	4.33	
7	.082	2.83	.67	.90	7.92	6.42	$\star$	.074	1.71	1.00	.78	10.95	7.38		.092	3.63	.75	.97	8.50	4.18	
8	.046	1.96	1.00	.71	18.03	10.58		.051	2.35	1.00	.85	16.87	8.25		.062	20.74	.69	.96	15.38	1.29	$\star$
9	.048	1.44	1.00	.68	16.33	13.03		.064	2.66	.63	.97	8.96	9.39		.083	19.85	.69	.96	11.36	1.00	$\star$
10	.058	2.09	1.00	.86	14.37	7.91		.062	3.25	.66	.96	10.78	7.75		.146	1.15	1.00	.69	4.98	4.97	
11	.039	8.82	1.00	.99	24.49	3.20		.055	5.35	1.00	.88	16.91	3.64		.068	2.48	1.00	.95	12.63	5.87	
12	.044	5.31	1.00	.89	21.28	4.61		.050	7.84	1.00	.89	19.05	2.80		.048	2.94	1.00	.71	18.37	7.18	
13	.050	17.53	1.00	.96	19.45	1.28		.044	11.56	1.00	.96	21.79	2.17		.044	3.89	1.00	.97	20.84	6.17	
14	.042	7.34	1.00	.81	22.40	3.51		.042	7.95	1.00	.62	22.99	3.33		.046	2.92	1.00	.75	19.00	7.48	
15	.044	5.48	1.00	.94	21.03	4.42		.041	4.84	1.00	.96	22.39	5.33		.049	5.91	1.00	.96	19.38	3.78	
16	.046	8.70	1.00	.97	20.88	2.76		.041	6.37	1.00	.85	23.14	4.18		.052	4.99	1.00	.90	17.86	4.12	
17	.043	4.23	1.00	.95	21.49	5.85		.042	6.28	1.00	.98	22.47	4.12		.050	5.32	1.00	.89	18.56	4.01	
18	.044	5.64	1.00	.98	21.14	4.32		.036	6.65	1.00	.91	26.38	4.57		.048	2.69	1.00	.99	18.06	7.74	
19	.043	4.97	1.00	.91	21.40	4.95		.044	5.30	1.00	.92	21.24	4.62		.051	3.93	1.00	.99	17.73	5.19	
20	.044	6.78	1.00	.95	21.30	3.62		.042	3.63	1.00	.81	21.46	6.80		.049	3.35	1.00	.86	18.35	6.31	
21	.043	7.40	1.00	.95	22.35	3.48		.040	5.76	1.00	.98	23.51	4.70		.045	8.91	1.00	.99	21.26	2.75	
22	.044	6.31	1.00	.99	21.62	3.94		.036	4.94	1.00	.94	25.68	5.98		.043	7.77	1.00	.97	22.30	3.31	
mean	.048	5.52	.99	.86	19.30	5.43		.049	4.91	.97	.89	19.25	5.56		.060	5.58	.96	.91	16.43	4.79	
mean*	.047	5.65	1.00	.86	19.85	5.39		.049	4.91	.97	.89	19.25	5.56		.059	4.11	.99	.91	16.73	5.16	

Table 3.1: Psychometric curve fitting results for closed contours. The table lists the parameter values for scale (a), shape (b) and shrink parameter (c) obtained for the Weibull model (3.11) with the Levenberg-Marquardt algorithm, as well as the goodness of fit in terms of the ratio of explained to total variation (η^2), the absolute 0.75 point (v_0) for the psychometric curve (3.10) and the standard deviation estimate (σ_0) obtained from (3.4) by evaluating the slope of $F(v)$ at half amplitude (see Footnote 4). The cases that were labelled as outliers with the Q-Q plot method (see below) are marked by an asterisk. The second last line shows the means of all parameter estimates, the last line shows the means for the samples cleared for outliers.

	UNI							SEMI-MULTI							MULTI						
no.	a	b	c	η^2	v_0	σ_0		a	b	c	η^2	v_0	σ_0		a	b	c	η^2	v_0	σ_0	
1	.068	2.96	1.00	.87	13.02	5.06		.070	5.74	1.00	.86	13.44	2.69		.057	1.55	1.00	.91	13.94	10.39	
2	.071	3.91	1.00	.96	12.84	3.78		.058	3.18	1.00	.85	15.37	5.57		.059	1.33	1.00	.99	12.96	11.23	
3	.054	3.64	1.00	.91	16.88	5.33		.051	1.89	1.00	.58	16.01	9.75		.059	4.03	1.00	.99	15.54	4.43	
4	.050	2.95	1.00	.87	17.62	6.88		.053	5.07	1.00	.74	17.41	3.95		.057	2.38	1.00	.96	14.99	7.25	
5	.074	3.61	1.00	.51	12.17	3.88		.082	1.86	1.00	.83	9.97	6.17		.055	6.42	.55	.93	12.76	5.62	
6	.080	3.81	1.00	.52	11.28	3.41		.113	1.96	1.00	.84	7.34	4.31		.066	6.86	.55	.93	10.91	4.38	
7	.053	5.36	.65	.81	14.78	5.89		.091	1.39	1.00	.64	8.44	6.99		.099	1.40	.62	.99	3.44	10.23	$\star$
8	.073	.79	.75	.97	4.30	16.96		.058	1.48	.69	.84	7.96	15.15		.076	1.26	1.00	.96	9.78	8.97	$\star$
9	.062	1.12	.75	.98	7.16	15.90		.088	1.57	.69	.86	5.51	9.58		.072	1.29	1.00	.96	10.38	9.28	
10	.146	6.73	1.00	.97	6.49	1.11	$\star$	.188	.91	1.00	.86	3.57	4.50		.362	.62	1.00	.92	1.54	2.83	$\star$
11	.051	5.00	1.00	.70	18.37	4.23		.056	5.27	1.00	.84	16.64	3.64		.072	4.63	1.00	.90	12.79	3.18	
12	.049	2.99	1.00	.72	17.91	6.90		.053	6.04	1.00	.91	17.81	3.39		.064	3.04	1.00	.92	13.85	5.24	
13	.052	4.32	1.00	.99	17.69	4.71		.054	3.57	1.00	.93	16.65	5.37		.074	3.02	1.00	.84	11.99	4.57	
14	.052	4.17	1.00	.84	17.67	4.87		.052	5.86	1.00	.99	18.03	3.54		.061	3.32	1.00	.87	14.58	5.05	
15	.047	3.22	1.00	.86	18.88	6.75		.047	3.15	1.00	.97	18.89	6.90		.066	5.12	1.00	.89	14.13	3.18	
16	.056	2.10	1.00	.77	14.99	8.23		.055	3.26	1.00	.85	16.28	5.75		.065	1.49	1.00	.89	11.97	9.25	
17	.049	4.98	1.00	.98	18.96	4.38		.037	2.81	1.00	.77	23.79	9.73	$\star$	.067	2.80	1.00	.84	13.00	5.35	
18	.048	3.63	1.00	.97	19.02	6.04		.040	2.45	1.00	.91	21.54	10.12		.053	2.32	1.00	.81	16.23	8.04	
19	.041	1.96	1.00	.81	20.38	11.96	$\star$	.048	3.41	1.00	.92	18.63	6.30		.063	2.43	1.00	.89	13.57	6.42	
20	.046	1.98	1.00	.94	18.08	10.50	$\star$	.048	4.36	1.00	.92	19.11	5.04		.072	3.25	1.00	.97	12.33	4.36	
21	.053	5.02	1.00	.96	17.38	3.98		.056	5.27	1.00	.95	16.72	3.65		.065	2.71	1.00	.87	13.41	5.69	
22	.053	3.81	1.00	.83	16.99	5.13		.050	7.50	1.00	.98	19.15	2.94		.055	3.06	1.00	.91	15.99	6.02	
mean	.060	3.55	.96	.85	15.13	6.63		.066	3.55	.97	.86	14.92	6.14		.079	2.92	.94	.92	12.28	6.41	
mean*	.058	3.55	.95	.84	15.15	6.44		.067	3.58	.97	.82	14.50	5.97		.063	3.21	.95	.91	13.44	6.26	

Table 3.2: Psychometric curve fitting results for open contours. Conventions as in Table 3.1.

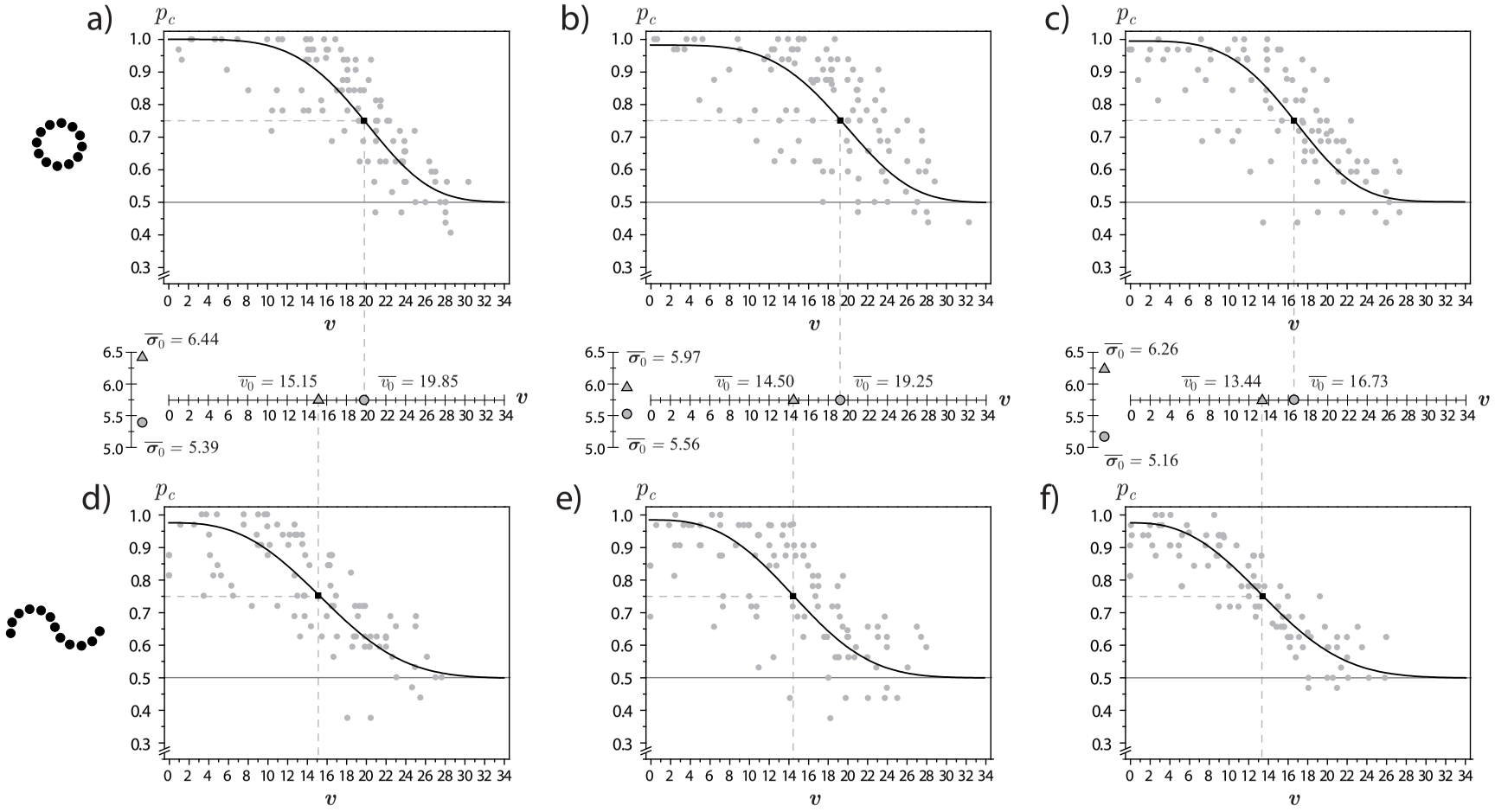

Figure 3.3: Psychometric curve data for closed (upper row) and open contours (lower row) for no spatial frequency jitter (left column), spatial frequency jitter in background (middle) and spatial frequency jitter in background and along the contour (right). Data points represent a proportion correct measure. The data shown are cleared for outliers, as described below. For each experimental condition a summary psychometric curve is drawn (solid line). This curve is a Weibull function that intersects at the between subject mean tilt angle threshold, $\overline{v_0}$, and has slope calculated from the mean standard deviation estimate. Mean jitter threshold and standard deviation estimates are projected onto a common axis (middle horizontal panel) to enable a first inspection of the effects of contour type on these variables (closed contours: circles; open contours: triangles).

As can be seen from the mean estimates of v_0 and σ_0, open contours have higher average tilt angle thresholds, and their psychometric curves tend to be steeper. These differences in the standard deviation estimates between both contour types are consistent over all spatial frequency jitter levels. The effects are illustrated by the summary psychometric curves shown in Figure 3.3, which are drawn through the mean tilt angle threshold, $\overline{v_0}$. Their scale and shape parameters were adjusted such to match the slope value, as calculated from the mean standard deviation estimates, $\overline{\sigma_0}$, via (3.3). This was done in order to enable capturing the effects of spatial frequency jitter level on both jitter threshold and slope directly from the psychometric curves.[3] It is seen that the curves for closed contours are clearly rightward shifted relative to the curves for open contours, and their steepness is some degree higher, and clearly higher for the condition with spatial frequency jitter on contour and background. Most extreme estimates of jitter threshold and standard deviation are obtained for open contours in this condition (see Figure 3.3f and Table 3.2).

3.5.2 Data Clearing and Preparation of Statistical Testing

In order to prepare statistical testing with both dependent variables mean jitter level and standard deviation estimate we cleared the data for outliers, and we verified bivariate normality of each sample. A proper method of outlier identification is provided in multivariate distribution fitting analysis. The logic of outlier exclusion is to consider the cases as outliers that show strong deviation from the expected quantiles in a Q-Q plot. In most cases, these are the observations with larger quantiles than the largest expected quantile calculated for a multivariate normal distribution with sample size N. After outlier exclusion a test can be applied that proves the degree to which empirical quantiles and expected quantiles coincide (see Johnson & Wichern, 2003, p. 184ff). This method was applied to the two-digit data vectors $\mathbf{x}$ composed of v_0 and σ_0 in each of the six experimental conditions with sample size $N = 22$. For each of the $j = 1, \ldots, 6$ groups, a bivariate normal density can be estimated according to[4]

$$f_j(\mathbf{x}) = \frac{1}{2\pi|\mathbf{S}_j|^{1/2}} \exp\left(-\frac{1}{2}(\mathbf{x} - \overline{\mathbf{x}}_j)'\mathbf{S}_j^{-1}(\mathbf{x} - \overline{\mathbf{x}}_j)\right). \tag{3.12}$$

Here, $\mathbf{S}_j^{-1}$ is the inverse of the unbiased estimate of the variance-covariance matrix in group c_j, $\mathbf{x}$ is an observation, and $\overline{\mathbf{x}}_j$ is the unbiased estimate of the centroid of group c_j.[5] In (3.12), all points $\mathbf{x}$ with squared Mahalanobis distance

$$D_j^2(\mathbf{x}) = (\mathbf{x} - \overline{\mathbf{x}}_j)'\mathbf{S}_j^{-1}(\mathbf{x} - \overline{\mathbf{x}}_j) = \chi_2^2(p) \tag{3.13}$$

[3] The Weibull functions shown in Figure 3.3 have shape parameter $b = \delta_0\overline{v_0}\exp(\ln 2)/\ln(2)$ and scale parameter $a_0 = \ln(2)/\overline{v_0}^b$ with $\delta_0 = \left(\overline{\sigma_0}\sqrt{2\pi}\right)^{-1}$. This means that the steepness of the curves is exactly inversely proportional to the mean standard deviation estimates given in Tables 3.1 and 3.2.

[4] Vectors are typed boldface, and the inverted comma denotes transposing.

[5] The unbiased sample variance-covariance matrix $\mathbf{S}$ has (i,k)th entry $(N-1)^{-1}\sum_{l=1}^{n}(x_{li} - \overline{x}_i)(x_{lk} - \overline{x}_k)$.

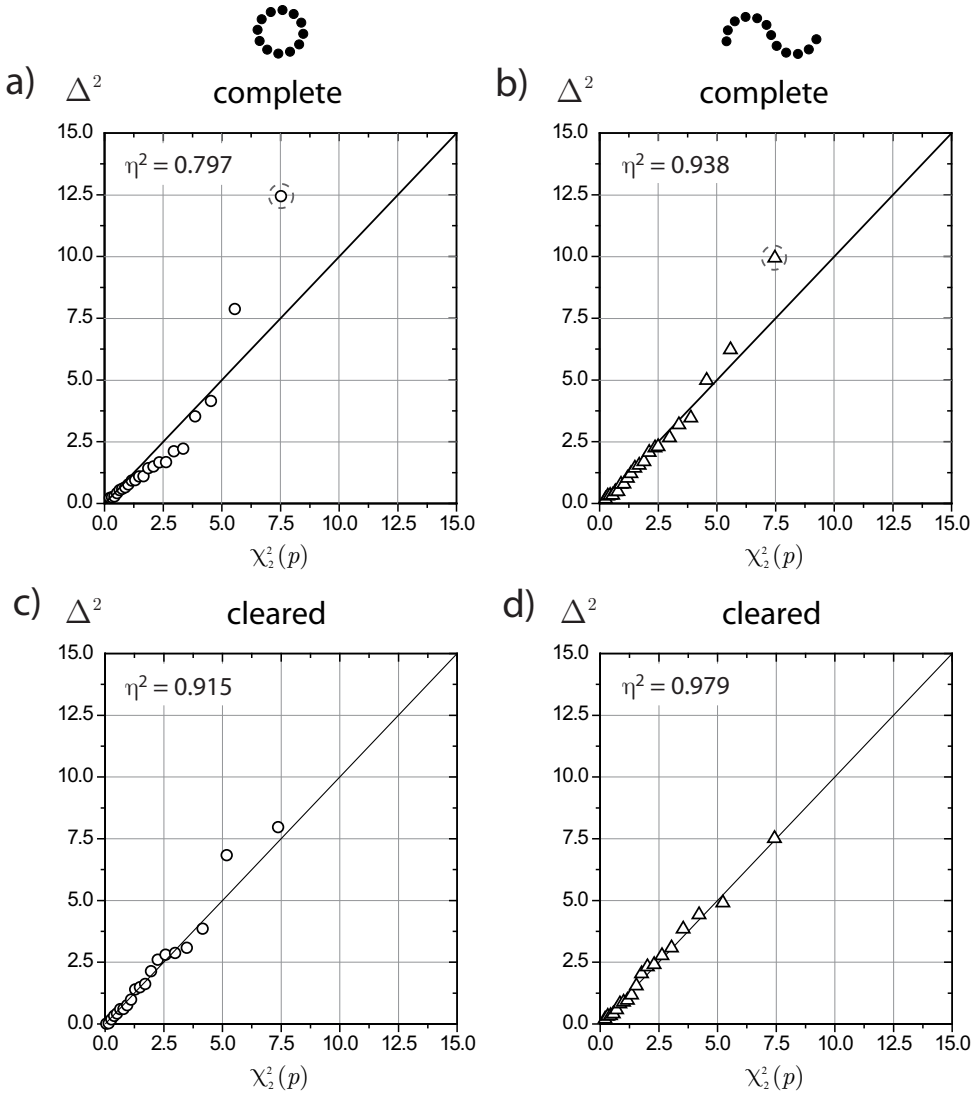

Figure 3.4: Assessing bivariate normality with a Q-Q plot method. The plots show the observed squared Mahalanobis distances D^2 as the quantiles for a rough approximation to the distribution function on the Y- axis, and the expected quantiles (Chi-squares), as derived from the χ^2- distribution with 2 degrees of freedom, on the X- axis. The diagonal is the line where observed and expected quantiles coincide. The η^2 measure reflects the degree of coincidence in terms of the ratio of explained to total variation. The left panel shows the data for closed contours with jitter in spatial frequency and orientation along the contour and in the background. The right panel shows the data for open contours with orientation jitter only. The upper panel contains the complete data sets with outliers marked by dashed grey circles, the lower panel the data sets after removing outliers and recalculation of squared Mahalanobis distances. Improvement of the η^2 measure due to the elimination of one outlier is about 12% for the example shown to the left, and about 4% for the example shown to the right.

	closed					open				
	complete			cleared		complete			cleared	
	η^2	r	ΔN	η^2	r	η^2	r	ΔN	η^2	r
uni	0.797	0.944	1	0.915	0.976	0.842	0.934	3	0.936	0.972
semi-multi	0.919	0.981	0	0.919	0.981	0.902	0.965	1	0.980	0.991
multi	0.962	0.971	2	0.988	0.994	0.938	0.981	3	0.979	0.990

Table 3.3: Results of evaluating the degree of coincidence of empirical quantiles and the quantiles expected from the assumption of bivariate normality. The table shows the ratio of explained to total variation, η^2, and the pearson correlation coefficient of empirical and expected quantiles, r, for open (cols. 2-6) and closed contours (cols. 7-11), before and after outlier exclusion, and for the three jitter conditions. Also shown is the number of excluded outliers, ΔN.

form the $p-$th quantiles of a bivariate normal distribution (see Johnson & Wichern, 2003, p. 155). This means that, if $\mathbf{x}$ and $\mathbf{u}$ are bivariate normally distributed, then for the squared Mahalanobis distance $D^2(\mathbf{x})$ the likelihood

$$P\left(D^2(\mathbf{u}) \leq D^2(\mathbf{x})\right) = F_{(\chi^2_2;2)}\left(D^2(\mathbf{x})\right) \tag{3.14}$$

is given by the distribution function of a Chi-Square distribution with 2 degrees of freedom.

From (3.13) and (3.14) a simple test for bivariate normality derives, that also enables a method of outlier exclusion. For the i- th data point of each class c_j, calculate $\chi^2_2((N - i + 0.5)/N)$, then calculate squared Mahalanobis distances $D^2_j(\mathbf{x}_{ij})$ and plot them in ascending order against the χ^2_2 quantiles to result in a Q-Q plot. The coincidence of empirical quantiles, $D^2_j(\mathbf{x}_{ij})$, and expected quantiles, $\chi^2_2((N - i + 0.5)/N)$, can be evaluated by the ratio of explained to total variation

$$\eta^2_j = 1 - \frac{\sum_i (D^2_{ij} - \chi^2_i)^2}{\sum_i (D^2_{ij} - \overline{D^2_j})^2} \tag{3.15}$$

and by the Pearson correlation coefficient of the quantiles

$$r_j = \frac{\sum_i \left(D^2_{ij} - \overline{D^2_j}\right)\left(\chi^2_i - \overline{\chi^2_i}\right)}{\sqrt{\sum_i \left(D^2_{ij} - \overline{D^2_j}\right)^2 \sum_i \left(\chi^2_i - \overline{\chi^2_i}\right)^2}}. \tag{3.16}$$

The results of applying (3.15) and (3.16) to the Q-Q plot data are shown in Table 3.3. An illustration of the method is given in Figure 3.4. The figure shows Q-Q plot data for complete data sets, and cleared for outliers. The figure shows for two examples that the coincidence of observed and expected quantiles is impaired by one outlier in the complete

Sample size	Significance level α		
N	0.01	0.05	0.10
5	0.8299	0.8788	0.9032
10	0.8801	0.9198	0.9351
15	0.9126	0.9389	0.9503
20	0.9269	0.9508	0.9604
25	0.9410	0.9591	0.9665

Table 3.4: Critical correlation values for the Q-Q plot method test of multivariate normality, as derived by Filliben (1975). Critical correlations are listed for three significance levels and up to sample sizes of $N = 25$.

data sets, but becomes well after removing the outlier, which is, for both examples shown, the observation with largest squared Mahalanobis distance.

Table 3.3 shows that data clearing was highly efficient by improving the ratio of explained to total variation η^2 to values of beyond $.91$ by excluding maximally 3 of $N = 22$ observations.

A statistical test can be applied to judge whether the assumption of bivariate normality is hurt, even at small sample sizes as given here. This test is based on the quantile correlation r, and enables to reject the assumption of bivariate normality at a level of significance, α, if r falls below a critical correlation, r_0 (Filliben, 1975). A sketch of critical correlation values is given in Table 3.4. Comparison with the critical values listed there shows that it is not possible to reject the assumption of bivariate normality for the cleared data sets at a significance level of smaller than $\alpha = 0.1$. This means that bivariate normality can be assumed for the six data sets, which is a prerequisite of multivariate statistical testing, and of correlation analysis.[6]

3.5.3 Statistical Testing

Jitter threshold and standard deviation estimates derived from the psychometric curve data and subsequently cleared for outliers, as described above, were fed into MANOVA procedures, which allowed to test the effects of contour type (open and closed contours), jitter level (univariate, semi-multivariate and multivariate) and their interaction with univariate and multivariate routines. Both factors, contour type and jitter level, are repeated measurements factors. Outliers, since it were few (see Table 3.3), were treated as missing data, and were replaced by between subject cell means. Tables 3.5 and 3.6 summarize the results of the univariate analyses for both dependent measures, and Table 3.7 gives a MANOVA results survey. Figure 3.5 illustrates the major findings.

[6]Note that bivariate normality implies normality of each univariate marginal distribution.

Source of Variation	*SS*	*df*	var'	*F*	*P*
Contour type (A)	594.673	1	594.673	85.539	0.000
Jitter level (B)	138.058	2	69.029	7.464	0.002
A × B	14.881	2	7.441	1.761	0.184
A × Vpn	145.994	21	6.952		
B × Vpn	388.422	42	9.248		
Residual	177.448	42	4.225		

Table 3.5: ANOVA results for the tilt angle threshold estimates, v_0. The table shows the source of variation, sum of squares, SS, degrees of freedom, df, variance estimate, var', F- ratio, F, and significance level, P.

Source of Variation	*SS*	*df*	var'	*F*	*P*
Contour type (A)	7.217	1	7.217	2.755	0.112
Jitter level (B)	1.037	2	0.518	0.155	0.857
A × B	4.675	2	2.337	0.609	0.548
A × Vpn	55.012	21	2.620		
B × Vpn	140.320	42	3.341		
Residual	161.119	42	3.836		

Table 3.6: ANOVA results for the standard deviation estimates, σ_0. Conventions as in Table 3.5.

75% thresholds decline with increasing level of spatial frequency jitter for open and closed contours in a similar way, and are reached for closed contours at much larger tilt angles. Both factors, frequency jitter level and contour type, are highly significant with no significant interaction for the jitter threshold estimates v_0 (see Table 3.5). For the standard deviation estimates σ_0 there neither is an effect of jitter level, nor of contour type (see Table 3.6). For open contours the estimates are consistently higher, but the difference to closed contours is not significant (see Table 3.6). Multivariate testing with both dependent measures yields the same overall statistical result as univariate testing with the jitter threshold estimates only (see Table 3.7).

Planned pairwise comparisons of jitter threshold estimates show that thresholds without any frequency jitter are higher than for frequency jitter along the contour and in background, for open and closed contours (see Table 3.8).[7] For closed contours, also the second jitter condition differs significantly from the third. Generally, closed contours are detected at significantly larger tilt angles, and the fact that closed contours with spatial frequency

[7]Planned pairwise comparisons were also computed in the bivariate space using Hotelling's T^2 test. It turned out that nearly the same results are obtained with both dependent variables, so the judgements with respect to the experimental conditions qualitatively agree for both ways of testing.

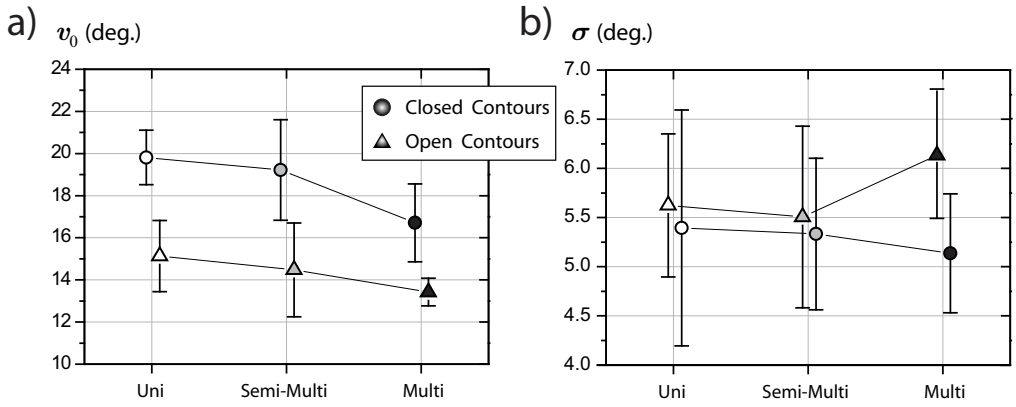

Figure 3.5: Between subject means of tilt angle threshold estimates v_0, defined as the 0.75 points of the psychometric curves (a), and the standard deviation estimates σ_0 (b), for open (triangles) and closed (circles) contours, plotted for the three jitter conditions. Error bars denote the 95% confidence limits of the means, based on the standard error derived from the residual variance estimates of the ANOVA procedures.

jitter along contour and in background (black filled circle in Figure 3.5a) are seen even slightly (but not significantly) better than open contours without any spatial frequency jitter (open triangle) illustrates the strength of the closure effect with the jitter threshold measure.

Besides the fact that standard deviation estimates are seemingly independent of the frequency jitter level and are only marginally higher for open contours, it is striking that contour detection in displays with background frequency jitter is as good as without any frequency jitter. This result is independent of contour type, and is illustrated best by the centroids of both conditions, which are nearby in the space spanned by jitter threshold and standard deviation estimates (see open and grey filled symbols in Figure 3.6). In this space one also sees that performance deteriorates with open contours and spatial frequency jitter along contour and in background. This condition yields largest standard deviation and lowest jitter threshold estimates. Multivariate pairwise testing of this condition to the mean of both conditions with less, respectively, no spatial frequency jitter shows that this increase in standard deviation and decrease of jitter threshold is significant (Hotelling's T^2 test, $F = 3.552, df_t = 2, df_e = 20, P = 0.047$; see dashed ellipse and dashed circle in Figure 3.6).

3.5.4 Within Group Correlation Analysis

While the analysis of jitter threshold and standard deviation estimates for different levels of spatial frequency jitter shows that both measures are seemingly uncorrelated across jitter

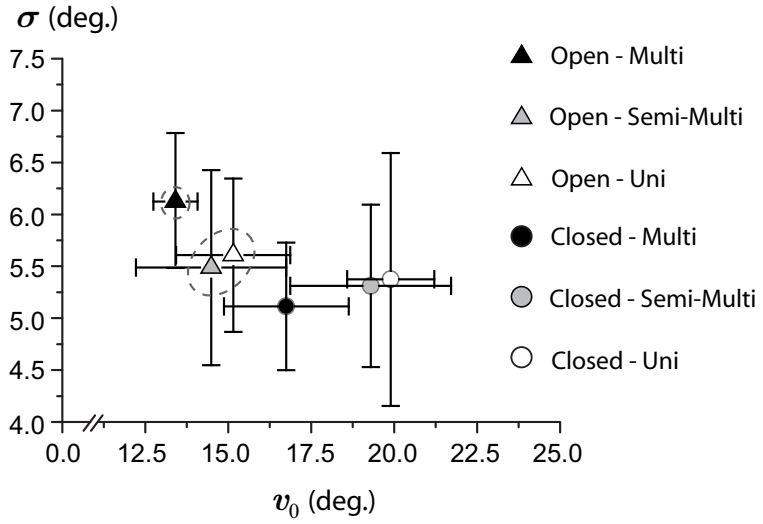

Figure 3.6: Centroids defined by tilt angle threshold (X-component, v_0) and standard deviation estimate (Y-component, σ_0). Error bars denote the 95% confidence limits of each mean component.

Source of Variation	*Wilk's* Λ	F	df_t	df_e	P
Contour type (A)	0.193	41.832	2	20	0.000
Jitter level (B)	0.393	6.964	4	18	0.001
A × B	0.865	0.705	4	18	0.599

Table 3.7: MANOVA results for the jitter threshold and standard deviation estimates. The table shows source of variation, Wilk's lambda, Λ, F- ratio, F, degrees of freedom for treatment, df_t, and error, df_e, and level of significance, P.

		$F_{(1,21)}$					P				
Group	j	1	2	3	4	5	1	2	3	4	5
Closed-Uni	1										
Closed-S-Multi	2	0.554					0.465				
Closed-Multi	3	17.681	13.038				0.000	0.002			
Open-Uni	4	53.161	20.119	2.344			0.000	0.000	0.141		
Open-S-Multi	5	61.892	86.717	9.270	0.726		0.000	0.000	0.006	0.404	
Open-Multi	6	131.859	35.107	14.958	5.772	1.261	0.000	0.000	0.001	0.026	0.274

Table 3.8: Results table for the univariate contrast analysis of the jitter threshold estimates. The table shows the F- statistic, $F_{(1,21)}$, (cols. 3-7), and corresponding significance levels, P, (cols. 8-12), for pairwise comparisons of the cell means shown in Figure 3.5a.

	closed			open		
Group	Uni	S-Multi	Multi	Uni	S-Multi	Multi
r	-0.648	-0.264	0.115	-0.461	-0.034	0.000
df	19	20	18	17	19	17
t	-3.711	-1.224	0.493	-2.142	-0.149	0.001
P	0.001	0.235	0.628	0.047	0.883	0.999

Table 3.9: Pearson correlation coefficients for the within group relation of tilt angle threshold estimates, v_0, and and standard deviation estimates, σ_0. The table lists the pearson correlation, r, degrees of freedom, $df = N - 2$, the t-statistic, $t = r\sqrt{N-2}/\sqrt{1-r^2}$, and level of significance, P.

conditions, it may be that there is a correlation among both measures within samples. Table 3.9 shows Pearson correlation coefficients and the results of testing them for statistical significance. The table shows that for the two conditions with spatial frequency jitter a correlation among thresholds estimate and standard deviation is lacking, while without spatial frequency jitter, there is a significant correlation. Closer analysis reveals that this correlation in not due to some extreme values, but indeed characterizes the global form of the empirical data ellipses (see Figure 3.7). The correlation is negative, reflecting that standard deviation estimates tend to decrease with increasing mean parameter estimates. This means that in the condition without spatial frequency jitter psychometric curves tend to be steeper with increasing jitter thresholds.

3.5.5 Analysis of Variation Coefficients

When introducing the variation coefficient (see Introduction) it was pointed out that crozier's law holds if the standard deviation rises proportional to the mean parameter of a physical quantity. Naturally, a prerequisite for crozier's law is that performance *rises* monotonically with the physical quantity. Since increasing the orientation tilt angle v of the Gabor element relative to the contour path leads to decreasing performance, the tilt angle variable must be properly transformed in order to enable analysis in terms of variation coefficients. An appropriate transform is the linear transform

$$v' = \beta - v \tag{3.17}$$

with β some constant. If β is chosen as the maximum tolerable angle for inter-element locking to occur, v' measures the similarity of contour and Gabor element rotation in units of tilt angle. Using (3.11) we may now define

$$\begin{aligned} F_A(v) &= F(v) \\ F_B(v) &= F(\beta - v). \end{aligned} \tag{3.18}$$

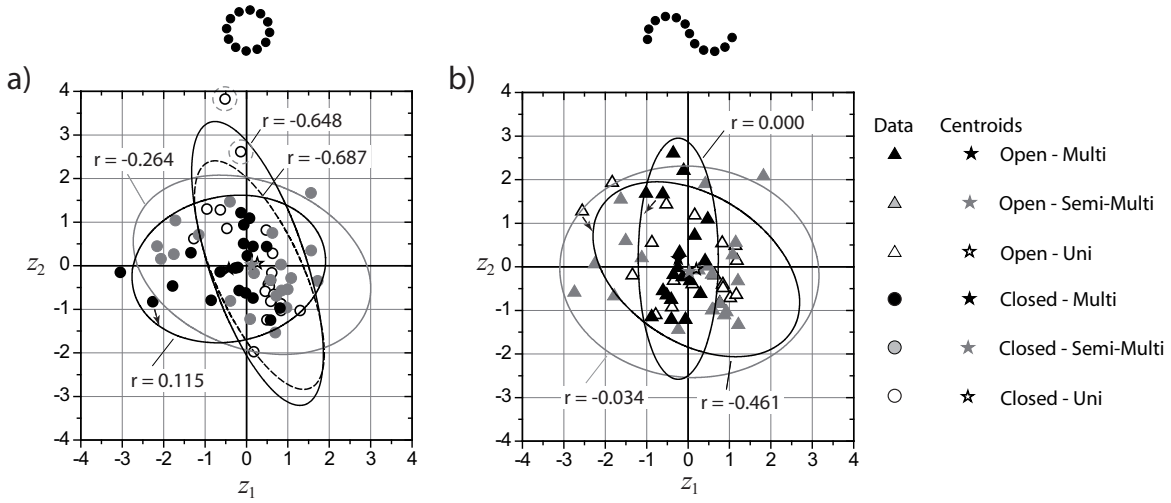

Figure 3.7: Data ellipses of standardized jitter threshold (z_1) and standard deviation estimates (z_2) for closed (a) and open contours (b). The 95% quantiles of bivariate normal densities (3.12) calculated for the standardized data are shown as solid ellipses for each of the three data ensembles of each contour type. Pearson correlation coefficients are shown for each data ensemble. Arrows mark belongingship of data and 95% normal quantiles. The dashed ellipse is the 95% normal quantile that results for closed contours with no spatial frequency jitter if the two data points marked by dashed circles are removed. Removing these two data points further increases the correlation coefficient.

$F_B(v)$ is mirrored and shifted with respect to $F_A(v)$, which implies corresponding psychometric curves $P_A(v)$ and $P_B(v)$ with the same symmetry properties. Psychometric curve $P_B(v)$, since it is mirrored with respect to $P_A(v)$, rises monotonically as a function of v. With this function conditions eliciting better performance are characterized by leftward shifted curves on v. Since mirroring and shifting does not affect the variance of a statistical variable, $P_B(v)$ will just be changed in the sign of slope compared to $P_A(v)$, but not in its absolute value (see Figure 3.8). As a guideline for the possible range of β consider that Field and others (Field et al., 1993; Beaudot & Mullen, 2003) have shown that there is inter-element locking up to at least $30°$ tilt angle, so β should be chosen larger than $30°$. On the other hand, orthogonal arrangements of Gabor element also lead to element grouping along a contour, so β must be some amount smaller then $90°$. A screening test would be to calculate generalized variation coefficients for $\beta \in [30°, 75°]$, and to compare their values for open and closed contours. To execute this test we calculated generalized variation coefficients (3.6) using (3.3),

$$q_0' = \frac{\overline{\sigma_0}\sqrt{2\pi}}{\overline{v_0'}} \tag{3.19}$$

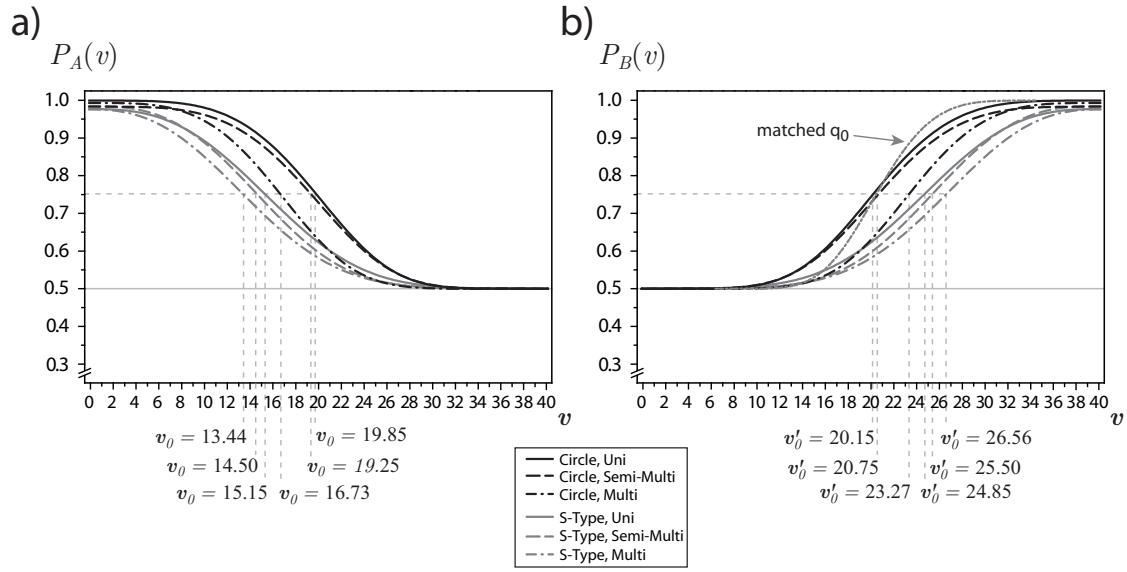

Figure 3.8: Psychometric curves $P_A(v)$ (a) and $P_B(v)$ (b), for circles (black lines) and S-type contours (grey lines), and all three spatial frequency jitter conditions. (a) is a re-plot of the psychometric curves shown in Figure (3.3). For the functions $P_B(v)$ shown in (b) $\beta = 40$ was chosen. The 0.75 points of P_A and P_B, v_0, are complementary with respect to β (see dashed vertical lines in (a) and (b)). Comparing slopes shows that the curves for closed contours are only marginally steeper, but clearly shifted on the scale. An exception is the condition with spatial frequency jitter in contour and background. There, $P_B(v)$ is slightly shifted but clearly steeper, resulting in about the same value of the variation coefficient as found for the three curves for open contours (see Table 3.10). The curves $P_B(v)$ for closed contours in the other two jitter conditions have larger variation coefficients. The smooth grey dot line (see arrow in (b)) shows a psychometric curve with the same variation coefficient as found for the curves for open contours. This curve, centered in $v'_0 = 20.45$, is much steeper than the two ones observed about this scale position, and illustrates the increase in steepness necessary to obtain the same constant value of the variation coefficient in order to compensate for a leftward shift on the scale.

by inserting the sample means for σ_0 and v'_0, particularly, $\overline{v'_0} = \beta - \overline{v_0}$.[8] Generalized variation coefficients q'_0 are listed in Table 3.10 for different values of β.

Table 3.10 shows that for mirrored and shifted psychometric curves $P_B(v)$, where higher values of v correspond to a smaller difference of local element orientation and path angle, variation coefficients are different among experimental conditions, and become quite close

[8]Note that v'_0 are the 0.75 points of $P_B(v)$ (see also Figure 3.8).

	closed			open		
β	Uni	Semi-Multi	Multi	Uni	Semi-Multi	Multi
30	1.329	1.241	0.969	0.948	0.889	0.927
35	0.891	0.847	0.704	0.709	0.672	0.712
40	0.670	0.643	0.552	0.567	0.540	0.578
45	0.537	0.518	0.455	0.472	0.452	0.487
50	0.448	0.434	0.386	0.404	0.388	0.420
55	0.384	0.373	0.336	0.353	0.340	0.369
60	0.336	0.327	0.297	0.314	0.303	0.330
65	0.299	0.292	0.266	0.282	0.273	0.298
70	0.269	0.263	0.241	0.257	0.248	0.271
75	0.245	0.239	0.221	0.235	0.228	0.249

Table 3.10: Generalised variation coefficients q_0' calculated for all experimental conditions for psychometric functions $P_B(v)$ for increasing values of the maximum tolerable tilt angle β.

with increasing values of β. Most striking, the Table shows that variation coefficients for closed contours without spatial frequency jitter and with spatial frequency jitter only in background are consistently *larger* for all choices of β. The implications of this are illustrated in Figure (3.8), for a choice of $\beta = 40°$. The psychometric curves $P_B(v)$ for these two conditions have strongest leftward shift (see Figure (3.8b)), but their steepness is only slightly larger than the steepness of the curves obtained for open contours. If evaluation of standard deviations is done relative to the position on the scale, then these psychometric curves turn out to be not as steep as the corresponding psychometric curves for open contours. In order to reach the same steepness relative to the 0.75 point, the reduction in the standard deviation would have to be larger than the marginal and non-significant reduction effect which was actually observed. For closed contours with spatial frequency jitter along contour and in background we find variation coefficients that are in the same range as the values obtained for open contours.

Taken together, an evaluation of psychometric curve slope relative to location on the scale gives no indication that closed contours are more efficiently detected, and this results does not depend on the hypothetical value of β.

3.6 Discussion

In order to assess whether contour detection is more efficient in background noise for closed compared to open contours we had 22 subjects measure psychometric curves for orienta-

tion tilt angle along the contour, for various levels of spatial frequency jitter. For each spatial frequency jitter level circle contours could be detected with the same accuracy as S-type contours at larger tilt angles, so there was a clear detection advantage. However, the slopes of psychometric curves were only slightly larger for the circle contours, and the difference was not statistically significant. Since there was a clear mean shift we analyzed psychometric curve slopes relative to their location on the scale by calculating variation coefficients. Variation coefficients were found to be equal or larger for circles, which means that psychometric curves tend to be flatter relative to their position on the scale.

Detection advantage for closed circular contours was much larger as found by Tversky et al. (2004), and was in the same order of magnitude as found recently by Mathes and Fahle (2007a).[9] However, as pointed out by the authors, when evaluating the contribution of closure, curvature and smoothness, it is smoothness (i.e. the absence of turning points), and not closure, which has the strongest modulating effect on detection performance. Balancing the number of elements and matching for smoothness there remains an effect that may be attributable to closure, but the size of this effect seems to be rather moderate. So, as also pointed out by (Braun, 1999), the facilitation observed for closed contours is not in the order of magnitude to justify speculation that there might be sensory routines particularly involved with closure.

The assumption of particular closure mechanisms would appear justified if it could be shown that the states of having detected and not having detected a closed contour are sharply separated on the orientation jitter scale, with a high degree of selectivity. However, the results obtained for the slopes of psychometric curves do not support that detection of circular contours is more immediate or efficient. The hypothesis that detection of circles is particularly efficient is somewhat tempting, since circles are pattern prototypes abundantly present in natural and cultural environments. Recently, evidence from natural image statistics was provided that the relative frequency of the angular separation of two line segments is maximal at fixed angles in the plane, which are given by the closed circles to which the two lines are tangents (Sigman, Cecchi, Gilbert, & Magnasco, 2001). This was taken to indicate a cocircularity principle in vision, provided the validity of the general principle that neural structures in the visual system capture prototypical structures of the visual word. Disappointingly, we find no support in favor of a particularly effective detection scheme associated with circularity, and therefore also not for closed contours in general.

Besides the role of closure there is another interesting aspect of the data. Note that, generally, a correlation of slope and mean parameter is absent, both in between and within

[9]The discrepancy in the observed detection advantage effects for the same stimuli and the same kind of variation is somewhat puzzling. A possible reason for same detection tilt angle thresholds for S-type and circular contours in the study of Tversky et al. is the fact that one target contour element always fell on the display center. A further difference to the method of Tversky et al. is the spatial algorithm. We used the same algorithm as Mathes and Fahle (2007a, 2007b).

group data, except for the condition with no spatial frequency jitter at all (univariate). There we find, and strongest for closed contours, that better tilt angle threshold performance comes along with steeper psychometric curves (see Figure 3.7). The correlation among mean and standard deviation is not due to outliers, but represents the structure of the data ellipses. This clearly suggests that crozier's law holds when there is no spatial frequency jitter at all. So, introducing spatial frequency jitter apparently introduces other processing levels, exerting an impairing overall effect on performance.

Generally, our scheme of results suggests that adding spatial frequency jitter impairs performance on a global rather than a local level of processing. This becomes plausible in the light of the following considerations. Note that detection performance for the two conditions where the contour spatial frequency is constant (*univariate* and *semi-multivariate*) is very close in both tilt angle threshold and standard deviation estimate (see Figure 3.6). By assuming only a local grouping mechanism serving to lock collinear elements within the same spatial frequency bands (Field et al., 1993; Polat & Sagi, 1993; Grossberg & Williamson, 2001; Z. Li, 1998, 1999; Yen & Finkel, 1997; Herzog, Ernst, Etzold, & Eurich, 2003; Schinkel et al., 2005) it cannot be explained why contour detection in univariate surrounds is as good as in surrounds varying in spatial frequency and orientation. Within surrounds jittering in both dimensions, neighbors flanking the contour are hardly proper locking mates, since they must coincide within both feature dimensions, while mates along the contour have to match just in orientation. Hence, the probability for path elements to lock with neighbor distractor elements is reduced. Further, also the probability for false positives is generally reduced in the multivariate background, so the target paths should be more salient. However, detection performance with univariate and multivariate backgrounds is the same, and only introducing spatial frequency jitter also along the contour lets performance deteriorate (see Figure 3.6). This suggests that the positive effects of spatial jitter on the local locking probabilities are overshadowed by impairing global effects of spatial frequency noise. A global effect most likely to interfere with an improved chance for correct local locking is spatial frequency uncertainty, which enters here (see below). Moreover, there is accumulating evidence that contour integration is not explainable just by local locking on distal and feature specific processing levels, but takes place on multiple scales with an involvement of higher visual areas.

It is crucial for our argument that selectivity for spatial frequency matters for the local grouping mechanism in contour integration. This has been shown by Dakin and Hess (1998, 1999), who demonstrated that co-aligned elements lock within the same carrier spatial frequency band, but hardly between. They found spatial frequency bandwidth estimates for contour detection in the range of 5/4 octaves for straight contours down to 3/4 octaves for curves with 30° path angle. Consistent with the tilt angle thresholds observed here they found larger bandwidths for closed contours compared to open ones. However, a striking difference of the studies of Dakin and Hess and our experiments is that they used only two

spatial frequencies simultaneously, while our displays contained random distributions of frequencies taken from a two octave range. This means that both experiments had different certainty conditions. As stated above, the certainty conditions are one possible candidate for explaining the similar detection performance for univariate and semi-multivariate displays with homogeneous carrier frequency along the contour. It might be that the benefit for local locking along the contour in surrounds with multiple feature variation is overshadowed by the higher uncertainty of the observer, who has to monitor lockings and false positives in multiple spatial frequency bands simultaneously. The uncertainty due to the necessity of monitoring multiple spatial frequency bands for possible targets reduces performance remarkably (Kramer, Graham, & Yager, 1985; Hübner, 1993, 1996a), and enters as a global factor at the decision stage.

Further, it is important to take into account that contour detection does not solely depend on local locking of neighboring primary coding units selectively sensitive to combinations of orientation and spatial frequency, but is a process that takes place on many spatial scales simultaneously. Recent neuroimaging studies show that in higher ventral areas, as the parietal cortex, inferio-temporal cortex (IT), and the lateral occipital complex (LOC), similarity grouping is accomplished on a larger scale, and contour parts are connected to form the outlines of figures and shapes (Kourtzi & Kanwisher, 2000; Kourtzi & Huberle, 2005; Lerner, Hendler, Ben-Bashat, Harel, & Malach, 2001). On higher levels not only orientation, but a variety of cues, such as shading, texture, motion, or luminance is used for form completion. Particularly the LOC responds to perceived global shape relatively independent of the nature of the local shape cue, and is particularly sensitive to line drawings. LOC responses are not modulated by object familiarity, which suggests a stimulus driven analysis (Kourtzi & Kanwisher, 2000). BOLD responses in V1 and V2 are strongly modulated by a change of local element orientation, but hardly by a change in global shape. Vice versa, the LOC responds most strongly to a change of global form, and moderately to local feature change. Cue integration stabilizing global form detection is stronger in the LOC than in V1 and V2 (Altmann et al., 2003; Kourtzi & Huberle, 2005). Meanwhile, there is ample evidence that contour integration and form completion are processes that concern simultaneous neural processing across the hierarchy (Roelfsema, Lamme, & Spekreijse, 1998, 2000, 2004). Consequently, a higher level global mechanism searching smooth curvature on different scales would successfully integrate circle and S-type fragments in spatial frequency maps, as long as these forms have homogeneous carrier frequency. In the course of the experiment observers learn to reduce uncertainty by ignoring spatial frequencies that are unlikely candidates for a target by forming quasi matched filters (Hübner, 1993, 1996b). So, repeated experience with the same degrees of curvature may also help to build adaptive form tuned global units within the same spatial frequency bands via principles of Hebbean learning (Mortensen & Nachtigall, 2000).

Taken together, our data show that contour integration is not well understood by assum-

ing just local locking processes on distal and feature specific layers. Global mechanisms of form completion and handling of decision uncertainty are certainly involved. Mechanisms of form completion may adapt to global features such as path curvature, but comparing detection performance of S- shapes and circles gives no indication that there are particular efficient routines for closeness.

4 Contour Integration across Spatial Frequency

Synopsis

Association field models of contour integration suggest that local band-pass elements are spatially grouped to global contours within limited bands of spatial frequency (Field et al., 1993). In order to study whether contour integration occurs across spatial frequency we measured contour detection performance as a function of element orientation jitter along the contour for various degrees of spatial frequency jitter applied to both contour and the embedding field. The results show that contour detection performance is essentially not affected when the contour elements differ in spatial frequency at least about 1.25 octaves. Even when the contour elements are separated about 2.25 octaves, threshold impairment amounts to 20% for closed contours and about 37% for open contours, compared to uniform spatial frequency patterns. To explore whether spatial frequency alone is sufficient for contour grouping we had subjects detect contours formed by spatial frequency homogeneous elements in fields with strong spatial frequency random jitter up to 3.0 octaves. For both isotropic (circular) bandpass elements and Gabor elements with fully random orientation we found that contours were essentially not detected by spatial frequency homogenization along the path. The results point to a contour detection mechanism that privileges orientation and operates across larger ranges of spatial frequency, but benefits from the restriction to a narrow spatial frequency band.

4.1 Introduction

A vast majority of studies on contour integration concentrated on the rules of contextual interaction among V1 cells selectively sensitive to limited ranges of orientation and spatial frequency (Field et al., 1993; Kovacs & Julesz, 1993; Pettet et al., 1998; Field et al., 2000; Hess et al., 2000; Ledgeway et al., 2005; Wang & Hess, 2005). Although primary sensory mechanisms are jointly tuned to both parameters, orientation was particularly focused upon, and most studies on contour integration were dedicated to the effects of orientation jitter, global curvature, closeness and inter-element spacing at a fixed spatial frequency of contour and background elements. This is surprising, since knowing the bandpass prop-

erties of the lateral interconnections in V1 would enable making precise predictions about contour integration performance. If it turned out that the spatial frequency tuning of human contour integration performance can be predicted from the bandpass tuning of local contextual interaction, then this would be further support for the local association field model of contour integration. If, on the other hand, contours were integrated across larger spatial frequency bands than predicted by the bandpass tuning of the local interactions, then this would be evidence for the involvement of additional mechanisms and higher order integration processes in contour integration.

The bandpass tuning within the minimum response field of early orientation and spatial frequency selective mechanisms is well understood. Psychophysical contrast detection experiments with superimposed (spatially coincident) gratings yield estimates for the full bandwidth at half height in the range of 1.0 to 1.75 octaves (Graham & Rogowitz, 1976; Graham, 1977; Mostafavi & Sakrison, 1976; Robson & Graham, 1981; Watson, 1982). With suprathreshold stimuli and an oblique mask technique Wilson and colleagues found evidence for variable bandwidths, which are about 2 to 2.5 octaves at the lowest frequencies of 0.7 cpd and 1.5 cpd and narrow down to 1.5 to 1.25 octaves at the highest frequencies of 8 cpd and 16 cpd (Wilson et al., 1983; Wilson & Gelb, 1984). All these estimates are corrected for the artificial narrowing due to the effects of spatial probability summation. Microelectrode recordings in area V1 of the macaque substantiate bandwidth estimates between 1 and 2 octaves (De Valois, Albrecht, & Thorell, 1982). In contrast to early mechanism tuning for spatially coincident frequencies only some studies explored how local spatial frequencies interact across space (Chubb et al., 1989; Sagi & Hochstein, 1985). The most systematic contribution to this issue comes from the target plus flanker experiments of Polat and Sagi (1993, 1994a). They studied how the contrast threshold of a central Gabor target is affected by the presence of suprathreshold flanking Gabors, as a function of the spatial test to flanker distance. These threshold curves turned out to be biphasic, with a short inhibitory lobe followed by a long excitatory one, which extended up to a test to flanker distance of about 8 wavelength units. By additionally manipulating the similarity of test and flanker in orientation and spatial frequency, they obtained an estimate of how the modulation of the curve vanishes with increasing dissimilarity of test and flanker in the parameter under investigation. For spatial frequency they found that the amplitude of the excitatory lobe is more than halved at test-flanker wavelength ratios of $1/2$ and 2 (1 octave) and vanishes completely at ratios of $1/4$ and 4 (2 octaves) (see Figure 7 in Polat & Sagi, 1993). This means that the tuning of orientation and spatial frequency selective mechanisms to spatially adjacent frequencies is about 2 octaves in a full bandwidth at half height measure, which is slightly broader than the tuning to coincident spatial frequencies.

With this estimate it is possible to derive an expectation for contour integration performance when the elements along the contour jitter in spatial frequency. If contour integration in cluttered images is solely based on the local inter-element locking of spatial frequency

and orientation selective mechanisms, then contour detection should be seriously impaired if the spatial frequency separation of the elements along the path is larger than about 1 octave, the half-bandwidth at half height bandwidth estimate derived from the data of Polat and Sagi (1993). It should be impossible with a spatial frequency separation of about 2 octaves. If contour integration proves much more robust against spatial frequency jitter in this order of magnitude, then this is a strong indication that additional mechanisms enter in contour integration. For the most part, these concern integration across larger ranges of spatial frequencies. But also, other global aspects may be important that are ignored by local locking approaches. These concern processing of first and second order feature statistics of the surrounding field, spatial and spatial frequency uncertainty characteristics of the display, and the influence of external noise on the detection process.

The spatial frequency tuning of human contour integration in cluttered images was studied by Dakin and Hess (1998, 1999). In their experiments spatial frequency could take two distinct values in background and along the contour, contour elements were nearly perfectly aligned with the path, and the effect of spatial frequency separation of the two concurrent micropattern families on contour detection performance was measured. They found that proportion correct was halved in the range of $5/4$ octaves for straight contours down to $3/4$ octaves for curves with a 30° path angle. Although these results seemingly substantiate local inter-element locking of early orientation and spatial frequency tuned mechanisms at first glance, it is worth looking at the actual arrangement of the experiment.[10]

Contour detection in random fields with alternating spatial frequencies is a difficult task, because false positives occur in two distinct spatial frequency bands, and the observer has to monitor the outputs of two channel families across space. Experiments on the detection of second order feature modulation have shown that the use of two concurrent spatial frequency bands deteriorates detection of orientation modulated waveforms, although net feature contrast is enlarged by introducing a second frequency component (Kingdom & Keeble, 2000). Besides uncertainty, deterioration is due to higher level influence, since concurrent groupings occur in two separated spatial frequency bands overlayed in transparency. These effects let the dual frequency band configuration appear not quite appropriate for studying a more or less low level property such as spatial frequency bandwidth of

[10]Note that one should be cautious in identifying these octave ranges as bandwidth estimates of human contour integration. Usually, bandwidth is defined as the half-sensitivity range of the parameter on a tuning-curve, where sensitivity is the reciprocal of a threshold contrast estimate. This means that each point on a tuning curve derives from a complete psychometric curve, and refers to a constant proportion of correct judgements. Dakin and Hess (1998) instead defined bandwidth as the half-width at half-height proportion correct range of the parameter, i.e. the points on their tuning curves were proportions of correct judgements, and they looked in which range of the spatial frequency parameter proportion correct was halved. It is clear from these different definitions that the bandwidth estimates of Dakin and Hess are not directly comparable to the estimates derived from classical tuning curve measurements experiments (Wilson et al., 1983; Wilson & Gelb, 1984; Wilson & Regan, 1984; Watson, 1982). See Discussion.

contour integration.

These considerations let us revisit the spatial frequency tuning of human contour detection using random fields continuously jittering in spatial frequency and orientation. We recorded the classical tilt angle versus proportion correct curves for various degrees of spatial frequency jitter applied to both contour and the surrounding field. This was done in order to judge the effect of additional spatial frequency jitter on the common performance measure for contour integration performance, namely the 0.75 proportion correct tilt angle threshold. With a particular quasi-randomization technique we controlled that at least every third element along the contour preserved a critical octave distance to its foregoing elements. To anticipate the findings, it turned out that contour integration can be done at reasonable performance levels even if the critical frequency separation of the elements along the contour is larger than 2 octaves. A distance of 1.25 octaves just leads to marginal impairment. Control experiments with fully random orientations of the contour elements, as well as with circular bandpass micropatterns, show that contour integration is not possible when spatial frequency homogeneity is the only grouping cue for the contour in the random element field. Hence, our results show that contour integration is possible across ranges of spatial frequency which are larger than the bandwidth estimates obtained from experiments on single patch center-surround interaction (see above), but, however, that it is not possible to do contour grouping by spatial frequency alone. Similar to results found in various experiments on orientation discrimination with complex grating patterns (Olzak & Thomas, 1992; Olzak & Wickens, 1997; Olzak & Thomas, 1999, 2003), our findings indicate a mechanism which integrates orientation from larger spatial frequency ranges. This mechanism must be located at later stages, since the medium bandwidth of local primary mechanism interactions precludes orientation locking across wide spatial frequency bands.

4.2 Experimental Outline

Two experiments were executed to explore the role of spatial frequency in contour integration. Experiment 1 aimed at measuring the effect of three experimental conditions differing by the magnitude of Gabor carrier spatial frequency jitter applied to contour and background elements on contour detection performance, and comparing the performance for open and closed contours within these conditions. Performance was measured in terms of tilt angle threshold (Field et al., 1993), defined as the 0.75 point v_0 of the psychometric curve for a 2AFC measurement. Additionally, we derived a standard deviation estimate $\hat{\sigma}$ from the psychometric curve. In Experiment 2 we tested whether contour integration is possible by sole homogeneity of carrier spatial frequency in the absence of orientation cues to the contour. This was done with two stimulus settings. First we probed whether

contour detection was possible by spatial frequency homogenization along the contour, embedded in frequency heterogeneous backgrounds. Gabor element orientations on contour and background were fully random. Second, we tested whether contours could be detected by spatial frequency homogenization in fields with Gaussian patches of circular cosine micropatterns, conveying no orientation information at all. Performance measures were the same as in experiment 1. Details about the experimental methods are provided in the respective section.

4.3 Procedure

4.3.1 Calibration of Individual Parameter Values

Parameter levels were calibrated at five performance levels for both contour types and all three spatial frequency conditions, and individually for each subject. In preparation measurements psychometric function data were recorded, and fit with Weibull distribution functions. This was done twice, and separately for each target condition. On the basis of the curve fitting results of the second measurement a set of parameter levels was extrapolated for each experimental condition, which corresponded to five fixed levels of proportions of correct judgements. These levels were selected as rates of 0.59, 0.67, 0.75, 0.83 and 0.91.

4.3.2 Main Experiment

For the main experiment the individually calibrated sets of parameter levels were used in the target conditions for each subject. In many but not all cases detection rates for the zero tilt angle were additionally measured in order to achieve a more stable estimate for saturated maximum performance on the psychometric curve. After calibration of the parameter level sets for each subject the main experiment was executed where all target conditions were randomly intermixed in a single experimental block.

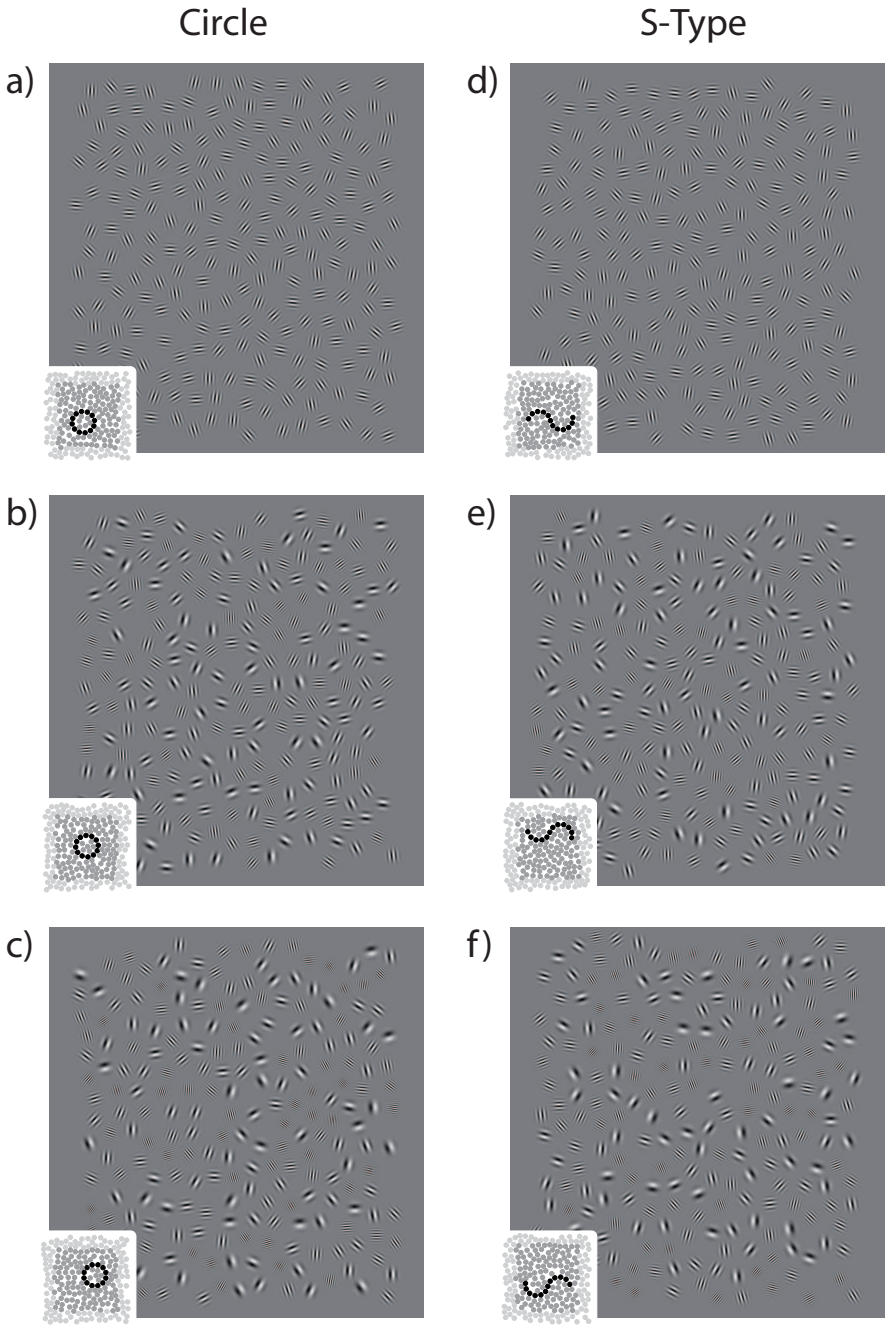

Figure 4.1: Examples of Gabor stimulus displays with closed target contours (left panel) and open target contours (right panel), without spatial frequency jitter (upper panel, (a) and (d)), with medium spatial frequency jitter spanning 2.0 octaves (middle panel, (b) and (e)), and high spatial frequency jitter spanning 2.9 octaves (lower panel, (c) and (f)). In the examples, the tilt angle, i.e. the rotation angle of the Gabor elements relative to the contour path, is set to 0°. The pictographs in each image indicate the position of the contour in the field.

4.4 Experiment 1

4.4.1 Methods

Stimulus Micropatterns

Stimulus displays consisted of contours made up by Gabor micropatterns aligned along a smooth path, embedded in Gabor random fields. Detectability of target contours was modulated by rotating a Gabor element away from its perfect alignment with the contour by an angle of v. Increasing this tilt angle results in decreasing contour detection performance (see Field et al., 1993). Gabor micropatterns were defined as in (2.1).

Orientation and Spatial Frequency Jitter

Orientation jitter was applied to the background elements in all experimental conditions. Orientation jitter was maximum, sampling φ uniformly from the interval $[0°, 180°]$.

Spatial frequency jitter was assigned to all stimulus elements. Three levels of spatial frequency jitter were used, which were no spatial frequency jitter (UNI), medium spatial frequency jitter, sampled from an interval of 2 octaves (MEDIUM), and high spatial frequency jitter, sampled from an interval spanning 2.9 octaves (HIGH).

For obtaining spatial frequencies of random distribution we defined spatial frequencies as $f = 2^u$ and sampled u from a uniform distribution in the interval $[1, 3]$ for the MEDIUM condition and $[0.43, 3.33]$ for the HIGH condition. Measured in units of cycles per degree, (cpd), spatial frequencies of the micropatterns were sampled from the interval $[2, 8]$ for the MEDIUM condition, and $[1.35, 10.05]$ for the HIGH condition. In the UNI condition background and contour elements were assigned a constant spatial frequency of $f_0 = 4.33$ cpd, which is the expected value of the two spatial frequency distributions ($f_{0,MED} = f_{0,HIGH} = f_0 = 4.33$). According to Feldman (2001), a minimum contour length of three elements is required to enable contour integration. Due to the random sampling of element spatial frequencies there is a considerable likelihood of three or more adjacent contour elements being assigned similar spatial frequency levels. Observed contour integration performance could thus be artificially enhanced by frequency homogeneous chains of sufficient length being accidentally taken for a target contour. To counter this unintended effect, a quasi-random procedure was devised for sampling spatial frequencies for contour elements, by which it was ascertained that at most two adjacent contour elements could be sampled from the same spatial frequency band. The minimum distance of at least every third contour element to its predecessor was $f = 1.25$ octaves in the MEDIUM condition and $f = 2.25$ octaves in the HIGH condition. Stimulus examples for the three spatial frequency jitter conditions, for open and closed contours, are shown in Figure 4.1.

Main Experiment

In the calibration phase detection rates were measured twice for 5 tilt angles in 6 target conditions, each with 32 replications, which means that each subject had to get through 1920 trials before the main experiment. This took about two hours. In the main experiment detection rates for the calibrated parameter values were then measured ones, also with 32 trial replications, resulting in 960 trials. All trials of the main experiment were completely randomized across experimental conditions and tilt angles, and were administered in a single one hour session with a brief pause.

4.4.2 Subjects

22 undergraduate students served as observers. Fourteen subjects were female, eight male. All subjects had normal or corrected to normal vision. The students had no former psychophysical experience, were paid and not informed about the purpose of the experiment.

4.4.3 Results

Psychometric Curves

Psychometric curves were obtained for each subject in each of the six experimental conditions. As a function of the tilt level v, they had the general form

$$P(v) = 1 - 0.5F(v), \tag{4.1}$$

where F is a distribution function. Equation (4.1) means that detection rates *decrease* with increasing tilt angle v. For fitting psychometric curves the Weibull model

$$F(v) = 1 - c\exp\left(-av^b\right) \tag{4.2}$$

was chosen for the distribution function for convenience, and its three parameters a, b and c were estimated with the Levenberg-Marquardt algorithm (Press, Teukolsky, Flamery, & Vetterling, 1996). Figure 4.2 gives an overview of the results, and Tables 4.1 and 4.2 list the parameter estimates, as well as the absolute 0.75 point (v_0), and the standard deviation estimate ($\hat{\sigma}$), as derived from (4.2) by using the variance of a Weibull distribution

$$\sigma^2 = \frac{\left(\Gamma\left(\frac{2}{b}+1\right) - \left(\Gamma\left(\frac{1}{b}+1\right)\right)^2\right)}{a^{2/b}}, \tag{4.3}$$

and taking its square-root, scaled by the shrink parameter c

$$\hat{\sigma} = \frac{\sigma}{c} \tag{4.4}$$

In (4.3) the symbol Γ denotes the Euler Gamma-function. The standard deviation estimate (4.4) describes the spread of an underlying distribution, and yields values which are close to estimates obtained from fitting cumulative Gaussians (see Persike and Meinhardt, 2007).

	NO							MEDIUM							HIGH						
no.	$a^{1/b}$	b	c	η^2	v_0	σ_0		$a^{1/b}$	b	c	η^2	v_0	σ_0		$a^{1/b}$	b	c	η^2	v_0	σ_0	
1	.041	6.588	1.000	.94	22.83	4.00		.046	3.672	1.000	.99	19.658	5.94		.049	5.512	1.000	.97	19.06	3.94	
2	.041	3.276	1.000	.90	21.71	7.31		.057	3.650	1.000	.98	15.81	4.80		.052	2.580	.698	.95	12.56	10.17	
3	.048	6.497	1.000	.93	19.69	3.49		.052	3.883	1.000	.90	17.45	5.00		.063	2.072	.776	.91	10.64	9.14	
4	.054	5.581	1.000	.93	17.36	3.55		–	–	–	–	–	–	⋆	.046	2.451	1.000	.96	18.89	8.47	
5	–	–	–	–	–	–	⋆	.062	4.653	1.000	.97	14.83	3.59		.070	4.707	.850	.99	12.56	3.75	
6	.045	5.519	.718	.97	18.43	5.97		.083	2.830	1.000	.97	10.65	4.13		.066	1.706	.689	.72	7.82	11.91	
7	.041	2.224	1.000	.98	20.78	10.31		.068	2.475	1.000	.95	12.63	5.61		.055	1.396	.839	.99	11.32	14.30	
8	.045	6.124	1.000	.96	20.84	3.91		.048	2.944	1.000	.71	18.37	6.86		.056	3.740	.746	.93	14.09	6.50	
9	.054	3.444	.850	.90	15.47	6.31		.044	3.890	1.000	.97	20.84	5.96		.059	4.007	1.000	.94	15.40	4.29	
10	.047	2.931	.787	.81	16.36	9.02		.049	5.907	1.000	.96	19.38	3.76		.057	2.640	1.000	.91	15.23	6.34	
11	.063	2.350	1.000	.83	13.55	6.35		.052	4.989	1.000	.90	17.86	4.05		.069	2.973	.624	.97	8.73	7.60	
12	.048	3.912	.840	.81	17.45	6.36		.051	3.930	1.000	.99	17.73	5.02		.063	2.727	1.000	.99	13.96	5.62	
13	.059	2.026	.870	.83	12.64	8.90		.049	3.348	1.000	.86	18.35	6.05		.052	3.980	1.000	.92	17.62	4.93	
14	.039	4.391	1.000	.98	23.73	6.06		.047	3.613	1.000	.97	19.37	5.94		.047	3.806	1.000	.98	19.38	5.66	
15	.049	6.999	1.000	.98	19.31	3.20		.046	3.506	1.000	.91	19.51	6.16		.041	5.305	.919	.88	21.99	5.25	
16	.045	5.693	1.000	.93	20.99	4.21		.040	2.961	1.000	.92	21.99	8.17		.043	4.476	1.000	.93	21.55	5.41	
17	.049	8.584	1.000	.96	19.44	2.66		.053	4.865	1.000	.92	17.61	4.09		.053	3.225	1.000	.94	16.90	5.78	
18	.044	5.591	1.000	.91	21.08	4.30		.048	6.242	1.000	.99	19.59	3.61		.063	1.727	.775	.77	9.90	10.96	
19	.048	8.595	1.000	.96	19.86	2.72		.052	3.987	1.000	.99	17.57	4.91		.064	2.062	1.000	.86	13.10	7.05	
20	.045	3.974	1.000	.87	20.26	5.68		.046	4.395	1.000	.99	19.87	5.07		–	–	–	–	–	–	⋆
21	.053	2.540	1.000	.87	16.19	7.00		.053	4.478	1.000	.99	17.51	4.39		–	–	–	–	–	–	⋆
22	.045	5.670	1.000	.96	20.71	4.17		.051	4.069	1.000	.66	17.87	4.90		.043	4.845	1.000	1.00	21.76	5.07	
mean	.048	4.88	.96	.92	18.98	5.50		.052	4.01	1.00	.93	17.83	5.14		.055	3.30	.90	.93	15.12	7.11	

Table 4.1: Psychometric curve fitting results for closed contours. The table lists the parameter values for scale (a), shape (b) and shrink parameter (c) obtained for the Weibull model (4.2) with the Levenberg-Marquardt algorithm, as well as the goodness of fit in terms of the ratio of explained to total variation (η^2), the absolute 0.75 point (v_0) for the psychometric curve (4.1) and the standard deviation estimate ($\hat{\sigma}$) according to (4.4). Since the estimates for a take very small values, $a^{1/b}$ is listed instead. Cases where the fitting algorithm failed to converge were treated as missing, and are marked by an asterisk. The last line shows the between subject means of the parameter estimates.

	NO							MEDIUM							HIGH						
no.	$a^{1/b}$	b	c	η^2	v_0	σ_0		$a^{1/b}$	b	c	η^2	v_0	σ_0		$a^{1/b}$	b	c	η^2	v_0	σ_0	
1	.045	5.733	1.000	.98	20.92	4.17		–	–	–	–	–	–	⋆	.050	3.697	1.000	.99	18.21	5.46	
2	.059	1.817	1.000	.85	13.97	8.66		.057	1.545	1.000	.91	13.94	10.51		.054	1.869	.550	.88	4.12	16.61	
3	.061	3.064	1.000	.91	14.46	5.20		.059	1.328	1.000	.99	12.96	11.94		.051	1.769	.557	.90	3.28	18.41	
4	.079	2.009	1.000	.91	10.58	5.86		.083	3.515	.612	.99	7.70	5.61		.046	2.266	.518	.80	2.16	8.99	
5	.072	3.319	.813	.95	11.13	5.07		.049	3.051	1.000	.87	18.26	6.59		.076	1.385	.798	.93	7.59	10.99	
6	.074	2.076	1.000	.88	11.28	6.03		.076	1.256	1.000	.96	9.78	9.77		.086	1.127	.587	.77	2.30	16.96	
7	.048	2.329	.582	.80	9.28	14.45		.072	1.287	1.000	.96	10.38	10.00		.049	3.168	.541	.91	9.13	11.68	
8	.058	3.186	1.000	.95	15.36	5.31		.074	3.018	1.000	.84	11.99	4.37		.085	2.259	.740	.90	7.76	6.58	
9	–	–	–	–	–	–	⋆	.061	3.320	1.000	.87	14.58	4.85		.073	1.649	.507	.97	1.07	15.10	
10	.045	1.662	.734	.76	12.37	16.57		.065	1.489	1.000	.89	11.97	9.45		.069	3.477	.525	.98	6.04	7.90	
11	.079	1.568	1.000	.72	9.97	7.38		.053	2.325	1.000	.81	16.23	7.69		.054	1.833	.622	.73	6.75	15.01	
12	–	–	–	–	–	–	⋆	.063	2.432	1.000	.89	13.57	6.13		.071	5.202	.657	.96	11.67	4.34	
13	.072	1.811	1.000	.96	11.28	7.02		.065	2.714	1.000	.87	13.41	5.43		.064	5.962	.813	.97	14.96	3.45	
14	.047	4.185	1.000	.87	19.32	5.16		.057	2.382	1.000	.96	14.99	6.93		.046	3.196	.876	.93	16.48	7.60	
15	.060	1.660	1.000	.71	13.32	9.19		.065	2.746	1.000	.97	13.47	5.39		.067	3.540	.855	.99	11.76	4.94	
16	.052	4.320	1.000	.99	17.69	4.59		–	–	–	–	–	–	⋆	–	–	–	–	–	–	⋆
17	.063	2.249	1.000	.91	13.53	6.64		.070	2.090	1.000	.85	11.98	6.35		.050	2.185	.508	.70	2.07	16.91	
18	.063	3.343	.878	.97	13.29	5.32		.047	2.414	1.000	.95	18.38	8.38		.054	3.843	.563	.99	10.67	8.67	
19	.054	3.645	1.000	.91	16.88	5.14		.070	2.090	1.000	.85	11.98	6.35		.046	1.548	.702	.98	10.78	18.29	
20	.062	3.636	1.000	.95	14.50	4.42		.057	4.675	1.000	.99	16.19	3.90		–	–	–	–	–	–	⋆
21	.050	5.769	.675	.91	16.36	5.55		.078	3.806	1.000	.94	11.63	3.40		.054	4.229	1.000	.99	16.98	4.49	
22	.053	5.025	1.000	.96	17.38	3.92		.061	2.659	1.000	.84	14.26	5.89		.046	2.737	.695	.96	14.47	10.96	
mean	.060	3.12	.93	.89	14.14	6.78		.064	2.51	.98	.91	13.38	6.95		.060	2.85	.68	.91	8.91	10.67	

Table 4.2: Psychometric curve fitting results for open contours. Conventions as in Table 4.1

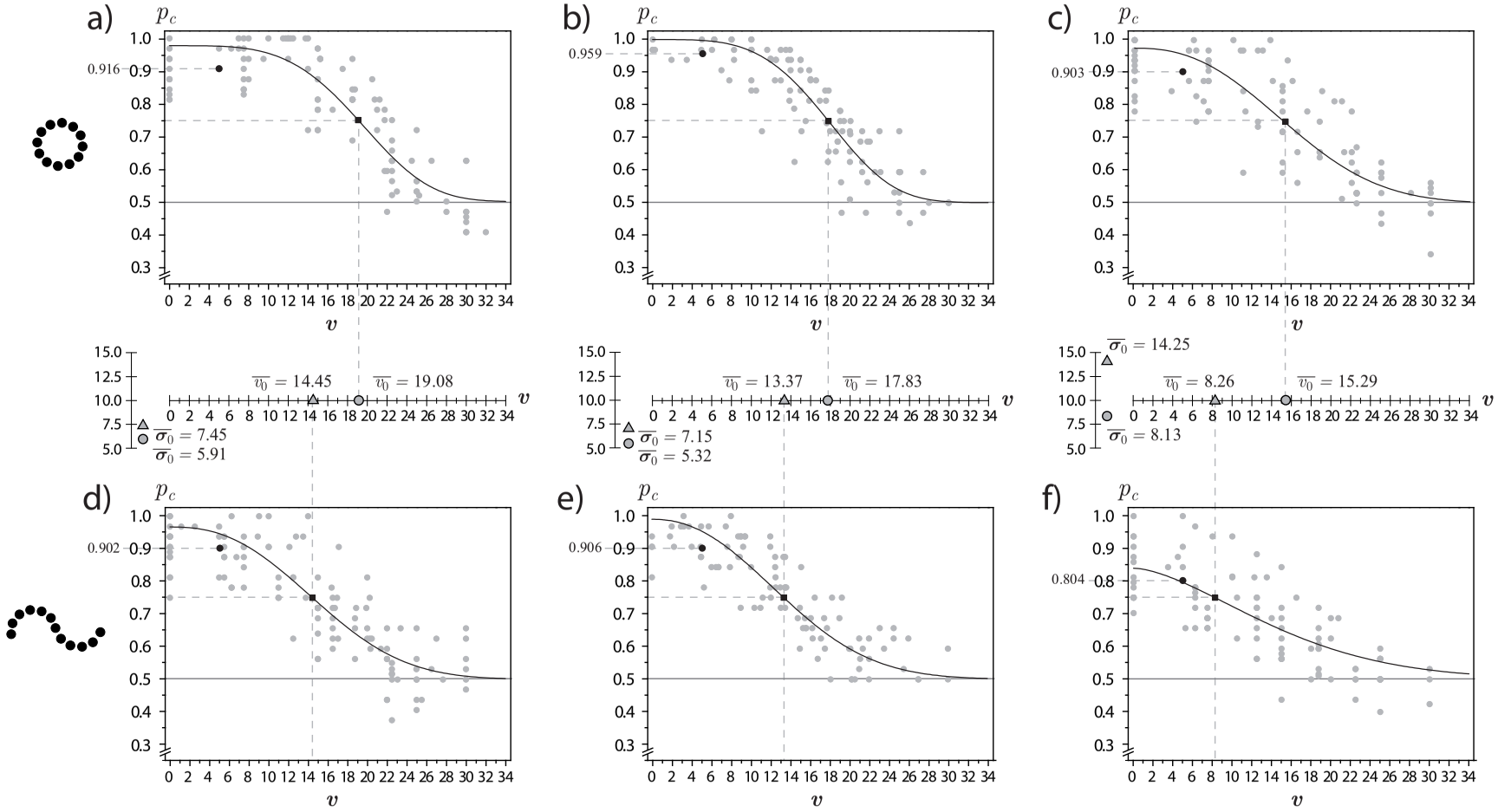

Figure 4.2: Psychometric curve data for closed (upper row) and open contours (lower row) for no spatial frequency jitter (left column), medium spatial frequency jitter (middle) and high spatial frequency jitter (right). Data points represent a proportion correct measure. The data shown are cleared for outliers, as described below. For each experimental condition a summary psychometric curve is drawn (solid line). This curve is a Weibull function that intersects at the between subject mean tilt angle threshold, $\overline{v_0}$, and has slope calculated from the mean standard deviation estimate. Mean jitter threshold and standard deviation estimates are projected onto a common axis (middle horizontal panel) to enable a first inspection of the effects of contour type on these variables (closed contours: circles; open contours: triangles).

As can be seen from the mean estimates of v_0 and $\hat{\sigma}$, closed contours have higher average tilt angle thresholds, and their psychometric curves tend to be steeper. These differences in the standard deviation estimates between both contour types are consistent over all spatial frequency jitter levels. The effects are illustrated by the summary psychometric curves shown in Figure 4.2, which are drawn through the between subject mean tilt angle threshold, $\overline{v_0}$. Their scale and shape parameters were adjusted such that they matched the slope value, as calculated from the mean standard deviation estimates $\overline{\hat{\sigma}}$ in each of the 6 experimental conditions. This was done in order to enable capturing the effects of spatial frequency jitter level on both jitter threshold and slope directly from the psychometric curves.[11] It is seen that the curves for closed contours are clearly rightward shifted relative to the curves for open contours, and their steepness is some degree higher, and clearly higher for the HIGH condition with a large degree of spatial frequency jitter. Most extreme estimates of jitter threshold and standard deviation are obtained for open contours in this condition (see Figure 4.2f and Table 4.2).

Statistical Testing

Tilt angle threshold and standard deviation estimates derived from psychometric curve data were analyzed with the general linear model, which allows to test the effects of contour type (open and closed contours), jitter level (UNI, MEDIUM, and HIGH), and their interaction with univariate and multivariate routines. Both factors, contour type and spatial frequency jitter level, are repeated measurement factors. Missing data (see Tables 4.1 and 4.2), were few, therefore they were replaced by between subject cell means. Tables 4.3 and 4.4 summarize the results of the separate analyses for the two dependent measures, and Table 4.5 gives a results survey of the multivariate test. Figure 4.3 illustrates the major findings.

Statistical testing shows a unique and consistent picture for both dependent variables. 75% tilt angle thresholds decline with increasing level of spatial frequency jitter for open and closed contours in a similar way, and are reached for closed contours at constantly larger tilt angles. Both factors, spatial frequency jitter level and contour type, are highly significant, and the parallel course of the mean threshold over spatial frequency jitter level indicates that they do not show any interaction (see Table 4.3). Pairwise comparisons show no significant differences of the first two spatial frequency jitter levels, both aggregated and for each contour type tested individually. The mean difference of MEDIUM to HIGH (D_{23}), however, is highly significant for both contour types in a conservative a-posteriori Scheffé-test, which indicates a critical cell-mean difference of $D_{(crit;0.95)} = 1.86$ (Closed: $D_{23} = 2.71$; Open: $D_{23} = 4.47$).[12]

[11] The Weibull functions shown in Figure 4.2 were derived such that their steepness in the mean parameter $\overline{v_0}$ is exactly inversely proportional to the mean standard deviation estimates given in Tables 4.1 and 4.2.

[12] With $n = 22$ subjects, 5 cell degrees of freedom (df_{cell}) and 42 degrees of freedom of the residual variance

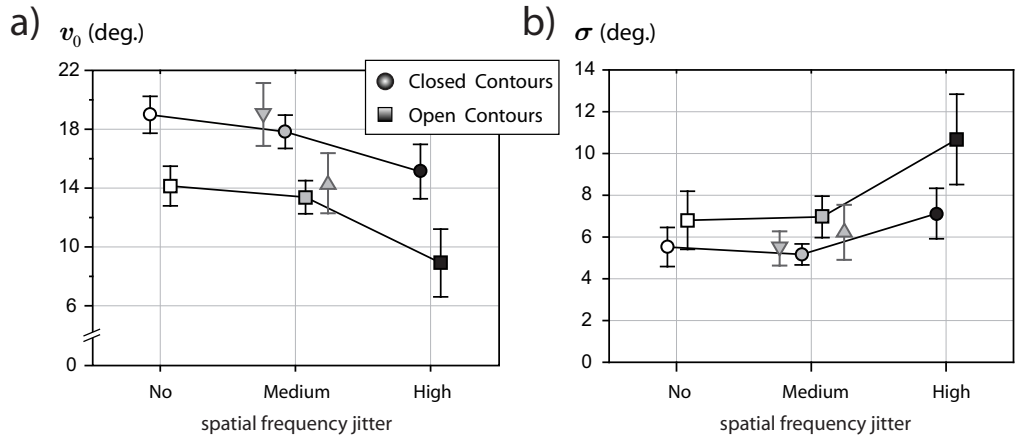

Figure 4.3: Between subject means of tilt angle threshold estimates v_0, defined as the 0.75 points of the psychometric curves (a), and the standard deviation estimates $\hat{\sigma}$ (b), for open (squares) and closed (circles) contours, plotted for the three jitter conditions. Error bars denote the 95% confidence limits of the means, based on the standard error derived from the residual variance estimates obtained for each cell. Triangle symbols refer to measurements for spatial frequency homogeneous contours embedded in surrounds with spatial frequency jitter of MEDIUM intensity. Up-triangles refer to closed contours, down triangles to open contours.

Source of Variation	*SS*	*df*	var'	*F*	*P*
Contour type (A)	881.120	1	881.120	99.881	.000
Jitter level (B)	505.617	2	252.808	22.012	.000
A $\times$ B	18.848	2	9.424	1.511	.233
A $\times$ Vpn	185.256	21	8.822		
B $\times$ Vpn	482.381	42	11.485		
Residual	262.036	42	6.239		

Table 4.3: ANOVA results for the tilt angle threshold estimates, v_0. The table shows the source of variation, sum of squares, SS, degrees of freedom, df, variance estimate, var', F- ratio, F, and significance level, P.

on the cell level (df_{res}), the critical cell-mean difference on a 5% significance level is given by

$$D_{(crit;0.95)} = \sqrt{\frac{2 \cdot df_{cell} \cdot var'_{res}}{n} \cdot F_{(df_{cell};df_{res})}\,(0.95)}. \tag{4.5}$$

Source of Variation	*SS*	*df*	var'	*F*	*P*
Contour type (A)	161.910	1	161.910	21.635	.000
Jitter level (B)	229.217	2	114.608	11.938	.001
A × B	31.370	2	15.685	3.125	.054
A × Vpn	157.153	21	7.483		
B × Vpn	403.214	42	9.600		
Residual	210.746	42	5.018		

Table 4.4: ANOVA results for standard deviation estimates, $\hat{\sigma}$. Conventions as in Table 4.3.

Source of Variation	*Wilk's* Λ	F	df_t	df_e	P
Contour type (A)	.169	49.127	2	20	.000
Jitter level (B)	.322	9.458	4	18	.000
A × B	.789	1.203	4	18	.343

Table 4.5: MANOVA results for the jitter threshold and standard deviation estimates. The table shows source of variation, Wilk's lambda, Λ, F- ratio, F, degrees of freedom for treatment, df_t, and error, df_e, and level of significance, P.

Qualitatively, the same scheme of results is obtained for the standard deviation estimate, $\hat{\sigma}$. Again, there are strong main effects of spatial frequency jitter level and contour type with no interaction. Psychometric curves for open contours are consistently and significantly flatter on the tilt angle scale. As found for tilt angle threshold, pairwise comparisons show no significant differences of the first two jitter levels. The mean difference of MEDIUM to HIGH (D_{23}) is larger than the critical Scheffé distance of $D_{(crit;0.95)} = 1.65$ for both contour types (Closed: $D_{23} = 1.96$; Open: $D_{23} = 3.72$). The multivariate test for the joint effects of both dependent variables substantiates the scheme of results with frequency jitter level and contour type as the two significant main factors with no interaction (Table 4.5).

4.5 Experiment 2

Experiment 2 was designed to explore whether contour detection is possible with spatial frequency homogeneity as the only cue to contour presence. We used two different stimulus display types, one with Gabor patches having totally random orientation along the contour and in background, and one with radially symmetric stimulus micropatterns conveying no orientation information at all. Gabor micropatterns were defined according to (2.1), circular sinusoidal patches as in (2.2). Circular sines were used in addition to Gabor micropatterns because the detection of contours due to the homogeneity of spatial frequency may be impaired by conflicting information from orientation detectors, such as false positives due

to orientation based locking, and the global presence of a further but nonvalid cue.

4.5.1 Methods

Orientation and Spatial Frequency Jitter

Orientation jitter was applied to Gabor elements on contour and background. Orientation jitter was maximum, sampling φ uniformly from the interval $[0°, 180°]$.

Spatial frequency jitter was assigned to all background stimulus elements. For obtaining spatial frequencies of random distribution we used exactly the same sampling technique as in the HIGH condition of Experiment 1 (a 2.9 octaves range).

To generate target stimuli, spatial frequency of all contour elements in a stimulus was set to the expected value of the background spatial frequency distribution ($f_0 = 4.33$). Detectability of target contours was modulated by adding jitter to the spatial frequency of contour elements. Spatial frequency jitter δ was defined as the octave range of spatial frequencies around the mean spatial frequency f_0, and defined the size of the interval where the octave number u was uniformly sampled from. With increasing δ spatial frequency heterogeneity along the contour increases, and thus the visibility of the contour decreases. Examples of target instances are shown in Figure 4.4.

Controlling for Alternative Cues

Homogenizing spatial frequency of contour elements onto the expected value of the spatial frequency distribution of background elements alters the probability of stimulus elements with mean spatial frequencies in the central $10° \times 10°$ target region. Setting the spatial frequency of $N_{FG} = 12$ contour elements to a constant mean frequency amounts to altering the spatial frequency of about 10% of the stimuli in the possible target region. Results from preliminary tests indicated that observers were able to discriminate target from distracter stimuli above chance level by only the different first order statistics of crucial stimulus features in the possible target region. Albeit a contour is never really seen by the observer, a detection strategy favoring the stimulus display with a higher perceived density of elements with mean spatial frequencies enables detection rates well above chance level. To account for this bias, $N_{bg} = 12$ arbitrary background elements within the possible target region of each distracter stimulus were assigned a spatial frequency akin to the distribution of target spatial frequencies.

Subjects

15 of the 22 undergraduate students who had taken part in experiment 1 served as observers. Nine subjects were female, six male.

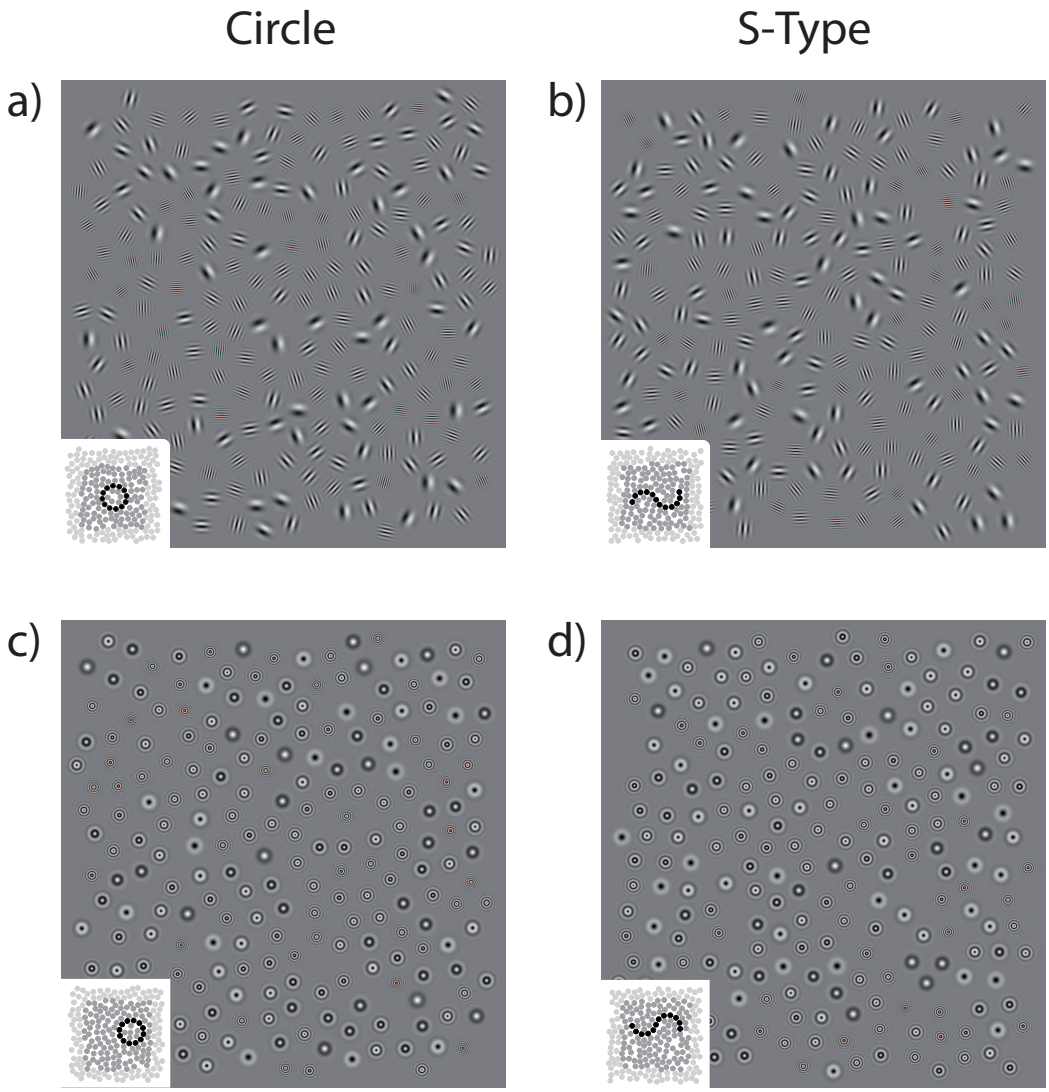

Figure 4.4: Examples of target stimuli and their spatial arrangement. The iconic figures in the lower left corner are symbolic representations of the larger stimulus displays. Stimulus element locations are indicated by dots. Mean grey dots represent locations of stimulus elements which were always sampled from the background distribution, light grey dots the approximate lattice of possible target stimulus positions. Actual target positions are indicated by black dots. Stimulus elements at possible target stimulus positions which were not part of a target figure were sampled from the background distribution. The two panels of I) show instances of Gabor stimuli, the two panels of II) instances of stimuli constructed from circular sines. In both element type conditions, target contours were shaped as a) a circle or b) an S-type figure.

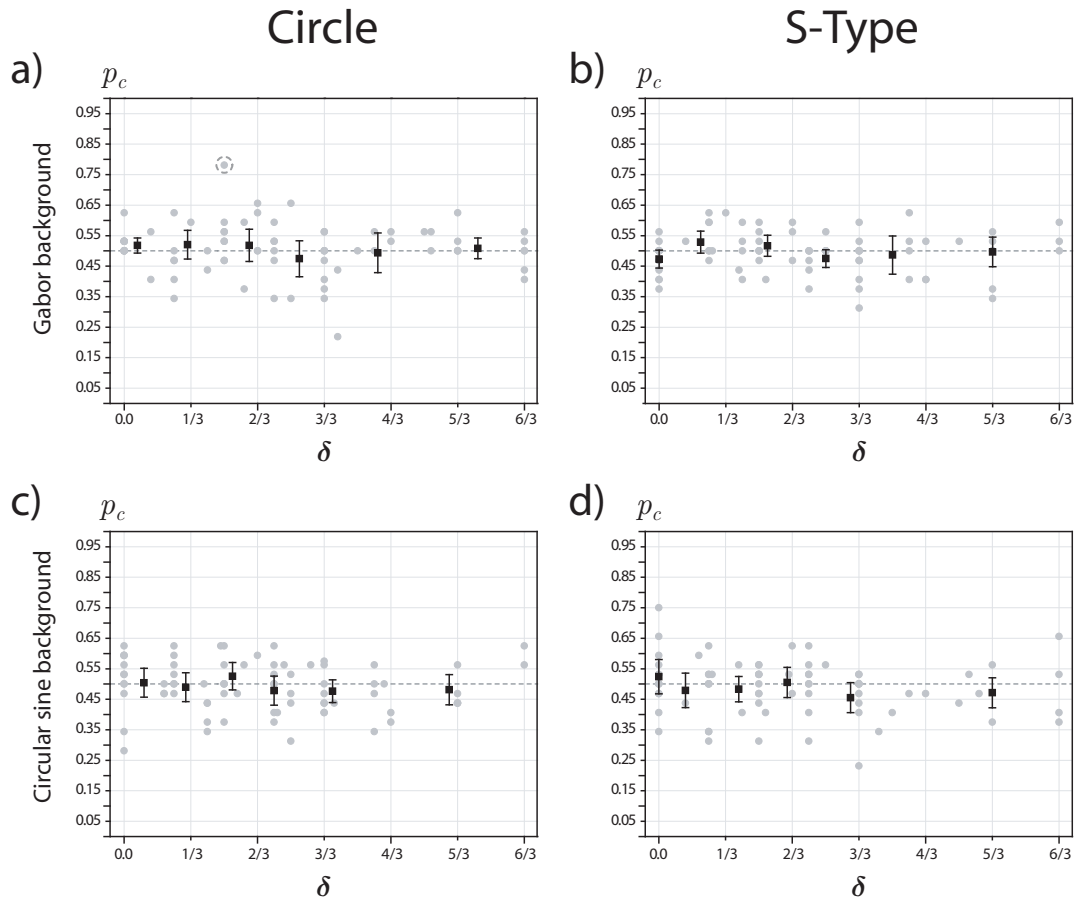

Figure 4.5: Results of measuring contour integration performance as a function of contour spatial frequency jitter level homogeneity (δ). Data are average proportion correct rates with their 95% confidence intervals, separately for each experimental condition. Proportion correct means and confidence intervals were estimated using an optimal binning procedure (see text). The upper row shows the data for Gabor micropatterns, the lower row for circular sine patches.

4.5.2 Results

Figure 4.5 depicts the effects of the four experimental conditions on the proportion correct rate measure. The complete range of contour spatial frequency jitter levels used in the main experiment spans $\delta = [0.0, 2.0]$. To summarize the results, data from all four experimental conditions were pooled separately for each condition by means of an optimal binning procedure. Bin sizes were calculated based on the empirical quantiles of the observed data. Proportion correct rates for data points within each bin interval were linearly averaged and assigned a single abscissa value, the midpoint of the respective bin. Confidence intervals

were estimated for each mean proportion correct rate and separately for each bin. Results for the binned data are summarized in Table 4.6.

It is apparent that subjects were generally not able to detect contours defined by spatial frequency homogeneity, neither with randomly oriented Gabor patches, nor with circular sine patches. Regardless of figure (Circle or S-Type) and patch type (Gabor or circular sine), confidence intervals for all calculated bins overlap $p_c = 0.5$, the chance level for the employed 2AFC task.[13]

In the calibration phase of the experiment we attempted to measure psychometric function data twice for 15 subjects in all four experimental conditions, which is a total of 120 data sets. Only nine data sets (7.50%) allowed a psychometric function estimation with reasonable fit quality, four of these with an ordinate intercept equal or greater than $p_c = 0.80$. During calibration subjects were informed about figure and patch type of the target contours. Nevertheless, subjects were largely inapt to detect visual contours defined by spatial frequency homogeneity. As substantiated by the data of the main experiment, without certainty about contour shape and cue type it is not possible to perform better than chance level with just a spatial frequency homogeneity cue to visual contours.

4.6 Discussion

We have found evidence that contour detection in Gabor random fields is rather robust against spatial frequency jitter. Spatial frequency jitter arranged such that at least every third element differed at least about 1.25 octaves from its neighbors along the contour leads to threshold impairment of just about 5% compared to spatial frequency homogeneous fields. Also the slopes of psychometric curves are practically not affected by spatial frequency jitter of this range. Larger jitter of about 2.25 octaves along the contour leads to threshold impairment, which is about 20% for closed contours and 37% for open contours, indicating that closed contours appear more robust against external noise. However, viewed generally, the impairment due to heterogeneous spatial frequencies in orientation based contour integration is not large. In particular, it is much smaller than can be expected from the bandpass spatial frequency tuning properties of the lateral interconnections of early orientation selective mechanisms, as revealed by the test plus flanker experiments of Polat & Sagi (1993, 1994) (see Introduction). A frequency separation of more than 2 octaves along the contour should have resulted in precluding contour grouping at all. As our data show, contour integration still works well with a spatial frequency separation of this range, although there is a stronger modulating influence of contour type.

[13] Among all four experimental conditions, only one observation exceeds detection threshold ($p_c = 0.75$). The respective data point is marked by a grey circle in Figure 4.5.

a) Gabor background

						95% confidence interval for $\overline{p_c}$	
Figure	Bin no.	Bin midpoint	$\overline{p_c}$	N	$\hat{\sigma}_{\overline{p_c}}$	Lower Limit	Upper Limit
Circle	1	0.100	0.518	14	0.013	0.493	0.542
	2	0.475	0.520	17	0.024	0.473	0.567
	3	0.938	0.518	12	0.027	0.465	0.571
	4	1.313	0.474	11	0.030	0.416	0.533
	5	1.900	0.494	10	0.033	0.429	0.559
	6	2.650	0.509	11	0.017	0.474	0.543
Snake	1	0.000	0.474	13	0.015	0.444	0.503
	2	0.313	0.529	14	0.018	0.493	0.565
	3	0.813	0.517	11	0.018	0.483	0.551
	4	1.250	0.475	20	0.015	0.446	0.504
	5	1.750	0.487	7	0.032	0.424	0.549
	6	2.500	0.497	10	0.025	0.448	0.546

b) Circular sine background

						95% confidence interval for $\overline{p_c}$	
Figure	Bin no.	Bin midpoint	$\overline{p_c}$	N	$\hat{\sigma}_{\overline{p_c}}$	Lower Limit	Upper Limit
Circle	1	0.150	0.504	15	0.024	0.457	0.552
	2	0.463	0.490	12	0.024	0.442	0.537
	3	0.813	0.526	11	0.023	0.480	0.571
	4	1.125	0.478	13	0.024	0.431	0.526
	5	1.563	0.476	14	0.019	0.439	0.513
	6	2.438	0.481	10	0.025	0.432	0.531
Snake	1	0.000	0.524	13	0.029	0.468	0.580
	2	0.200	0.479	12	0.029	0.423	0.536
	3	0.600	0.483	13	0.021	0.442	0.525
	4	0.963	0.505	12	0.025	0.456	0.555
	5	1.438	0.455	13	0.025	0.406	0.505
	6	2.500	0.471	12	0.025	0.422	0.520

Table 4.6: Results from optimal binning of the data obtained in the main experiment. For each of the four experimental conditions, six bins were constructed from the empirical quantiles of the observed data. Proportion correct rates were linearly averaged and standard errors estimated individually for each bin. To characterize the location of each bin, the bin midpoint is displayed. The table summarizes mean proportion correct rates with their standard errors, the number of data points included in each bin, and the lower and upper limit of the 95% confidence interval for each mean value, as defined by $\overline{p_c} \pm 1.96\ \hat{\sigma}_{\overline{p_c}}$.

One may argue that the spatial frequency separated elements fail to preclude detection of the whole contour because these elements may be spatially bridged, and contour detection may occur across them. However, this alternative explanation can be excluded, since it has been formerly shown (Dakin & Hess, 1998; W. Li & Gilbert, 2002) that contour detection performance deteriorates down to chance level if there are spatial gaps within a contour of 2° or larger. So, our data indicate that orientation based contour integration in cluttered images works across much larger ranges of spatial frequency than can be expected just from local locking of neighboring spatial frequency and orientation selective mechanisms on early visual stages. On the other hand, the data of Experiment 2 show that it is not possible to do contour integration when spatial frequency homogeneity is the only cue to the global contour. Even when all elements along the path share the same carrier frequency, a global contour is not perceived better than chance level. Apparently, contour integration is possible across wide ranges of spatial frequency for orientation based grouping, but not at all with spatial frequency as the only grouping cue.

Dakin and Hess (Dakin & Hess, 1998, 1999) measured the reduction in the proportion of correct contour detection as a function of the difference of two concurrent spatial frequencies used in surround and along the contour. The micropatterns were completely aligned with the contour (0° tilt angle), and a 10 element length was used for contours with 30° path angle. We used a 12 element length for the open and closed versions of contours with 30° path angle.[14] To have a rough comparison with the results of Dakin and Hess we calculated average proportion correct rates for tilt angles up to 10°, where performance is close to its maximum (see black circles in the right upper quadrants of the data panels shown in Figure 4.2).[15] Qualitatively, the results (see Table 4.7 and Figure 4.2) reveal the same basic aspect of the data as the 0.75 tilt angle thresholds: There is practically no impairment compared to no spatial frequency jitter when at least every third element differs from its neighbors at least about 1.25 octaves. Even with at least 2.25 octaves separation only a negligible reduction of 1.3% occurs for closed contours, and of 10.7% for open contours.[16] So, our results with small tilt angles in continuous spatial frequency distributions are in strong contrast to the results of Dakin and Hess with two concurrent spatial frequency populations. They found that proportion correct is halved when the octave difference of the two spatial

[14] Dakin and Hess (1998) used path length to adjust performance across path angle. Path length was 4 elements for straight paths, 6 for 10° paths, 8 for 20° paths, and 10 for 30° paths. Path length is extremely crucial for contour integration performance, since the likelihood to confuse a target contour with a false positive in the surround falls rapidly with increasing path length. Straight paths are very easy to see for lengths of 10 and beyond. So the results of this study and the study of Dakin and Hess are comparable only for the 30° paths, which had similar length.

[15] The zero tilt angle was not used in all cases (see Methods), however, including the data for moderate tilt angles gives a good and stable estimate for the highest performance achieved in the 3 spatial frequency jitter level conditions.

[16] The percent reduction is calculated from the data of Table 4.7 as $\Delta r = \Delta p / p$.

	closed			open		
	No	Medium	High	No	Medium	High
Mean	0.916	0.959	0.903	0.902	0.906	0.804
N	29	23	38	42	35	38

Table 4.7: Mean proportions of correct contour detections (Mean) and number of aggregated proportions (N) for tilt angles up to 10° for closed (cols. 2-4) and open (cols. 5-7) contours with the three degrees of spatial frequency jitter.

frequency families becomes larger than 0.7.

A first explanation at hand for this strong discrepancy is that there are concurrent groupings and a lot of false positive lockings within each element population when only two discrete spatial frequency values are in the display (see Figure 8 in Dakin & Hess (1998)). This makes contour detection a difficult task *per se*. The danger of false positive lockings is pronounced with shorter path lengths. Particularly, spurious groupings in the low frequency population are salient in a high frequency environment (see Figure 4 in Dakin & Hess (1998)). It appears that in displays with only two spatial frequencies the spatial frequency cue, although invalid, is extremely distractive. Displays with a continuous distribution of spatial frequencies avoid this disadvantage, and help to focus just on orientation. This is a serious hint that the certainty conditions of the observer are quite important in contour detection experiments. The uncertainty due to the necessity of monitoring multiple spatial positions and multiple spatial frequency bands for possible targets reduces performance remarkably (Kramer et al., 1985; Hübner, 1993, 1996a), and enters as a global factor at the decision stage. In our experiment target contours always had a mean spatial frequency of $f_0 = 4.33$, so some of the spatial frequency uncertainty could be reduced by the repeated experience of the observer that target contours could be expected in a band around a known mean carrier frequency. This was not the case in the experiment of Dakin & Hess (1998), where the mean path carrier was shifted away from the reference carrier of 3.2 cpd from trial to trial, dependent on the carrier of the second Gabor population. Together with the uncertainty about contour length and the increased likelihood of false positives all across the display particularly for the shorter contours there are several differences to our experimental situation, which makes it difficult to give a unique explanation for the conflicting experimental findings.

As our data indicate, the hypothetical contour detection mechanism integrates smooth orientation defined paths over spatial frequency discrepancies of about 1.25 octaves without appreciable impairment compared to spatial-frequency homogeneous displays. If just the locking probability of neighboring elements matters (Field et al., 1993; Herzog et al., 2003; Schinkel et al., 2005) one could argue that this result can be expected, as long as there is some inter-element locking across 1.25 octaves. For proper locking, neighboring

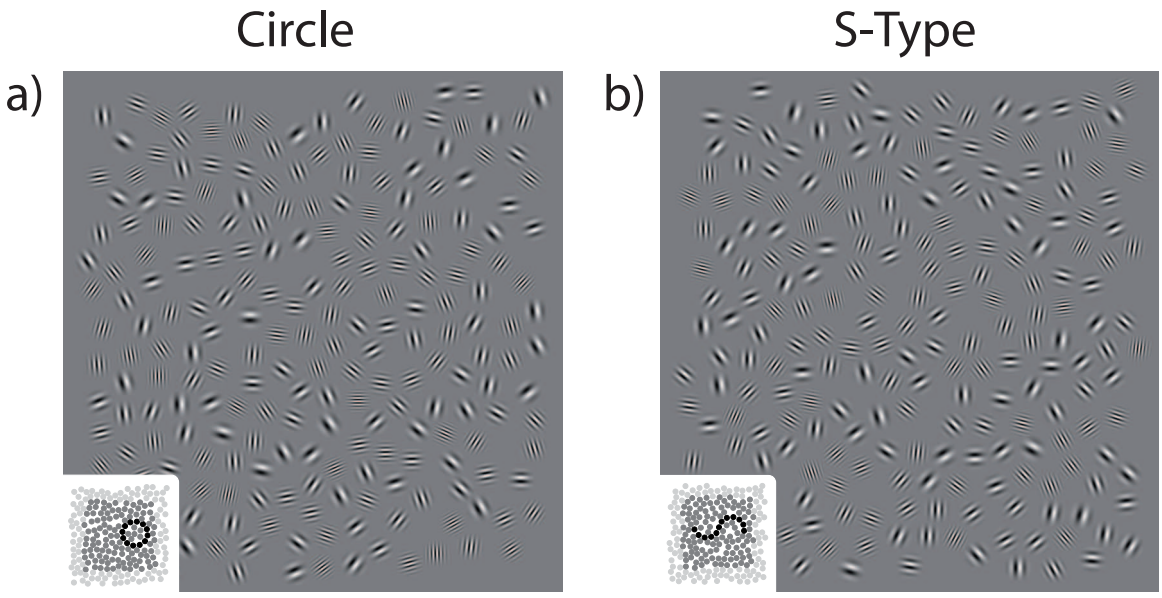

Figure 4.6: Examples of Gabor stimulus displays with closed target contours (left) and open target contours (right) for the control measurements with spatial frequency homogeneous contours embedded in surrounds with spatial frequency jitter of MEDIUM intensity (2 octave range). The pictographs in each image indicate the position of the contour in the field.

elements must fit in orientation and spatial frequency. If spatial frequency jitters in the surround and along the contour, the segregation effect of spatial frequency mismatch is the same along the contour, and from contour towards surrounding elements. Therefore, contour detection performance in spatial-frequency homogeneous and heterogeneous random fields should not strongly differ. In order to prove this, we placed completely spatial-frequency homogeneous contours ($f_{cont} = f_0$) in random fields with spatial frequency jitter of MEDIUM intensity (see Figure 4.6), and measured tilt angle versus proportion correct curves, as in Experiment 1. Mean 0.75 thresholds and standard deviation estimates are shown in Figure 4.3 as down triangle symbols. As the data show, threshold and standard deviation estimates are the same as found with no spatial frequency jitter, and thresholds are slightly better than with MEDIUM jitter along the contour and in surround. This result poses a problem for approaches which explain contour integration just with local grouping among neighboring orientation and spatial frequency selective units. Within surrounds jittering in both dimensions, neighbors flanking the contour are hardly proper locking mates, since they must coincide within both feature dimensions, while mates along the contour have to match just in orientation. So, spatial-frequency homogeneous contours should be much more salient than spatial frequency heterogenous contours in spatial frequency het-

erogenous surrounds. As the data show, they are not. Moreover, comparison for the results of the NO jitter condition are also problematic for a simple inter-element locking approach. In this condition, false locking of elements on the contour with surround elements is more likely than in the case of frequency homogeneous contours embedded in spatial frequency jittering surrounds. So there should also be a clear detection advantage in the latter condition compared to completely spatial-frequency homogeneous displays. Again the data show, there isn't any.

These considerations make it clear that there must be processes involved in contour integration which are not captured by approaches which try to explain contour integration solely by local contextual integration fields. These processes concern global aspects, as the already mentioned certainty conditions of the task, and, most important, integration across larger bands of spatial frequency in later stages. Contour detection in the current task is critically dependent upon the orientation of component Gabor elements, but the detecting mechanism sums over a wide range of spatial frequencies as well as over space. Mechanisms that integrate over multiple spatial scales, but only within a very narrow orientation range, have been shown to mediate orientation discriminations between complex gratings and have been described mathematically in a model of neural recoding (Olzak & Thomas, 1992; Olzak & Wickens, 1997; Olzak & Thomas, 1999; Thomas & Olzak, 1996). These mechanisms, or their outputs, integrate over a large area; discrimination performance continues to improve up to the largest diameter the equipment could produce: just under four degrees of visual angle (Olzak, unpublished data). We speculate that these mechanisms, or a mechanism summing over their outputs, are prime candidates to serve as a contour detector.

There is accumulating evidence, particularly from neuroimaging studies combined with the assessment of psychophysical performance, that contour detection does not solely depend on local locking of neighboring primary coding units selectively sensitive to combinations of orientation and spatial frequency, but is a process that takes place on many spatial scales simultaneously (Altmann et al., 2003; Kourtzi & Kanwisher, 2000; Kourtzi & Huberle, 2005; Lerner et al., 2001). Recent studies show that higher ventral areas, as the parietal cortex, inferio-temporal cortex (IT), and the lateral occipital complex (LOC), similarity grouping is accomplished on a larger scale, and contour parts are connected to form the outlines of figures and shapes (Kourtzi & Kanwisher, 2000; Kourtzi & Huberle, 2005; Lerner et al., 2001). On higher levels not only orientation, but a variety of cues, such as shading, texture, motion, or luminance is used for form completion. Particularly the LOC responds to perceived global shape relatively independent of the nature of the local shape cue, and is particularly sensitive to line drawings. Responses of this area are not modulated by object familiarity, which suggests a stimulus driven analysis (Kourtzi & Kanwisher, 2000). In early areas as V1 and V2, BOLD responses are strongly modulated by a change of local element orientation, but hardly by a change in global shape. In contrast, the LOC

responds most strongly to a change of global form, and moderately to local feature change. Cue integration stabilizing global form detection is stronger in the LOC than in V1 and V2 (Altmann et al., 2003; Kourtzi & Huberle, 2005). Meanwhile, there is ample evidence that contour integration and form completion are processes that concern simultaneous neural processing across the hierarchy (Roelfsema et al., 1998, 2000, 2004). Consequently, a higher level global mechanism searching smooth curvature would successfully integrate circle and S-type fragments across different spatial scales. In the course of the experiment observers learn to reduce uncertainty by ignoring spatial frequencies that are unlikely candidates for a target by forming quasi matched filters (Hübner, 1993, 1996a). So, repeated experience with the same degrees of curvature may also help to build adaptive form tuned global units via principles of Hebbean learning (Mortensen & Nachtigall, 2000).

Taken together, the finding that closed and S- shaped contours are detected across wide ranges of carrier spatial frequencies poses serious problems for approaches that assume the inter-element locking of neighboring orientation tuned early mechanisms as the only mechanism effective in contour integration. Many spatial scales, and the interaction among them, have to be included to arrive at a more realistic description of human contour detection performance in cluttered images. The advantage of multiplex processing should be a challenge for the many models of contour integration that included just a single spatial scale so far (Field et al., 1993; Grossberg & Williamson, 2001; Z. Li, 1998, 1999; Yen & Finkel, 1997, 1998; Herzog et al., 2003; Schinkel et al., 2005).

5 Contour Integration by Cue Combination

Synopsis

The interaction of local orientation alignment cues and spatial frequency cues in global contour salience was studied with Gabor random fields having elements jittering in local carrier spatial frequency and orientation. Target contours were defined by local orientation alignment, a mean spatial frequency difference of the contour elements to the surround, or both cues, and subjects had to indicate in a 2AFC task which frame contained the contour, and to identify its type (circle or S-type). The effect of cue summation, defined as the performance benefit due to the combination of the alignment with a spatial frequency cue, was evaluated and tested against the predictions derived from probability summation and linear summation. Cue summation was strong and increased with the performance level achieved with single cues until it was bounded by ceiling effects. Cue summation was particularly large when the spatial frequency deviation of contour elements and surround was realized by lowering the carrier frequency of the contour elements. Together with the robustness of alignment based contour integration over wide ranges of spatial frequency (Persike, Olzak, & Meinhardt, 2007) the results indicate two distinct grouping mechanisms in contour integration. The first one mediates similarity and feature–segregation based grouping among the contour defining elements, and works independent of local alignment. The second one is purely alignment based, and integrates over other locally variable features. Cooperation of both mechanisms leads to strong location binding and highly salient global contours. The implications of these findings for feature based detection of shape and for side conditions of modeling contour detection are discussed.

5.1 Introduction

Detecting visual objects requires to decompose a visual scene into parts and to reintegrate these parts into meaningful wholes. Several principles of information processing are implemented into the nervous system to accomplish segregation and reintegration. One basic principle for segregation is border detection. Object borders usually define the outlines of objects and are formed by local feature differences, such as spatial transitions in lumi-

nance, contrast, color, orientation, spatial frequency, motion, or texture. Ample research in the last three decades was dedicated to proving that the outlines of objects, established by local differences in feature modulation, can be extracted with a relatively simple feed-forward mechanism, comprising a stage of linear orientation selective filters followed by a local nonlinearity and a second stage of isotropic filtering. (Caelli, 1982; Bergen & Julesz, 1983; Bergen & Adelson, 1988; Landy & Bergen, 1991; Rubenstein & Sagi, 1990, 1996; Sagi, 1991; Malik & Perona, 1990). The outcome of processing, a spatial map containing object borders, is considered the preliminary stage of object recognition in theories of object vision (Sagi, 1995; Marr, 1982; Biederman, 1987).

Other principles that underlie detection of shapes and objects concern grouping of similar elements and linking them across space into larger configurations. From the well known Gestalt rules proposed in the twenties of the last century we expect elements to be grouped particularly by proximity, similarity and good continuation. However, these principles remain relatively ambiguous in complex stimulus situations. For example, the degree of similarity of elements varies with the context in which they appear. The contextual dependency of similarity grouping was first demonstrated by Beck (Beck, 1966, 1972, 1982), who showed that elements, which appear very similar when viewed as single entities, may define strongly segregating regions when presented together as opposite regions, while other seemingly very different single elements do not form very different regions when they are arranged as spatial groups.

In search of the local principles that define spatial element grouping in textures and cluttered images, many studies of the nineties of the last century provided evidence that local orientation signals are crucial for linking spatially distributed elements into global spatial structures. Field et al. (1993) proposed a 'local association field' as a means to govern the rules of how spatially distributed local elements become integrated into a contiguous whole very early in the visual pathway. Psychophysical studies (Kovacs & Julesz, 1993; Hess & Demanins, 1998; Hess & Field, 1999; Hess & Dakin, 1999; Hess et al., 2001; Polat & Bonneh, 2000; Polat & Sagi, 1993, 1994a; Ledgeway et al., 2005; Persike et al., 2007), neuroanatomical investigations (Bauer & Heinze, 2002; Kourtzi & Huberle, 2005; Mandon & Kreiter, 2005; Mathes & Fahle, 2007a), and model simulations (Z. Li, 1998; Feldman, 2001; Mundhenk & Itti, 2005; Schinkel et al., 2005; Samonds et al., 2006) have supported the notion of contour integration being accomplished by linking the outputs of neighboring orientation selective cells to form paths in a spatial map. Expressed in terms of the Gestaltists, association field models implement the principle of good continuation for detecting structure in cluttered images.

In most studies of contour detection the principle of good continuation was put into focus by capitalizing on the effect of global-local path alignment of the contour defining elements. Varying only the orientation of local elements, other principles that contribute to overall contour salience were left out of account to some extent. For example, varying

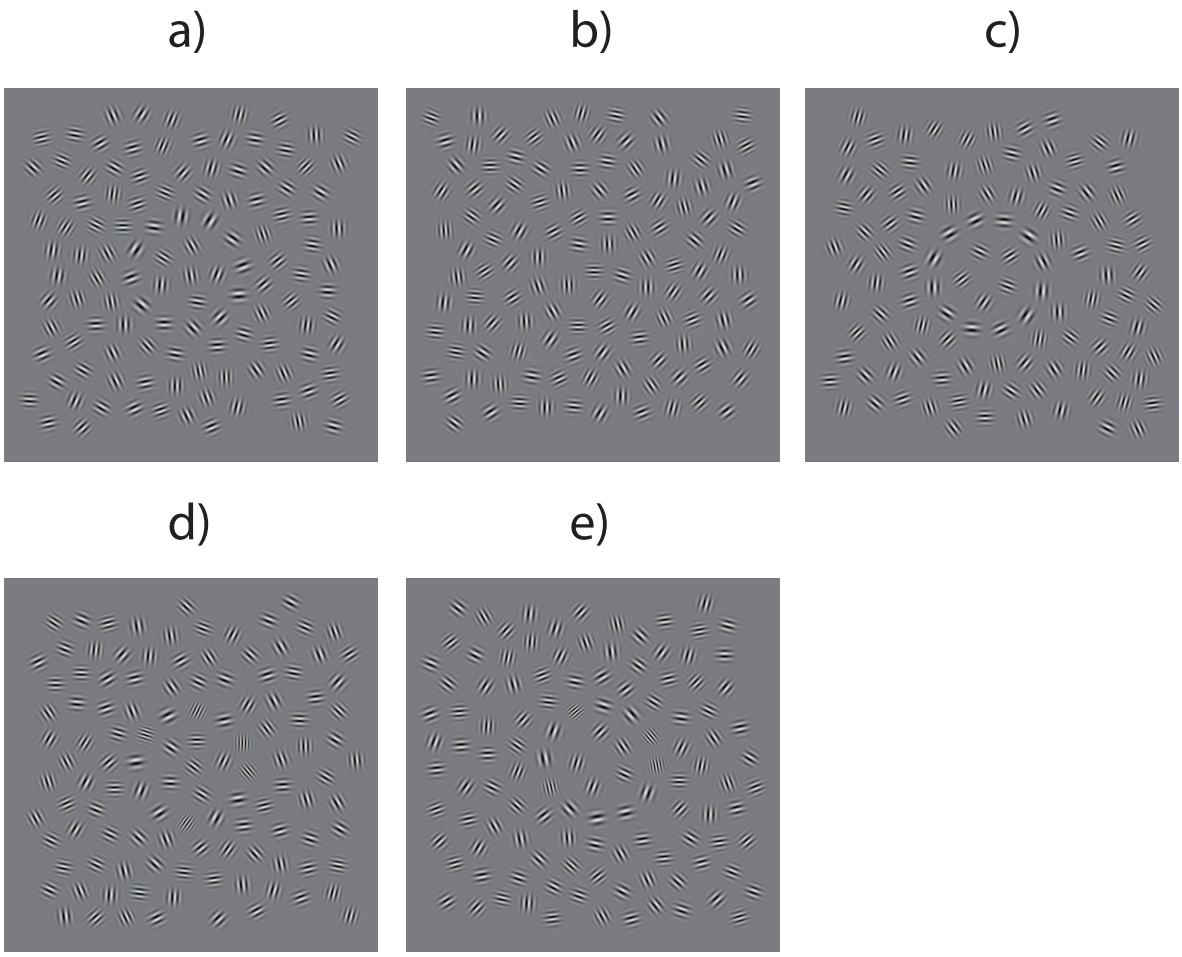

Figure 5.1: Perceptual effects of feature contrast, alignment and similarity cues on the salience of a global circular contour in Gabor random fields. In a) the twelve contour defining elements have the same random orientation than the surrounding elements, but an octave lower carrier frequency. The contour defining elements segregate from the surround, and are similar to each other. b) shows contour defining elements with local orientations aligned with the global path. Elements belonging to the contour have the same carrier frequency than the surrounding elements. In c) the contour defining principles of a) and b) are combined, which makes the global path highly salient. d) shows elements along the circular path which have an octave lower or higher carrier frequency than the surround, and random orientation. These elements segregate from the embedding field, but are not similar. In e) feature contrast in carrier frequency is combined with global path alignment.

spatial frequency or size of the elements in a random field could provide valuable hints about the effect of inter-element similarity on grouping phenomena in contour integration. Unfortunately, only few studies were dedicated to the effect of additional cues in contour integration so far. Variation of spatial frequency cues was used to study just the robustness of alignment based grouping against an additional source of variation (Dakin & Hess, 1998, 1999). Defining contours by path alignment and additional cues such as color (Mathes et al., 2006b), motion (Ledgeway et al., 2005) and depth (Hess et al., 1997; Ledgeway et al., 2005; Mathes et al., 2006b) showed that the performance benefit obtained for the combined features
is in a order of magnitude as can be expected from assuming cue independence, yielding just a moderate increase of the overall contour salience compared to single cue contour salience.

As Nothdurft (2000) has pointed out, the effect of combining features is highly dependent on the specific pairing of features. In a feature contrast salience matching task with single texture elements (singletons) he found that color and orientation did not show much salience summation, while adding a luminance cue to orientation produced a much stronger salience gain. This suggests that there are constraints in the architecture of the visual system which rule the degree to which different features might interact. It is therefore challenging to look whether features, which are coded on a common site, interact stronger than can be expected from assuming independent feature selective processing in a contour integration task.

As propagated by Sagi (1988), combinations of spatial frequency and orientation are effortlessly perceived and produce strong pop-out effects in a search display. According to Sagi (Sagi, 1988; Rubenstein & Sagi, 1990) this is probably due to the fact that these combinations are jointly coded on an early site. Since in the realm of association field models, contour integration is viewed as the result of inter-element locking of orientation and spatial frequency selective units located on an early site, it is straightforward to ask whether combining path alignment with a spatial frequency cue produces a strong contour detection gain by emphasizing inter-element grouping along the path. From the Gestaltist approach, one may ask whether adding a similarity cue to good continuation of the elements along the path results in strong salience enhancement of the global contour.

Figure 5.1 shows exemplary stimulus arrangements with fields of Gabor elements and their perceptual effects on contour salience. In Figure 5.1a Gabor elements with a carrier spatial frequency about half an octave lower compared to the surround are arranged along a circular path, producing the impression of a global circle. In Figure 5.1b Gabor elements having the same carrier frequency as the surround are aligned with the path, which also results in a strong circular global figure. In Figure 5.1c the variations of Figure 5.1a and Figure 5.1b are combined. The perceptual result is a highly salient circular figure. In Figure 5.1d the elements along the circular path have half an octave lower or higher carrier

frequency compared to the surrounding elements, alternating randomly. In Figure 5.1e this kind of variation is combined with path alignment. While no circle is visible just by spatial frequency contrast, the figure becomes visible by alignment. However, the perceptual salience is lower compared its spatial frequency homogeneous counterpart shown in Figure 5.1c, which evokes the strongest impression of a global figure.

A closer look at Figure 5.1a-e shows that the examples given there demonstrate the perceptual effects of three principles, namely *feature contrast*, *similarity* and *good continuation* on the salience of a global contour. Comparison of the variations shown in a) and d) reveals the contribution of similarity grouping as added to feature contrast, since in a) there is feature contrast based segregation and homogeneity of the contour element carrier frequency while in d) there is segregation by feature contrast only. Apparently, the contribution of the feature contrast cue to global contour salience is weak. Contour salience purely by path alignment is illustrated in b). The perceptual salience of this kind of variation was demonstrated in many studies (Kovacs & Julesz, 1993; Geisler et al., 2001; Braun, 1999; Mathes et al., 2006b). The example shown in e) demonstrates the effect of combining a pure feature cue with an alignment cue.[17] The strong global contour salience of the example shown in c) is the result of perceptual summation among all three types of cues, feature contrast, alignment and similarity.

In the present study the effects of feature contrast, similarity and good continuation are investigated by employing the kind of variations outlined in Figure 5.1a-c. The results obtained for these variations are discussed together with the results of a preceding study (Persike et al., 2007), which employed the type of variations illustrated in Figure 5.1d and 5.1e. In both studies the same measure of salience was applied, and the same technique to reveal the degree of cue summation for multiple cue displays. Comparing the results of these two studies and other studies from the field, the contribution of the three types of cues to a global contour is outlined, and the association field model is evaluated in the context of the new insights that derive from studying cue summation phenomena in contour integration.

5.2 Methods

5.2.1 Stimulus Micropatterns

Stimulus displays consisted of contour paths made up by Gabor micropatterns, embedded in Gabor random fields. Gabor elements were defined according to (2.1).

[17] Note that alignment and orientation similarity are not confounded in b) and c), since the elements along the circle take all possible orientations, and the surrounding field is randomly sampled from all possible orientations. So the elements along the circle do only show good continuation, but no higher order orientation similarity than the surrounding elements.

5.2.2 Orientation and Spatial Frequency of Stimulus Patches

Orientation and spatial frequency jitter were applied to the background elements in all experimental conditions. Orientation jitter was maximum, sampling φ uniformly from the interval $[0°, 180°]$. For obtaining spatial frequencies of random distribution we defined spatial frequencies as $f = 2^u$ and sampled u from the uniform distribution $U(a, b)$ with a and b the lower and upper limit. Within the scope of the study, let $\mu_f = \frac{a+b}{2}$ and $r_f = \frac{b-a}{2}$, whereby u is sampled from $U(\mu_f \pm r_f)$. We chose $\mu_f = 2.087$ octaves and $r_f = .175$ octaves as parameters for the reference distribution of background spatial frequencies. The range parameter r_u was identical for target and reference patterns and constant throughout the experiment. Measured in units of cycles per degree (cpd), spatial frequencies of background micropatterns were sampled from the interval $[3.74, 4.76]$.

Detectability of target contours was modulated by orientation of contour elements, their spatial frequencies, or both. Target patterns with orientation contours were formed by initially aligning the orientation of contour elements perfectly with the global contour curvature, then introducing a deviation of element orientation from the contour. Increasing 'tilt angle' v corrupts the fit of local element orientation with global path curvature and thus results in deteriorating contour detection performance. Target patterns comprising spatial frequency contours were generated by sampling spatial frequencies of contour elements from a distribution with a different mean parameter $\mu_{f,tar} = \mu_{f,ref} + \Delta f$, but unchanged range parameter. Note that depending on experimental condition, Δf could take positive or negative values, so that the distribution of target contour spatial frequencies was shifted relative to the background distribution either in upward or downward direction.

5.2.3 Experimental Design

Target figures could consequently be defined by orientation tilt angle, upward or downward spatial frequency shift (single cue targets; denoted as ϕ, f_{up}, or f_{down}, in what follows), or the two pairwise combinations of orientation with each spatial frequency shift direction (double cue targets; denoted as $\phi + f_{up}$ or $\phi + f_{down}$), each at five visibility levels. Contour type was not assumed a separate experimental condition, but was randomly chosen with equal likelihood on each trial. See Figure 5.2 for examples of all stimulus types used in the experiment, and Procedure for a summary of actual parameter levels used in the main experiment.

5.2.4 Subjects

25 undergraduate students served as observers. Sixteen subjects were female, nine male. All subjects had normal or corrected to normal vision. The students had no former psychophysical experience, were paid and not informed about the purpose of the experiment.

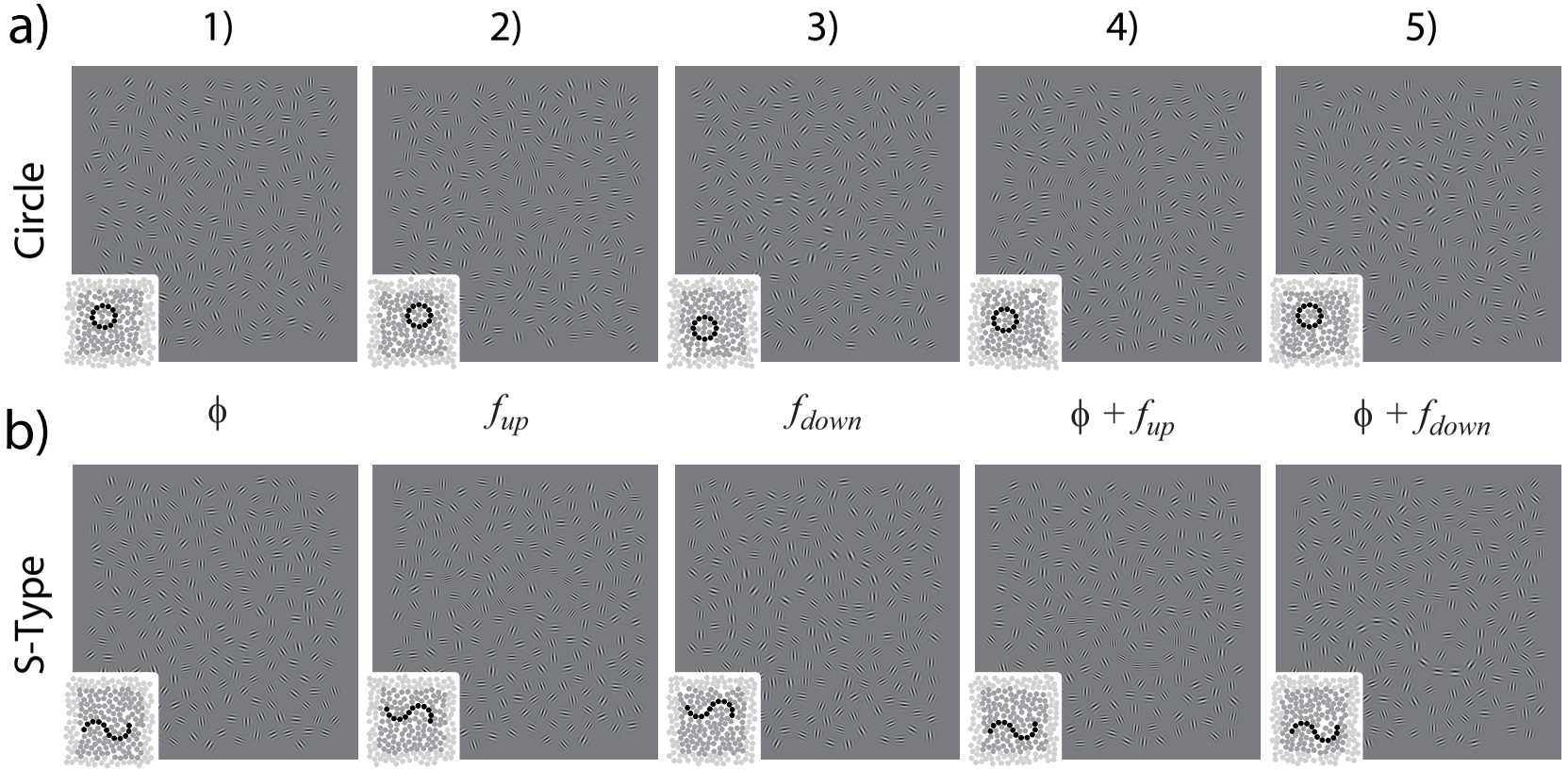

Figure 5.2: Examples of target patterns with circles (a) and S-type (b) contours. (a) shows a circle (see pictograph), defined by orientation (1), upward directed spatial frequency contrast (2), downward spatial frequency contrast (3) and the conjunctions of orientation with each of the two spatial frequency feature contrasts (3 and 4). With only a single feature cue (see panels 1 through 3) the mean parameter difference of the inner and the outer region is too small to readily enable detection and identification of target contours. With the same parameter difference but in both feature dimensions simultaneously (double cue target definition), visibility of contours is markedly increased. Note the apparent salience benefit of contours defined by the conjunction type $\phi + f_{down}$ (panel 5) relative to $\phi + f_{up}$ (panel 4), although the single cue components are perceptually equivalent.

5.2.5 Procedure

Detection Performance Level

For all single feature dimensions (ϕ, f_{up}, or f_{down}) we established five visibility levels by varying orientation tilt angle v or spatial frequency shift Δf, the latter taking positive values for f_{up} and negative values for f_{down}. The five visibility levels were individually calibrated for each subject such as to correspond to the same definite performance levels in the feature contrast detection task. For double cue targets ($\phi + f_{up}$ and $\phi + f_{down}$) the visibility levels of two feature dimensions were then combined at each detection performance level. A rather wide range of detection levels was chosen in order to be able to judge the degree of cue summation for low and higher target visibility in both tasks.

Calibration of Individual Detection Performance Levels

Calibration measurements served an important purpose in determining perceptually equivalent feature contrast levels of all single features, in order to define double cue targets with equally detectable components (see Persike & Meinhardt, 2006). To achieve this, subjects measured psychometric curves for feature contrast detection in a 2AFC task. All calibration measurements were done twice by every subject on two different days to obtain reliable psychometric function estimates. Psychometric function data sets from the two days were then merged and fit with Weibull functions by estimating their shape and scale parameters using the Levenberg-Marquardt algorithm. On the basis of the fitting functions we extrapolated the set of feature contrasts which corresponded to proportions of correct judgements of 0.62, 0.68, 0.74, 0.80, and 0.86 in the detection task, which are levels of 0.432, 0.661, 0.910, 1.190 and 1.528, expressed as a d' measure. This was done individually by each subject for the three feature dimensions (ϕ, f_{up}, and f_{down}) and both figure types. In the main experiment exactly the estimated sets of parameter values were used for the single cue targets, as well as for the pairwise conjunctions of single features at each visibility level for the double cue targets ($\phi + f_{up}$ and $\phi + f_{down}$). Measuring two psychometric functions for three feature dimensions with five intensity levels, separately for circular and S-type contours, each with 32 replications, means that each subject had to get through at least 960 trials before the main experiment. This took about two hours.

Main Experiment

After calibration of the parameter sets for each subject, correct key assignment and figure type categorization learning was verified in a training period with highly salient target patterns. Finally, the main experiment was executed. With 32 replications of each experimental condition and contour type the main experiment comprised 1600 trials. The trials

were randomly intermixed and divided into two blocks, each lasting about one hour. Both blocks were run at the same day.

5.2.6 Performance Measures

d' Data Transformation

In order to enable data analysis within the framework of factorial designs it is necessary to have an unbounded variable with at least an interval scale of measurement. Proportion correct is not appropriate, since it is a bounded measure whose distribution become seriously skewed as the mean gets close to the upper or lower end of the scale. The sensitivity measure d' avoids this disadvantage and is uniquely related to proportion correct in a 2AFC task (see McMillan & Creelman, 2005, p. 172). d' is obtained from proportion correct by

$$d' = \sqrt{2}\Phi^{-1}(p)\,. \tag{5.1}$$

Measure of Cue Summation

The detection and discrimination of compound stimuli is treated by signal detection theory. It is assumed that the observer maps each stimulus component onto a random variable through a sensory transformation, and all random variables together span a multivariate space of sensory states. The observer's performance can be described by comparisons along each axis with decision bounds, and sensitivity is determined by the distances of the centroids for each stimulus alternative (McMillan & Creelman, 2005; Tanner, 1956; Ashby & Townsend, 1986). For two stimulus dimensions and two stimulus alternatives, the distance between the centroids of target and reference distribution is given by

$$d'_{\phi+f} = \sqrt{\left(d'_\phi\right)^2 + \left(d'_f\right)^2 + 2d'_\phi d'_f \cos\gamma}. \tag{5.2}$$

Here, γ is the angle enclosed by both random variables, d'_ϕ is the mean distance for feature ϕ and d'_f the corresponding mean distance for feature f. If both features are processed by the same sensory mechanism both random variables coincide (i.e. $\gamma = 0°, \cos\gamma = 1$), which implies linear summation, (5.2) reduces to $d'_{\phi+f} = |d'_\phi + d'_f|$. If both random variables are independent in the sense of dimensional orthogonality (Tanner, 1956), then $\gamma = 90°$ and $\cos\gamma = 0$, hence (5.2) becomes

$$d'_\perp = \sqrt{\left(d'_\phi\right)^2 + \left(d'_f\right)^2}. \tag{5.3}$$

The prediction of dimensional orthogonality (5.3) enables a statistical test of whether the observed d' sensitivity for feature conjunctions, $d'_{\phi+f}$, is larger than expected for the case of independent sensory coding of both features, $d'_\perp$. In the latter case

$$\Delta d'_\perp = d'_{\phi+f} - d'_\perp \tag{5.4}$$

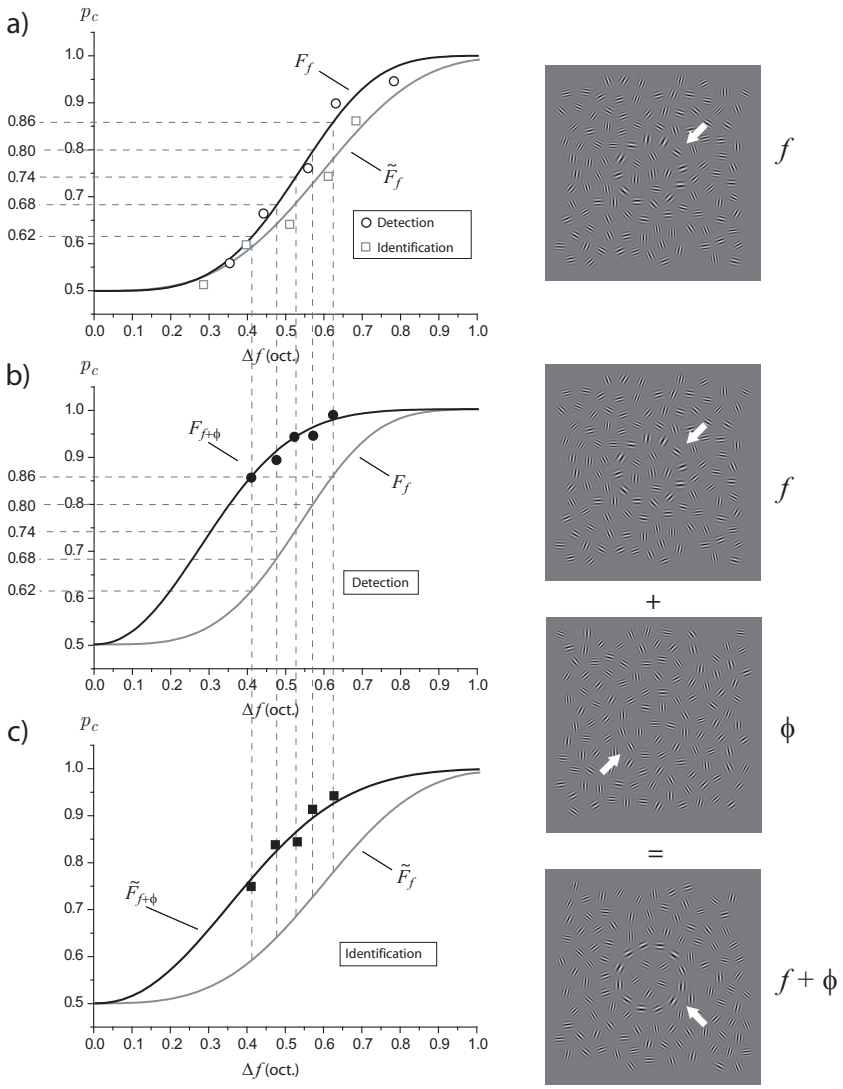

Figure 5.3: Screening measurements for cue summation effects. The plots show proportion correct data (p_c) as a function of the mean difference of target and reference distribution for the spatial frequency cue. The stimulus examples on the right side provide a vivid illustration of the visibility difference between single and double cues. Data are shown for one subject exemplarily. (a) Proportion correct data obtained in 2AFC measurements fitted by Weibull functions in the feature contrast detection (open black circles and black line, F_f) and figure identification task (open grey squares and grey line, $\widetilde{F}_f$). The dashed projection lines illustrate the correspondence of the five detection performance levels chosen for the main experiment (intersection with ordinate) to the feature contrast values (projection on abscissa). (b) Psychometric curves for the spatial frequency cue alone (grey line, F_f) and double cue targets (black line and solid black circles, $F_{f+\phi}$) for the feature contrast detection task. The vertical curve distances along the projection lines denote the improvement due to the additional and equally detectable spatial frequency cue. (c) Psychometric curves for single cue (grey line, $\widetilde{F}_f$) and double cue targets (black line and solid squares, $\widetilde{F}_{f+\phi}$) for the figure identification task.

has zero expected value and its standard error derives from the factorial decomposition of the experimental design employed for statistical testing. Note that (5.3) predicts a relatively large degree of summation among independent feature specific variables and is therefore a stern benchmark for testing cue summation effects. In case of dimensional orthogonality, just $2^{-1/2} = 0.707$ units of d' are necessary for each of two equally visible single cues in order to reach one unit of d' in the overall performance. This means that there is approximately 29% 'redundancy gain' for dimensional orthogonality, and this prediction is hard to beat. Probability summation in the formulation of Quick's model (Quick, 1974) implies a single component strength of $2^{-1/k}$, where k is the shape parameter of the Weibull distribution function (Watson, 1982; Meinhardt & Persike, 2003; Meinhardt, 1999, 2000). Since k varies from 2.7 to 4.6 in 2AFC experiments (Robson & Graham, 1981; Graham, 1989), the gain expected from probability summation in a double cue experiment ranges between 14% and 22.6% in a threshold measure.

5.2.7 Data Clearing and Handling of Outliers

The measure of cue summation (5.4) is based on a triplet of d' values $(d'_{\phi}, d'_{f}, d'_{\phi+f})$, which is obtained from each subject for each experimental condition. In the present study, two different triplets were obtained from the combination of orientation with upward directed spatial frequency contrast $(d'_{\phi}, d'_{f}, d'_{\phi+f_{up}})$, and such with downward spatial frequency contrast $(d'_{\phi}, d'_{f}, d'_{\phi+f_{down}})$. For the lowest visibility levels, which allow performance levels only slightly above chance, also negative d' values can be expected to occur due to proportion correct rates falling below guessing probability incidentally. The prediction for independent feature processing (5.3), however, cannot become negative, since it is defined as an absolute value. Consequently, the inevitable occurrence of negative d' values at low visibility levels makes the independence prediction (5.3) too stern. Since negative d' values indicate that a subjects' performance is at chance level, we set them to zero for subsequent analysis. This was necessary for 6 out of 625 observations in the detection task (0.96%) and for 8 observations in the identification task (1.28%). Proportions correct for perfect performance were replaced by $1 - (2N)^{-1}$, where N is the number of replications. This correction was applied to 19 observations in the detection task and to 13 observations in the identification task.

5.3 Results

5.3.1 Parameter Ranges

Visibility of orientation contours was modulated by rotating each contour element away from its perfect alignment with the contour by different tilt angles, randomly in clock-

wise or counterclockwise direction. Tilt angle values for the lowest visibility level among all subjects in the main experiment fell within the range of $[20.0°, 28.5°]$ for circles and $[15.8°, 26.8°]$ for S-type contours. To elevate detection performance up to the highest intended visibility level, tilt angles in the interval $[12.5°, 22.0°]$ were needed for circles and $[8.9°, 17.1°]$ for S-type contours. Spatial frequency contrast was realized by shifting the uniform spatial frequency distribution of contour elements away from the reference distribution in upward or downward direction. Measured in octaves, the lowest visibility level required shifts from the interval $[.11, .52]$ for upward spatial frequency contrasts (f_{up}) and $[.08, .26]$ for downward feature contrasts (f_{down}), whereas the highest visibility level was attained with shifts of $[.26, .66]$ octaves in f_{up} and $[.18, .51]$ octaves in f_{down} among all subjects. Feature contrast levels here did not differ significantly between the two contour types. In total, spatial frequencies spanned 4.03 cpd to 7.52 cpd for upward feature contrasts and 2.61 cpd to 4.52 cpd in downward direction.

Contrast matching experiments with suprathreshold standards at the same luminance level than used in this experiment show that sensitivity is almost constant within the range used here (Peli, Arend, & Labianca, 1996). Also, Gabor element root mean square (RMS) contrast is practically constant within this range of spatial frequencies at the chosen Gabor element size.

5.3.2 Screening of Cue Summation Effects

Figure 5.3 shows data from calibration measurements of spatial frequency feature contrast, as well as screening measurements for the cue summation effect. The screening measurements were done by the author and two other staff members, who are experienced observers. Doing the feature detection tasks with targets defined by two equally detectable feature cues ($\phi + f$) elevates the proportion of correct judgements at each of the five detection performance levels relative to the single cue f. As a result, the psychometric curve for double cue targets is leftward shifted relative to the one obtained for the spatial frequency cue alone (see Figure 5.3b). The magnitude of leftward shift thus represents the double cue benefit. When the figure identification task is done at the same visibility levels, performance is only marginally weaker compared to the detection task (see Figure 5.3a and Figure 5.3c, grey curves).

5.3.3 Observed and Calibrated Single Cue Sensitivity Level

Figure 5.4 shows the observed sensitivity level of each single cue feature in the main experiment as a function of the calibrated d' detection sensitivity level (see Methods), separately for the detection and identification task. The diagonal with slope 1 is the line where calibrated and observed detection performances coincide, indicating a perfect match of

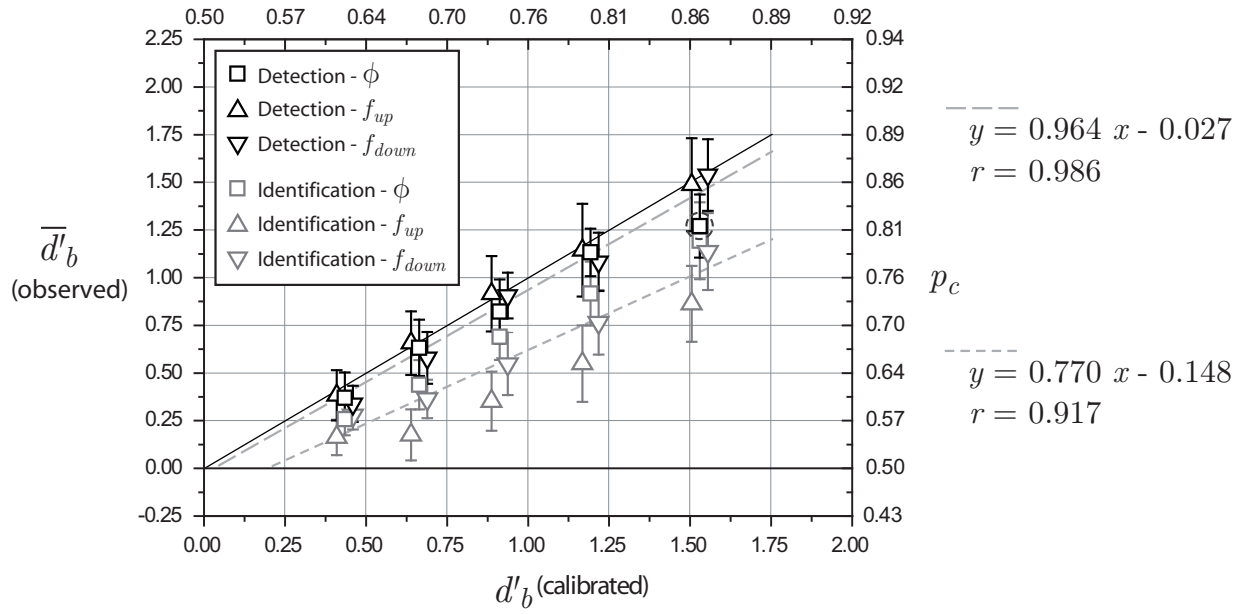

Figure 5.4: Observed base sensitivity level according to (5.5), measured in d' units, as a function of the calibrated base sensitivity level in the feature contrast detection and identification task. The right and upper axes show the proportion correct scale for comparison. Data for the feature contrast detection task are indicated by circles, data for the contour type identification task are indicated by squares. The data means were fitted by linear regression functions, which are drawn as dashed lines (long dashing: detection task; short dashing: identification tasks; see right keys for regression parameters). The straight solid line is the positive diagonal with slope 1. Error bars denote 95% confidence limits of the mean.

intended and observed visibility levels. The relation of all variables is almost perfectly linear[18]. The regression line for the detection data is practically identical to the diagonal with slope 1, only at the highest feature level for ϕ a notable divergence of calibrated and observed sensitivity level occurs.

5.3.4 Performance as a Function of Feature Contrast Level

Figure 5.5 summarizes the effects of experimental variation on the performance in the feature contrast detection task (black symbols) and the contour type identification task (grey

[18]Figure 5.4 indicates that the base sensitivity levels for each task and figure type are linear functions of the calibrated d' detection level. Linear approximations were done separately for each task, but combined for the three single cue features (ϕ, f_{up}, and f_{down}). The Pearson correlation between observed and calibrated base sensitivity level is larger than .910 for each of the data sets. Consequently, also the relation of the base sensitivity levels among both tasks is linear.

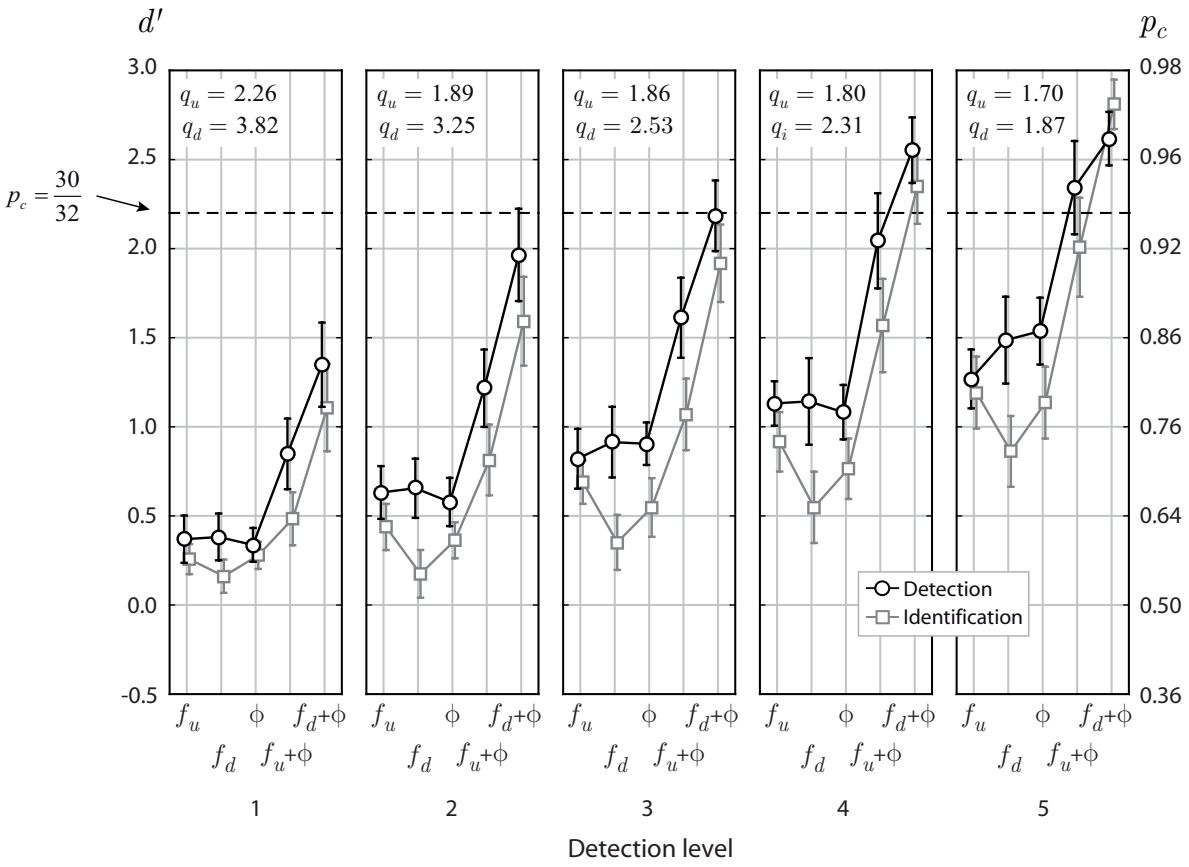

Figure 5.5: Summary of main effects. The figure depicts mean d' sensitivity for feature contrast detection (black circles) and figure identification (grey squares) for contours defined by orientation (ϕ), upward or downward directed feature contrast in spatial frequency (f_{up} and f_{down}), and the double cues ($\phi + f_{up}$ and $\phi + f_{down}$). Data are shown for the five detection levels. Error bars denote 95% confidence limits of the mean, based on the standard error of measurement of each cell. The latter was estimated based on the residual cell variance calculated within a complete factorial repeated measurements MANOVA. The right ordinate shows the proportion correct scale, which directly corresponds to d' in a 2AFC task. The performance level which corresponds to 30 hits of the 32 trials is marked by a dashed line. The q- values (see Table 5.1) indicate the ratio of mean double cue sensitivity in the detection task, $\overline{d'}_{f+\phi}$, to the mean sensitivity achieved with both single cues, $\overline{d'}_b$, for double cues with f_{up} (q_u) and with f_{down} (q_d), respectively.

symbols). The figure emphasizes the notion of Figure 5.4 that the calibration procedures successfully established perceptual equivalence among all three single cues, since their mean d' values differ only fractionally among each other. Sensitivity rises with feature contrast level and is only marginally higher for detection than for identification. The iden-

		Detection				Identification			
Conjunction	FC-Level	$\overline{d'}_b$	$\overline{d'}_{\phi+f}$	$\overline{\Delta}d'_b$	q	$\overline{d'}_b$	$\overline{d'}_{\phi+f}$	$\overline{\Delta}d'_b$	q
$\phi + f_{up}$	1	.376	.848	.473	2.258	.210	.484	.274	2.308
	2	.644	1.217	.573	1.890	.306	.814	.508	2.658
	3	.868	1.612	.744	1.858	.521	1.070	.549	2.055
	4	1.137	2.044	.907	1.798	.732	1.569	.837	2.143
	5	1.378	2.342	.964	1.700	1.027	2.008	.981	1.955
$\phi + f_{down}$	1	.354	1.349	.995	3.815	.268	1.108	.840	4.135
	2	.605	1.965	1.360	3.248	.401	1.593	1.192	3.975
	3	.863	2.184	1.321	2.530	.619	1.918	1.299	3.101
	4	1.107	2.552	1.446	2.306	.840	2.351	1.510	2.797
	5	1.403	2.617	1.214	1.865	1.164	2.810	1.646	2.414

Table 5.1: Sensitivity advantage of double cue targets compared to the base sensitivity level. The table shows the base sensitivity level, $\overline{d'}_b$, mean sensitivity for double cue targets, $\overline{d'}_{\phi+f}$, mean sensitivity difference, $\overline{\Delta}d'_b$, and the ratio of double cue and single cue performance, $q = \overline{d'}_{\phi+f}/|\overline{d'}_b|$. Data are shown for both tasks and feature conjunction types at the five detection levels.

tification task therefore proves its purpose as a control task, asserting that not only small segments but a sufficiently large part of the whole contour were seen by the observers. Sensitivity is consistently higher with double cues than with single cues. Hence, we generally find a clear and stable cue summation effect, particularly at larger visibility levels in both tasks. At the highest visibility levels mean proportion correct rates of more than 30 hits of 32 trials are reached with double cues in five cases (see dashed lines). This is the utmost of what can be expected in forced choice experiments. Moreover, Figure 5.5 suggests a systematic difference in magnitude of the cue summation effects between the two double cue combinations $\phi + f_{up}$ and $\phi + f_{down}$.

Further analysis concerns statistical testing of the cue summation effect, and elaborates on how cue summation gains are modulated by the base sensitivity level and the direction of spatial frequency feature contrast (i.e., f_{up} or f_{down}).

5.3.5 The Cue Summation Effect

Comparing Double Cue to Single Cue Performance

With perceptual equivalence among the single cues ϕ, f_{up}, and f_{down}, as found in Figure 5.4, a 'base sensitivity level' can be defined as

$$\overline{d'}_b = \frac{d'_\phi + d'_f}{2}. \tag{5.5}$$

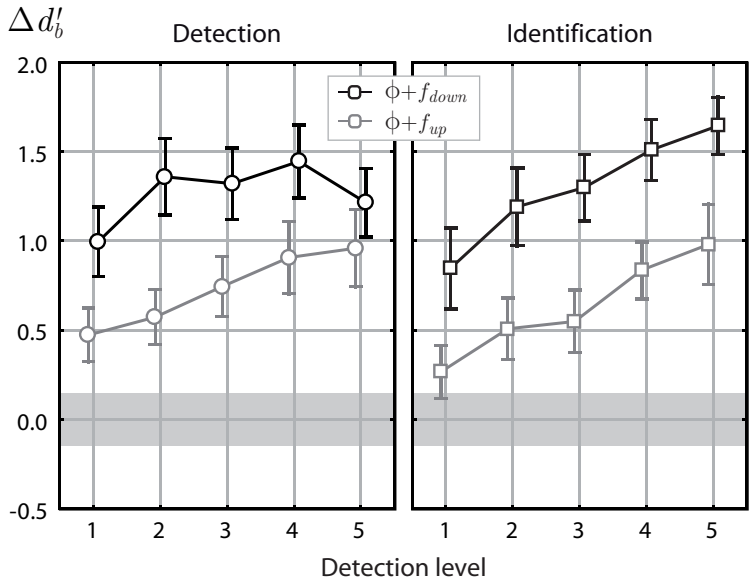

Figure 5.6: Sensitivity difference of double cue targets to the average sensitivity achieved with a single cue $\Delta d'_b$ (5.6). The plot shows cell means and their 95% confidence limits, based on the residual variance of each cell (see error bars). The confidence interval for the distribution of means with zero expected value was calculated from the overall residual variance, and is shown as grey shaded area. Data for the detection task are indicated by black circles, data for the identification task are drawn as grey squares.

Here, $\overline{d'}_\phi$ and $\overline{d'}_f$ are the d' values obtained for the single features, where f is either f_{up} or f_{down}. From (5.5) the sensitivity advantage of double cue targets relative to the performance achieved with a single cue is reflected by the sensitivity difference of double cue targets to the base sensitivity achieved with both single cues,

$$\Delta d'_b = d'_{\phi+f} - \frac{d'_\phi + d'_f}{2}. \tag{5.6}$$

This difference can be calculated from each raw data triplet $(d'_\phi, d'_f, d'_{\phi+f})$, and analyzed by ANOVA routines with feature (5 levels, i.e. ϕ, f_{up}, f_{down}, $\phi+f_{up}$, and $\phi+f_{down}$) and visibility level (5 levels) as repeated measurement factors. Table 5.1 lists the cue summation measure (5.6), Tables 5.2 and 5.3 show the results of the univariate analyses of variance for detection and identification, respectively. Figure 5.6 presents a plot of the cell means.

The advantage of double cue targets is modulated by visibility level, and by feature type (see Tables 5.2 and 5.3). The curves for both tasks, shown in Figure 5.6, take the same principle course, the cue summation gain is only marginally higher for detection than for identification. However, a strong asymmetry is observed for feature type. Doubles cues

Source of Variation	*SS*	*df*	$\hat{\sigma}^2$	*F*	*P*
Conjunction (A)	17.960	1	17.960	45.106	.000
Detection level (B)	5.570	4	1.392	8.042	.000
$A \times B$	1.796	4	.449	3.330	.013
$A \times$ subjects	9.556	24	.398		
$B \times$ subjects	16.621	96	.173		
$A \times B \times$ subjects	12.944	96	.135		

Table 5.2: ANOVA results for the difference measure $\Delta d'_b$ (5.6) in the feature contrast detection task. The table shows the source of variation, sum of squares (SS), degrees of freedom (df), variance estimate ($\hat{\sigma}^2$), F- ratio, (F), and significance level, P.

Source of Variation	*SS*	*df*	$\hat{\sigma}^2$	*F*	*P*
Conjunction (A)	28.123	1	28.123	132.363	.000
Detection level (B)	17.314	4	4.328	20.246	.000
$A \times B$	.183	4	.046	.351	.843
$A \times$ subjects	5.099	24	.212		
$B \times$ subjects	20.524	96	.214		
$A \times B \times$ subjects	12.522	96	.130		

Table 5.3: ANOVA results for the difference measure $\Delta d'_b$ (5.6) in the figure identification task. Conventions as in Table 5.2.

formed by orientation and upward spatial frequency feature contrast ($\phi + f_{up}$) evince a lower cue summation gain than double cues of orientation and downward directed spatial frequency contrast ($\phi + f_{down}$). Cue summation rises monotonically with visibility level for $\phi + f_{up}$, whereas for $\phi + f_{down}$ a plateau is reached already at the second visibility level, followed by a minor decline at the highest visibility level. The reason for the decline in the cue summation measure (5.6) for $\phi + f_{down}$ conditions is most likely a ceiling effect (see Section *Cue summation as a function of the base sensitivity level*) due to the very high level of single cue visibility. Ceiled data do not occur for $\phi + f_{up}$.

The statistical significance of the difference measure $\Delta d'_b$ can be evaluated at the level of cell means with their confidence limits, calculated on the basis of the overall residual variance estimate $\hat{\sigma}^2_{res} = \hat{\sigma}^2_{A \times B \times subjects}$. The residual variance estimates are quite close for both tasks (see Tables 5.2 and 5.3), which allows to pool them in order to obtain just a single confidence interval for both tasks. This enables to judge the statistical significance of the double cue advantage directly from the cell means plot. A cell mean is significant if

		Detection				Identification			
Conjunction	FC-Level	$\overline{d'}_{\perp}$	$\overline{d'}_{\phi+f}$	$\overline{\Delta}d'_{\perp}$	q	$\overline{d'}_{\perp}$	$\overline{d'}_{\phi+f}$	$\overline{\Delta}d'_{\perp}$	q
$\phi + f_{up}$	1	.376	.848	.473	2.258	.210	.484	.274	2.308
	2	.644	1.217	.573	1.890	.306	.814	.508	2.658
	3	.868	1.612	.744	1.858	.521	1.070	.549	2.055
	4	1.137	2.044	.907	1.798	.732	1.569	.837	2.143
	5	1.378	2.342	.964	1.700	1.027	2.008	.981	1.955
$\phi + f_{down}$	1	.354	1.349	.995	3.815	.268	1.108	.840	4.135
	2	.605	1.965	1.360	3.248	.401	1.593	1.192	3.975
	3	.863	2.184	1.321	2.530	.619	1.918	1.299	3.101
	4	1.107	2.552	1.446	2.306	.840	2.351	1.510	2.797
	5	1.403	2.617	1.214	1.865	1.164	2.810	1.646	2.414

Table 5.4: Sensitivity advantage of double cue targets compared to the prediction of dimensional orthogonality (5.3). The table shows the mean prediction, $\overline{d'}_{\perp}$, mean sensitivity for double cue targets, $\overline{d'}_{f+\phi}$, mean sensitivity difference, $\overline{\Delta}d'_{\perp}$, as defined by (5.4), and the ratio of double-cue sensitivity and prediction, $q = \overline{d'}_{f+\phi}/|\overline{d'}_{\perp}|$. Data are shown for both tasks and figure types at the five detection levels.

it lies outside the interval

$$0 \pm t_{(df_{res};1-\alpha/2)} \frac{\hat{\sigma}_{res}}{\sqrt{N}} \tag{5.7}$$

(see grey shaded area in Figure 5.6). With $N = 25$ and $t_{(96;.975)} = 1.98$, this interval is $0 \pm .145$. Figure 5.6 shows all cell means to lie above the upper boundary of this range.

Testing Cue Summation Against the Independence Assumption

As for the cue summation measure (5.6), also the double cue advantage relative to the prediction of dimensional orthogonality (5.4) can be calculated for each raw data triplet, and can be analyzed by ANOVA procedures. Table 5.4 lists this measure for all experimental conditions, and Tables 5.5 and 5.6 show the ANOVA results. The corresponding cell means plot is shown in Figure 5.7. Generally, the results are akin to those found for the advantage relative to single cue performance (see Tables 5.5 and 5.6). When comparing the curves for d'_b (see Figure 5.6) and $d'_{\perp}$ (see Figure 5.7) one finds them to follow the same trends, but $d'_{\perp}$ values are downward shifted, and the plateau of the detection data after the second visibility level for $\phi + f_{down}$ is more pronounced. The confidence interval, based on the pooled residual variance, is only marginally larger ($0 \pm .152$), and, as found for the advantage over single cue performance, also the double cue advantage over the independence prediction

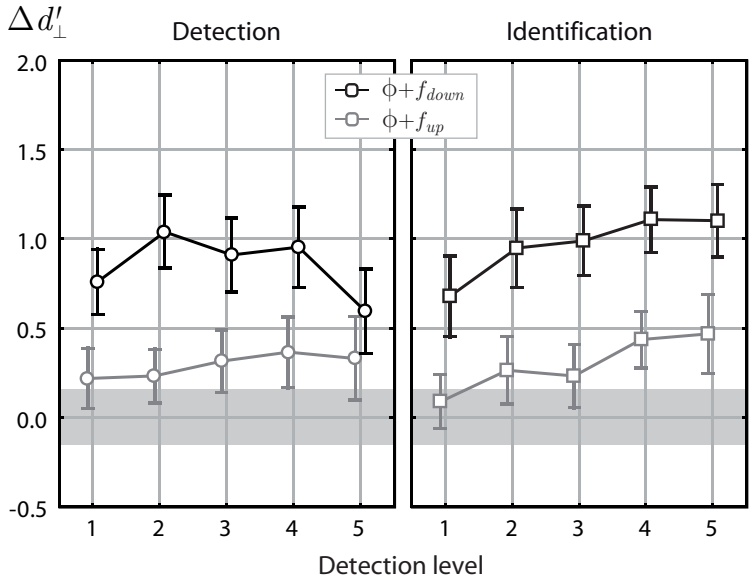

Figure 5.7: Sensitivity difference $\Delta d'_{\perp}$ of double cue targets to the prediction of independent feature specific sensory mechanisms according to (5.4). Conventions as in Figure 5.6.

(5.3) is significant for all visibility levels, except the lowest level of the double cue $\phi + f_{up}$ in the identification task.

Cue Summation as a Function of the Base Sensitivity Level

The amount of cue summation is apparently different for the two types of double cues, while cue summation is fairly comparable among tasks for both double cue types. It is now worth to analyze how the difference measure $\Delta d'_b$ depends on the observed base sensitivity level, $\overline{d'}_b$. This function illustrates how much sensitivity adds to the base sensitivity level to result in double cue performance. Plotting the between subject means of $\Delta d'_b$ against the between subject means of $\overline{d'}_b$ this relation is depicted in Figure 5.8.[19] The bottom grey shaded area marks the positive half of the confidence interval for the distribution of means with zero expected value, as displayed in Figure 5.6. The oblique grey shaded area shows the analogous interval for the advantage relative to the independence prediction (5.4). Its upper bound is obtained by adding half the confidence interval for the mean sensitivity difference $\overline{\Delta} d'_{\perp}$ (see Figure 5.7) to the gain expected from the independence assumption, $\Delta d'_{(b,\perp)}$. An estimate for this difference is obtained by substituting the base sensitivity level

[19] It is important to note that the data shown in Figure 5.8 are mean data. So each data point is a centroid obtained by averaging across the data of the 25 subjects. For each of the four data families, the plot of $\Delta d'_b$ against $\overline{d'}_b$ may therefore be viewed as a 5 point sample of the 2D sampling distribution.

Source of Variation	*SS*	*df*	$\hat{\sigma}^2$	*F*	*P*
Conjunction (A)	19.565	1	19.565	50.323	.000
Detection level (B)	1.624	4	.406	1.860	.124
$A \times B$	1.886	4	.472	2.969	.023
$A \times$ subjects	9.331	24	.389		
$B \times$ subjects	20.957	96	.218		
$A \times B \times$ subjects	15.247	96	.159		

Table 5.5: ANOVA results for the difference measure $\Delta d'_{\perp}$ (5.6) in the feature contrast detection task. Conventions as in Table 5.2.

Source of Variation	*SS*	*df*	$\hat{\sigma}^2$	*F*	*P*
Conjunction (A)	27.909	1	27.909	143.333	.000
Detection level (B)	5.307	4	1.327	5.199	.001
$A \times B$	.191	4	.048	.352	.842
$A \times$ subjects	4.673	24	.195		
$B \times$ subjects	24.498	96	.255		
$A \times B \times$ subjects	13.033	96	.136		

Table 5.6: ANOVA results for the difference measure $\Delta d'_{\perp}$ (5.6) in the figure identification task. Conventions as in Table 5.2.

for the two single feature d' sensitivities in (5.3). When two perceptually equivalent cues are combined according to (5.3), its advantage relative to the base sensitivity level (5.5) is

$$\Delta d'_{(b,\perp)} = \overline{d'}_b \left(\sqrt{2} - 1 \right). \tag{5.8}$$

Formula (5.8) means that double cue performance is expected to be about a factor of $\sqrt{2}$ larger than single cue performance. Plotted against the base sensitivity level, $\overline{d'}_b$, it is a linear function with slope $\sqrt{2} - 1$. This function is shown as the lower end of the oblique grey shaded area (see dashed grey line marked by an arrow).

As becomes obvious in Figure 5.8, the cue summation gain, $\overline{\Delta} d'_b$, rises monotonically with the base sensitivity level, and shows an approximately linear trend in each of the four data families. For one data family ($\phi + f_{low}$ combination in detection) this trend is overlayed by ceiling effects (see below). Closer analysis in terms of 2D confidence regions reveals further important aspects of the cue summation effect. Note that the centroids of the four data families follow 2D sampling distributions with Mahalanobis distance condition

$$\widetilde{\Delta}_j^2 (\boldsymbol{\mu}) = n \left(\overline{\mathbf{x}}_j - \boldsymbol{\mu} \right)' \hat{\boldsymbol{\Sigma}}^{-1} \left(\overline{\mathbf{x}}_j - \boldsymbol{\mu} \right) \leq c^2 = \frac{(n-1)p}{n-p} F_{(2,n-2)}(1-\alpha) \tag{5.9}$$

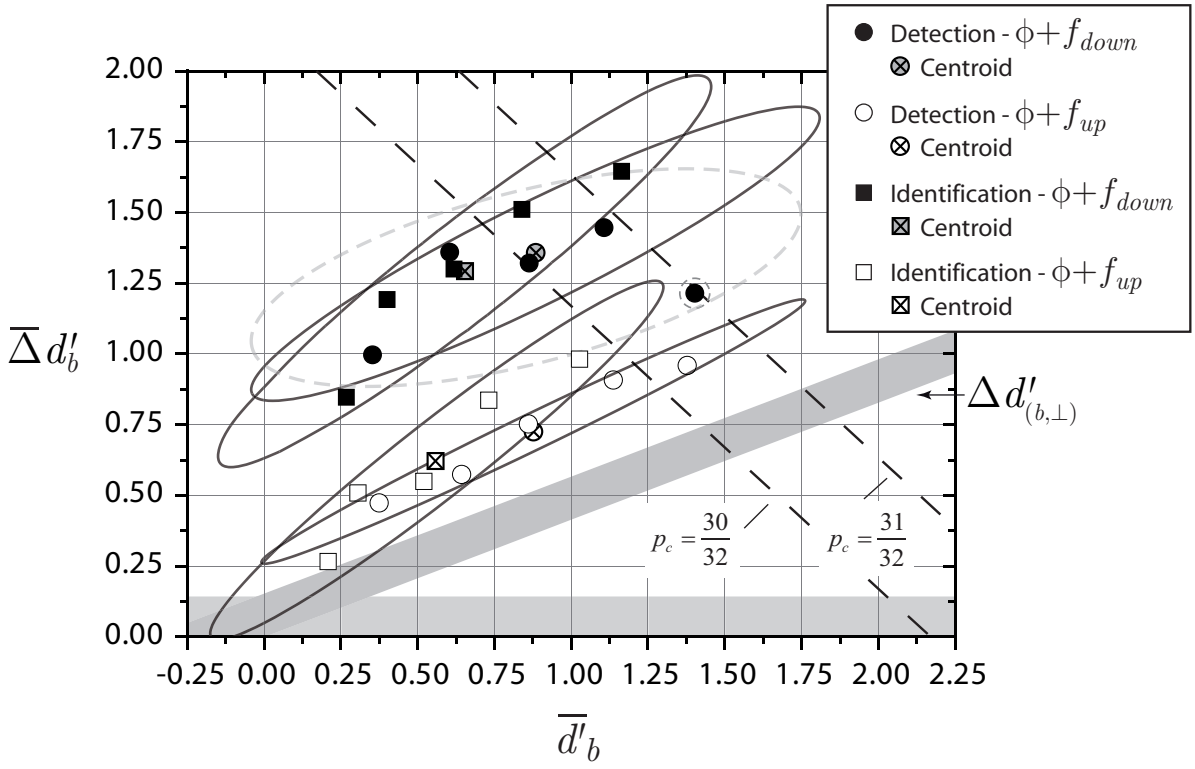

Figure 5.8: Mean sensitivity advantage of double cue targets compared to single cue targets, $\overline{\Delta} d'_b$, as a function of the base sensitivity level, $\overline{d'}_b$. Data for the figure identification task are indicated as squares, data for the feature contrast detection task are shown as circles. Open symbols refer to the $\phi + f_{up}$ double cue, filled symbols denote feature conjunctions $\phi + f_{down}$. The upper right line with long dashing marks the d' sensitivity which corresponds to 31 of 32 correct decisions, the lower one the sensitivity which corresponds to 30 hits. The oblique grey area marks the upper half of the confidence interval for the prediction derived from the assumption of independent feature specific mechanisms. Its lower bound is this prediction, $\Delta d'_{(b,\perp)}$, according to (5.8) (see arrows). The bottom grey area is the upper half of the confidence interval for the null hypothesis $\mu\left(\Delta d'_b\right) = 0$. Dashed circles mark ceiling effect outliers. The solid ellipsoids are the 95% contours of the bivariate normal distributions for the four ensembles, obtained from the unbiased estimates $\mathbf{S}_j$ and $\overline{\mathbf{z}}_j$ for the true variance-covariance matrix, $\mathbf{\Sigma}_{z_j}$, and the true centroid, $\boldsymbol{\mu}_{z_j}$, respectively. Ellipsoid centroids are denoted as light grey symbols with an inscribed cross. The dotted normal ellipsis denotes the ellipses for the cleared data set for condition $\phi + f_{down}$.

which defines the critical distance to the centroid $\overline{\mathbf{x}}_j$ for a $1-\alpha$ confidence region. In 5.9, $F_{(2,n-p)}(1-\alpha)$ is the 95% quantile of the F-distribution with 2 denominator and $n-2$ nominator degrees of freedom, $\hat{\mathbf{\Sigma}}^{-1}$ is the inverse of the unbiased estimate of the variance-covariance matrix of the 2D data vectors, $\overline{\mathbf{x}}_j$ is the centroid of the j-th data family, $j=1,\ldots,4$, and $\boldsymbol{\mu}$ is an arbitrary mean vector taking the role of an assumed true centroid for data family j. The bivariate normal distributions which satisfy (5.9) are shown in Figure 5.8 as solid ellipses for the four data families. The first eigenvector of the unbiased estimate of the variance covariance matrix, $\hat{\mathbf{\Sigma}}$, scaled by a factor $c\sqrt{\lambda/n}$, with λ the eigenvalue associated with the first eigenvector, is the first principal component of $\hat{\mathbf{\Sigma}}$. It coincides with the regression of $\overline{d'}_b$ on $\overline{\Delta}d'_b$ by minimizing the error sum of squares in the direction perpendicular to the regression axis (see Flury, 1997, p. 584).

First, not only the centroids, but also the principal axes of all four data families are far above the independence prediction (5.8), which illustrates that cue summation at each base sensitivity level is far better than predicted by assuming independent processing of cues. Second, the slope of the first principal axis precisely predicts the psychophysical task: for each task the slopes for $\phi + f_{down}$ and $\phi + f_{up}$ are the same, while the slopes for detection and identification are different (see Table 5.7). This corresponds to parallel confidence ellipses within tasks, and lack of parallelism between tasks (see Figure 5.8). Slopes for identification are larger, indicating more cue summation gain with rising base sensitivity levels, and therefore a better exploitation of the second cue when the task requires recognition of form compared to the mere detection of target presence. Similar results were found for the task dependency of cue summation in combined shape detection and identification tasks (Persike & Meinhardt, 2008; Meinhardt et al., 2006).

For $\phi + f_{down}$, cue summation rises monotonically up to the highest base sensitivity level, where the decline in cue summation indicates saturated performance at the maximum achievable performance level (see the dashed circle in Figure 5.8). This data point reflects a ceiling effect, caused by a tradeoff of single cue performance level and double cue benefit at the maximum performance level. For base sensitivity levels in the vicinity or beyond 1.5 d' units, double cue performance is at the maximum rate of about 31 to 32 correct decisions out of 32 trials (see Persike & Meinhardt, 2008).[20] Ceiling effects therefore limit the gain in cue summation with the base performance level for $\phi + f_{down}$, and preclude to reveal the exact relationship of both variables at these high base performance levels. After clearing for the one ceiling effect datum, cue summation is strongly correlated among both types of double cue ($r = .928, t = 6.60, p = .000$), and the two confidence ellipses for each task turn out to be exactly parallel (see Table 5.7).

In order to substantiate specific cue summation schemes for different directions of spatial frequency feature contrast and task, Hotelling's T^2 tests were computed for all six pairwise

[20] The marked data point indicates a mean d' sensitivity of 2.61 (see Table 5.1), which correspond to proportions correct of .967. Note that a rate of $p_c = 31/32 = .968$ corresponds to $d' = 2.63$.

combinations of the four data families. The outlier shown in Figure 5.8 was removed from the data set, and did not enter testing. Owing to the incomplete data sets after clearing for the outlier, independent T^2 statistics were computed to account for the different data set sizes, which is a conservative ways of testing, since the strong correlations among data sets (see Table 5.7) do not enter the comparisons. With Hotelling's T^2–statistic, the null hypothesis that a difference vector of sample means has zero true centroid is rejected at significance level α if

$$T^2 = \mathbf{d}' \left(\left(\frac{1}{n_1} + \frac{1}{n_2} \right) \hat{\mathbf{\Sigma}}_{pooled} \right)^{-1} \mathbf{d} > \frac{(n_1 + n_2 - 2)p}{n_1 + n_2 - p - 1} F_{(p, n_1+n_2-p-1)}(1-\alpha), \quad (5.10)$$

where $\mathbf{d} = (\overline{\mathbf{x}}_2 - \overline{\mathbf{x}}_1)$ is the difference vector of the p mean components from two samples with n_1 and n_2 observations, $\hat{\mathbf{\Sigma}}_{pooled}$ is the unbiased estimate of the pooled variance-covariance matrix of the variables, and the single quote mark denotes transposing. From (5.10) it follows that

$$F_{(p, n_1+n_2-p-1)} = \frac{n_1 + n_2 - p - 1}{(n_1 + n_2 - 2)p} \, T^2. \quad (5.11)$$

Table 5.8 shows F-values and significance levels for the pairwise comparisons of group centroids.[21] The results confirm that the group centroids observed for cue summation gains in the two different tasks stem from the same population, illustrated in Figure 5.8 by the largely overlapping ellipses for detection and identification. On the other hand, all pairwise comparisons for the different directions of spatial feature frequency contrast reveal that the group centroids are separated with a high degree of statistical certainty at significance levels beyond a Bonferroni corrected alpha level of $\alpha/6$, with $\alpha = 0.05$. Pairwise comparisons thus provide conclusive evidence that more cue summation relative to the actual base sensitivity level is obtained for the $\phi + f_{down}$ double cue than for $\phi + f_{up}$ in both detection and identification.

Together with the slope analysis of the first principal axes of the confidence ellipses we obtain a very unique result. The two types of cue combinations, $\phi + f_{down}$ and $\phi + f_{up}$, are discriminated by the amount of cue summation, $\Delta d'_b$. The two tasks are discriminated by the slope of the first principal axes of the confidence ellipses. The latter result indicates that observers are generally more efficient in exploiting the additional cue in the identification task than in the detection task.

[21] The critical F-values for $\alpha = 0.05$ and $\alpha = 0.01$ are $F_{(2;5)}(.95) = 5.786$ and $F_{(2;5)}(.99) = 13.274$, respectively.

Group	Group No. (j)	r_{xy}	λ	$\mathbf{e}$	$\tilde{\mathbf{e}}$	a_e
$\phi + f_{up}$ - Detection	1	0.926	0.2167	(0.880,0.474)	(0.925,0.498)	1.857
$\phi + f_{up}$ - Identification	2	0.949	0.2169	(0.759,0.651)	(0.798,0.684)	1.166
$\phi + f_{down}$ - Detection	3	0.987	0.1990	(0.885,0.465)	(0.891,0.469)	1.902
$\phi + f_{down}$ - Identification	4	0.967	0.1859	(0.762,0.648)	(0.741,0.631)	1.175

Table 5.7: Results of the eigenvalue decomposition of the estimated variance-covariance matrix, $\hat{\mathbf{\Sigma}}_j$, for each of the four data families. The table shows the Pearson correlation among the coordinates $\overline{d'}_b$ and $\overline{\Delta} d'_b$, $r_{x,y}$, eigenvalue of the first eigenvector, λ, the first eigenvector, $\mathbf{e}$, the scaled first eigenvector, $\tilde{\mathbf{e}} = \mathbf{e} \cdot c\sqrt{\lambda/n}$, and the slope of the first principal axis, a_e. The value of the distance constant is $c = 5.047$, which results for $n = 5$ cases and $p = 2$ variables from the right hand side of (5.9).

		$F_{(p;n-p)}$			P		
Group	Group No. (j)	1	2	3	1	2	3
$\phi + f_{up}$ - Detection	1						
$\phi + f_{up}$ - Identification	2	2.817			0.127		
$\phi + f_{down}$ - Detection	3	75.424	27.744		$0.000^\star$	$0.001^\star$	
$\phi + f_{down}$ - Identification	4	66.840	51.801	0.426	$0.000^\star$	$0.000^\star$	0.671

Table 5.8: Results table for the contrast analysis of the cue summation data with Hotelling's T^2 statistic. The table shows the F- statistic, $F_{(p;n-p)}$, (cols. 3-5), and the corresponding significance levels, P, (cols. 6-8) for pairwise comparisons of the group centroids shown in Figure 5.8 with Hotelling's T^2-test. Significant contrasts after Bonferroni correction are marked with an asterisk.

5.4 Discussion

Employing spatial frequency contrast as a cue to a global contour shows that contour integration is indeed possible due to just this cue without local orientation collinearity. Since in our stimulus configurations with open and closed contours formed by 12 elements target detection is only moderately better than global form identification (see Figure 5.5) we can conclude that global contours are already detected in most of the trials with just a spatial frequency cue, and local alignment with the global path is not necessary for enabling contour integration.

Second, combining a spatial frequency cue with path alignment results in a strong enhancement of global contour salience. The cue combination gain is larger than what can be expected from the assumption of independent processing of spatial frequency and collinearity cues (see Figure 5.7, and Tables 5.5 and 5.6). Particularly for the low frequency contours

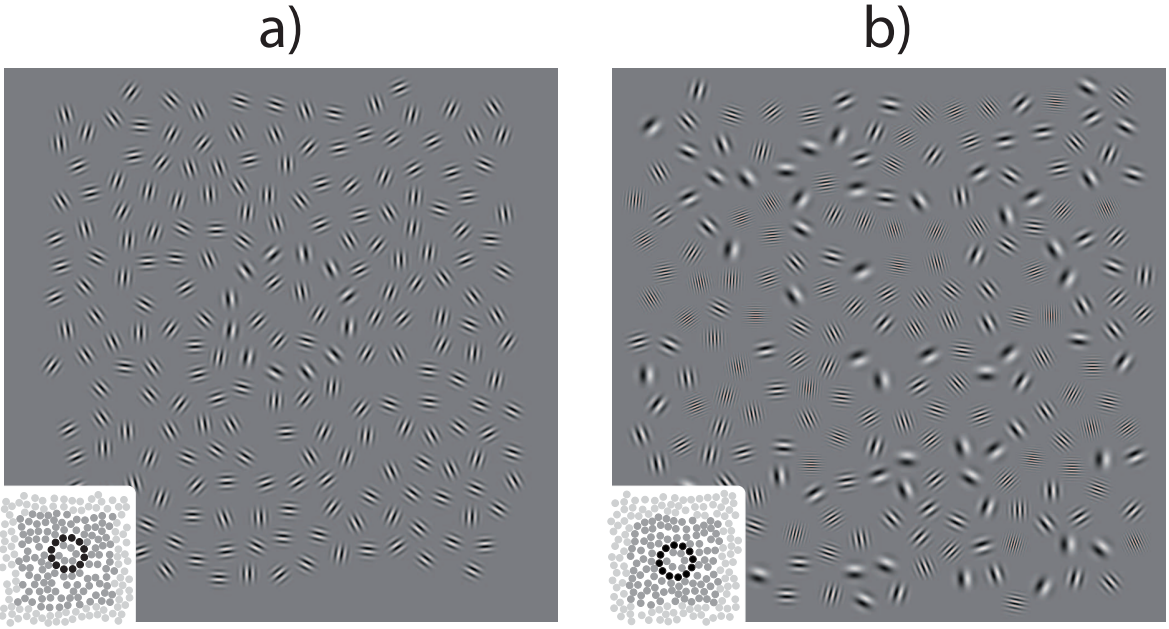

Figure 5.9: Illustration of contour integration with spatial frequency as the only cue in a field with random local orientations. a) shows a circle defined by contour elements with lower carrier spatial frequency than the surround, thus introducing a mean shift in the spatial frequency parameter. A contour is clearly perceived. In b) the same contour is defined by a spatial frequency homogeneous arrangement of the Gabor elements along the circular path, all sharing the mean frequency of the background elements. No global contour is visible. The pictograph between the figures indicates the relative position of the circular paths in the fields.

it is *oversummative* in all but one case (see Table 5.1). This means that combining the spatial frequency cue with the collinearity cue results in a d' sensitivity which is larger than the sum of both individual d' values. Oversummative effects point to a nonlinear integration rule and involvement of additional mechanisms for the combination of cues (see below).

Third, the gain in contour salience is stronger when low spatial frequency deviants from the surround are aligned with the path than for high spatial frequency deviants, although both types of spatial frequency defined contours were perceptually equivalent (see Figure 5.8 and Tables 5.2 and 5.3). Hence, we find an asymmetry in cue combination: The synergistic effect of adding the collinearity cue is much larger when combined with lower than with higher spatial frequencies of the contour defining elements.

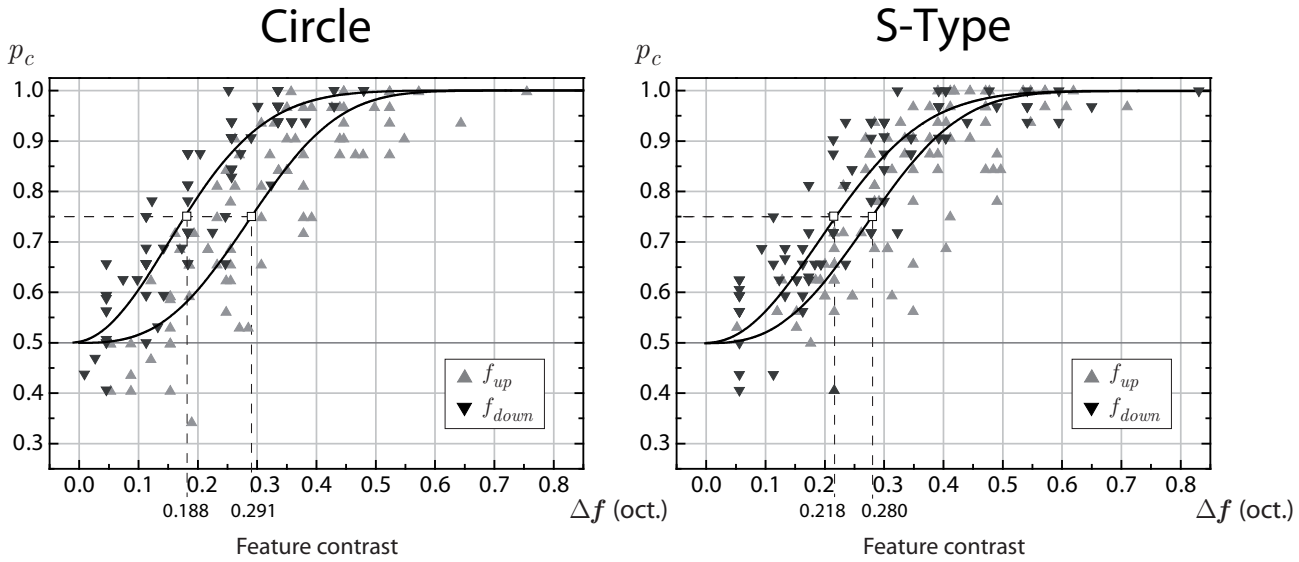

Figure 5.10: Psychometric curve data from the calibration measurements of 16 subjects for closed (left) and open contours (right) for the f_{low} and the f_{high} condition. For each experimental condition a psychometric curve is drawn that represents the general trend (solid line). This curve is a Weibull function that intersects at the between subject mean spatial frequency feature contrast threshold Δf, and has slope calculated from the mean standard deviation estimate. Mean threshold estimates are projected onto the horizontal axis to enable a first inspection of the effects of feature contrast direction on detection rates (f_{up}: upright triangles; f_{down}: inverted triangles).

5.4.1 Spatial Frequency as the Only Cue to the Contour

The finding that contour integration is enabled with spatial frequency is not surprising at first glance, since it has formerly been shown to work also with depth, motion and color cues (see Introduction). But it is in the light of recent findings showing that contour paths, when defined by spatial frequency homogeneous Gabor elements, are not visible for human observers in surrounds jittering in orientation and spatial frequency (Persike et al., 2007). The critical variation upon spatial frequency is that path elements must exhibit other first order statistics, i.e. a different frequency histogram in the spatial frequency parameter, in order to be integrated into a global form. A different spatial frequency variance of path elements and background is not sufficient to enable grouping (see Figure 5.9). This is a crucial finding, which implies that feature contrast is necessarily involved with spatial frequency based contour grouping, and similarity in the spatial frequency property alone, even as a neighbor to neighbor transitive process, is not sufficient to enable local elements to be integrated into a global spatial path.

It is striking that the frequency shifts enabling purely frequency mediated grouping are not large, and display an asymmetry in favor of lower frequency target contours. In the f_{low} condition subjects required a 0.2 octave shift on average to reach a 75% correct performance level. In the f_{high} condition about 0.3 octaves are necessary to reach this performance level (see Figure 5.10). This mean shift in spatial frequency complies with the range of thresholds for spatial frequency discrimination (Wilson et al., 1983; Wilson & Gelb, 1984), and also the observed detection asymmetry in favor of spatial frequency decrements (Regan & Beverley, 1983) suggests involvement of a spatial frequency discrimination mechanism. Alternatively, it may indicate involvement of a feedforward texture discrimination mechanism, as suggested by Rubenstein and Sagi (1990). Referring to the results of Gurnsey and Browse (1987), who found that 'L' texture elements are more easily detected when embedded in '+' elements than vice versa, Rubenstein and Sagi were able to show that this asymmetry can be attributed to the different noise energies associated with the texture elements when used as backgrounds, and that this asymmetry is accounted for by a multi-scale feedforward Filter-Rectify-Filter model. With this processing scheme it can be revealed that orientation jitter of 'L' texture elements produces much more noise energy than orientation jitter of '+' elements. This is due to the fact that orientation jitter of 'L' texture elements produces noise energy located in low spatial frequency regions, while noise energies associated with orientation jitter of '+' elements are located in higher spatial frequency bands, and reach much smaller energy levels. Targets with less energy are difficult to detect when embedded in backgrounds with strong noise energy levels, consequently a '+' texture embedded in an 'L' texture is less salient than an 'L' texture embedded in a '+' texture.

The threshold asymmetry for low frequency and high frequency deviants from the background, as observed here, is precisely the kind of asymmetry as accounted for by Rubenstein and Sagi (1990). If Gabor carrier frequency is lowered, low frequency targets with high orientation noise energy levels are embedded in a higher frequency background with less noise energy, which is a favorable relation of foreground and background texture noise energy. If Gabor carrier frequency is increased relative to the surround, the opposite holds, and the foreground to background noise energy relation is disadvantageous. Whether the observed asymmetry in the detection thresholds for spatial frequency defined target contours involves spatial frequency discrimination or texture segregation, in any way it seems to imply a pure *segregation* mechanism, that separates one pattern class from another.

Since the task was a dual task requiring target detection and contour type identification, a pure segregation mechanism is not sufficient to explain the subjects' performance with spatial frequency defined contours. Since a segregation mechanism is blind for the definite spatial distribution of the targets, a further mechanism is needed to explain contour integration with a spatial frequency cue.[22] The argument is verified by comparing Figure

[22]Spatial frequency discrimination models capable of explaining the high spatial frequency discriminability

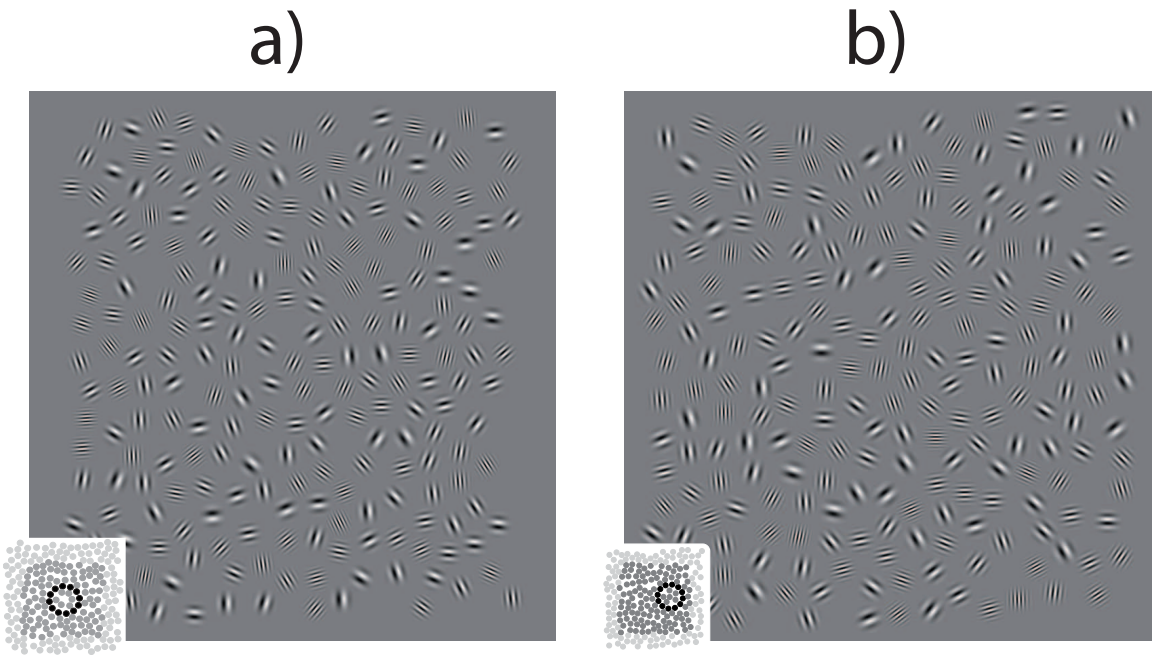

Figure 5.11: Collinearity based contour integration in Gabor fields randomly jittering in spatial frequency and orientation. In both examples the spatial frequency sampling range is 2 octaves. In (a) this range is applied to contour and background, in (b) the contour is spatial frequency homogeneous at the mean carrier frequency of the whole field. Both displays lead to the same contour detection performance by human observers (Persike, Olzak, & Meinhardt, 2007). The pictographs indicate the positions of the contours in the fields.

5.1a and Figure 5.1d. Apparently, it is possible to detect that there are spatial frequency targets in displays containing spatial frequency increments and decrements randomly alternating along the contour and jittering randomly in orientation (Figure 5.1d). Such a contour induces a strong local energy signal, since local feature contrasts are strongest along the contour, much stronger than in the background. However, it is a tedious task to recognize the spatial course of the deviating elements, and to combine them into a smooth contour.

of the visual system which is far better than the tuning of single spatial frequency selective neurons exploit a population code among all activated units, thus calculating a multivariate distance between target and background pattern (Wilson & Gelb, 1984; Wilson & Regan, 1984; Baldi & Heiligenberg, 1988; Meinhardt, 2001). The multivariate distance is compared to a threshold value. The locations that generate strongest contributions to this measure do not enter the comparison. The same holds for texture segregation mechanisms, which compare net texture energies calculated by aggregation over space (Rubenstein & Sagi, 1990; Sagi, 1995). Comparison of the spatial outlines of texture energies requires to assume additional spatial matching mechanisms, however, the described asymmetry is just captured by the summed responses.

Only when the contour elements share similar local carrier frequencies recognition of shape is enabled (Figure 5.1a). The information that all the deviating elements belong to the same class is necessary to enable robust spatial grouping by the tapped mechanism. Apparently, this mechanism serves to bind spatial frequency deviants with similar spatial frequencies. So, similarity grouping is necessarily involved for contour grouping by spatial frequency in the absence of collinearity cues. Comparing the examples shown in Figure 5.1a and Figure 5.1d shows that element grouping does not work very well across some distance, i.e. it is not really possible for the example shown in Figure 5.1d to bind only the similar low frequency patches, or the high frequency pathes into a contour, bridging the spatial gaps. In the terminology of Geisler and Super (2000) we may say that contour grouping just by spatial frequency must be *transitive*, which means that the direct spatial neighbors must share the same attribute in order to enable grouping to a global form (connectedness by the same attribute).[23] Our results show that contour integration by local carrier frequency is enabled if the contour defining elements share very similar carrier frequencies, and these carrier frequencies are distinct from the carrier frequencies of the surrounding field in their first order statistics. So both principles, transitive similarity grouping *and* feature contrast are necessary for contour integration by spatial frequency without local collinearity cues. It is important to note that association field models of contour integration (see Introduction) cannot account for this type of grouping, since all Gabor elements of the display have random orientation, precluding any local orientation based neighbor locking.

5.4.2 Contour Integration with Local Collinearity Cues and Variable Spatial Frequency

Contour integration performance with local orientation cues to the global contour in spatial frequency homogeneous displays (see example in Fig 1b) has been described with local contextual response fields that regulate the strength of neighbor interaction (Geisler et al., 2001; Polat & Sagi, 1994b; Polat et al., 1998; Polat, 1999; Kapadia et al., 1999, 2000; Polat & Bonneh, 2000). Contour integration in spatial frequency homogeneous displays is often viewed as a typical example of the Gestalt principle of good continuation (Hess & Field, 1999; Geisler & Super, 2000; Spillmann, 2001). However, as the results for the spatial frequency cue suggest, one may ask whether also similarity grouping must be necessarily involved for grouping that complies with the Gestalt principle of good continuation. This question cannot be answered with spatial frequency homogeneous displays, but only with displays jittering in spatial frequency. In the orientation condition (ϕ) of this experiment, as well as in most studies on contour integration with bandpass stimuli, the Gestalt principles of similarity and good continuation are somewhat confounded, since all path elements share the same carrier frequency, and orientation transitions between path element neighbors

[23] A classical example of intransitive grouping would be highlighting critical locations of a form with similar elements, e.g. marking just the edges of a square with red dots in a field of blue and green dots.

are smooth. So, neighboring elements share the same carrier frequency and similar local orientations, and, since local orientation is the only feature that varies in the display, they are *similar*. Hence, the question is whether just local alignment with a global path is sufficient, and contour integration occurs across variable carrier frequencies, or whether the elements must also coincide in local carrier frequency in order to be integrated into a smooth contour.

The illustration given in Figure 5.1e indicates that path elements do *not* need to share the same carrier frequency to enable contour integration. In this example the carrier frequency of the path elements differs by approximately 2 octaves, but it is still possible to detect a circular figure. Contour grouping in the stimulus example may be due to the fact that the spatial frequency heterogeneous path is perceived because it contrasts with the spatial frequency homogeneous background. A systematical study of the dependency on spatial frequency homogeneity proves this not to be the case. The first experiment from Chapter 4 studied contour integration in Gabor fields varying randomly in spatial frequency and orientation. Contour integration performance was very robust against spatial frequency jitter. Performance was essentially the same for spatial frequency homogeneous displays (as in Figure 5.1b) and displays with spatial frequency jitter within a 2 octave range, with path elements differing more than 1.25 octaves in carrier frequency (see Figure 5.11a). Even a separation of more than 2.25 octaves along the path led to only a 12% drop in a percent correct measure. Most striking, spatial frequency homogeneous contours were not seen better when embedded in backgrounds jittering in orientation and spatial frequency than contours with the same jitter in carrier frequency as the background (see Figure 5.11b). These results show that contour integration works across wide ranges of spatial frequency, and that similarity grouping is neither necessary for collinearity based grouping to work, nor does it contribute much to enhance the global contour. So it can indeed be said that good continuation, mediated by local orientation alignment with a global path, works as an *independent transitive grouping principle* besides similarity based grouping in contour integration. Despite locally varying spatial frequency, the contour integration mechanism is able to embark on just the local alignment information and effectively uses this information for binding local elements into a global form.

5.4.3 Combining Local Collinearity and Spatial Frequency Cues

If feature contrast and similarity based grouping by local carrier frequency and alignment based grouping by local orientation are brought together, global contour salience surges in a nonlinear, synergistic fashion, reaching the largest amounts of cue summation that can be obtained within the intervals of a single psychometric curve measurement (see Results). This stands in contrast to most other additional cues (color, motion and depth) studied in contour integration so far, which lead to a cue summation gain that is compatible with the

notion of independent grouping sources. With these additional cues, contour salience mediated by the additional cue or the collinearity cue, and, occasionally, by both cues. In contrast, the synergistic cue summation gain of local carrier spatial frequency and orientation collinearity, leading to contour sensitivity which is larger than the sum of the two single cue contour sensitivities, rules out any passive integration scheme, and points to a new sensory mechanism for the combination of cues.

Results from neuroimaging studies suggest that weaker cue summation gain in shape perception can be expected if both cues are not processed at the same site early on the visual pathway. Altmann et al. (2003) found cue summation of depth and collinearity cues in contour integration in the order of magnitude of probability summation among independent sources, and were able to show that enhancement in common areas was weak in V1 and V2, but much stronger in LOC. In the same way, the failure to find stronger interaction for color and collinearity cues (Mathes, Trenner, & Fahle, 2006a) may be due to the fact that color and orientation are processed by distinct mechanisms in V1, and their combination occurs at later stages. Color is processed in area V1 only on layer 4, where predominantly isotropic cells reside, while simple cells are specific for local carrier frequency, orientation and contrast, but not for color. The earliest level where considerable integration of the outputs of orientation and color selective cells occurs are complex thin stripe sensitive cells located in V2 (Livingstone & Hubel, 1984, 1987, 1988). Higher levels, possibly area V4, which also responds shape selective (Desimone & Duncan, 1995; Desimone, 1996), are more likely candidates for the fusion of color, local orientation and form. Because of its hierarchical channeling, color and orientation may be viewed as a classical example of a 'early channeling – later integration' scheme of feature processing, which is reflected by feature independence when early layers are tapped by the psychophysical task (Treisman & Gelade, 1980; Treisman, 1988).

Orientation and spatial frequency, however, are jointly coded at early sites (V1, V2), which are strongly activated by orientation based contours and shapes (Kourtzi & Kanwisher, 2000, 2001; Altmann et al., 2003; Kourtzi et al., 2003; Altmann et al., 2004). Hence, the fact that local alignment and spatial frequency strongly sum in contour integration, while combinations with other cues studied so far do not show substantial cue summation gain suggests that joint coding on a common site is the source of the strong interaction of orientation and spatial frequency.

5.4.4 Task Specifity

Interaction of spatial frequency and orientation cues has also been studied in other tasks than contour integration, such as texture segregation (Bach, Schmitt, Quenzer, Meigen, & Fahle, 2000), texture border localization (Landy & Kojima, 2001), feature contrast detection (Meinhardt & Persike, 2003), and texture figure detection and identification

(Meinhardt et al., 2004, 2006; Persike & Meinhardt, 2006, 2008). Strong summation among both cues was only found in texture figure detection and identification, with summation effects significantly larger than predicted by independent cue processing.[24] In these studies the cue summation effect was comparable, but slightly weaker than found in the contour integration experiments reported here. In the studies by Meinhardt and coworkers, as well as here, it was found that the cue summation effect is larger in identification than in detection when judged at the same base sensitivity level. Moreover, the higher slopes of the first principal axes of the confidence ellipses in identification, as found here, indicate that observers handle the additional cue more efficiently in shape identification than in simple target detection. These findings suggests that combining local orientation with spatial frequency cues plays a significant role in perceiving shape and object outlines, and is a mechanism which serves to stabilize early form perception in noisy environments.

5.4.5 Hypothetical Mechanism

The discussion of the principles good continuation, feature contrast, and similarity grouping may have conveyed the impression that these principles are independent principles of perceptual organization that may interact as independent sources when brought together in a given stimulus set. While it is possible to disentangle the perceptual effects of all three principles on contour salience with appropriately chosen stimulus displays (see Figure 5.1 and discussion above), the results of this study with respect to the combination of spatial frequency with the local alignment cue show that the coincidence of cues leads to contour salience which is far larger than predicted by an additive component model. A model of the form

$$y = af_a(v_a) + bf_b(v_b) \tag{5.12}$$

where v_a, v_b are the single cues, and f_a, f_b transformations that map feature cues to salience, linearly combines the single cue saliences to a new variable that determines overall salience of the combined stimulus. Now, any linear combination of cues cannot account for over-summative combination effects, since the gain due to linearly combining two sources cannot exceed an upper bound set by the triangle inequality. Note that the single cues were normed in this study such that $f_a(v_a) \mapsto d'_a$, $f_b(v_b) \mapsto d'_b$, and $d'_a = d'_b$ for all salience levels. Even if the single cue saliences f_a, f_b are highly correlated, the sensitivity d'_{a+b} for

[24] Strong fusion of orientation and spatial frequency should also occur in texture segregation. The failure to find a stronger synergy effect in the study of Bach et al. (2000) may be due to the fact that the feature contrast for the single features was already very high, with strengths eliciting strong pop-out. For high feature contrast levels no synergy effect can be expected, since saturation of the neuronal responses is already reached with the individual features (see Zipser, Lamme, & Schiller, 1996; Meinhardt & Persike, 2003; Meinhardt et al., 2006)

the cue combination is bounded by

$$d'_{a+b} \leq d'_a + d'_b \tag{5.13}$$

which is the triangle inequality for d' sensitivities (see Appendix C). So the only possible transformation to overall salience that allows for oversummative effects in the d' sensitivity measure has the general form

$$y = \varphi\left(f_a(v_a), f_b(v_b)\right), \tag{5.14}$$

with φ a nonlinear function that integrates single cue saliences.

Linear combination models of cue combination have been discussed recently in the context of optimal cue combination for cue reliability and consistency (Landy & Kojima, 2001). It can easily be shown that two *independent* cues x_1, x_2 can be weighted such that an estimator $y = a_1x_1 + a_2x_2$ has minimum variance, setting $a_1 = \sigma_1^{-1}/(\sigma_1^{-1} + \sigma_2^{-1})$ and $a_2 = 1 - a_1$. The cue that has smaller variance is more reliable and therefore given more weight, such that the cue combination is optimally localized on the scale. Consistency means that cues which coincide in their target prediction are given more weight, while conflicting cues are generally suppressed since they do not contribute to a unique and reliable representation for solving the visual task.

Although optimal linear weighting of cues cannot explain oversummative cue combination effects, weighting according to reliability definitely plays a role in contour integration. While spatial frequency homogeneity alone cannot be exploited as a cue to the global contour, spatial frequency variance was necessary in this experiment to preclude that a lower or higher carrier frequency indicated contour presence with absolute reliability. In the calibration phase prior to the main experiment the amount of spatial frequency jitter was chosen such that a spatial frequency deviation of half an octave did not indicate target presence with absolute certainty, and local alignment and spatial frequency cues appeared fairly balanced with respect to cue reliability. The fact that the deviations between calibrated detection rates and observed detection rates in the main experiment are negligible (see Figure 5.4), and that perceptual equivalence of individual cues was maintained for each of the two pairings (see Figure 5.5) suggests that intermixing displays with both type of cues in the main experiment did not lead to reweighing, attending one cue at the cost of the other in order to optimize cue usage due to a perceived difference in cue reliability.

Spatial Uniqueness Principle of Contour Coding

The data presented here impose systematic constraints for a hypothetical contour integration mechanism. Two distinct grouping principles underly the integration of local elements into global contours. The first one requires similarity of attributes combined with local

feature contrast. The second one just requires local orientation collinearity. Both types of grouping must be *transitive* in the sense of contiguity, i.e. the grouping principle must be realized from neighbor to neighbor, otherwise a global contour is not represented unambiguously. If these two principles coincide, the salience of the global contour surges, and the structure pops out of a noisy surround.

Neighbor to neighbor grouping was found to be necessary for good continuation based grouping in many studies. Particularly, it was shown that gaps between contour elements must not be larger than 2° to be bridged, and intermitting false elements let contour detection performance deteriorate (Dakin & Hess, 1998; Kovacs & Julesz, 1993; W. Li & Gilbert, 2002), which suggests involvement of an early site with a limited size of the contextual response field, as found in V1 (Kapadia et al., 1999, 2000; Gilbert et al., 2000). On the other hand, integration across larger ranges of spatial frequencies indicates that contour coding is well performed with good continuation and element collinearity as the prevalent grouping cues, which is only possible if the contour signal does not directly depend on local locking among spatial frequency and orientation selective cells at an early site, as stated by association field models. With two orientations at one location anchored in different spatial frequency bands Olzak and colleagues (Olzak & Thomas, 1992; Olzak & Wickens, 1997; Olzak & Thomas, 1999) showed that observers could not evaluate orientations in two widely separated spatial frequency bands independently, but instead judged the orientation of a whole grating patch based on orientation information collapsed over the different frequencies. When both spatial frequency components were tilted into the same direction, the observers were quite accurate in their orientation judgements of both components. When one frequency component was tilted left and the other one right, subjects were unable to say which one was leftward, and which one rightward. These results indicate a spatial uniqueness principle in local orientation judgements. Subjects tend to assign one orientation to one location, and are not able to differentiate among orientations depending on the value of other local attributes. Although the situation is somewhat more complicated with contour integration since the perceived orientation of a patch is modulated by the orientations of the neighbors, the findings of Olzak and colleagues indicate a similar principle in contour coding. The fact that contours are integrated across wide ranges of local carrier frequencies as long as the elements are aligned with the path suggests that observers tend to ascribe a unique path angle to a smooth curve by picking only the relevant attribute. This may be viewed as a kind of subservience principle of higher order properties upon local properties: In order to be able to detect a meaningful structure within a spatial random field, namely a smooth curve, differences in other local attributes, which are not consistent over the course of the path, are ignored. Hence, what is extracted is what is invariant with the global structure, namely the local alignment of the elements. Besides our findings of contour integration across wide ranges of spatial frequencies, further evidence for such an invariance principle comes from studying the effect of color and depth varia-

tion. McIlhagga and Mullen (1996) showed that a collinearity based contour is spatially integrated with isoluminant color modulation of the Gabor elements. The path remained visible with alternating isoluminant color and luminance modulations, which indicates that the contour integration mechanism integrates information from feature specific processing at the level of area V2 or higher. The finding implies that contour integration cannot be based solely on locking among spatial frequency and orientation selective cells located in V1, but binds the outputs of these cells with the outputs of orientation and color sensitive cells located at the level if V2 or higher into a spatial contour. Similar evidence comes from studies on the role of depth in contour integration (Hess & Field, 1995). Authors were able to show that a collinearity based contour is spatially integrated across different depth planes, i.e. the contour is still seen when the elements along the contour exhibit different disparity parameters. This result also shows that local alignment is extracted as the invariant property across different values in an additional feature, which requires to integrate the outputs of V2 cells tuned to respond optimally in the presence of the same image features for locations at large disparities (Hubel & Wiesel, 1970).

The invariance of local alignment information across other locally variable features remains to be further validated. If it can be proven successfully over a broad collection of additional features, this will substantiate the prevalence of orientation collinearity over other possible cues in contour integration and early shape perception.

Spatial Frequency Asymmetry of the Synergy Effect

It was found that contour salience enhancement is much stronger when the collinearity cue is combined with low spatial frequency deviants than with high deviants of the spatial frequency contrast cue. Different noise energies, as mentioned above, cannot account for this asymmetry, since the f_{low} and f_{high} cues that were combined with collinearity were perceptually equivalent. However, lower spatial frequencies are ascribed with some advantages in the attentional prerequisites of processing, and are much more effective in capturing spatial attention for the regions of interest (Shulman & Wilson, 1987). Therefore, contours defined by combinations of orientation collinearity with low spatial frequency deviants have advantageous certainty conditions and are more easily found in a random display. With enhanced spatial and spatial frequency certainty, the local alignment mechanism can operate much more effective.

Low spatial frequencies are more salient in search displays, where orientation targets with low spatial frequencies are detected faster and more accurately than high spatial frequency targets (Carrasco, McLean, Katz, & Frieder, 1998). They are conducted faster (Maffei & Fiorentini, 1973; Roufs & Blommaert, 1981), and are effective in salience driven bottom-up attentional capture (Navon, 1977; Shulman & Wilson, 1987; Kimchi et al., 2007). Fast, scale selective pathways tuned to low spatial frequencies within the dor-

sal stream modulate the processing of more slowly conducted feedforward inputs to areas V1, V4, and IT (Chen et al., 2007). The notion of a global preprocessing scheme during the acquisition of visual scene information, relying predominantly on low spatial frequencies, is widely supported by neuroanatomical (Sugase, Yamane, Ueno, & Kawano, 1999; Tamura & Tanaka, 2001), psychophysical (Schyns & Oliva, 1994; Loftus & Harley, 2004), and computational studies (Rodrigues & Buf, 2006b, 2006a). Hence, faster preprocessing and attentional capture by low frequency deviants effectively prime the positions where contour integration might be successful. This is verified by the example given in Figure 5.9, where low frequency deviants capture spatial attention (Figure 5.9a) and are effective as distracters (Figure 5.9b). In the f_{low} condition low frequency deviants are reasonably reliable cues to the region of interest, and local alignment based locking is facilitated in this region, whereas in the f_{high} condition, low frequency distracters effectively disturb focusing of the target area. As shown by studies on spatial and spatial frequency certainty, performance is boosted by limiting attention to the locations and frequency channels of interest (Yager, Kramer, Shaw, & Graham, 1984; Kramer et al., 1985). Cueing of the correct spatial frequency channels boosts performance in a way comparable to introducing matched filtering of the known signal (Hübner, 1996b). Hence, effective spatial and spatial frequency preselection might be responsible for the strong and oversummative cue combination effect observed for low frequency deviants from the surrounding field.

5.4.6 Side Conditions for Modeling Contour Integration

As the major results with spatial frequency variable displays for human contour integration performance we have found:

a. *Transitive similarity grouping and feature contrast.* Contour integration is not possible if the contour defining elements are similar in local carrier frequency while the background elements display carrier frequency jitter around the same mean carrier frequency. In order to be integrated to a global contour, the contour defining elements must be *(i)* different from the background in the local carrier frequency mean, *(ii)* must have similar carrier frequency, and *(iii)* carrier frequency similarity must be transitive, from neighbor to neighbor, along the contour.

b. *Alignment based grouping across wide ranges of spatial frequency.* If an orientation collinearity cue is present, contour integration works across wide ranges of carrier frequencies, and is still possible even when the contour defining elements differ about more than 2.25 octaves.

c. *Salience enhancement by combining alignment with spatial frequency feature contrast and similarity.* As a result of combining both types of cues, the global contour becomes a highly salient and stable structure that pops out of a noisy surround. Salience

enhancement is oversummative and asymmetric with respect to the direction of the carrier spatial frequency deviation, in favor of low spatial frequency deviants.

These findings pose side conditions for modeling contour integration in cluttered images. Existing computational approaches to contour integration have focused on the principles of collinearity and local locking among orientation and spatial frequency selective neurons, as found in V1 (Field et al., 1993; Yen & Finkel, 1997, 1998; Z. Li, 1998, 1999; Ursino & La Cara, 2004; Schinkel et al., 2005). This means that, based on the fields of local contextual interaction (Polat & Sagi, 1993; Kapadia et al., 1999, 2000), local locking of elements occurs when contiguous stimuli agree in local carrier frequency within a tolerance of not exceeding 1 octave and a local orientation difference of not exceeding $60°$. Comparison with the main results found with spatial frequency heterogenous displays shows that local locking based models can neither account for the finding of transitive similarity grouping and feature contrast, nor for the result of alignment based grouping across wide ranges of spatial frequency. In order to account for both findings one needs to implement alignment based contour integration in a much more robust fashion, and has to introduce a further contour integration mechanism that is not based on local alignment at all. Moreover, attentional guidance and spatial and featural preselection mechanisms have to enter a model which is capable of describing human contour integration in a more realistic fashion.

If transitive similarity grouping and feature contrast can be proven as a general principle of contour integration that works with many different features, a mechanism has to be implemented that is able to bind neighboring locations sharing a common attribute which is different from the surround. Such a feature independent mechanism can only be located in higher visual areas, such as IT and LOC. It would correspond to findings in recent neuroimaging studies, which demonstrate that these areas respond to perceived global shape independent of the primary feature modulation, performing a stimulus driven analysis without reference to stored knowledge about specific object form (Kourtzi & Kanwisher, 2000; Kourtzi & Huberle, 2005).

Alignment based grouping across wide ranges of spatial frequency shows that the alignment based contour integration mechanism is much more robust against other features that do not match from neighbor to neighbor. For integration across locally jittering spatial frequencies this means that the contour integration mechanism cannot be located within a single layer which is specific for combinations of orientation and carrier frequency. It must be located at higher cortical levels, possibly in area V2, where information from many local scales converges on one orientation at each location. The contributions from different local scales may be reweighed to increase neighbor to neighbor congruity in orientation collinearity across local scales. However, a problem with any purely bottom-up approach is that bandwidth measurements of the contextual response field with pairs of stimuli have shown a half amplitude at half height bandwidth of one octave (Polat & Sagi, 1993). There-

fore, the much larger bandwidth in contour integration must have a global source, where the presence of the whole contour exerts a modulating effect on the feature selectivity of lower level neurons, as shown by Lamme and colleagues (Zipser et al., 1996; Lamme, 1995; Lamme, Rodriguez-Rodriguez, & Spekreijse, 1999). Since alignment based contour integration is seemingly robust against jitter in other feature dimensions which are not jointly processed with orientation at early sites, such as color and depth (see above), a mechanism must exist which extracts local orientation independent of other features at the same spatial locations, and builds a local orientation map. Contour integration by orientation collinearity is special in the sense that the feature statistics of local orientation are no cue to contour presence. For smooth curvilinear contours there is no mean difference in local orientation to the surround and of the two displays which are to be compared in the 2AFC task. In transitive similarity grouping based on other features than orientation there *must* be such a mean difference, otherwise a contour is not perceived. In local orientation the contour is defined by a smooth change of local orientation from neighbor to neighbor, so it is the locking among neighbors, and not feature contrast based segregation, which mediates grouping with local orientation. The robustness of collinearity based contour integration across locally jittering features, combined with fact that neighbor to neighbor similarity alone is insufficient for contour grouping, underlines the special role of orientation collinearity for coding outlines and shapes, and its prevalence over other grouping principles in contour detection. From the outlined constraints it is clear that modeling contour grouping requires multiple, adaptively weighted scales and feedback connections with feature independent higher order shape coding layers. However, models of local alignment based grouping have not yet implemented multiple scales and their interaction in order to reach stabilized contour perception so far.

The findings regarding salience enhancement by combining alignment with spatial frequency feature contrast and similarity indicate that a realistic model must also include mechanisms of spatial and featural tagging, attentional capture and dynamic selection. Bottom up attentional capture works as a prime to the relevant locations and scales, which should lead to a reweighing of local scales when calculating contour salience. These are adaptive mechanisms, which alter cue integration rules, and therefore can explain oversummative cue interaction with the collinearity cue.

As outlined, a realistic model of human contour integration performance comprises implementations for feature contrast based transitive similarity grouping with multiple features, robust alignment based grouping across many scales and other features, and active selection and guidance mechanisms apt to optimize reweighing of scales in the spatial binding process.

6 General Discussion

6.1 Principles of Perceptual Organization in Contour Integration

Three studies were conducted to examine the role of three major principles of perceptual organization, namely *closure*, *similarity* and *good continuation*, for the integration of contours in cluttered images. As a source of variation widely ignored so far in the study of human contour integration the carrier spatial frequency of the local stimulus elements with bandpass characteristic was varied in all three experiments on contour integration. Thus, the standard stimulus display was a Gabor random field with variation of local orientation *and* local carrier spatial frequency. The simultaneous variation of both local orientation and carrier frequency is a novel aspect of pathfinder stimulus displays, since in almost all studies on contour integration just local orientation was varied at a fixed and somewhat arbitrarily chosen local carrier frequency. Most of the data recorded in the presented experiments are based on psychometric curves obtained for orientation variation of the contour elements relative to the global contour path (the *tilt angle*), as used in many studies on contour integration.

In this chapter principles of contour integration are outlined, which become apparent by combining the results of all experiments. As motivated in the introduction, the principles of contour integration are described in terms of Gestalt rules, and are discussed with respect to possible general guidelines of feature processing. Generalizations of the findings to other features are formulated as propositions, which may guide further experimentation on general routines of feature processing and their interaction in the human visual system.

6.1.1 Closure

In search of a sensory routine particularly associated with closure the efficiency of contour detection in noise was compared for open and closed contours in Chapter 3. To this end a rigorous psychometric curve analysis and an analysis of slope relative to the location parameter of the distribution function was applied. Psychometric curve slopes for closed contours tend to be slightly steeper than the corresponding curves for open contours. However, the effect is small and not statistically significant. Analysis in terms of the variation coefficient showed that the effect vanishes when the slopes are evaluated relative to the location of the psychometric function on the tilt angle scale. Taken together, there is no

indication from psychometric curve analysis that closed contours are detected more efficiently in noise than open contours. Closed (circular) contours were found to be detected with the same accuracy at significantly larger tilt angle values than open contours. The tilt angle threshold difference of open and closed contours is relatively large with nonoverlapping confidence intervals at all degrees of background element random jitter tested. As shown by various studies (see Introduction), alternative explanations properly account for the tilt angle threshold advantage of closed contours, namely the absence of turning points in the global stimulus (Mathes & Fahle, 2007a), the lack of curvature change in most stimulus instances used (Schinkel, 2007), and the better detectability by independent linking mechanisms (Tversky et al., 2004). As shown by Tversky et al. (2004), contour integration performance deteriorates when 2 elements are removed from contours of short length smaller than 12 elements, but this concerns open and closed contours in the same manner. Hence, the finding of Kovacs and Julesz (1993) that contour integration performance deteriorates if only two contour elements are removed is due to using just a small number of contour elements, and is not attributable to contour closure, as initially proposed by the authors. Since there is also a serious confound in the nearest neighbor statistics of displays with open and closed contours in the study of Kovacs and Julesz (1993), as well as with eccentricity (Braun, 1999), it appears that, at the time, there is no convincing psychophysical evidence for a particular closure mechanism, or a reverberating excitatory circuit involved with closed contours. The existence of such a mechanism can be questioned further, since there is evidence that closure is perceived to different degrees in spiral element arrangements with their ends unconnected (Elder & Zucker, 1993; Mathes & Fahle, 2007a). Existing evidence suggests that closure does not play a major role in mediating contour integration performance, and there is no need to postulate special routines for the processing of closed contours.

6.1.2 Similarity

The two-dimensional variation of the Gabor fields allowed to study the effect of homogeneity in local carrier spatial frequency along the global path independent of local orientation variation. This allowed for investigation whether similarity in only the spatial frequency parameter is sufficient to enable contour integration. It was found in Chapter 4 that similarity in local carrier frequency but with randomly varying local orientation is not sufficient to enable integration of local elements to global contours. Control measurements with isotropic bandpass elements conveying no local orientation information showed that also with these stimuli global contours are not seen in cluttered displays when all the elements along the path have the same local carrier frequency, while the surrounding elements are randomly varying in this parameter, and all other local features characterizing the local grating patch (color, size, contrast) are held at a constant value. Since the value of lo-

cal carrier frequency shared by all elements along the path matched the mean value of the whole display, this observation means that a difference in the variance parameter of contour and background while the mean parameters are held identical in both areas is not sufficient for a human observer to see a contour in a cluttered display. Upon introduction of a mean shift in the local carrier frequency contours defined by similar local carrier frequencies, which are distinct from the carrier frequencies of the surrounding, elements become detectable by human observers (see Chapter 5), and the larger the separation of mean carrier frequencies of contour and surrounding elements, the better contours are detected. Hence, similarity in local carrier frequency leads to contour grouping in a random display if, and only if, the carrier frequencies of contour and surrounding elements *segregate* in their mean values. As a major finding of this thesis, this result may lead to a generalized principle of contour integration mediated by feature similarity in other features than local orientation. It is taken down in the following proposition.

Proposition 1 *In contour grouping based on similarity of local features other than orientation, contiguous local elements are grouped into global contours if the contour defining elements are similar in the grouping feature and have sufficiently different mean value. Similarity and feature contrast are sufficient for salient contour grouping according to a weak principle of good continuation.*

It is already implied by Proposition 1 that local orientation is a special feature for which specific contour grouping principles apply. It is further implied that other features, if they are capable of enabling similarity based contour grouping, both similarity and feature contrast must be given for contour integration to occur. This is a strong assertion, which needs to be validated by further testing of different local features.

To illustrate the validity of proposition 1 the same scheme of variation as used with local carrier frequency in Chapter 4 and Chapter 5 can be applied to isoluminant color. The Figures 6.1 and 6.2 depict random fields of local elements varying in isoluminant color from green (510 nm wavelength) to red (650 nm wavelength), and show variation in local carrier frequency according to the same principles. Figure 6.1 illustrates the grouping principle stated by Proposition 1 for isoluminant color and local carrier frequency with local elements randomly varying in orientation, and Figure 6.2 illustrates the same principle with circular symmetric stimuli conveying no local orientation information. As shown by the left panels of both figures, the circular contour defined by assigning all contour elements a feature value identical to the background mean is difficult to see. If the contour elements are set to a feature value at the lower end of the scale (right panel of both figures) the circular contour emerges. This holds even if contour elements jitter randomly in orientation (Figure 6.1), or convey no local orientation information (Figure 6.2). Hence, irrespective of the nature of the feature (isoluminant color or local carrier frequency), feature contrast combined with similarity enables seeing a global contour in cluttered displays.

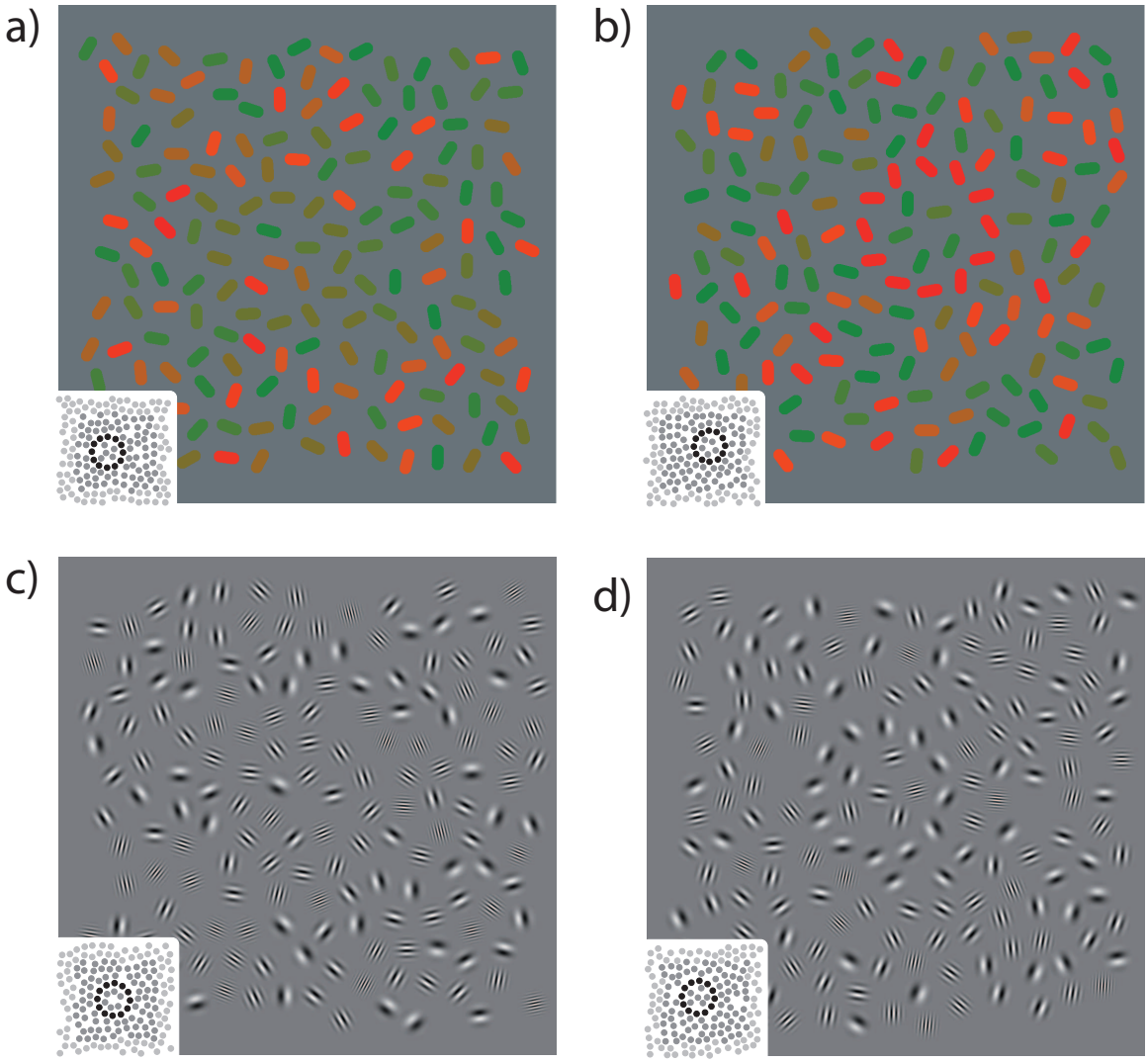

Figure 6.1: Similarity and feature contrast based grouping with isoluminant color and local carrier frequency in line element and Gabor random fields. The upper panel (a and b) shows the variation of isoluminant color from green to red, the lower panel variation of local carrier frequency according to the same principle. In the examples of the left panel (a and c) a circle is defined by a constant feature value, which is the mean of the total random display. In the examples of the right panel (b and d) the circle defining elements have feature contrast to the surround. In (b) they have a red value which is 3 units of standard deviation apart from the mean color of the display. In (d) they have local carrier frequency which is 3 units of standard deviation lower than the mean carrier frequency, measured on an octave scale. Sampling was done from normal distributions in all instances shown.

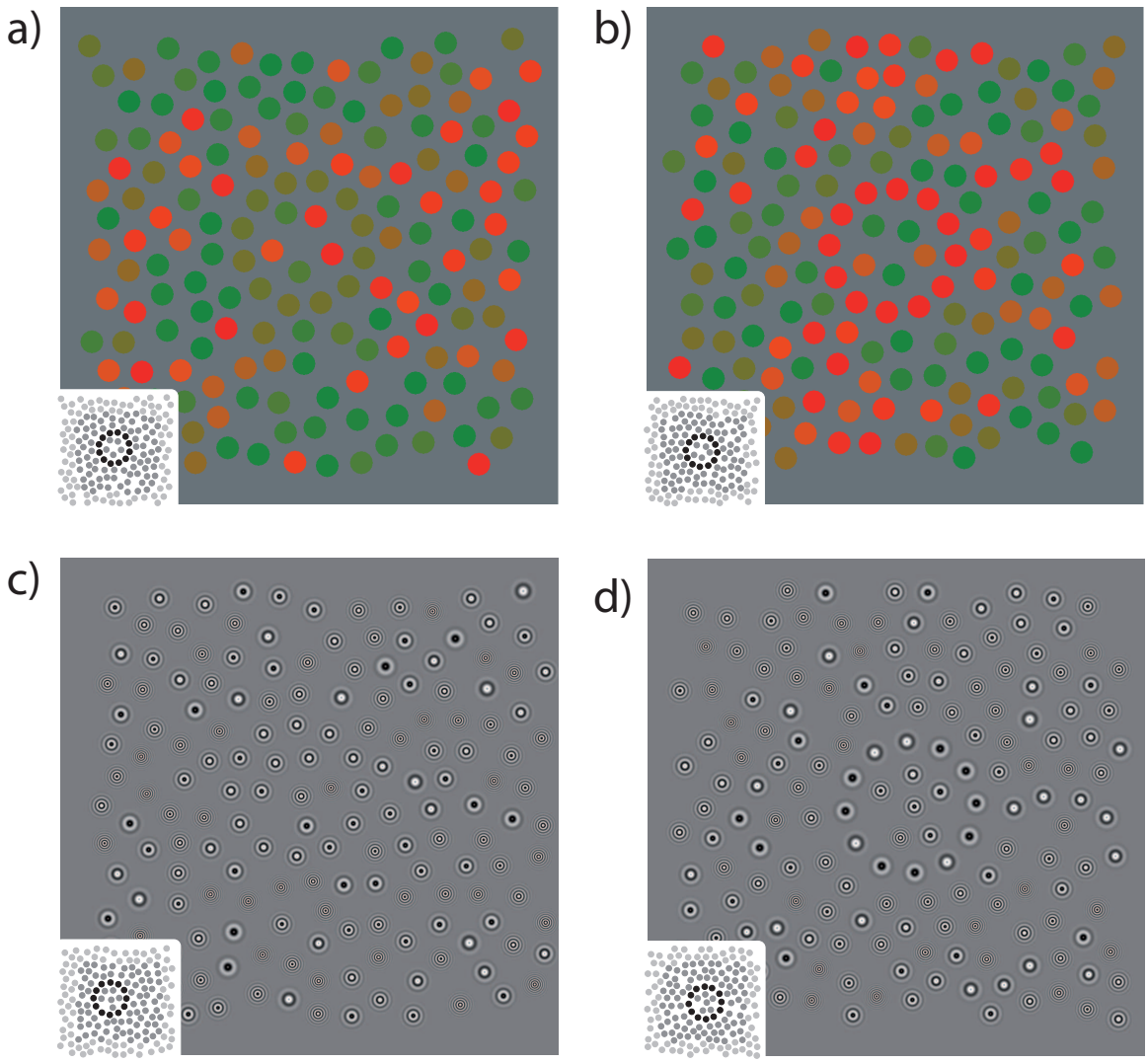

Figure 6.2: Similarity and feature contrast based grouping with isoluminant color and local carrier frequency in fields of isotropic stimulus elements. The scheme of variation is the same as shown in Figure 6.1, but applied to circular symmetric stimulus elements.

The conclusion that it is the *combination* of feature contrast and similarity that enables contour integration is justified if it can be shown that a pure feature contrast cue alone does not lead to grouping, since a pure similarity cue apparently fails to enable perception of the global contour (see left panels of Figures 6.1 and 6.2). Figure 6.3 lends support to this hypothesis: With isoluminant color (see Figure 6.3a,b) as well as local carrier frequency (see Figure 6.3c,d) it is not possible to see a global contour if the contour elements deviate from the mean feature value of the display in both directions, alternating randomly along the course of the contour. Hence, feature contrast, without similarity, is not apt to enable integration of elements to a global path. This allows to conclude that feature contrast *per se* does not lead to grouping in cluttered displays. Note that feature contrasts are maximum along the contour due to the alternating sign of the feature contrast values. Analyzing with a Filter-Rectify-Filter processor shows that local energy is maximum along the course of the contour. However, grouping only occurs when the feature deviation is in the same direction on the feature continuum, establishing feature contrast values which are homogeneous along the contour but different from the surround (see Figures 6.1 and 6.2). This points out that grouping is not enabled by maximum feature contrast, but by feature contrast combined with homogeneity of the segregating features along the global form.

In the introduction it was outlined that contour integration can be understood as a case of good continuation, which requires the principle of transitivity for the locking of neighboring elements. A contour is integrated if, and only if, for elements a, b, c the transitivity relation $aRb \cap bRc \Rightarrow aRc$ holds, where R means "locking" among the two elements. Locking can in principle be mediated by contiguity in any feature. For features that obey Proposition 1 element locking requires feature contrast of the grouped elements from the surround. The kind of features that follow this grouping principle do not carry local information about the direction of the path. Proposition 1 therefore may be viewed to formulate the definitory precondition of good continuation for contour integration (see Introduction). Element properties that already highlight contour substrings are mandatory to convey information about the direction of the global path. Besides good continuation and contiguity, another feature property of the contour defining elements is necessary to enable the grouping process.

6.1.3 Local Alignment

The second major finding, which was made possible by using displays varying in local orientation and local carrier frequency is that local alignment based contour grouping appears rather robust against jitter in the carrier frequency feature. As outlined in Chapter 4, this finding is surprising at first glance, and it is against the expectation derived from a local association field model assuming contour integration to be mediated by locking among orientation and spatial frequency tuned mechanisms, as found in V1. The bandwidth estimates

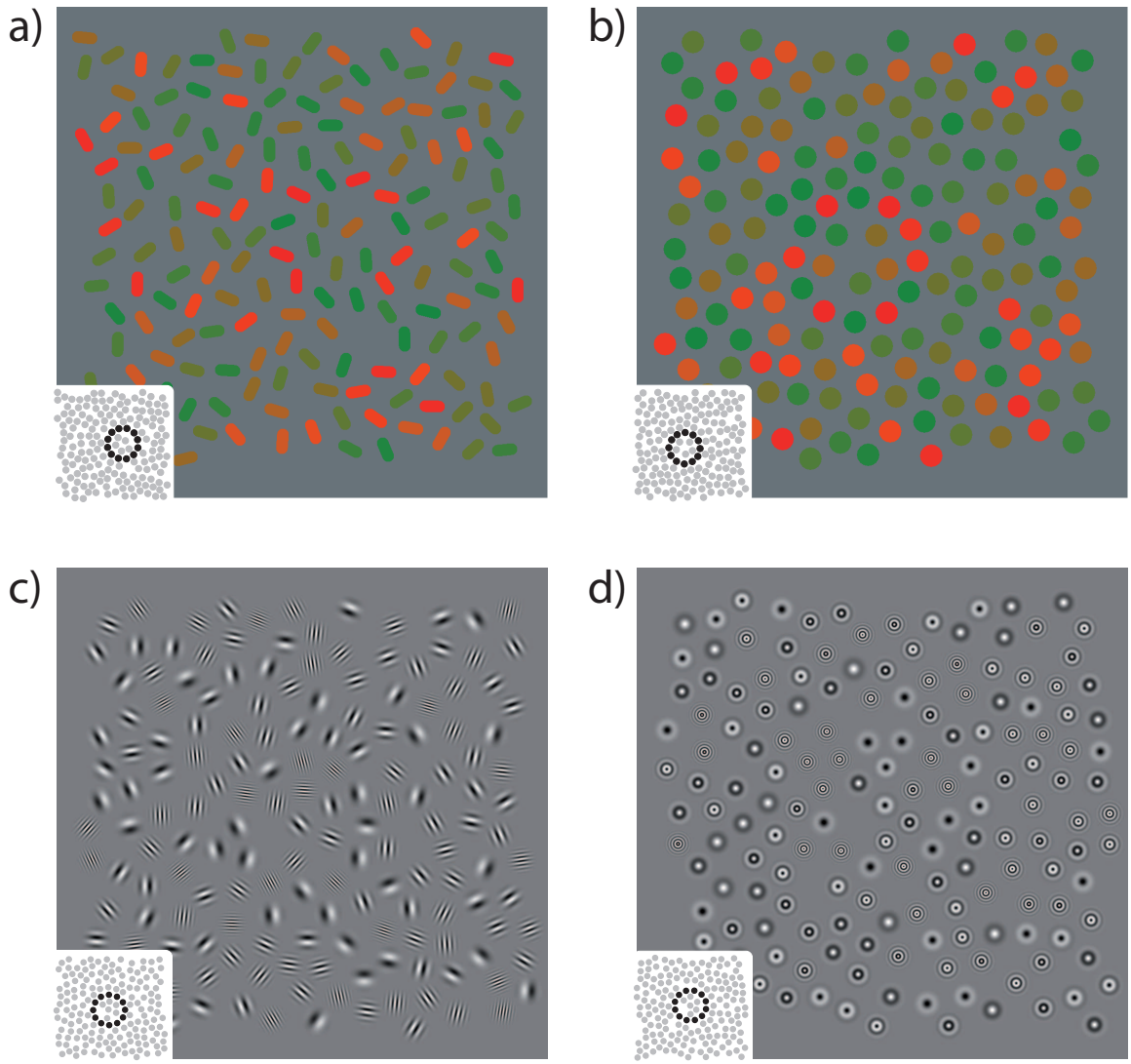

Figure 6.3: Feature contrast in isoluminant color and local carrier frequency does not enable contour grouping in displays with local orientation jitter (left panel) and displays with no local orientation information (right panel). All displays contain contours defined by alternating between the minimum and the maximum feature value of the background distribution, yielding substrings of elements with maximum feature contrast along the circular contour. In a) and b) this is shown with isoluminant color, and c) and d) show stimuli with maximum difference in local carrier frequency.

for the contextual response field derived from the measurements of Polat and Sagi (1993, 1993) show that interaction among neighboring Gabor patches should be weak if they are more than 1 octave apart in local carrier frequency, the half-bandwidth at half height bandwidth estimate found in their dual patch experiments. In the contour detection experiments of Chapter 4 it is shown that in this task, executed at comparable conditions (contrast, patch-sizes, local carrier frequency range), a carrier frequency separation of about 1.25 octaves leads to no considerable performance impairment, and even with a separation of more than 2 octaves subject still reach reasonable contour detection performance levels. These results show that contour detection cannot solely depend on local locking of orientation and spatial frequency tuned elements, but must involve integration of the local alignment signal over wider ranges of carrier frequencies. Corresponding to this finding it was found that contour integration is possible across depth planes (Hess & Field, 1995; Hess et al., 1997) and across isoluminant color and luminance variation (McIlhagga & Mullen, 1996). Particularly the findings of McIlhagga and Mullen (1996) are crucial for the local association field model. In this study it was shown that contours are integrated in random fields with aligned elements bearing just chromatic modulation but no luminance modulation. Further, it was shown that alternating luminance and isoluminant chromatic modulation along the contour still enables contour integration at reasonable performance levels. These results indicate that contour integration involves layers where color and orientation are combined, and these layers are located at area V2 and higher. They further imply that color and luminance are integrated at the level of contour processing, which means that there must be an interaction among luminance modulated orientation and carrier spatial frequency selective cells on the one hand and color modulated orientation selective cells on the other, both sharing the same local scale. Also, this interaction can only be located on a level of processing which is higher than V1.

In Chapter 4 it was outlined that integration of oriented contour elements across variation of other features suggests an invariance principle for extracting local orientation alignment. This invariance principle becomes apparent from two observations: First, the above mentioned robustness of contours defined by the local alignment with a global path against other randomly varying features, and second, the tendency of human observers to assign a unique local orientation to one point in space (Olzak & Thomas, 1992; Olzak & Wickens, 1997; Olzak & Thomas, 1999). Local alignment is a feature that takes a particular role in contour integration, since already the local elements carry information about the possible course of the global path. Each element indicates a direction in space, and locking among few elements enables to predict the further course of a trajectory.

An important property of contour grouping mediated by locally oriented elements is that it does not require feature contrast and similarity of neighboring elements, as stated in Proposition 1. Only *local* orientation similarity is necessary, meaning a *smooth change* of local orientation from neighbor to neighbor. Contours are integrated based on a local align-

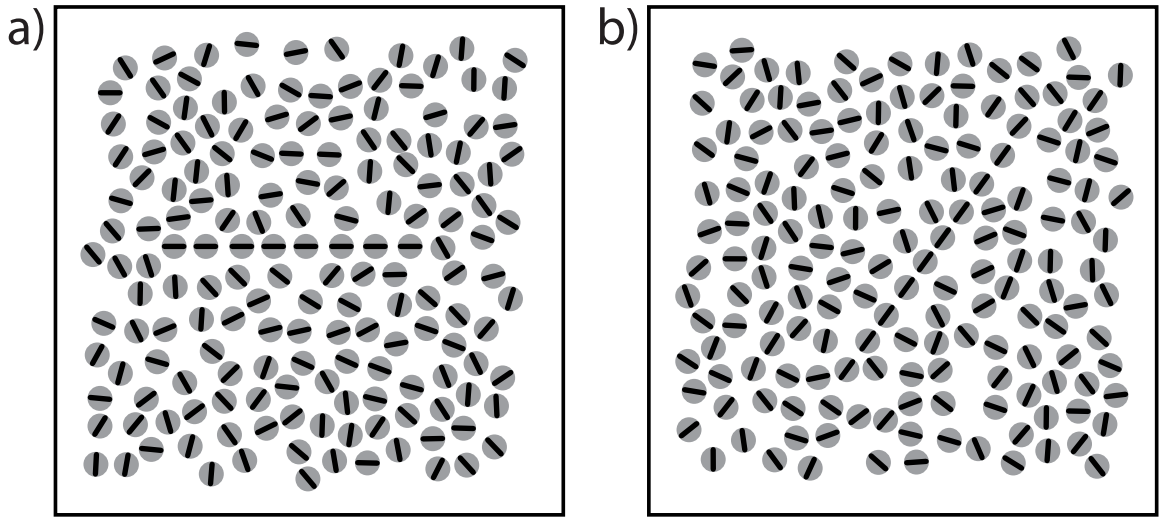

Figure 6.4: Straight contours with moderate orientation jitter in horizontal (a) and oblique direction (b) embedded in a field with mean orientation of 0°. Both contours are easily and effortlessly seen.

ment cue irrespective of the mean local orientation value of the contour defining elements relative to the surround. For example, the local elements along a straight contour can be set to the mean orientation of the surrounding field, but the contour is easily and effortlessly found in the random display. A deviation from the mean feature value does not enhance performance any further. This is illustrated in Figure 6.4. The mean orientation of the random field elements is set to 0°, and straight contours can be defined along the cardinal and the oblique axes. All such contours are effortlessly integrated, and there is no significant detection advantage for contours with specific global angles (see Polat & Sagi, 1994a).

The validity of the contour grouping principle formulated in Proposition 1 was substantiated by the results obtained for local carrier frequency, and was illustrated further with isoluminant color as a feature for which the same principle applies. Robustness of contour integration mediated by local alignment as found across local carrier frequency variation can also be shown to across high levels of isoluminant color variation.

In Chapter 4 it was reported that contour integration in random fields with jitter in local orientation and local carrier frequency jitter in the range of about 2 octaves operates at approximately the same performance level, irrespective of whether this jitter level is applied also to the elements along the contour or not. This is illustrated in the upper panel of Figure 6.5: Visibility of the spatial frequency homogeneous contour (b) is as high as for the contour with local carrier frequency jitter along the path (a). The lower panel of Figure 6.5 shows the analogous stimulus instances, but for variation of isoluminant color. The alignment based circular contour is well visible in a random field with orientation and

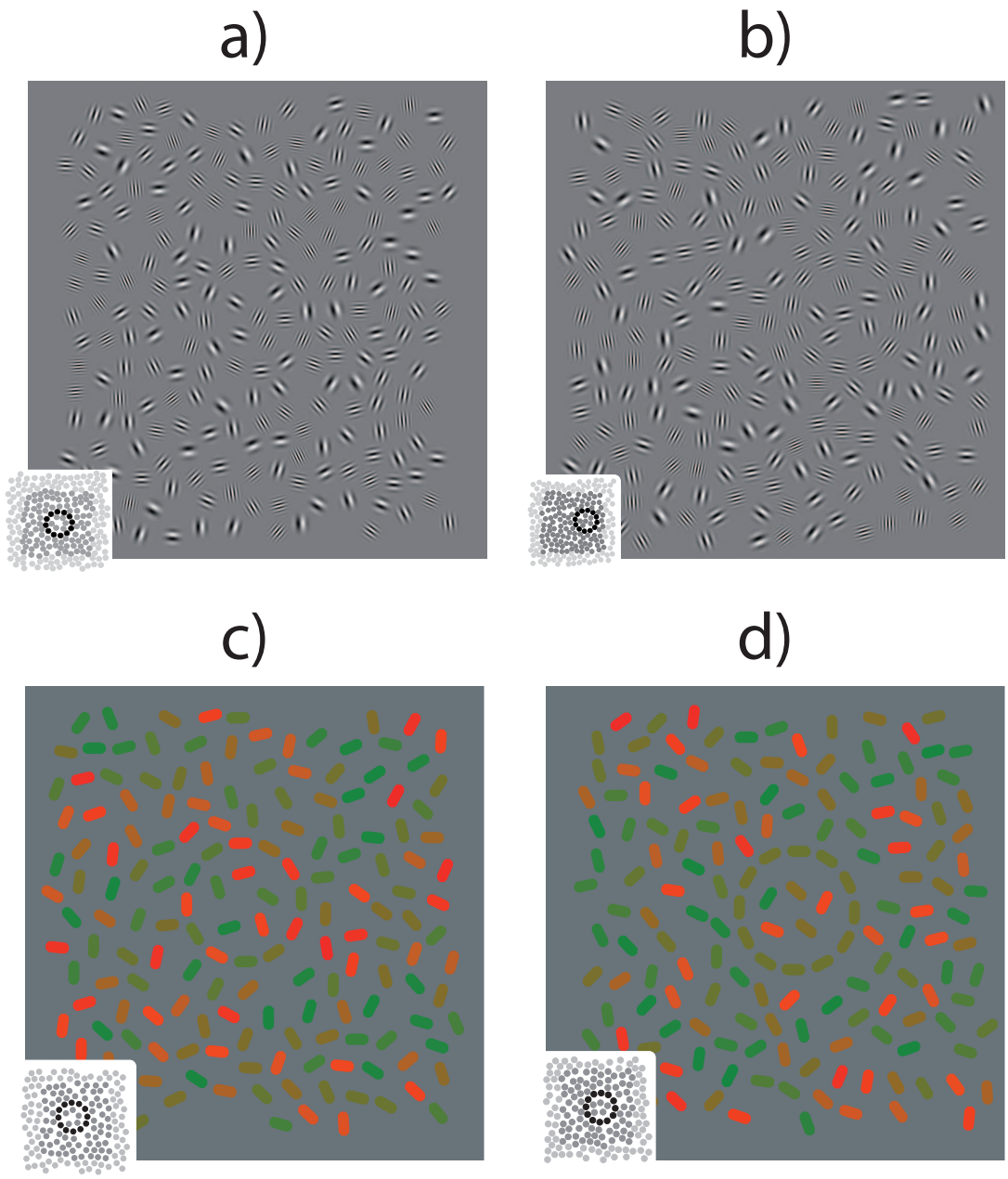

Figure 6.5: Robustness of local alignment based grouping across local carrier frequency and isoluminant color variation. Alignment based contour grouping in random fields with local carrier frequency jitter in the range of 2 octaves (upper panel) is possible with carrier frequency jitter along the contour (a), or not (b). Analogously, in fields with isoluminant color jitter alignment based contour grouping is possible with color jitter along the path (c), or not (d).

color jitter, with color jitter along the contour (c), or without (d). Both examples show that the contour detection mechanism is capable of extracting the invariant local alignment cue in environments with randomly jittering features, and to integrate this cue across space.

Contour integration due to local orientation alignment can be viewed as the addition of orientation collinearity to the rule of good continuation (see Introduction), with direction information transmitted by each element which is uniquely extracted and robustly integrated across other varying features, without the necessity of segregating the elements along the contour from the surround. It appears that just similarity of local orientation among neighbors is sufficient to built the transitive locking relation from neighbor to neighbor, which results in a globally integrated path. This principle of contour integration is taken down in the following proposition.

Proposition 2 *In contour grouping based on local alignment, elements are grouped into global contours if there is similarity of local orientation among neighbors. The value of local orientation may smoothly change from neighbor to neighbor. Contour grouping occurs across other locally varying features along the contour in surrounds with multiple varying features.*

6.2 Combining Local Alignment with Similarity and Feature Contrast

In the foregoing sections two principles of contour grouping were defined, which emerge as generalizations from the results obtained with random displays varying in local orientation and carrier spatial frequency. Each principle of contour grouping was illustrated with isoluminant color as an additional feature for which the same principles apply.

It is tempting to generalize from the findings on combining a local alignment cue (Proposition 2) with local carrier frequency as an additional similarity and feature contrast cue obeying the weak law of good continuation (Proposition 1), towards a general principle of combining these two types of cues, independent of the nature of the additional cue. Considering generalizations of the contour grouping examples illustrated in Figure 5.1 with local orientation and carrier frequency (see Chapter 5) to combinations of other local features with the alignment cue shows that generalizations should be done only with caution.

It was stressed in the discussion of Chapter 5 that the asymmetry of the cue combination effect for local carrier frequency implies that combining a local alignment cue with a low frequency deviant involves other contour detection mechanisms than the combination with a high frequency deviant, involving superior spatial and spatial frequency certainty conditions (see Section 5.4.5). The assumption of specific sensory mechanisms responsible for processing low spatial frequency deviants was due to the oversummative nature of cue summation gains for low frequency deviants, since the magnitude of salience enhancement due to combining with a high frequency deviant fell within the range expected for passive summation rules among different sensory sources.

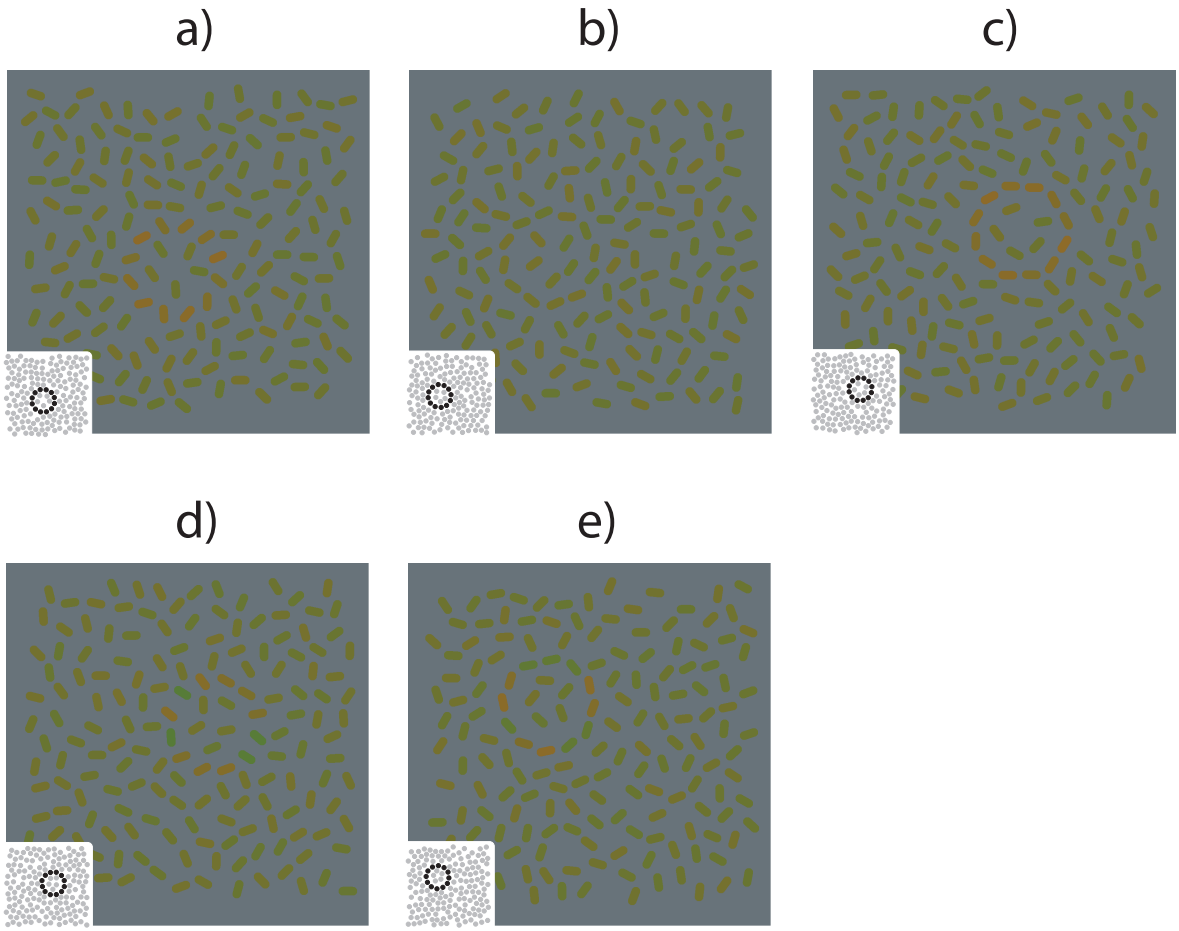

Figure 6.6: Perceptual effects of feature contrast, collinearity and similarity cues on the salience of a global circular contour in orientation random fields with isoluminant line elements. In a) contour elements were assigned the same random orientation than the surrounding elements, but a mean shift in isoluminant color towards a red hue. The contour defining elements segregate from the surround, and are similar in color. Panel b) shows contour defining line elements with local orientations aligned with the global path in a field where contour elements and surround carry similar hue. In c) the contour defining principles of a) and b) are combined, which makes the global path more salient. Panel d) shows a background of randomly oriented elements where elements along the circular contour deviate from the surround by their hue, randomly alternating in green and red direction. These elements segregate from the embedding field, but are not similar. In e) feature contrast in isoluminant color is combined with global path alignment.

The introductory example in Chapter 5 (see Figure 5.1), illustrates the perceptual effects of the different cues of orientation collinearity (Figure 5.1b), feature contrast (Figure 5.1d), feature contrast and similarity (Figure 5.1a), alignment and feature contrast (Figure 5.1e), and collinearity combined with similarity and feature contrast (Figure 5.1c). It becomes clear that feature contrast in carrier frequency alone does not enable contour integration, whereas combinations with similarity in carrier frequency (Proposition 1) or alignment (Proposition 2) render a global contour visible.[25] Combining feature contrast in carrier frequency and similarity in this feature with local alignment makes a contour highly salient, and leads to a robust and stable global percept in a cluttered display. Figure 6.6 shows an example which is analogous to the introductory example of Chapter 5 with isoluminant color. The color cue is established by increasing the red component value of contour elements, thus providing them with a faint red hue. Comparing Figure 5.1 to Figure 6.6 shows that, essentially, the same effects of feature contrast and its combination with similarity, alignment, and with both principles appear. However, the salience gain due to combining similarity and feature contrast (Proposition 1) with local alignment (Proposition 2) appears much weaker for color than for spatial frequency. This phenomenological impression needs to be substantiated by comparing cue summation measures in an experimental setting. As a convenient circumstance, cue summation proved oversummative for low spatial frequency deviants and within the range of expectation for passive summation rules for high spatial frequency deviants, but, in any case, stronger than expected from the assumption of summation among independent cues. This is a clear scheme of summation which can be compared to summation schemes found with combinations of local alignment with other features obeying Proposition 1. Without exact cue summation measurements at hand, statements about the generality of the findings obtained for the combination of alignment with spatial frequency remain speculative.

There are several reasons why the effects of combining the local alignment cue with other feature cues obeying Proposition 1 should depend on the nature of the feature, and its site of primary processing on the visual pathway. Note that spatial frequency and local alignment are jointly processed on a common site early in area V1. This means that interaction among both cues is a matter of the vertical and horizontal connections among layers within the same site. Strong cue combination effects could be achieved by adaptive selection mechanisms, giving the layers comprising those spatial scales with strongest local orientation neighbor locking more weight in constructing the global path (see discussion in Chapter 5). Hence, the site of interaction among both cues is early, which explains its large magnitude. Different conditions apply when combining orientation collinearity and color

[25] The fact that similarity in local carrier frequency alone does not lead to contour integration was already shown in Chapter 4. Combining feature contrast of carrier frequency with local alignment (Figure 5.1e) demonstrates the robustness of alignment based contour integration against jitter in another feature (Proposition 2).

cues. In area V1 both cues have no common site, and the earliest locus of cue integration is area V2, where slit detectors reside which integrate the outputs of isotropic color sensitive cells from layer 4 of area V1. Accordingly, perception of orientation with just color appears somewhat difficult, much more difficult than with luminance modulated local stimuli.[26] Shape detection based on color is reported to be located higher, in areas V4 and above (Desimone & Duncan, 1995; Desimone, 1996). A much weaker interaction among orientation and color compared to orientation and luminance was found by Nothdurft (2000) in a salience matching task, and Mathes et al. (2006a) failed to find any significant interaction among both cues in contour integration. The stimulus examples given in Figure 6.6 demonstrate that there is a moderate cue summation gain, but it remains to be seen how strong this interaction is compared to the combination of orientation and local carrier spatial frequency. For these cues a good correspondence in early shape detection is reported for higher ventral areas, as the inferior-temporal cortex, the parietal cortex, and the LOC with early sites (Altmann et al., 2003; Kourtzi & Kanwisher, 2000; Kourtzi & Huberle, 2005; Lerner et al., 2001), suggesting that cooperation among higher ventral areas and V1 and V2 regulates scale invariant early shape extraction preferably from luminance modulated stimuli.

[26] A striking demonstration of contour integration with isoluminant oriented local elements is found in the stimulus examples of McIlhagga and Mullen (1996, see Figure 1 ibid.)

7 Concluding Remarks

Two fundamental propositions were derived from the experimental findings presented in this thesis. First, it was proposed that the rule of good continuation is not sufficient to enable contour grouping within the visual system, but has to be complemented by other grouping cues. If the Gestalt rule of similarity is used as the additional grouping principle, similar elements also need to exhibit a salient feature contrast cue in order to establish a stable contour percept. Second, it was concluded that a principle of good continuation that rests on local orientation collinearity enables salient contiguity grouping even in environments with high feature noise, allowing for robust integration of contours in cluttered surrounds. These two propositions defer to requirements and opportunities of future work, which will be briefly outlined in what follows.

One of the most auspicious directions of future research is the generalization of both propositions across a broad range of features. Validity of Proposition 1 would be substantiated by showing that the mutual dependency between similarity and feature contrast, when used as a complementary cue to the rule of good continuation, is invariant against the specific feature transmitting similarity information. Incidental evidence has already been reported for depth and motion as local features. The stimulus displays shown in the general discussion also qualify the color processing pathway to dovetail with this notion. If converging evidence for feature independence of Proposition 1 was obtained, the principle of coherent similarity and feature contrast would qualify as a general functional principle of neural organization in contour integration.

Further, the generality of the assertion that similarity and feature contrast do not enable perceptual grouping when used as single cues to a global contour requires experimental scrutiny with many different features. Particularly the apparent ineptitude of feature similarity as a salient grouping principle to aid contour integration calls for further examination. In the scope of this thesis, only the combination of good continuation with local carrier frequency as one possible similarity cue has been studied. If similarity conveyed by arbitrary features would consistently prove inefficient to establish a solid contour percept, a serious constraint would be imposed on the Gestalt rule of similarity. Similarity would then not stand as a self-contained principle of perceptual grouping, but as a mere precondition that is contingent on a complementary segregation cue.

The differential effects of cue summation found for low and high local carrier frequency deviants led to the assumption that additional mechanisms may enter visual processing, de-

pending on the cues' aptitude to trigger bottom up attentional capture serving to highlight the spatial scale of contour integration. This hypothesis may be tested by attentional cueing of the spatial frequency contrast direction of the deviant. If this interpretation holds, an external cue informing the subject about the local scale of contour elements in the forthcoming trial should eliminate the observed cue summation asymmetry, and summation of the carrier frequency deviant with the alignment cue should become equal for low and high frequency contour targets.

Finally, the quantification of cue summation effects presents itself as a promising enterprize. While it appears beyond debate *that* multiple grouping cues can combine synergistically in contour integration, the magnitude of the visibility advantage due to additional cues has only been estimated among very few features like spatial frequency and motion. A systematic evaluation of the relative suitability of different features to complement good continuation with a salient similarity and feature contrast cue, as accomplished by Nothdurft (2000) for feature contrast detection tasks, could prove valuable in understanding how and on which level within the visual hierarchy the respective features are integrated. Particularly by combining features which have their primary processing sites close and far apart along the processing hierarchy could help to elucidate the functional relationship among major areas of visual feature processing in the human brain.

References

Abramowitz, M., & Stegun, I. A. (1972). *Handbook of mathematical functions* (10th ed.). New York: Dover.

Altmann, C. F., Bülthoff, H. H., & Kourtzi, Z. (2003). Perceptual organization of local elements into global shapes in the human visual cortex. *Current Biology*, *13*(4), 342–349.

Altmann, C. F., Deubelius, A., & Kourtzi, Z. (2004). Shape saliency modulates contextual processing in the human lateral occipital complex. *Journal of Cognitive Neuroscience*, *16*(5), 794–804.

Anderson, J. R. (2004). *Cognitive psychology and its implications* (6th ed.). New York: Palgrave Macmillan.

Ashby, F. G., & Townsend, J. T. (1986). Varieties of perceptual independence. *Psychological Review*, *93*(2), 154–179.

Bach, M., Schmitt, C., Quenzer, T., Meigen, T., & Fahle, M. (2000). Summation of texture segregation across orientation and spatial frequency: Electrophysiological and psychophysical findings. *Vision Research*, *40*(26), 3559–3566.

Baldi, P., & Heiligenberg, W. (1988). How sensory maps could enhance resolution through ordered arrangements of broadly tuned receivers. *Biological Cybernetics*, *59*(4-5), 313–318.

Bauer, R., & Heinze, S. (2002). Contour integration in striate cortex. Classic cell responses or cooperative selection? *Experimental Brain Research*, *147*(2), 145–152.

Beaudot, W. H., & Mullen, K. T. (2003). How long range is contour integration in human color vision? *Visual Neuroscience*, *20*(1), 51–64.

Beck, J. (1966). Effects of orientation and shape similarity on perceptual grouping. *Perception & Psychophysics*, *1*, 300–302.

Beck, J. (1972). Similarity grouping and peripheral discriminability under uncertainty. *American Journal of Psychology*, *85*, 1–19.

Beck, J. (1982). Textural segmentation. In J. Beck (Ed.), *Organization and representation in perception* (p. 285-318). Hillsdale: Erlbaum.

Beck, J., Rosenfeld, A., & Ivry, R. (1989). Line segregation. *Spatial Vision*, *4*(2-3), 75–101.

Bergen, J. R., & Adelson, E. H. (1988). Early vision and texture perception. *Nature*, *333*(6171), 363–364.

Bergen, J. R., & Julesz, B. (1983). Parallel versus serial processing in rapid pattern discrimination. *Nature*, *303*(5919), 696–698.

Bertamini, M., & Croucher, C. J. (2003). The shape of holes. *Cognition*, *87*(1), 33–54.

Bertamini, M., & Farrant, T. (2006). The perceived structural shape of thin (wire-like) objects is different from that of silhouettes. *Perception*, *35*(12), 1679–1692.

Bex, P. J., Simmers, A. J., & Dakin, S. C. (2001). Snakes and ladders: The role of temporal modulation in visual contour integration. *Vision Research*, *41*(27), 3775–3782.

Biederman, I. (1987). Recognition-by-components: a theory of human image understanding. *Psychological Review*, *94*(2), 115–147.

Blackwell, H. R. (1963). Neural theories of simple visual discriminations. *Journal of the Optical Society of America*, *53*, 129–160.

Bosking, W. H., Zhang, Y., Schofield, B., & Fitzpatrick, D. (1997). Orientation selectivity and the arrangement of horizontal connections in tree shrew striate cortex. *The Journal of Neuroscience: The Official Journal of the Society for Neuroscience*, *17*(6), 2112–2127.

Bradley, A., Skottun, B. C., Ohzawa, I., Sclar, G., & Freeman, R. D. (1987). Visual orientation and spatial frequency discrimination: a comparison of single neurons and behavior. *Journal of Neurophysiology*, *57*(3), 755–772.

Braun, J. (1999). On the detection of salient contours. *Spatial Vision*, *12*(2), 211–225.

Bredfeldt, C. E., & Ringach, D. L. (2002). Dynamics of spatial frequency tuning in macaque V1. *The Journal of Neuroscience: The Official Journal of the Society for Neuroscience*, *22*(5), 1976–1984.

Caelli, T. (1982). On discriminating visual textures and images. *Perception & Psychophysics*, *31*(2), 149–159.

Carrasco, M., McLean, T. L., Katz, S. M., & Frieder, K. S. (1998). Feature asymmetries in visual search: Effects of display duration, target eccentricity, orientation and spatial frequency. *Vision Research*, *38*(3), 347–374.

Chen, C. M., Lakatos, P., Shah, A. S., Mehta, A. D., Givre, S. J., Javitt, D. C., et al. (2007). Functional anatomy and interaction of fast and slow visual pathways in macaque monkeys. *Cerebral Cortex*, *17*(7), 1561–1569.

Choe, Y., & Miikkulainen, R. (2004). Contour integration and segmentation with self-organized lateral connections. *Biological Cybernetics*, *90*(2), 75–88.

Chubb, C., Sperling, G., & Solomon, J. A. (1989). Texture interactions determine perceived contrast. *Proceedings of the National Academy of Sciences of the United States of America*, *86*(23), 9631–9635.

Crozier, W. J. (1936). On the sensory discrimination of intensities. *Proceedings of the National Academy of Sciences of the United States of America*, *22*(6), 412–416.

Crozier, W. J., & Holway, A. H. (1937). On the law for minimal discrimination of intensities: I. *Proceedings of the National Academy of Sciences of the United States of America*, *23*(1), 23–28.

Dakin, S. C., & Hess, R. F. (1998). Spatial-frequency tuning of visual contour integration. *Journal of the Optical Society of America. A, Optics, Image Science, and Vision*, *15*(6), 1486–1499.

Dakin, S. C., & Hess, R. F. (1999). Contour integration and scale combination processes in visual edge detection. *Spatial Vision*, *12*(3), 309–327.

Dakin, S. C., Williams, C. B., & Hess, R. F. (1999). The interaction of first- and second-order cues to orientation. *Vision Research*, *39*(17), 2867–2884.

Das, A., & Gilbert, C. D. (1999). Topography of contextual modulations mediated by short-range

interactions in primary visual cortex. *Nature*, *399*(6737), 655–661.

Desimone, R. (1996). Neural mechanisms for visual memory and their role in attention. *Proceedings of the National Academy of Sciences of the United States of America*, *93*(24), 13494–13499.

Desimone, R., & Duncan, J. (1995). Neural mechanisms of selective visual attention. *Annual Review of Neuroscience*, *18*, 193–222.

De Valois, R. L., Albrecht, D. G., & Thorell, L. G. (1982). Spatial frequency selectivity of cells in macaque visual cortex. *Vision Research*, *22*(5), 545–559.

Ehrenstein, W. H., Spillmann, L., & Sarris, V. (2003). Gestalt issues in modern neuroscience. *Axiomathes*, *13*(3–4), 433–458.

Elder, J. H., & Goldberg, R. M. (2002). Ecological statistics of gestalt laws for the perceptual organization of contours. *Journal of Vision*, *2*(4), 324–353.

Elder, J. H., & Zucker, S. W. (1993). The effect of contour closure on the rapid discrimination of two-dimensional shapes. *Vision Research*, *33*(7), 981–991.

Elder, J. H., & Zucker, S. W. (1994). A measure of closure. *Vision Research*, *34*(24), 3361–3370.

Farag, A. A., & Delp, E. J. (1992). Edge linking by sequential search. In R. M. Larson & H. H. Nasr (Eds.), *Model-based vision development and tools* (Vol. 1609, pp. 198–216).

Feldman, J. (2001). Bayesian contour integration. *Perception & Psychophysics*, *63*(7), 1171–1182.

Feldman, J., & Singh, M. (2005). Information along contours and object boundaries. *Psychological Review*, *112*(1), 243–252.

Field, D. J., Hayes, A., & Hess, R. F. (1993). Contour integration by the human visual system: evidence for a local "association field". *Vision Research*, *33*(2), 173–193.

Field, D. J., Hayes, A., & Hess, R. F. (2000). The roles of polarity and symmetry in the perceptual grouping of contour fragments. *Spatial Vision*, *13*(1), 51–66.

Filliben, J. J. (1975). The probability plot correlation coefficient test for normality. *Technometrics*, 111–117.

Flury, B. (1997). *A first course in multivariate statistics* (Vol. 1). Berlin: Springer.

Geisler, W. S., Perry, J. S., Super, B. J., & Gallogly, D. P. (2001). Edge co-occurrence in natural images predicts contour grouping performance. *Vision Research*, *41*(6), 711–724.

Geisler, W. S., & Super, B. J. (2000). Perceptual organization of two-dimensional images. *Psychological Review*, *107*(4), 677–708.

Gibson, B. S. (1994). Visual attention and objects: One versus two or convex versus concave? *Journal of Experimental Psychology. Human Perception and Performance*, *20*(1), 203–207.

Gigus, Z., & Malik, J. (1991). *Detecting curvilinear structure in images* (Tech. Rep.). University of California.

Gilbert, C., Ito, M., Kapadia, M., & Westheimer, G. (2000). Interactions between attention, context and learning in primary visual cortex. *Vision Research*, *40*(10-12), 1217–1226.

Goldstone, R. L., Medin, D. L., & Gentner, D. (1991). Relational similarity and the nonindependence of features in similarity judgments. *Cognitive Psychology*, *23*(2), 222–262.

Goolsby, B. A., Grabowecky, M., & Suzuki, S. (2005). Adaptive modulation of color salience contingent upon global form coding and task relevance. *Vision Research*, *45*(7), 901–930.

Graham, N. (1977). Visual detection of aperiodic spatial stimuli by probability summation among narrowband channels. *Vision Research*, *17*(5), 637–652.

Graham, N. (1989). *Visual pattern analyzers* (Vol. 16). New York: Oxford University Press.

Graham, N., & Rogowitz, B. E. (1976). Spatial pooling properties deduced from the detectability of fm and quasi-am gratings: a reanalysis. *Vision Research*, *16*(9), 1021–1026.

Grossberg, S., & Pessoa, L. (1998). Texture segregation, surface representation and figure-ground separation. *Vision Research*, *38*(17), 2657–2684.

Grossberg, S., & Williamson, J. R. (2001). A neural model of how horizontal and interlaminar connections of visual cortex develop into adult circuits that carry out perceptual grouping and learning. *Cerebral Cortex*, *11*(1), 37–58.

Gurnsey, R., & Browse, R. A. (1987). Micropattern properties and presentation conditions influencing visual texture discrimination. *Perception & Psychophysics*, *41*(3), 239–252.

Herzog, M. H., Ernst, U. A., Etzold, A., & Eurich, C. W. (2003). Local interactions in neural networks explain global effects in gestalt processing and masking. *Neural Computation*, *15*(9), 2091–2113.

Hess, R. F., Baker, J., C. L., & Wilcox, L. M. (1999). Comparison of motion and stereopsis: Linear and nonlinear performance. *Journal of the Optical Society of America. A, Optics, Image Science, and Vision*, *16*(5), 987–994.

Hess, R. F., Beaudot, W. H., & Mullen, K. T. (2001). Dynamics of contour integration. *Vision Research*, *41*(8), 1023–1037.

Hess, R. F., & Dakin, S. C. (1997). Absence of contour linking in peripheral vision. *Nature*, *390*(6660), 602–604.

Hess, R. F., & Dakin, S. C. (1999). Contour integration in the peripheral field. *Vision Research*, *39*(5), 947–959.

Hess, R. F., & Demanins, R. (1998). Contour integration in anisometropic amblyopia. *Vision Research*, *38*(6), 889–894.

Hess, R. F., & Field, D. (1999). Integration of contours: New insights. *Trends in Cognitive Sciences*, *3*(12), 480–486.

Hess, R. F., & Field, D. J. (1995). Contour integration across depth. *Vision Research*, *35*(12), 1699–1711.

Hess, R. F., Hayes, A., & Kingdom, F. A. (1997). Integrating contours within and through depth. *Vision Research*, *37*(6), 691–696.

Hess, R. F., Ledgeway, T., & Dakin, S. (2000). Impoverished second-order input to global linking in human vision. *Vision Research*, *40*(24), 3309–3318.

Hoffman, D. D., & Singh, M. (1997). Salience of visual parts. *Cognition*, *63*(1), 29–78.

Hubel, D. H., & Wiesel, T. N. (1970). Stereoscopic vision in macaque monkey. Cells sensitive to binocular depth in area 18 of the macaque monkey cortex. *Nature*, *225*(5227), 41–42.

Hübner, R. (1993). Different ways of modeling spatial-frequency uncertainty in visual signal detection. *Biological Cybernetics*, *69*(5-6), 457–462.

Hübner, R. (1996a). The efficiency of different cue types for reducing spatial-frequency uncertainty. *Vision Research*, *36*(3), 401–408.

Hübner, R. (1996b). Specific effects of spatial-frequency uncertainty and different cue types on contrast detection: Data and models. *Vision Research*, *36*(21), 3429–3439.

Johnson, R. A., & Wichern, D. W. (2003). *Applied multivariate statistical analysis*. Upper Saddle River (New Jersey): Prentice Hall.

Kapadia, M. K., Westheimer, G., & Gilbert, C. D. (1999). Dynamics of spatial summation in primary visual cortex of alert monkeys. *Proceedings of the National Academy of Sciences of the United States of America*, *96*(21), 12073–12078.

Kapadia, M. K., Westheimer, G., & Gilbert, C. D. (2000). Spatial distribution of contextual interactions in primary visual cortex and in visual perception. *Journal of Neurophysiology*, *84*(4), 2048–2062.

Kimchi, R., Yeshurun, Y., & Cohen-Savransky, A. (2007). Automatic, stimulus-driven attentional capture by objecthood. *Psychonomic Bulletin & Review*, *14*(1), 166–172.

Kingdom, F. A., & Keeble, D. R. (2000). Luminance spatial frequency differences facilitate the segmentation of superimposed textures. *Vision Research*, *40*(9), 1077–1087.

Kiorpes, L., & Bassin, S. A. (2003). Development of contour integration in macaque monkeys. *Visual Neuroscience*, *20*(5), 567–575.

Koffka, K. (1935). *Principles of Gestalt psychology*. New York: Hartcourt.

Kourtzi, Z., & Huberle, E. (2005). Spatiotemporal characteristics of form analysis in the human visual cortex revealed by rapid event-related fMRI adaptation. *Neuroimage*, *28*(2), 440–452.

Kourtzi, Z., & Kanwisher, N. (2000). Cortical regions involved in perceiving object shape. *The Journal of Neuroscience: The Official Journal of the Society for Neuroscience*, *20*(9), 3310–3318.

Kourtzi, Z., & Kanwisher, N. (2001). Representation of perceived object shape by the human lateral occipital complex. *Science*, *293*(5534), 1506–1509.

Kourtzi, Z., Tolias, A. S., Altmann, C. F., Augath, M., & Logothetis, N. K. (2003). Integration of local features into global shapes: Monkey and human fMRI studies. *Neuron*, *37*(2), 333–346.

Kovacs, I. (1996). Gestalten of today: Early processing of visual contours and surfaces. *Behavioral Brain Research*, *82*(1), 1–11.

Kovacs, I., & Julesz, B. (1993). A closed curve is much more than an incomplete one: Effect of closure in figure-ground segmentation. *Proceedings of the National Academy of Sciences of the United States of America*, *90*(16), 7495–7497.

Kramer, P., Graham, N., & Yager, D. (1985). Simultaneous measurement of spatial-frequency summation and uncertainty effects. *Journal of the Optical Society of America. A, Optics and Image Science*, *2*(9), 1533–1542.

Kubota, T. (2004). Massively parallel networks for edge localization and contour integration–adaptable relaxation approach. *Neural Networks: The Official Journal of the International Neural Network Society*, *17*(3), 411–425.

Lamme, V. A. (1995). The neurophysiology of figure-ground segregation in primary visual cortex. *The Journal of Neuroscience: The Official Journal of the Society for Neuroscience*, *15*(2), 1605–1615.

Lamme, V. A., Rodriguez-Rodriguez, V., & Spekreijse, H. (1999). Separate processing dynam-

ics for texture elements, boundaries and surfaces in primary visual cortex of the macaque monkey. *Cerebral Cortex*, *9*(4), 406–413.

Landy, M. S., & Bergen, J. R. (1991). Texture segregation and orientation gradient. *Vision Research*, *31*(4), 679–691.

Landy, M. S., & Kojima, H. (2001). Ideal cue combination for localizing texture-defined edges. *Journal of the Optical Society of America. A, Optics, Image Science, and Vision*, *18*(9), 2307–2320.

Ledgeway, T., & Hess, R. F. (2002). Rules for combining the outputs of local motion detectors to define simple contours. *Vision Research*, *42*(5), 653–659.

Ledgeway, T., & Hess, R. F. (2006). The spatial frequency and orientation selectivity of the mechanisms that extract motion-defined contours. *Vision Research*, *46*(4), 568–578.

Ledgeway, T., Hess, R. F., & Geisler, W. S. (2005). Grouping local orientation and direction signals to extract spatial contours: Empirical tests of "association field" models of contour integration. *Vision Research*, *45*(19), 2511–2522.

Lee, D. T., & Schachter, B. J. (1980). Two algorithms for constructing a delaunay triangulation. *International Journal of Parallel Programming*, *9*(3), 219–242.

Lee, S. H., & Blake, R. (2001). Neural synergy in visual grouping: When good continuation meets common fate. *Vision Research*, *41*(16), 2057–2064.

Leeuwenberg, E., & Boselie, F. (1988). Against the likelihood principle in visual form perception. *Psychological Review*, *95*(4), 485–491.

Lerner, Y., Hendler, T., Ben-Bashat, D., Harel, M., & Malach, R. (2001). A hierarchical axis of object processing stages in the human visual cortex. *Cerebral Cortex*, *11*(4), 287–297.

Levitt, J. B., & Lund, J. S. (2002). The spatial extent over which neurons in macaque striate cortex pool visual signals. *Visual Neuroscience*, *19*(4), 439–452.

Li, C. Y., & Li, W. (1994). Extensive integration field beyond the classical receptive field of cat's striate cortical neurons–classification and tuning properties. *Vision Research*, *34*(18), 2337–2355.

Li, W., & Gilbert, C. D. (2002). Global contour saliency and local colinear interactions. *Journal of Neurophysiology*, *88*(5), 2846–2856.

Li, Z. (1998). A neural model of contour integration in the primary visual cortex. *Neural Computation*, *10*(4), 903–940.

Li, Z. (1999). Visual segmentation by contextual influences via intra-cortical interactions in the primary visual cortex. *Network*, *10*(2), 187–212.

Liu, Z., Jacobs, D. W., & Basri, R. (1999). The role of convexity in perceptual completion: Beyond good continuation. *Vision Research*, *39*(25), 4244–4257.

Livingstone, M. S., & Hubel, D. (1988). Segregation of form, color, movement, and depth: Anatomy, physiology, and perception. *Science*, *240*(4853), 740–749.

Livingstone, M. S., & Hubel, D. H. (1984). Anatomy and physiology of a color system in the primate visual cortex. *The Journal of Neuroscience: The Official Journal of the Society for Neuroscience*, *4*(1), 309–356.

Livingstone, M. S., & Hubel, D. H. (1987). Psychophysical evidence for separate channels for the

perception of form, color, movement, and depth. *The Journal of Neuroscience: The Official Journal of the Society for Neuroscience*, *7*(11), 3416–3468.

Loftus, G. R., & Harley, E. M. (2004). How different spatial-frequency components contribute to visual information acquisition. *Journal of Experimental Psychology. Human Perception and Performance*, *30*(1), 104–118.

Lord, F. M., & Novick, M. R. (1968). *Statistical theories of mental test scores*. Reading: Addison-Wesley.

Lorenceau, J., Giersch, A., & Series, P. (2005). Dynamic competition between contour integration and contour segmentation probed with moving stimuli. *Vision Research*, *45*(1), 103–116.

Maffei, L., & Fiorentini, A. (1973). The visual cortex as a spatial frequency analyser. *Vision Research*, *13*(7), 1255–1267.

Malach, R., Amir, Y., Harel, M., & Grinvald, A. (1993). Relationship between intrinsic connections and functional architecture revealed by optical imaging and in vivo targeted biocytin injections in primate striate cortex. *Proceedings of the National Academy of Sciences of the United States of America*, *90*(22), 10469–10473.

Malik, J., & Perona, P. (1990). Preattentive texture discrimination with early vision mechanisms. *Journal of the Optical Society of America. A, Optics and Image Science*, *7*(5), 923–932.

Mallot, H. A., Arndt, P. A., & Bülthoff, H. H. (1996). A psychophysical and computational analysis of intensity-based stereo. *Biological Cybernetics*, *75*(3), 187–198.

Mandon, S., & Kreiter, A. K. (2005). Rapid contour integration in macaque monkeys. *Vision Research*, *45*(3), 291–300.

Marr, D. (1982). *Vision: A computational investigation into the human representation and processing of visual information.* New York: Freeman.

Masin, C. M. (2001). Absolute and relative effects of similarity and distance on grouping. *Perception*, *31*(7), 799–811.

Mathes, B., & Fahle, M. (2007a). Closure facilitates contour integration. *Vision Research*, *47*(6), 818–827.

Mathes, B., & Fahle, M. (2007b). The electrophysiological correlate of contour integration is similar for color and luminance mechanisms. *Psychophysiology*, *44*(2), 305–322.

Mathes, B., Trenner, D., & Fahle, M. (2006a). Do subthreshold colour-cues increase contour detection performance? In *Beiträge zur 48. Tagung experimentell arbeitender Psychologen* (p. 82). Lengerich: Pabst Science Publishers.

Mathes, B., Trenner, D., & Fahle, M. (2006b). The electrophysiological correlate of contour integration is modulated by task demands. *Brain Research*, *1114*(1), 98–112.

May, K. A., & Hess, R. F. (2007a). Dynamics of snakes and ladders. *Journal of Vision*, *7*(12), 13, 1–19.

May, K. A., & Hess, R. F. (2007b). Ladder contours are undetectable in the periphery: a crowding effect? *Journal of Vision*, *7*(13), 9, 1–15.

McIlhagga, W. H., & Mullen, K. T. (1996). Contour integration with colour and luminance contrast. *Vision Research*, *36*(9), 1265–1279.

McMillan, N. A., & Creelman, C. D. (2005). *Detection theory: A user's guide*. London: Erlbaum.

Meinhardt, G. (1999). Evidence for different nonlinear summation schemes for lines and gratings at threshold. *Biological Cybernetics*, *81*(3), 263–277.

Meinhardt, G. (2000). Detection of compound spatial patterns: Further evidence for different channel interactions. *Biological Cybernetics*, *82*(4), 269–282.

Meinhardt, G. (2001). Learning a grating discrimination task broadens human spatial frequency tuning. *Biological Cybernetics*, *84*(5), 383–400.

Meinhardt, G., & Persike, M. (2003). Strength of feature contrast mediates interaction among feature domains. *Spatial Vision*, *16*(5), 459–478.

Meinhardt, G., Persike, M., Mesenholl, B., & Hagemann, C. (2006). Cue combination in a combined feature contrast detection and figure identification task. *Vision Research*, *46*(23), 3977–3993.

Meinhardt, G., Schmidt, M., Persike, M., & Röers, B. (2004). Feature synergy depends on feature contrast and objecthood. *Vision Research*, *44*(16), 1843–1850.

Metzger, W. (1975). *Gesetze des sehens* (3rd ed.). Frankfurt: Verlag Waldemar Kramer.

Metzger, W. (2006). *Laws of seeing*. Cambridge, MA: MIT Press.

Morita, H., Morita, M., & Kumada, T. (2003). Integration process of contours defined by different attributes. *Brain Research. Cognitive Brain Research*, *15*(3), 324–327.

Mortensen, U. (2002). Additive noise, weibull functions and the approximation of psychometric functions. *Vision Research*, *42*(20), 2371–2393.

Mortensen, U. (2007a). An analysis of visual detection by temporal probability summation. *Journal of Mathematical Psychology*, *51*(3), 164–182.

Mortensen, U. (2007b). Detection of visual stimuli in correlated noise. *Journal of Mathematical Psychology*, *51*(3), 183–197.

Mortensen, U., & Nachtigall, C. (2000). Visual channels, Hebbian assemblies and the effect of Hebb's rule. *Biological Cybernetics*, *82*(5), 401–413.

Mortensen, U., & Suhl, U. (1991). An evaluation of sensory noise in the human visual system. *Biological Cybernetics*, *66*(1), 37–47.

Mostafavi, H., & Sakrison, D. J. (1976). Structure and properties of a single channel in the human visual system. *Vision Research*, *16*(9), 957–968.

Mullen, K. T., Beaudot, W. H., & McIlhagga, W. H. (2000). Contour integration in color vision: a common process for the blue-yellow, red-green and luminance mechanisms? *Vision Research*, *40*(6), 639–655.

Mundhenk, T. N., & Itti, L. (2005). Computational modeling and exploration of contour integration for visual saliency. *Biological Cybernetics*, *93*(3), 188–212.

Navon, D. (1977). Forest before trees: the precedence of global features in visual perception. *Cognitive Psychology*, *9*(3), 353–383.

Nothdurft, H. C. (2000). Salience from feature contrast: Additivity across dimensions. *Vision Research*, *40*(10-12), 1183–1201.

Nugent, A. K., Keswani, R. N., Woods, R. L., & Peli, E. (2003). Contour integration in peripheral vision reduces gradually with eccentricity. *Vision Research*, *43*(23), 2427–2437.

Olzak, L. A., & Thomas, J. P. (1992). Configural effects constrain fourier models of pattern discrimination. *Vision Research*, *32*(10), 1885–1898.

Olzak, L. A., & Thomas, J. P. (1999). Neural recoding in human pattern vision: Model and mechanisms. *Vision Research*, *39*(2), 231–256.

Olzak, L. A., & Thomas, J. P. (2003). Dual nonlinearities regulate contrast sensitivity in pattern discrimination tasks. *Vision Research*, *43*(13), 1433–1442.

Olzak, L. A., & Wickens, T. D. (1997). Discrimination of complex patterns: Orientation information is integrated across spatial scale; spatial-frequency and contrast information are not. *Perception*, *26*(9), 1101–1120.

Parent, P., & Zucker, S. W. (1989). Trace inference, curvature consistency, and curve detection. *IEEE Transactions on Pattern Analysis and Machine Intelligence*, *11*(8), 823–839.

Pashler, H. (1988). Cross-dimensional interaction and texture segregation. *Perception & Psychophysics*, *43*(4), 307–318.

Peli, E., Arend, L., & Labianca, A. T. (1996). Contrast perception across changes in luminance and spatial frequency. *Journal of the Optical Society of America. A, Optics, Image Science, and Vision*, *13*(10), 1953–1959.

Persike, M., & Meinhardt, G. (2005). Contour integration by cue combination. *Perception*, *34*, 163.

Persike, M., & Meinhardt, G. (2006). Synergy of features enables detection of texture defined figures. *Spatial Vision*, *19*(1), 77–102.

Persike, M., & Meinhardt, G. (2007). Does closure stabilize contour integration? *Perception*, *36*, 108.

Persike, M., & Meinhardt, G. (2008). Cue summation enables perceptual grouping. *Journal of Experimental Psychology. Human Perception and Performance*, *34*(1).

Persike, M., Olzak, L. A., & Meinhardt, G. (2007). Contour integration across spatial frequency. *Journal of Experimental Psychology. Human Perception and Performance*, *(submitted)*.

Pettet, M. W. (1999). Shape and contour detection. *Vision Research*, *39*(3), 551–557.

Pettet, M. W., McKee, S. P., & Grzywacz, N. M. (1998). Constraints on long range interactions mediating contour detection. *Vision Research*, *38*(6), 865–879.

Polat, U. (1999). Functional architecture of long-range perceptual interactions. *Spatial Vision*, *12*(2), 143–162.

Polat, U., & Bonneh, Y. (2000). Collinear interactions and contour integration. *Spatial Vision*, *13*(4), 393–401.

Polat, U., Mizobe, K., Pettet, M. W., Kasamatsu, T., & Norcia, A. M. (1998). Collinear stimuli regulate visual responses depending on cell's contrast threshold. *Nature*, *391*(6667), 580–584.

Polat, U., & Sagi, D. (1993). Lateral interactions between spatial channels: Suppression and facilitation revealed by lateral masking experiments. *Vision Research*, *33*(7), 993–999.

Polat, U., & Sagi, D. (1994a). The architecture of perceptual spatial interactions. *Vision Research*, *34*(1), 73–78.

Polat, U., & Sagi, D. (1994b). Spatial interactions in human vision: From near to far via experience-

dependent cascades of connections. *Proceedings of the National Academy of Sciences of the United States of America*, *91*(4), 1206–1209.

Poom, L., & Borjesson, E. (2004). Good continuation with kinetic edges. *Vision Research*, *44*(18), 2101–2108.

Press, W. H., Teukolsky, S. A., Flamery, B. P., & Vetterling, W. T. (1996). *Numerical recipes* (5th ed.). Oxford: Oxford University Press.

Prins, N., & Kingdom, F. A. (2003). Detection and discrimination of texture modulations defined by orientation, spatial frequency, and contrast. *Journal of the Optical Society of America. A, Optics, Image Science, and Vision*, *20*(3), 401–410.

Prytulak, L. S. (1974). Good continuation revisited. *Journal of Experimental Psychology*, *102*(5), 773–777.

Quick, J., R. F. (1974). A vector-magnitude model of contrast detection. *Kybernetik*, *16*(2), 65–67.

Quinlan, P. T., & Wilton, R. N. (1998). Grouping by proximity or similarity? Competition between the gestalt principles in vision. *Perception*, *27*(4), 417–430.

Regan, D., & Beverley, K. I. (1983). Spatial-frequency discrimination and detection: Comparison of postadaptation thresholds. *Journal of the Optical Society of America*, *73*(12), 1684–1690.

Rivest, J., & Cavanagh, P. (1996). Localizing contours defined by more than one attribute. *Vision Research*, *36*(1), 53–66.

Robson, J. G., & Graham, N. (1981). Probability summation and regional variation in contrast sensitivity across the visual field. *Vision Research*, *21*(3), 409–418.

Rock, I., & Brosgole, L. (1964). Grouping based on phenomenal proximity. *Journal of Experimental Psychology*, *67*, 531–538.

Rodrigues, J., & Buf, J. M. du. (2006a). Cortical object segregation and categorization by multi-scale line and edge coding. In J. Braz, A. Ranchordas, H. Arajo, & J. Jorge (Eds.), *Visapp.* Setbal: Springer.

Rodrigues, J., & Buf, J. M. du. (2006b). Multi-scale keypoints in V1 and beyond: Object segregation, scale selection, saliency maps and face detection. *Biosystems*, *86*(1-3), 75–90.

Roelfsema, P. R., Lamme, V. A., & Spekreijse, H. (1998). Object-based attention in the primary visual cortex of the macaque monkey. *Nature*, *395*(6700), 376–381.

Roelfsema, P. R., Lamme, V. A., & Spekreijse, H. (2000). The implementation of visual routines. *Vision Research*, *40*(10-12), 1385–1411.

Roelfsema, P. R., Lamme, V. A., & Spekreijse, H. (2004). Synchrony and covariation of firing rates in the primary visual cortex during contour grouping. *Nature Neuroscience*, *7*(9), 982–991.

Roelfsema, P. R., Scholte, H. S., & Spekreijse, H. (1999). Temporal constraints on the grouping of contour segments into spatially extended objects. *Vision Research*, *39*(8), 1509–1529.

Roufs, J. A. (1974). Dynamic properties of vision. IV. Thresholds of decremental flashes, incremental flashes and doublets in relation to flicker fusion. *Vision Research*, *14*(9), 831–851.

Roufs, J. A., & Blommaert, F. J. (1981). Temporal impulse and step responses of the human eye obtained psychophysically by means of a drift-correcting perturbation technique. *Vision Research*, *21*(8), 1203–1221.

Rubenstein, B. S., & Sagi, D. (1990). Spatial variability as a limiting factor in texture-discrimination

tasks: implications for performance asymmetries. *Journal of the Optical Society of America. A, Optics and Image Science*, *7*(9), 1632–1643.

Rubenstein, B. S., & Sagi, D. (1996). Preattentive texture segmentation: the role of line terminations, size, and filter wavelength. *Perception & Psychophysics*, *58*(4), 489–509.

Saarinen, J., & Levi, D. M. (1999). The effect of contour closure on shape perception. *Spatial Vision*, *12*(2), 227–238.

Sagi, D. (1988). The combination of spatial frequency and orientation is effortlessly perceived. *Perception & Psychophysics*, *43*(6), 601–603.

Sagi, D. (1991). Spatial filters in texture segmentation tasks. In E. Blum (Ed.), *Channels in the visual nervous system: Neurophysiology, psychophysics and models* (pp. 397–424). London: Freund.

Sagi, D. (1995). The psychophysics of texture segmentation. In T. V. Papathomas, C. Chubb, A. Gorea, & E. Kowler (Eds.), *Early vision and beyond* (pp. 69–78). London: MIT Press.

Sagi, D., & Hochstein, S. (1985). Lateral inhibition between spatially adjacent spatial-frequency channels? *Perception & Psychophysics*, *37*(4), 315–322.

Samonds, J. M., Zhou, Z., Bernard, M. R., & Bonds, A. B. (2006). Synchronous activity in cat visual cortex encodes collinear and cocircular contours. *Journal of Neurophysiology*, *95*(4), 2602–2616.

Schiller, P. H. (1996). On the specificity of neurons and visual areas. *Behavioral Brain Research*, *76*(1-2), 21–35.

Schinkel, N. (2007). *Contour integration models predicting human behavior*. Unpublished doctoral dissertation, Universität Bremen.

Schinkel, N., Pawelzik, K. R., & Ernst, U. A. (2005). Robust integration and detection of noisy contours in a probabilistic neural model. *Neurocomputing*, *65-66C*, 211–217.

Schmidt, K. E., Goebel, R., Lowel, S., & Singer, W. (1997). The perceptual grouping criterion of colinearity is reflected by anisotropies of connections in the primary visual cortex. *The European Journal of Neuroscience*, *9*(5), 1083–1089.

Schyns, P. G., & Oliva, A. (1994). From blobs to boundary edges: Evidence for time and spatial scale dependent scene regocnition. *Psychological Science*, *5*(4), 195–200.

Shulman, G. L., & Wilson, J. (1987). Spatial frequency and selective attention to local and global information. *Perception*, *16*(1), 89–101.

Sigman, M., Cecchi, G. A., Gilbert, C. D., & Magnasco, M. O. (2001). On a common circle: Natural scenes and gestalt rules. *Proceedings of the National Academy of Sciences of the United States of America*, *98*(4), 1935–1940.

Singh, M., & Fulvio, J. M. (2007). Bayesian contour extrapolation: Geometric determinants of good continuation. *Vision Research*, *47*(6), 783–798.

Sirovich, L., & Uglesich, R. (2004). The organization of orientation and spatial frequency in primary visual cortex. *Proceedings of the National Academy of Sciences of the United States of America*, *101*(48), 16941–16946.

Smits, J. T., & Vos, P. G. (1987). The perception of continuous curves in dot stimuli. *Perception*, *16*(1), 121–131.

Smits, J. T., Vos, P. G., & Oeffelen, M. P. van. (1985). The perception of a dotted line in noise: a model of good continuation and some experimental results. *Spatial Vision*, *1*(2), 163–177.

Spillmann, L. (1999). Gehirn und Gestalt: I. Metzgers Gesetze des Sehens. *Psychologische Beiträge*, *41*, 458–493.

Spillmann, L. (2001). Gehirn und Gestalt II. Neuronale Mechanismen. *Kognitionswissenschaft*, *9*(3), 122–143.

Sugase, Y., Yamane, S., Ueno, S., & Kawano, K. (1999). Global and fine information coded by single neurons in the temporal visual cortex. *Nature*, *400*(6747), 869–873.

Tamura, H., & Tanaka, K. (2001). Visual response properties of cells in the ventral and dorsal parts of the macaque inferotemporal cortex. *Cerebral Cortex*, *11*(5), 384–399.

Tanner, W. P. (1956). Theory of recognition. *Journal of the Optical Society of America*, *28*, 882–888.

Thomas, J. P., & Olzak, L. A. (1996). Uncertainty experiments support the roles of second-order mechanisms in spatial frequency and orientation discriminations. *Journal of the Optical Society of America. A, Optics, Image Science, and Vision*, *13*(4), 689–696.

Tootell, R. B., Switkes, E., Silverman, M. S., & Hamilton, S. L. (1988). Functional anatomy of macaque striate cortex. II. Retinotopic organization. *The Journal of Neuroscience: The Official Journal of the Society for Neuroscience*, *8*(5), 1531–1568.

Treisman, A. M. (1988). Features and objects: The fourteenth Bartlett memorial lecture. *Quarterly Journal of Experimental Psychology A*, *40*(2), 201–237.

Treisman, A. M., & Gelade, G. (1980). A feature-integration theory of attention. *Cognitive Psychology*, *12*(1), 97–136.

Tripathy, S. P., Mussap, A. J., & Barlow, H. B. (1999). Detecting collinear dots in noise. *Vision Research*, *39*(25), 4161–4171.

Ts'o, D. Y., & Gilbert, C. D. (1988). The organization of chromatic and spatial interactions in the primate striate cortex. *The Journal of Neuroscience: The Official Journal of the Society for Neuroscience*, *8*(5), 1712–1727.

Ts'o, D. Y., Gilbert, C. D., & Wiesel, T. N. (1986). Relationships between horizontal interactions and functional architecture in cat striate cortex as revealed by cross-correlation analysis. *The Journal of Neuroscience: The Official Journal of the Society for Neuroscience*, *6*(4), 1160–1170.

Tversky, T., Geisler, W. S., & Perry, J. S. (2004). Contour grouping: Closure effects are explained by good continuation and proximity. *Vision Research*, *44*(24), 2769–2777.

Ullman, S., & Sha'ashua, A. (1988). Structural saliency: the detection of globally salient structures using a locally connected network. In *International conference on computer vision* (pp. 321–327).

Ursino, M., & La Cara, G. E. (2004). A model of contextual interactions and contour detection in primary visual cortex. *Neural Networks: The Official Journal of the International Neural Network Society*, *17*(5-6), 719-35.

Uttal, W. R., Davis, N. S., Welke, C., & Kakarala, R. (1988). The reconstruction of static visual forms from sparse dotted samples. *Perception & Psychophysics*, *43*(3), 223–240.

Von der Heydt, R., Peterhans, E., & Baumgartner, G. (1984). Illusory contours and cortical neuron responses. *Science*, *224*(4654), 1260–1262.

Wang, Y. Z., & Hess, R. F. (2005). Contributions of local orientation and position features to shape integration. *Vision Research*, *45*(11), 1375–1383.

Watson, A. B. (1982). Summation of grating patches indicates many types of detector at one retinal location. *Vision Research*, *22*(1), 17–25.

Webster, M. A., & De Valois, R. L. (1985). Relationship between spatial-frequency and orientation tuning of striate-cortex cells. *Journal of the Optical Society of America. A, Optics, Image Science, and Vision*, *2*(7), 1124–1132.

Wertheimer, M. (1923). Untersuchungen zur Lehre von der Gestalt. II. *Psychologische Forschung*, *4*(1), 301–350.

Wertheimer, M. (1958). Principles of perceptual organization. In D. C. Beardslee & M. Wertheimer (Eds.), *Readings in perception.* Princeton: Van Nostrand.

Wilson, H. R., & Gelb, D. J. (1984). Modified line-element theory for spatial-frequency and width discrimination. *Journal of the Optical Society of America. A, Optics and Image Science*, *1*(1), 124–131.

Wilson, H. R., McFarlane, D. K., & Phillips, G. C. (1983). Spatial frequency tuning of orientation selective units estimated by oblique masking. *Vision Research*, *23*(9), 873–882.

Wilson, H. R., & Regan, D. (1984). Spatial-frequency adaptation and grating discrimination: Predictions of a line-element model. *Journal of the Optical Society of America. A, Optics and Image Science*, *1*(11), 1091–1096.

Wolfe, J. M. (1994). Guided search 2.0. *Psychonomic Bulletin & Review*, *1*(2), 202–238.

Yager, D., Kramer, P., Shaw, M., & Graham, N. (1984). Detection and identification of spatial frequency: Models and data. *Vision Research*, *24*(9), 1021–1035.

Yen, S. C., & Finkel, L. H. (1997). Identification of salient contours in cluttered images. In *Computer vision and pattern recognition* (pp. 273–279). San Juan, Puerto Rico: IEEE Computer Society.

Yen, S. C., & Finkel, L. H. (1998). Extraction of perceptually salient contours by striate cortical networks. *Vision Research*, *38*(5), 719–741.

Zhou, H., Friedman, H. S., & von der Heydt, R. (2000). Coding of border ownership in monkey visual cortex. *The Journal of Neuroscience: The Official Journal of the Society for Neuroscience*, *20*(17), 6594–6611.

Zipser, K., Lamme, V. A., & Schiller, P. H. (1996). Contextual modulation in primary visual cortex. *The Journal of Neuroscience: The Official Journal of the Society for Neuroscience*, *16*(22), 7376–7389.

Zucker, S. W., Stevens, K. A., & Sander, P. (1983). The relation between proximity and brightness similarity in dot patterns. *Perception & Psychophysics*, *34*(6), 513–522.

Appendix A

The Gaussian Function on Logarithmic Scales

If the physical variable x is expressed on a logarithmic scale, i.e. $\tilde{x} = \ln x$, the Gaussian distribution $F(x)$ becomes a log-normal distribution

$$G(x) = \frac{1}{\sqrt{2\pi}\sigma_l} \int_0^{\ln x} \exp\left(-\frac{1}{2}\left(\frac{\ln v - \mu_l}{\sigma_l}\right)^2\right) dv. \tag{A.1}$$

with parameters μ_l and σ_l. For expected value and variance on the original scales one obtains

$$\mu = \exp\left(\mu_l + \frac{\sigma_l^2}{2}\right) \tag{A.2}$$

$$\sigma^2 = \exp\left(2\mu_l + \sigma_l^2\right)\left(\exp\left(\sigma_l^2\right) - 1\right) \tag{A.3}$$

(see Abramowitz & Stegun, 1972), which resolve to the parameters on the logarithmic scale

$$\mu_l = \ln \mu - \frac{\sigma_l^2}{2} \tag{A.4}$$

$$\sigma_l^2 = \ln\left(\frac{\sigma^2}{\mu^2} + 1\right) = \ln\left(\rho^2 + 1\right). \tag{A.5}$$

Now, equations (A.4) and (A.5) imply that distributions with different mean parameter μ but the same variation coefficient ρ are displaced but parallel on a logarithmic continuum, since they have the same variance on this scale.

Appendix B

The Generalized Variation Coefficient for the Weibull Distribution Function

Assume the Weibull model (3.7)

$$F(x) = 1 - \exp\left(-ax^b\right) \tag{B.1}$$

for the distribution Function $F(x)$. It has derivative

$$f(x) = \frac{dF}{dx} = ab\exp\left(-ax^b\right)x^{b-1}. \tag{B.2}$$

For the quantile corresponding to $p_0 = 1 - 1/e \approx 0.632$ one obtains

$$1 - 1/e = 1 - \exp\left(-ax_0^b\right) \tag{B.3}$$

which resolves to

$$x_0 = a^{-1/b}. \tag{B.4}$$

The value of $f(x)$ in the quantile x_0 is

$$\begin{aligned} \delta_0 &= ab\exp\left(-a\left(a^{-1/b}\right)^b\right)x_0^b x_0^{-1} \\ &= abe^{-1}\left(a^{-1/b}\right)^b x_0^{-1} \\ &= be^{-1}x_0^{-1}. \end{aligned} \tag{B.5}$$

Hence, the generalized variation coefficient (3.6) becomes

$$q_0 = \left(be^{-1}x_0^{-1}x_0\right)^{-1} = \frac{e}{b}. \tag{B.6}$$

(B.6) shows that the generalized variation coefficient for the Weibull distribution function is independent of the scale parameter a, and depends just on the shape parameter b. If another quantile is chosen, only an additional constant enters. For $p_0 = 0.5$ one obtains

$$x_0 = \left(\frac{\ln 2}{a}\right)^{1/b} \tag{B.7}$$

and the generalized variation coefficient resolves to

$$q_0 = \frac{e^{\ln 2}}{b\ln 2}. \tag{B.8}$$

Appendix C

Sensitivity Measure for Variation in Two Feature Dimensions

Assume that a stimulus vector of feature contrasts $\mathbf{s}'_i = (\Delta f_i, \Delta\phi_i)$ elicits sensory states $\mathbf{u}' = (x, y)$ with bivariate normal density, centroids $\boldsymbol{\mu}'_i = (\mu_{x_i}, \mu_{y_i})$, and homogeneous variance-covariance matrices $\boldsymbol{\Sigma}_i$. Then, the d' value for joint features, d'_{x+y}, has a definite geometrical meaning. When the random variables x and y are standardized with respect to the noise distribution, the coordinates of the centroid of the noise distribution, $\mathbf{z}_{\mu_0}$, and of the signal plus noise distributions, $\mathbf{z}_{\mu_t}$, are

$$\mathbf{z}_{\mu_0} = \begin{pmatrix} 0 \\ 0 \end{pmatrix} \qquad \mathbf{z}_{\mu_t} = \begin{pmatrix} \frac{\mu_{tx}-\mu_{0x}}{\sigma_x} \\ \frac{\mu_{ty}-\mu_{0y}}{\sigma_y} \end{pmatrix}. \tag{C.1}$$

This means that the coordinates of $\mathbf{z}_{\mu_t}$ are

$$\mathbf{z}_{\mu_t} = \mathbf{d}'_{x+y} = \begin{pmatrix} d'_x \\ d'_y \end{pmatrix}. \tag{C.2}$$

Formula (C.2) shows that the coordinates of the standardized coordinate vector $\mathbf{z}_{\mu_t}$ are the d' values in each dimension, which define the vector $\mathbf{d}'_{x+y}$. Now, since $\mathbf{d}'_{x+y}$ is a linear combination of its component vectors

$$\mathbf{d}'_{x+y} = \mathbf{d}'_x + \mathbf{d}'_y \tag{C.3}$$

its length is given by

$$\begin{aligned} d'_{x+y} &= \|\mathbf{d}'_{x+y}\| = \sqrt{\left\langle \left(\mathbf{d}'_x + \mathbf{d}'_y\right), \left(\mathbf{d}'_x + \mathbf{d}'_y\right) \right\rangle} \\ &= \sqrt{\|\mathbf{d}'_x\|^2 + \|\mathbf{d}'_y\|^2 + 2\left\langle \mathbf{d}'_x, \mathbf{d}'_y \right\rangle} \\ &= \sqrt{\|\mathbf{d}'_x\|^2 + \|\mathbf{d}'_y\|^2 + 2\|\mathbf{d}'_x\|\|\mathbf{d}'_y\|\cos\gamma} \\ &= \sqrt{\left(d'_x\right)^2 + \left(d'_y\right)^2 + 2d'_x d'_y \cos\gamma} \end{aligned} \tag{C.4}$$

where γ is the angle enclosed by the axes x and y. If the two random variables x and y are uncorrelated (i.e. $r_{xy} = \cos\gamma = 0$), then (C.4) becomes equal to (5.3). If they lie on a common ray (i.e. $r_{xy} = \cos\gamma = 1$), then

$$d'_{x+y} = \sqrt{(d'_x)^2 + \left(d'_y\right)^2 + 2d'_x d'_y} = \sqrt{\left(d'_x + d'_y\right)^2} = \left|d'_x + d'_y\right|, \tag{C.5}$$

which means that the d' values sum linearly.

Zusammenfassung

(gemäß § 22 (5) der Promotionsordnung vom 26.07.2000, in der Fassung vom 15.08.2005)

Ziel der Arbeit ist die Analyse von Prinzipien der Konturintegration im menschlichen visuellen System. Die perzeptuelle Verbindung benachbarter Teile in einer visuellen Szene zu einem Ganzen wird durch zwei gestalttheoretisch begründete Propositionen gekennzeichnet, die komplementäre lokale Mechanismen der Konturintegration beschreiben.

Das erste Prinzip der Konturintegration fordert, dass lokale Ähnlichkeit von Elementen in einem anderen Merkmal als Orientierung nicht hinreicht für die Entdeckung von Konturen, sondern ein zusätzlicher statistischer Merkmalsunterschied von Konturelementen und Umgebung vorliegen muss, um Konturentdeckung zu ermöglichen.

Das zweite Prinzip der Konturintegration behauptet, dass eine kollineare Ausrichtung von Konturelementen für Konturintegration hinreicht, und es bei deren Vorliegen zu robuster Konturintegrationsleistung kommt, auch wenn die lokalen merkmalstragenden Elemente in anderen Merkmalen in hohem Maße zufällig variieren und damit keine nachbarschaftliche Ähnlichkeitsbeziehung entlang der Kontur aufweisen.

Als empirische Grundlage für die beiden vorgeschlagenen Prinzipien der Konturintegration werden drei Experimente berichtet, die zunächst die untergeordnete Rolle globaler Konturmerkmale wie Geschlossenheit bei der Konturentdeckung aufweisen und daraufhin die Bedeutung lokaler Mechanismen für die Konturintegration anhand der Merkmale Kollinearität, Ortsfrequenz sowie der spezifischen Art der Interaktion zwischen beiden Merkmalen beleuchten.

Im ersten Experiment wird das globale Merkmal der Geschlossenheit untersucht und gezeigt, dass geschlossene Konturen nicht effektiver entdeckt werden als offene Konturen. Das zweite Experiment zeigt die Robustheit von über Kollinearität definierten Konturen über die zufällige Variation im Merkmal Ortsfrequenz entlang der Kontur und im Hintergrund, sowie die Unmöglichkeit der Konturintegration bei nachbarschaftlicher Ähnlichkeit der Konturelemente, wenn Ähnlichkeit statt über kollineare Orientierung über gleiche Ortsfrequenzen realisiert ist. Im dritten Experiment wird gezeigt, dass eine redundante Kombination von kollinearer Orientierung mit einem statistischen Unterschied im Merkmal Ortsfrequenz zu erheblichen Sichtbarkeitsgewinnen bei der Konturentdeckung führt. Aufgrund der Stärke der Summationswirkung wird vorgeschlagen, dass durch die Kombination mehrerer Hinweisreize neue kortikale Mechanismen angesprochen werden, die die Konturentdeckung unterstützen.

Die Resultate der drei Experimente werden in den Kontext aktueller Forschung zur Objektwahrnehmung gestellt und ihre Bedeutung für die postulierten allgemeinen Prinzipien visueller Gruppierung in der Konturintegration diskutiert. Anhand phänomenologischer Beispiele mit anderen Merkmalen als Orientierung und Ortsfrequenz wird gezeigt, dass die gefundenen Prinzipien Generalisierbarkeit für die Verarbeitung von Konturen im visuellen System beanspruchen können.